The Numerical Modelling of Laminar and Turbulent Viscous Fluid Flow

A Thesis Presented

for the Degree of

Doctor of Philosophy

of the

University of Southampton

in the

Faculty of Engineering and

Applied Sciences

by

MICHAEL ANTHONY KAVANAGH

May 1982

This work is dedicated to the fond memory of my Uncle Noel.

TABLE OF CONTENTS

UNIVERSITY OF SOUTHAMPTON

ABSTRACT

FACULTY OF ENGINEERING AND APPLIED SCIENCES

Doctor of Philosophy

THE NUMERICAL MODELLING OF LAMINAR AND TURBULENT FLUID FLOW

by Michael Anthony Kavanagh

The numerical solution of the Navier-Stokes Equations is presented for a two-dimensional incompressible fluid in terms of stream function and vorticity. An uncoupled Galerkin formulation is derived from the governing equations and their respective natural boundary conditions. By assuming a polynomial variation of both unknowns within the flow domain an approximate solution is achieved by the finite element method.

In the first part of this work a successful solution of three laminar flow problems is achieved, i.e. the flow: within a square cavity, over a downstream step and past a circular cylinder. Adequate comparison is made with earlier work.

In the second part the solution scheme is extended to model developing turbulent flow in a channel by means of an algebraic closure of the time averaged equations.

In order to model a variety of flow problems the development of a suitable automatic mesh generating scheme is carried out. Providing a fast and efficient discretization of each flow region.

This work concentrates on evaluating the solution scheme by solving problems where previous work already exists. With the aid of the mesh generator the program can also be used as a practical predictive tool.

ACKNOWLEDGEMENTS

The author would like to thank Dr. C.A. Brebbia for his supervision and encouragement throughout the course of this work.

Thanks are also to the staff at the Rutherford Appleton Laboratory, Chilton, Didcot without whose fine computer facilities this work would not have been possible.

The author would also like to thank all his colleagues at Number 13 University Crescent both, past and present, for many hours of discussion. In addition thanks are also due to friends in the Department of Civil Engineering who helped to provide a suitable environment in which to carry out this work.

A special mention is reserved for my family and Louise whose patience and unswerving support have made the completion of this work possible.

Finally thanks are due to the Science and Engineering Research Council under whose auspices this research was instigated.

NOTATION

u_i	fluid velocity
U_i	time averaged velocity
p	fluid pressure
$\overline{P}$	time averaged pressure
t	time
x_i	spatial coordinates
s,n	local coordinates of a surface
b_i	body forces
T_{ij}	surface stresses
D_{ij}	rate of deformation tensor
$\overline{D_{ij}}$	time averaged rate of deformation tensor
ω	fluid vorticity
Ω	time averaged fluid vorticity
ψ	stream function
Ψ	time averaged stream function
$\delta\omega,\delta\psi$	the weighting functions of both unknowns
ϕ_j	the interpolation functions over one element
δ_{ij}	Kronecker delta, $\delta_{ij}=1$ if $i=j$, $=0$ if $i\neq j$
$(-)'$	fluctuating part of unknown (-)
$\frac{D(-)}{Dt}$	complete derivative of (-)
$\dot{(-)}$	time derivative of (-)
$\Delta(-)$	small increment of (-)
ρ	density of fluid
μ	dynamic viscosity of the fluid
ν	kinematic viscosity of the fluid
σ_{ij}	shear stress
Re	Reynolds number (ul/ν)

ν_a	apparent kinematic viscosity
ν_t	total kinematic viscosity
σ_w	wall shear stress
u^*	wall friction velocity
$\overline{u'_i u'_j}$	Reynolds stress
κ	universal mixing length
A	Van Driest damping constant

CHAPTER ONE

INTRODUCTION

1. Introduction

To model the flow of an incompressible viscous fluid in two dimensions the solution of the Navier-Stokes equation and the continuity equation is required, i.e. the (N.S) set of equations. They can be considered in either the steady state or the transient form. From the creeping flow of metal extrusion to the turbulent flow about an aeroplane wing; the governing equations are of the same form, and the same basic techniques are adopted. With such importance attached to this problem there is a great need to develop suitable solution techniques.

Great difficulties have been met in solving this problem analytically owing to the non-linearities of the momentum equation. It has been necessary to turn to approximate or numerical techniques to achieve solution for practical flow problems. An original work by Thom [1] to model the flow past a cylinder by the Finite Difference technique, (F.D.T), was presented in 1933. Subsequently this numerical technique has been developed to model a wide variety of flow problems; see Kawaguti [2], Apelt [3] and Gosman et al [4].

Inheriting many ideas from (F.D) work and also adopting the Finite Element Method (F.E.M) from solid mechanics the fluid dynamicist can now tackle flow problems of greater complexity. The inherent ability of the (F.E.M) to discretize the problem domain in an irregular fashion makes it most suitable for modelling fluid flow where localised regions within a domain have large variations of the unknowns, e.g. close to the solid wall. Furthermore it has the ability to handle natural boundary conditions with ease. Both are distinct advantages over the (F.D.T), as a consequence the (F.E.M) has superseded it for

most structural problems. In actual fact the (F.D.T) may be considered a special case of the more general (F.E.M).

As mentioned above the non-linearity of the momentum equation is the major difficulty when solving a flow problem. This is caused by the complete derivative of the velocity at a fixed point in the fluid w.r.t. time. Increasing the magnitude of the inertial effects increases the extent of the non-linearity, causing greater difficulty in achieving a solution. Numerically it is overcome by a quasi-linearisation of the momentum equation and the solution is achieved by an iterative process.

Writing the set of (N.S) equations in terms of velocity and pressure (u_j, P) a solution can be obtained in terms of these primitive variables. A (F.E) solution in this manner was first developed by Zienkiewicz [5] for slow creeping flow. In this case the problem is simplified as the viscous terms dominate and the non-linear inertial terms become negligible. By ignoring these terms the momentum equation reduces to the Stokes equation. Later the technique was extended to the full (N.S) equations with the inertial terms included by Taylor and Hood [6].

Further development of this approach has been carried out by Kawahara et al [7] and Nickell et al [8]. All these schemes experience the same major drawback when calculating the pressure in the formulation. It is not possible to calculate pressure with the same accuracy as velocity because the continuity condition is a constraint on the velocity alone and not a full relationship between pressure and velocity. It has been generally found that in order to solve the set of equations successfully the element interpolation of velocity needs

to be of one order greater then the pressure.

To by-pass the pressure problem, Fortin [9] developed a technique to solve the momentum equation with the null divergence of velocity explicit to the interpolation scheme chosen. This scheme enables the incompressibility, i.e. the continuity of the flow, to be inherent in the interpolation scheme. The pressure can then be eliminated from the formulation and a solution can be achieved. This technique does solve the problem of having to compute the pressure iteratively; however, construction of a suitable interpolation field is difficult. Fortin uses some approximations to demonstrate his ideas.

Extending the idea of defining the continuity directly, the momentum equation is written in terms of a variable whose definition applies continuity directly, i.e. stream function. Tuann and Olson [10] write the momentum equation in terms of stream function alone, (ψ), with the continuity applied by its definition. As the momentum equation is now of fourth order the element discretization has to be of C' compatibility. An approximate solution is reached in terms of quintic triangles for the stream function, with the velocity and pressure retrieved subsequently. Owing to the complication of the fourth order equation this technique has not proved attractive to other workers.

To reduce the order of this equation it can be written in terms of an intermediate variable, i.e. vorticity (ω). It is now necessary to solve two equations, i.e. the vorticity transport equation and the Poisson equation which relates stream function to vorticity. Strictly speaking the vorticity transport equation is produced by taking the curl of the momentum equation, with the fourth order stream function

equation derived from it subsequently. The solution of fluid flow in terms of stream function and vorticity has the advantage of excluding pressure as an unknown. Such an approach has found favour with several (F.D) engineers; see for example Burggraff [11] and Gosman [2]. The problem of defining the vorticity boundary condition on the no-slip wall has caused many (F.E) researchers to revert to the primitive approach, i.e. (u_i, P).

Separate work by Baker [12] and Cheng [13] has produced a Galerkin (F.E) solution technique for the transient problem in terms of stream function and vorticity, (ψ, ω). Owing to the problem of defining the vorticity on the no-slip wall directly a steady state solution has proved difficult. Instead an iterative solution is possible by integrating through time. The solution is stopped when the steady state has been reached or when a suitable amount of time has passed to describe adequately the transient problem.

Above, a general summary of the major approaches for solving the (N.S) equations is presented. Each solution has particular merits and drawbacks; currently much debate abounds as to the best scheme. In general the (F.D) engineers prefer the stream function vorticity approach, (ψ, ω), whereas the (F.E) engineers prefer the primitive variable approach; (u_i, P).

Here a (F.E) solution of two dimensional flow is presented, based on the transient stream function vorticity approach. Using the Galerkin method, Two seperate integral statements are constructed for the vorticity transport equation and the Poisson relationship. The solution of vorticity is obtained iteratively with the non-linearity expressed in terms of stream function, which is updated periodically by

solving the equivalent Poisson statement.

The time integration scheme is a semi-implicit technique based on a forward and backward integration, which is designed to reduce solution instability at high values of Reynolds number, Re; see Smith [14]. The no-slip vorticity boundary condition is applied as a natural condition based on a limiting equation at the wall.

A mesh generation program has been linked to the solver to allow large and varied flow conditions to be considered with a minimum of effort; see Nelson [15]. Similarly a contour plotting program is attached to the solution program to enable fast processing of results.

Finally the laminar model is extended to solve problems in the turbulent range. The mechanisms of turbulent flow are different from those of laminar flow, producing a superposition of random velocities on the overall mean motion. When solving a turbulent problem it is necessary to write the equations in terms of time averaged variables.

When expressing the momentum equation in terms of time averaged velocity and pressure an additional term is produced which is a function of the fluctuating velocities. This is known as the Reynolds stress and is caused by the lateral transfer of momentum. To solve the equations in this form the Reynolds stress has to be expressed in terms of the time averaged unknowns.

By assuming the turbulent stresses to be of the same form as the viscous stresses, Boussinesq related them to the gradient of the time averaged velocity. This was made possible by the introduction of turbulent or apparent viscosity, which differs from molecular viscosity in being a local function of the fluid motion and not a constant

property of the fluid.

The use of the turbulent viscosity concept was later extended by Prandtl [16]. In the molecular theory of gases the kinematic molecular viscosity is caused by the momentum transfer of molecules. Similarly, Prandtl proposed that the turbulent viscosity is caused by the momentum transfer of lumps of fluid. With this in mind he equated the turbulent viscosity to the product of mixing length and time averaged velocity. The variation of the mixing length within a flow region has been derived empirically for many flow problems. It is now possible to achieve closure of the time averaged equations and consequently a solution of such problems is possible.

Much (F.D) work has been carried out to produce such turbulent solutions. Solutions in terms of the primitive variables have been developed by Cebeci and Smith [17] and Patankar and Spalding [18]. Using the stream function and vorticity approach Gosman et al [4] have also produced a successful turbulent model.

More recently a (F.E) solution of the time averaged equations has been achieved in terms of the primitive variables by Hughes [19].

In this case a turbulent model in terms of stream function and vorticity is presented , adopting the mixing length concept to achieve closure of the equations. This model is developed by extending the existing time dependent solution scheme.

The aim of this work is to develop a general scheme designed to solve a variety of viscous flow problems in both the laminar and turbulent range. With the introduction of the mesh generator this is achieved with much reduced effort.

In chapter two the governing equations of fluid flow are presented . They are subsequently expressed in terms of stream function and vorticity as the unknowns. Finally the boundary conditions of the flow domain are explained.

In chapter three the set of governing equations is expressed in the (F.E) form, from which an approximate solution is obtained. The semi-implicit time integration scheme is outlined where the time step restrictions are explained. Finally the application of the vorticity condition on the no-slip wall is introduced.

In chapter four the interface between the data generator and the fluid flow program is outlined. A simple way of ensuring a suitable mesh discretization for flow problems is presented.

In chapter five a variety of flow problems is solved using this (F.E) scheme. All these problems are in the steady state laminar range, i.e. the flow in a square cavity, the flow over a downstream step and the flow past a circular cylinder. With the use of earlier numerical and experimental work an evaluation of the solution method is achieved.

Following on from this successful work the model is extended to handle turbulent conditions. In chapter six the theory of turbulent flow is discussed. The existing (F.E) program is extended by including an algebraic model of the turbulent mechanisms. Finally the complete solution of developing flow in a channel encompassing both the laminar and the turbulent range is presented.

CHAPTER TWO

THE THEORY OF FLUID FLOW

2. The Theory of Fluid Flow

2.1 Introduction

In this work the flow of a two-dimensional incompressible fluid is presented. Below, a brief description of the Navier-Stokes equations is given. Then these equations are written in a form to be solved. For a fuller explanation of the governing equations see Malvern [20]. However, many fluid mechanics text books provide a more complete discussion of the continuum equations; refer to the bibliography below.

The equations presented throughout this work are expressed in terms of Cartesian tensor notation. Subscript indicies are employed to represent the three component directions. A standard summation convention is introduced without the need to write summation symbols.

2.2 The Governing Equations of Fluid Flow

As in the solution of most engineering problems a fluid is considered to have continuum properties. This enables us to ignore its discrete molecular components and consider only the macroscopic scale.

By considering a small element of fluid, the conservation of mass is applied to it. The equations are expressed spatially; where u_i is velocity and ρ is fluid density.

$$\frac{\partial \rho}{\partial t} + \frac{\partial (\rho u_i)}{\partial x_i} = 0 \,. \qquad (2.2.1)$$

As the fluid is incompressible its density is constant throughout, therefore the equation is reduced to:

$$\frac{\partial u_i}{\partial x_i} = 0 \qquad (2.2.2)$$

Considering all the forces acting on a small element of fluid, and applying Newton's second law of motion, an equilibrium equation is obtained;

$$\frac{\rho \partial u_i}{\partial t} = \rho b_i + \frac{\partial T_{ij}}{\partial x_j} \qquad (2.2.3)$$

Above is the equation describing the conservation of momentum, the forces acting on an element of fluid being divided into body force, b_i, and surface force, T_{ij} which is known as Chauchy's stress tensor.

It is now necessary to express the constitutive equations relating the surface stresses to the strains. At this point the distinction must be made between solid and fluid continua.

In a solid continuum the shear stresses may be resisted, and so they are a function of the shear strains. A fluid, however, cannot hold shear stress, and so it will deform. Instead they are a function of the shear stress rate. The constitutive equations for a linear elastic material are derived from Hookes law, relating stress to strain. This was later extended to a fluid by Stokes, and so by applying Stokes law of friction the shear stresses can be expressed in terms of the strain rate; see appendix A1.

$$T_{ij} = -P_i \delta_{ij} + F(D_{ij}) \qquad (2.2.4)$$

δ_{ij} - Kronecker delta, $\delta_{ij} = 1$ if $i = j$, $= 0$ $i \neq j$

P_i - pressure

D_{ij} - the rate of deformation tensor

Above is the constitutive relationship of surface stresses with deformation for any fluid. In this case the fluid is isotropic, i.e. incompressible with a constant viscosity. This is also known as a Newtonian fluid, consequently the function above takes the following form:

$$T_{ij} = -P \delta_{ij} + \lambda D_{kk} \delta_{ij} + 2\mu D_{ij} \qquad (2.2.5)$$

λ - bulk viscosity

μ - dynamic viscosity

D_{kk} - the volumetric dilatation or rate of change of volume of a fluid element

The rate of deformation tensor, D_{ij}, is defined in a similar way to the strain tensor in solid mechanics, with velocity replacing deformation; see appendix A1.

$$D_{ij} = \frac{1}{2}\left(\frac{\partial u_i}{\partial x_j} + \frac{\partial u_j}{\partial x_i}\right) \qquad (2.2.6)$$

Substituting the constitutive relation, (2.2.5), into the momentum equation, (2.2.3), produces the Navier-Stokes equation for momentum. That, combined with continuity, (2.2.2), is the set of equations which governs the flow of an incompressible Newtonian fluid.

The derivation of T_{ij} is detailed in its general form; here a particular result shall be quoted, for further details see appendix A1. Differentiating equation (2.2.5) w.r.t x_i, and substituting into this the definition of the deformation tensor, D_{ij}. Applying continuity to this directly will produce:

$$\frac{\partial T_{ij}}{\partial x_j} = -\frac{dP}{dx_i} + \mu\frac{\partial}{\partial x_j}\left(\frac{\partial u_i}{\partial x_j}\right) \qquad (2.2.7)$$

The bulk viscosity may be cancelled for a fluid of an isotropic form. Substituting this into the momentum equation, (2.2.3), to obtain:

$$\rho\frac{\partial u_i}{\partial t} = \rho\, b_i - \frac{dP}{dx_i} + \mu\frac{\partial}{\partial x_j}\left(\frac{\partial u_i}{\partial x_j}\right) \qquad (2.2.8)$$

The body forces, b_i per unit mass, refer to any external force acting on the mass of fluid, e.g. magnetic or gravitational forces. Here the latter are more likely; however, this may be incorporated into the direct pressure gradient if there is no free surface.

At this stage an equation which relates the rate of change of momentum to forces expressed in terms of fluid deformation has been presented. So far this equation may refer to the motion of a particle through a fluid, the Lagrangian frame, or to the motion at one point in the fluid through time, the Eulerian frame. In the study of fluid flow the Eulerian approach is more convenient. This is in contrast to solid mechanics where the small deformation theory allows the Lagrangian frame of reference to be adopted; see Gallagher et al [21]. To consider the motion of a fluid at a fixed point it is necessary to take

the complete derivative of velocity with time. This is known as the substantial derivative and introduces the non-linear convective term as follows:

$$\frac{\partial u_i}{\partial t} = \frac{du_i}{dt} + \frac{\partial u_i}{\partial x_j}\frac{\partial x_j}{\partial t} \tag{2.2.9}$$

$$= \frac{du_i}{dt} + u_j \frac{\partial u_i}{\partial x_j}$$

$\frac{\partial}{\partial x_i}$ - is a general partial derivative defining the operator:

$$\frac{D(\ )}{Dt} = \frac{d(\ )}{dt} + u_j \frac{\partial(\ )}{\partial x_j} \tag{2.2.10}$$

In terms of an Eulerian field the momentum equation may be written:

$$\frac{Du_i}{Dt} = -\frac{1}{\rho}\frac{dP}{dx_i} + \nu\frac{\partial}{\partial x_j}\left(\frac{\partial u_i}{\partial x_j}\right) + b_i \tag{2.2.11}$$

ν - kinematic viscosity = μ/ρ

$\frac{d}{dx_i}$ - is a specific derivative in a single direction

The convective terms produced by this derivative cause great difficulty when solving the set of (N.S) equations. As the Re for a particular problem is increased these non-linear terms become larger. In order to solve any practical flow problem it is necessary to deal with a highly non-linear momentum equation. Analytical solutions are unavailable, and so it is necessary to turn to numerical methods to solve problems of any practical importance.

Above the derivation of the (N.S) set of equations describing the flow of fluid has been outlined. This derivation has been simplified by the assumption of constant fluid density and viscosity. Both are reasonable for the range of problems to be solved here.

Although this work is mainly concerned with the application of these equations, it is still necessary to present a working knowledge of their derivation.

2.3 To Express the Navier-Stokes Equations in Terms of Stream function and Vorticity

To solve the set of (N.S) equations by numerical techniques two major approaches exist; the solution in terms of the primitive variables, (u_i, P), by solving the equations presented in the previous section, and a solution in terms of alternative variables, stream function and vorticity (ψ, ω).

Writing the equations in terms of the latter enables the continuity of the fluid to be satisfied directly by the definition of stream function. For this reason many (F.D) engineers have adopted this approach successfully; e.g. Kawaguti [2] and Burggraf [11].

Furthermore the evaluation of pressure is no longer necessary ; this would involve a solution of the divergence form of the momentum equation ; see Tuann and Olson [10]. The disadvantage of solving the problem in this manner is in the application of a suitable vorticity boundary condition on the no-slip solid boundary.

In recent years the finite element method has been used to predict the unsteady flow past a circular cylinder; see Smith [14].

Leading on from this the solution of a variety of steady state flow problems is carried out here, with extensive comparison made with earlier work.

It is first necessary to express the governing equations in terms of stream function and vorticity.

Both these equations are written in spatial form. Here the two-dimensional form is considered, thus the vorticity is reduced to a scalar in the flow region.

Defining the variables stream function, (ψ), and vorticity, (ω):

$$u_1 = \frac{\partial \psi}{\partial x_2}$$

$$u_2 = - \frac{\partial \psi}{\partial x_1} \qquad (2.3.1)$$

$$\omega = \frac{\partial u_2}{\partial x_1} - \frac{\partial u_1}{\partial x_2} \qquad (2.3.2)$$

Where the vorticity is the curl of velocity acting along a line normal to the plane of two components; here it is treated as a scalar.

By taking the curl of the momentum equation the vorticity transport equation is now written:

$$\frac{D\omega}{Dt} - \nu \frac{\partial^2 \omega}{\partial x_j^2} = 0 \qquad (2.3.3)$$

This is of the same form as the momentum equation but with

vorticity as the unknown variable; both are particular examples of the transport equation. The original equation refers to the transport of momentum and the final equation refers to the transport of vorticity.

By substituting equation (2.3.1) into equation (2.3.2) a relationship between stream function and vorticity is obtained, see appendix A.2.

$$\frac{\partial^2 \psi}{\partial x_j^2} = -\omega \qquad (2.3.4)$$

Equations (2.3.3) and (2.3.4) represent the set of equations which govern viscous fluid flow in two dimensions. By substituting the definition of stream function, equation (2.3.1), into the continuity relationship, equation (2.2.2), it can be shown that the fluid continuity is satisfied directly, see appendix A.2.

2.4 The Boundary Conditions of the Problem

A two dimensional domain is considered in which the fluid flow is governed by the two equations above, i.e. equations (2.3.3) and (2.3.4). This domain is enclosed by a boundary defining the limits of the problem.

This boundary is separated into a flux type and a rigid type. The direction vectors (s,n) are lines tangential and normal to the boundary respectively.

2.4.1 The Rigid Boundary

(i) The Free-slip Boundary

This is not truly a rigid boundary but it is used to define the

limits of the domain. In the primitive scheme it is described as a line of zero shear stress. Here it is treated as a streamline boundary, by describing the stream function as:

$$\frac{\partial \psi}{\partial s} = 0 \text{ or } \psi = \overline{\psi} \qquad (2.4.1a)$$

The vorticity is a measure of the fluid rotation. This rotation will diminish with distance from the solid or no- slip wall. As the free- slip wall defines the limit of the domain it is reasonable to assume the vorticity to be zero along it; thus:

$$\omega = 0 \qquad (2.4.1b)$$

(ii) The No-slip Boundary

This boundary describes the line of a solid obstruction to the fluid flow. It also imposes restrictions on the flow in that region. The velocity along the no-slip boundary is zero; this is defined in terms of stream function gradients to produce:

$$\frac{\partial \psi}{\partial n} = 0 \qquad (2.4.2a)$$

$$\frac{\partial \psi}{\partial s} = 0$$

A value for the vorticity or its gradient normal to the boundary is also applied along this boundary:

$$\frac{\partial \omega}{\partial n} = \overline{g}_{\omega}$$

$$\omega = \overline{\omega} \qquad (2.4.2b)$$

The difficulty arises in expressing the boundary values $\overline{g}_{\omega}$ and $\overline{\omega}$ since knowledge of the distribution of vorticity along it is unavailable, at least until a solution is achieved. A typical no-slip boundary is a cylindrical obstruction in a flow regime.

2.4.2 The Flux Boundary

The flux condition permits the flow of fluid into and out of the domain. The conditions for the inflow boundary are:

Stream function:

$$\psi = \overline{\psi} \qquad (2.4.3a)$$

Vorticity:

$$\omega = \overline{\omega} \qquad (2.4.3b)$$

This means that the velocity at the inflow boundary can be specified as $\overline{\frac{\partial \psi}{\partial s}} = \overline{u}_n$.. If the vorticity is zero and the stream function has a linear variation along the boundary, the tangential velocity is also zero, consequently normal parallel flow is enforced.

The conditions for the outflow boundary are defined as:

Stream function:

$$\frac{\partial \psi}{\partial n} = \overline{g}_{\psi} \qquad (2.4.4a)$$

Vorticity:

$$\frac{\partial \omega}{\partial n} = \overline{g}_{\omega} \qquad (2.4.4b)$$

The choice of $\overline{g}_{\omega}$ and $\overline{g}_{\psi}$ is arbitrary; choosing them to be zero will produce a parallel flow condition normal to this boundary.

The application of an outflowing boundary defines the limits of the domain in the direction of the flow. To define this explicitly it is necessary to position it far enough downstream so that the flow is no longer influenced by any disturbances upstream, e.g. disturbances caused by a bluff body. Such a rigid condition would need to be located so far downstream that the resulting flow domain would be prohibitively large. Instead it is necessary to impose an implicit boundary condition at some practical distance from the obstruction of the form stated above.

In order to achieve a practical location for this boundary some speculation is necessary. However, it is not expected that this will affect flow upstream as long as it is placed well away from the disturbance.

In this chapter the equations governing fluid flow have been derived and expressed in terms of stream function vorticity, (ψ, ω). The boundary conditions necessary to solve a problem within a fluid domain have also been presented.

In order to solve such flow problems the Finite Element Method,

(F.E.M), is applied to the set of equations. By using this approximate method it is possible to overcome the problems inherent in solving the non-linear equations. In the next chapter the application of the (F.E.M) to the fluid flow equations is presented.

CHAPTER THREE

THE FINITE ELEMENT FORMULATION

3. The Finite Element Formulation

3.1 Introduction

The (F.E.M) is now applied to the governing equations derived in the last chapter.

In this method the differential equations are replaced by equivalent integral formulations, which both represent a stationary condition, written in terms of approximate unknowns. From these formulations an approximate solution of the dependent variables is obtained; here the variables are vorticity, (ω), and stream function, (ψ). The above formulation is obtained by multiplying a differential equation by a weighting function and integrating this expression over the entire domain of the problem.

In this problem there are two differential equations describing the flow behaviour and so either one equivalent formulation may be developed for them in a coupled form, or two separate formulations may be produced, see Tuann and Olson [10]. Here, two separate formulations are produced and the resulting matrix equations are treated independently.

At this stage the domain is discretized into small regions called finite elements. A simple variation of the unknown is taken over each element separately, and the effect of all the elements added together fulfills the relaxed stationary constraint. The choice of weighting function and approximate solution of a variable over an element will effect the accuracy of the solution, as will the discretization of the domain.

In a similar fashion the weighting technique can be applied to

approximate the natural or implied boundary equations. In this case the equation is weighted and integrated over the boundary side. In the (F.E.M) the sum of both the boundary term and the domain term is assumed to be stationary. This formulation is applied over each element and each contribution is added to the global system which describes the entire domain. At this point the essential boundary conditions are imposed directly to the system of equations. Finally the solution of a set of non-homogeneous equations is produced by standard matrix inversion techniques.

As this work is primarily concerned with the application of the (F.E.M), and so this brief explanation is sufficient. For further mathematical justification of this method see Connors and Brebbia [22] and Zienkiewicz [23].

The ease with which the (F.E.M) can model problems of an arbitrary shape coupled with its ability to mesh a domain with local concentration of nodes makes it attractive for all kinds of engineering problems. In the field of fluid mechanics this is particularly important where large gradients of vorticity and stream function occur close to the no-slip boundary, e.g. the wake behind a cylinder.

A further advantage when compared to the (F.D.T) is its ability to approximate the natural boundary condition as part of the formulation; some of these constraints have proved to be as difficult to describe directly as the governing equations.

Below, integral formulations are developed for the two governing equations. Here the particular weighted residual technique applied is the Galerkin method, where the weighting function is chosen to be of the same form as the local variation of the unknown, i.e. a

polynomial of the same order.

3.2 The Equivalent Formulations

The weighting technique is applied to the set of equations governing the two dimensional flow of an incompressible Newtonian fluid; see equation (2.3.3) and (2.3.4).

The (W.R.T) is the most general method by which an integral formulation is derived from a differential equation and its associated boundary conditions. When considering the equilibrium equation in elasticity it is possible to relate the weighted residual formulation to the principle of virtual work and the principle of minimum potential energy. Owing to the character of the momentum equation for a fluid continuum, whether in its present or original form, it is not possible to derive a variational statement from it. Many attempts have been made to develop restricted or pseudo-variational statements; see Tuann [10] and Finlayson [24]. In this work the generalized (W.R.T) is used to provide an equivalent integral formulation. Failing to obtain a variational form of the equations results in an unsymmetric matrix equation due to the presence of the convective terms. For a more extensive discussion of this problem see Zienkiewicz [23].

The vorticity transport equation is of the form;

$$\frac{D\omega}{Dt} = \frac{d\omega}{dt} + \frac{\partial\psi}{\partial x_2}\frac{\partial\omega}{\partial x_1} - \frac{\partial\psi}{\partial x_1}\frac{\partial\omega}{\partial x_2} = \nu\left(\frac{\partial^2\omega}{\partial x_1^2} + \frac{\partial^2\omega}{\partial x_2^2}\right) \text{ in A} \qquad (3.2.1)$$

with the relationship between stream function and vorticity being:

$$\frac{\partial^2\psi}{\partial x_1^2} + \frac{\partial^2\psi}{\partial x_2^2} = -\omega \text{ in } A \qquad (3.2.2)$$

As these two equations govern the fluid flow, two equivalent formulations are required. As mentioned in the previous section, the sum of the governing formulation and its natural boundary formulation is assumed to be stationary.

The boundary of the flow domain is split into two sections for each variable; see section 2.4. The boundary conditions for the two variables may be expressed:

Stream function:

$$\begin{aligned} \psi &= \overline{\psi} \quad \text{on } S_{\psi_1} \\ \frac{\partial\psi}{\partial n} &= \overline{g}_\psi \quad \text{on } S_{\psi_2} \end{aligned} \qquad (3.2.3a)$$

Vorticity:

$$\begin{aligned} \omega &= \overline{\omega} \quad \text{on } S_{\omega_1} \\ \frac{\partial\omega}{\partial n} &= \overline{g}_\omega \quad \text{on } S_{\omega_2} \end{aligned} \qquad (3.2.3b)$$

Where S_{ψ_1} and S_{ω_1} are the essential boundary sides for stream function and vorticity, and S_{ψ_2} and S_{ω_2} are the natural boundary sides.

The weighted formulations of both equations are:

$$\int_A \left[\frac{d\omega}{dt} + \frac{\partial\psi}{\partial x_2}\frac{\partial\omega}{\partial x_1} - \frac{\partial\psi}{\partial x_1}\frac{\partial\omega}{\partial x_2} - \nu\left(\frac{\partial^2\omega}{\partial x_1^2} + \frac{\partial^2\omega}{\partial x_2^2}\right)\right] \delta\omega \, dA -$$

$$\nu \int_{S_{\omega_2}} (\overline{g}_\omega - \frac{\partial\omega}{\partial n}) \, \delta\omega \, ds = 0 \qquad (3.2.4a)$$

$$- \int_A \left(\frac{\partial^2\psi}{\partial x_1^2} + \frac{\partial^2\psi}{\partial x_2^2} + \omega\right) \delta\psi \, dA +$$

$$\int_{S_{\psi_2}} \left(\frac{\partial\psi}{\partial n} - \overline{g}_\psi\right) \delta\psi \, ds = 0 \qquad (3.2.4b)$$

Where $\delta\omega$ and $\delta\psi$ are respectively the weighting functions for the momentum equation and the stream function vorticity relationship.

Integrating both formulations by parts will produce a weak form of the equations:

$$\int_A \left(\frac{d\omega}{dt} + \frac{\partial\psi}{\partial x_2}\frac{\partial\omega}{\partial x_1} - \frac{\partial\psi}{\partial x_1}\frac{\partial\omega}{\partial x_2}\right) \delta\omega \, dA$$

$$+ \nu\int_A \left(\frac{\partial\omega}{\partial x_1}\frac{\partial\delta\omega}{\partial x_1} + \frac{\partial\omega}{\partial x_2}\frac{\partial\delta\omega}{\partial x_2}\right) dA = \nu\int_{S_{\omega_2}} \overline{g}_\omega \, \delta\omega \, dS \qquad (3.2.5a)$$

$$\int_{\Lambda} \left(\frac{\partial \psi}{\partial x_1} \frac{\partial \delta\psi}{\partial x_1} + \frac{\partial \psi}{\partial x_2} \frac{\partial \delta\psi}{\partial x_2} \right) d\Lambda - \int_{\Lambda} \omega \delta\psi \, d\Lambda$$

$$= \int_{S_{\psi_2}} \overline{g}_{\psi} \, \delta\psi \, dS \qquad (3.2.5b)$$

Above are the two formulations governing the flow of fluid in the domain, A, bounded by the natural boundaries S_{ω_2} and S_{ψ_2}.

An approximate solution of the variables is now introduced. If the domain is discretized into small but finite elements it is possible to assume a polynomial variation over each element.

$$u = \sum_{n=1}^{n=NE} \sum_{j=1}^{j=NNE} \phi_j^T \, u_j^n \qquad (3.2.6)$$

NNE - number of node per element

NE - number of elements

$( )^T$ - the transpose of the matrix

Where u is the variable and is expressed in terms of interpolation functions, ϕ_j^T, and nodal unknown values of u, $\underline{u}^n$, over each element. Here there are two variables, however; the interpolation functions over each element are taken to be the same for both.

$$\psi = \sum_{n=1}^{n=NE} \phi_j^T \, \psi_j^n$$

$$\omega = \sum_{n=1}^{n=NE} \phi_j^T \, \omega_j^n \qquad (3.2.7)$$

As stated in section 3.1, a successful application of the weighted residual technique occurs when the weighting functions are of the same form as the approximate solution chosen; this particular weighting technique is attributed to Galerkin, see Finlayson [25].

The weighting functions are taken to be of the same form as equation (3.2.7) above:

$$\delta\omega = \sum_{n=1}^{n=NE} \phi_j^T \, \delta\omega_j^n$$

$$\delta\psi = \sum_{n=1}^{n=NE} \phi_j^T \, \delta\psi_j^n \qquad (3.2.8)$$

Substituting the approximate solution for vorticity and stream function, equations (3.2.7), and the weighting functions, equations (3.2.8), into the respective formulations , equations (3.2.5), produces:

$$\sum_{n=1}^{n=NE} \left[\iint_a \left\{ (\phi_j \cdot \phi_j^T) \, \dot{\omega}_j^n + \left(\phi_j \frac{\partial \phi_j^T}{\partial x_2} \psi_j^n \frac{\partial \phi_j^T}{\partial x_1} - \phi_j \frac{\partial \phi_j^T}{\partial x_1} \psi_j^n \frac{\partial \phi_j^T}{\partial x_2} \right) \omega_j^n \right.\right.$$

$$\left.\left. + \nu \left(\frac{\partial \phi_j}{\partial x_1} \frac{\partial \phi_j^T}{\partial x_1} + \frac{\partial \phi_j}{\partial x_2} \frac{\partial \phi_j^T}{\partial x_2} \right) \omega_j^n \right\} da = \nu \int_{s_{\omega_2}} \phi_j \, \overline{g}_\omega^n \, ds \right] \qquad (3.2.9a)$$

$$\sum_{n=1}^{n=NE} \left[\int_a \left\{ \left(\frac{\partial \phi_j}{\partial x_1} \frac{\partial \phi_j^T}{\partial x_1} + \frac{\partial \phi_j}{\partial x_2} \frac{\partial \phi_j^T}{\partial x_2} \right) \psi_j^n - (\phi_j \cdot \phi_j^T)\ \omega_j^n \right\} da \right.$$

$$\left. = \int_{s_{\psi_2}} \phi_j\ \bar{g}_\psi^n\ ds \right] \qquad (3.2.9b)$$

a - element area

s_{ω_2} ; s_{ψ_2} - the natural boundaries of the element

the element matricies are defined as:

$$\underline{m} = \int_a (\phi_j \cdot \phi_j^T)\ da$$

$$\underline{a} = \int_a \left[\phi_j \left(\frac{\partial \phi_j^T}{\partial x_2} \psi_j^e \frac{\partial \phi_j^T}{\partial x_1} - \frac{\partial \phi_j^T}{\partial x_1} \psi_j^e \frac{\partial \phi_j^T}{\partial x_2} \right) \right] da$$

$$\underline{k} = \int_a \left(\frac{\partial \phi_j}{\partial x_1} \frac{\partial \phi_j^T}{\partial x_1} + \frac{\partial \phi_j}{\partial x_2} \frac{\partial \phi_j^T}{\partial x_2} \right) da \qquad (3.2.10)$$

$$\underline{b}_\omega = \int_{s_{\omega_2}} \phi_j\ \bar{g}_\omega^e\ ds$$

$$\underline{b}_\psi = \int_{s_{\psi_2}} \phi_j\ \bar{g}_\psi^e\ ds$$

$( )^e$ - the element array

see appendix B for the results of the element integration.

Both equations are now written in element matrix form:

$$\sum_{n=1}^{n=NE} \underline{m}\ \dot{\underline{\omega}}^n + \underline{a}\ (\underline{\psi}^n)\ \underline{\omega}^n + \nu \underline{k}\ \underline{\omega}^n = \nu \underline{b}_\omega \qquad (3.2.11a)$$

$$\sum_{n=1}^{n=NE} \underline{k}\,\underline{\psi}^{n} - \underline{m}\,\underline{\omega}^{n} = \underline{b}_{\psi} \qquad (3.2.11b)$$

$\dot{\omega}$ - time derivative of vorticity

Both equations apply to each element separately within the domain A. As the formulations refer to an integral over the entire domain, it is necessary to sum all the element effects together, producing global matrix equations:

$$\underline{M}\,\dot{\underline{\omega}} + \underline{A}(\underline{\psi})\,\underline{\omega} + \nu\underline{K}\,\underline{\omega} = \nu\underline{B}_{\omega} \qquad (3.2.12a)$$

$$\underline{K}\,\underline{\psi} = \underline{M}\,\underline{\omega} + \underline{B}_{\psi} \qquad (3.2.12b)$$

Where $\underline{\psi}$ and $\underline{\omega}$ are the nodal arrays containing discrete values of stream function and vorticity respectively. These are the set of finite element equations governing fluid flow in terms of nodal variables. In this work three noded linear triangular elements are adopted, refer to appendix B. By using a local homogeneous coordinate system over each triangle the element matricies are calculated in a general manner, see Connors and Brebbia [22]. The global matricies are then assembled; subsequently the essential boundary conditions are applied directly to this system. Finally a set of (NxN) non-homogeneous equations is solved in terms of N unknowns, i.e the nodal variable array, using standard matrix inversion techniques; see Brebbia and Ferrante [26].

In order to solve the above system of equations two additional

problems need to be overcome. In order to solve the non-linear momentum equation it is necessary to linearize the convective matrix, i.e $A(\underline{\psi})$ of equation (3.2.12a). This equation also contains a time derivative and so some form of time integration scheme is required.

The following section deals with these problems and sets out the equations in a form suitable for computation.

3.3 The Solution Technique

In the previous section the equations are replaced by their finite element equivalent formulations. In this section these are rearranged into a form that can be solved, overcoming the non-linearity and time dependence of the momentum equation.

Earlier work by Smith [14] produced a set of such schemes by which the non-linear time-dependent matrix equations, (3.2.12), can be solved. The most successful scheme applied was the semi-implicit fractional step. This has proved to be stable at high values of Re; when other schemes break down.

Any such solution scheme employs a time marching technique solving a quasi-linear equation until a solution is achieved. The non-linear convective matrix $A(\underline{\psi})$ being linearized by evaluating it in terms of the previous time step value of stream function. Eventually the discrepancy between both solutions becomes negligible as the problem is iterated.

When employing the time-dependent form of the momentum equation the correct solution to a particular flow problem may not necessarily be of a steady state nature. The Re may be high enough for unsteady

flow to occur, for example at Re>40 for a cylindrical obstruction the fluid flow becomes unsteady; see the experimental work of Coutanceau and Bouard [27].

In the unsteady range of flow the motion can be periodic and cyclically steady, e.g. the development of the vortex street in cyclindrical flow. Some confusion may result in recognising when the correct solution has been achieved in this type of flow.

For example, a time dependent (F.D) solution to flow past a cylinder was presented by Payne [28] at Re=40 and 100. This work was later extended by Ingham [29] covering a greater time interval. The result of continuing the integration procedure produced results closer to the steady solution for Re=40.

To integrate the solution numerically in time, i.e. to march through time, a linear variation of the variable is assumed over a small time step:

$$\frac{(\underline{\omega}_{t+\Delta t} - \underline{\omega}_t)}{\Delta t} = \frac{\Delta \omega}{\Delta t} = \dot{\underline{\omega}} \qquad (3.3.1)$$

Due to the time dependent term above it is necessary to initially define the values of one of the unknown variables before commencing the solution.

(i) Starting with the initial values of vorticity, $\underline{\omega}_t$.

Using the stream function vorticity relationship; the stream function at time t is obtained:

$$\underline{K}\ \underline{\psi} = \underline{M}\ \underline{\omega} + \underline{B}_{\psi}$$

By letting $\underline{B}_{\psi}=0$ since $\frac{\partial \psi}{\partial n}=0$ on S_{ψ_2}, the outflow boundary, this equation is reduced to:

$$\underline{K}\ \underline{\psi}_t = \underline{M}\ \underline{\omega}_t \qquad (3.3.2)$$

(ii) Differentiating equation (3.3.2) w.r.t. time:

$$\underline{K}\ \dot{\underline{\psi}} = \underline{M}\ \dot{\underline{\omega}}$$

and substituting it into the momentum equation, (3.2.12), to produce:

$$\underline{K}\ \dot{\underline{\psi}} + \underline{A}(\underline{\psi}_{t+\Delta t})\ \underline{\omega}_t + \nu\ \underline{K}\ \underline{\omega}_t = \nu\ \underline{B}\ \omega$$

Rearranging the equation in terms of the unknown $\underline{\Delta\psi}$. Letting $\underline{B}_{\omega}=0$ then solving for stream function.

$$\left[\frac{\underline{K}}{\Delta t} - \underline{A}(\underline{\omega}_t)\right]\ \underline{\Delta\psi} = -\left[\underline{A}(\underline{\psi}_t)\ \underline{\omega}_t + \nu\ \underline{K}\ \underline{\omega}_t\right] \qquad (3.3.3)$$

(iii) This step involves computing $\underline{\omega}_{t+\Delta t}$ using the momentum equation;

$$\underline{M}\ \frac{(\underline{\omega}_{t+\Delta t} - \underline{\omega}_t)}{\Delta t} + \underline{A}(\underline{\psi}_{t+\Delta t})\underline{\omega}_t + \nu\ \underline{K}\ \underline{\omega}_t = \nu\ \underline{B}_\omega$$

The value of $\underline{B}_\omega$ on the no-slip boundary is non-trivial, being a function of both vorticity and stream function, see section 3.4 below.

$$\underline{B}_\omega = \underline{F}_1\ \underline{\psi} + \underline{F}_2\ \underline{\omega}$$

The momentum equation is written with $\underline{\Delta\omega}$ taken as the unknown:

$$\underline{M}\ \Delta\ \underline{\omega} = -\Delta t\left[\underline{A}(\underline{\psi}_{t+\Delta t})\ \underline{\omega}_t + \nu\ \underline{K}\ \underline{\omega}_t\right.$$

$$\left. - \nu\ \underline{F}_1\ \underline{\psi}_{t+\Delta t} - \nu\ \underline{F}_2\ \underline{\omega}_t\right] \qquad (3.3.4)$$

(iv) The second time step value for vorticity, $\underline{\omega}_{t+2\Delta t}$, is computed using the momentum equation again:

$$\underline{M}\ \frac{(\underline{\omega}_{t+2\Delta t} - \underline{\omega}_{t+\Delta t})}{\Delta t} + \underline{A}(\underline{\psi}_{t+\Delta t})\ \underline{\omega}_{t+2\Delta t}$$

$$+ \nu\ \underline{K}\ \underline{\omega}_{t+2\Delta t} = \nu\ \underline{F}_1\ \underline{\psi}_{t+\Delta t} + \nu\ \underline{F}_2\ \underline{\omega}_{t+2\Delta t}$$

This equation is written with $\underline{\Delta\omega}$ as the unknown array.

$$\left[\frac{\underline{M}}{\Delta t} + \underline{A}(\underline{\psi}_{t+\Delta t}) + \nu\ \underline{K} - \nu\ \underline{F}_2\right]\ \underline{\Delta\omega} =$$

$$- \left[\underline{A}(\underline{\psi}_{t+\Delta t}) + \nu\ \underline{K} - \nu\ \underline{F}_2\right]\ \underline{\omega}_{t+\Delta t} + \nu\ \underline{F}_1\ \underline{\psi}_{t+\Delta t} \qquad (3.3.5)$$

(v) In the final step the stream function is updated, $\underline{\psi}_{t+2\Delta t}$:

$$\underline{K}\ \underline{\psi}_{t+2\Delta t} = \underline{M}\ \underline{\omega}_{t+2\Delta t} \qquad (3.3.6)$$

Steps (i) to (v) outline one cycle of the fractional step method. The scheme marches through time by iterating from (ii) to (v) until a solution is reached.

In steps (iii) to (iv) the vorticity is computed over a period of $2\Delta t$. Step (iii) may be considered a forward step about time $t+\Delta t$. Conversely step (iv) is a backward step about time $t+\Delta t$. The combination of the two ensures increased stability of the solution. The overall centering of the two integration steps about time $t+\Delta t$ is clearly illustrated when equations (3.3.4) and (3.3.5) are summed.

$$\begin{aligned}\underline{M}\ \frac{(\underline{\omega}_{t+2\Delta t} - \underline{\omega}_t)}{2\Delta t} &= -\underline{A}(\underline{\psi}_{t+\Delta t})\ \frac{(\underline{\omega}_{t+2\Delta t} + \underline{\omega}_t)}{2} \\ -\nu\underline{K}\ &\frac{(\underline{\omega}_{t+2\Delta t} + \underline{\omega}_t)}{2} + \nu\ \underline{F}_1(\underline{\psi}_{t+\Delta t}) \\ + \nu\underline{F}_2\ &\frac{(\underline{\omega}_{t+2\Delta t} + \underline{\omega}_t)}{2}\end{aligned} \qquad (3.3.7)$$

An initial estimate of the vorticity array has to be made to evaluate the convective matrix in equation (3.3.3). The choice of the starting vorticity will effect the number of iterations required to reach a solution. The simple choice is to assume the vorticity to be zero throughout the region, i.e. orthogonal flow. However the vorticity solution of the same problem at a lower Re may be used in order to speed up the solution at high values of Re.

The choice of time step is critical to ensure convergence to a

correct solution. Failure to use a correct step causes either convergence to an incorrect solution or complete divergence of the solution. The former problem arises when at high Re the time step to ensure stability is larger then that required to achieve a correct solution. It is important to distinguish between the two.

An empirical formula to define a maximum time step to ensure stability for particular flow conditions and mesh size has been obtained; see section (3.5) below.

In this section the five matrix equations, (3.3.2) to (3.3.6), which are used to solve the flow iteratively are presented. When solving for vorticity the no-slip boundary condition is non-trivial and is a function of both stream function and vorticity. This boundary condition is expressed in a suitable (F.E) form outlined in the preceeding section.

3.4 The No-Slip Vorticity Boundary Condition

The problems associated with describing a vorticity constraint on this boundary have caused many researchers to rely on the primitive approach when implementing the (F.E.M); see Taylor and Hood [6] and Hutton [30]. The value of vorticity or its gradient along a normal to the no-slip boundary is unknown at the start of the solution. Instead it is necessary to develop an expression based on the limiting physical effects at the wall.

The development of such a constraint has been given sound treatment by (F.D) workers who have a preference for the stream function vorticity approach; see Gosman et al [4].

As the gradients in the direction tangential to the wall are much smaller then those in the normal direction, they are neglected. Resulting from this the momentum equation is reduced to its one-dimensional form, the resulting solution of which is linear:

$$\omega = A\,n + B \qquad (3.4.1)$$

n - normal to no-slip boundary

Here again constant viscosity and density of the fluid is assumed. The relationship between stream function and vorticity is also reduced to its one- dimensional form.

$$\frac{\partial^2 \psi}{\partial n^2} = -\omega \qquad (3.4.2)$$

Substituting this into equation (3.4.1) and integrating twice w.r.t. n produces:

$$\psi = -A\frac{n^3}{6} - B\frac{n^2}{2} + C_1 n + C_2 \qquad (3.4.3)$$

The constants of the equation are evaluated from boundary values of stream function and vorticity on the wall, at a point s:

$$A = \left(\frac{\partial \omega}{\partial n}\right)_s$$

$$B = \omega_s$$

$$C_1 = \left(\frac{\partial \psi}{\partial n}\right)_s$$

$$C_2 = \psi_s$$

Rewriting equation (3.4.3)

$$\psi = -\left(\frac{\partial\omega}{\partial n}\right)_s \frac{n^3}{6} - \omega_s \frac{n^2}{2} + \left(\frac{\partial\psi}{\partial n}\right)_s n + \psi_s \qquad (3.4.4)$$

Considering the stream function at a point x normal to the wall at a distance ℓ from s, produces:

$$\psi_x - \psi_s = -\left(\frac{\partial\omega}{\partial n}\right)_s \frac{\ell^3}{6} - \omega_s \frac{\ell^2}{2} + \left(\frac{\partial\psi}{\partial n}\right)_s \ell \qquad (3.4.5)$$

see figure 3.1

As the variation of vorticity normal to the wall is linear it is consistent to define its derivative numerically as:

$$\left(\frac{\partial\omega}{\partial n}\right)_s = \frac{\omega_x - \omega_s}{\ell}$$

Substituting this into equation (3.4.5) and rearranging it an expression for the vorticity at the wall is obtained; ω_s :

$$\omega_s = -\frac{3}{\ell^2}(\psi_x - \psi_s) - \frac{\omega_x}{2} + \frac{3}{\ell}\left(\frac{\partial\psi}{\partial n}\right)_s \qquad (3.4.6)$$

Equation (3.4.6) represents the vorticity at the wall in terms of calculable values. The value of $(\frac{\partial\psi}{\partial n})_s$ is usually zero, it represents the speed at which the no-slip wall is moving. In the classical problem of flow in a square cavity the top wall or 'moving lid' has a fixed velocity, and the equation becomes

$$\omega_s = -\frac{3}{\ell^2}(\psi_x - \psi_s) - \frac{\omega_x}{2} + \frac{3v_{mL}}{\ell} \qquad (3.4.7)$$

v_{mL} - is the velocity of the wall

Using the above equation it is possible to express the no-slip boundary matrix as used in section (3.3), in terms of discrete nodal values of stream function and vorticity. The boundary matrix may be expressed in terms of no-slip element side components:

$$\underline{B}_\omega = \sum_{i=1}^{NS} \underline{b}_\omega^i$$

NS - total number of no-slip boundary elements

From equation (3.2.10) each element component may be expressed in terms of nodal values of the unknowns and the interpolation functions.

$$\underline{b}_\omega^e = \int_{s_{NSB}} \phi_j \underline{g}_\omega^e \, ds = \int_{s_{NSB}} \phi_j \frac{\partial \omega_j^e}{\partial n} \, ds = \left[\int_{s_{NSB}} \phi_j \frac{\partial \phi_j^T}{\partial n} \, ds\right] \omega_j^e$$

ω_j^e - local no-slip boundary vorticity values expressed using equation (3.4.7)

s_{NSB} - is the no-slip boundary wall

Integrating the expression above along an element side by using a linear interpolation scheme produces;

$$\underline{b}_{\omega}^{e} = \frac{m^2}{4A}\,\omega^{e}\begin{bmatrix}1\\1\end{bmatrix}$$

ω^{e} - the boundary side vorticity value

m - the length of a boundary element side

See appendix B for the boundary side integration. The value of the vorticity on the no-slip wall may be obtained using the limiting equation obtained above:

$$\underline{b}_{\omega}^{e} = f_1\,\psi_j\begin{bmatrix}1\\1\end{bmatrix} + f_2\,\omega_j\begin{bmatrix}1\\1\end{bmatrix}$$

where:

$$\underline{f}_1\,\psi_j^{e} = \frac{3m^2}{4A\ell^2}\,(\psi_x - \psi_s)$$

$$\underline{f}_2\,\omega_j^{e} = \frac{m^2}{8A}\,\omega_x \qquad (3.4.8)$$

for the normal case where v_{mL} is equal to zero. Above is the expression used in section (3.3) steps (iii) and (iv).

In most cases the no-slip walls are stationary and so v_{mL} may be ignored. In the case of the cavity problem this extra constant term is placed into the load vector.

3.5 The Stability Criterion

An empirical formula is required to define the maximum time step to ensure a stable solution for the integration scheme based on properties of the mesh and the fluid flow. Such a formula was derived from work on cylinder flow problems.

In most integration schemes the stability criterion changes as the convective terms become significant and its stability is reduced. In the fractional step technique, owing to its inherent stability, one criterion suffices:

$$DT \leqslant \frac{0.7}{\nu\left[\frac{2}{\ell^2} + \frac{1}{m^2}\right]} \qquad (3.5.1)$$

ν - viscosity

ℓ - dimension of an element normal to the flow direction

m - dimension of an element parallel to the flow

DT - time step or interval in the integration technique

For this scheme the time step limit increases with Re.

It must be emphasised that this criterion ensures only a stable solution and not a correct one. At high Re the time step may satisfy stability but not produce a correct solution.

It must also be chosen on the basis of the distance travelled during the time step. If the distance travelled within the step is greater then an element side length, convergence to a correct solution is unlikely. Consequently this distance must be smaller then the mesh size to ensure a correct solution.

At some Re there is a cut-off time step DT_{max} describing the maximum allowable time step to ensure a correct solution for a particular mesh configuration. This may be expressed as:

$$DT_{max} < \frac{L}{u_m} \qquad (3.5.2)$$

L - minimum element dimension

u_m - mean fluid velocity

The stability criterion, equation (3.5.1), is obtained empirically from the solution of flow past a cylinder: it does not necessarily hold for other flow problems; however, it seems reasonable to use it as a guide.

In this chapter the set of equations governing fluid flow in a domain is rewritten in its finite element equivalent form.

To solve these two matrix equations the problem of time dependence and the non-linearity of the momentum equation has to be overcome. It is necessary to choose a time marching sequence which enables the solution of both variables iteratively.

The application of a vorticity condition on the no-slip boundary has also been dealt with. It is reasonable to assume that the stream function and vorticity variation parallel to the wall are negligible compared to normal variations. The momentum equation is expressed in a one dimensional form; from this an expression is obtained for wall vorticity in terms of calculable values. This expression is finally introduced into the no-slip condition.

Having presented a (F.E.M) solution procedure for the flow of fluid it is necessary to apply this technique to some practical problems. Previous work concentrated on the problem of unsteady flow past a cylinder. Here the solution of a greater variety of problems is possible, due to the incorporation of a general mesh generation

program.

The following chapter discusses in detail its inclusion in the (N.S) solution program.

CHAPTER FOUR

THE AUTOMATIC MESH GENERATOR

4. The Automatic Mesh Generator

4.1 Introduction

The solution technique used to solve the (N.S) equations by the (F.E.M) has been presented in the previous chapter.

In order to test the success of the technique a variety of flow conditions needs to be considered. The ease with which the (F.E.M) lends itself to problems of arbitrary shape, coupled with its ability to deal with large localised variable gradients, makes it suitable for fluid flow analysis. However, the problems involved in creating the large amount of data which is required to discretize such a flow region can be a major drawback. A great number of nodal points is needed to describe a region for flow of a practical nature due to the large variable gradients adjacent to the no-slip wall. Furthermore a variety of mesh patterns is often needed before a suitable one can be found to represent adequately a particular flow case. Obviously this requires the solution of some preliminary trail meshes in order to obtain some knowledge of the flow behaviour.

The introduction of an automatic mesh generator in front of the solver would reduce the man hours required to produce suitable problem data, consequently making it possible to try a variety of mesh patterns when modelling a particular problem. Such a mesh generator would also permit the modelling of a range of flow problems with much less effort. Work by Nelson [15] in 1976 resulted in a mesh generation program, this is adapted here to the particular needs of the fluid flow problem. The basis of the mesh algorithm is a fortran-extended language designed to discretize a two-dimensional domain with the minimum of information.

Here this mesh generation program is adapted to be interfaced with the solution program. It sits on top of the solver and its overall size in the program may be eliminated by a straight-forward overlay procedure.

The ease with which this fortran-extended language can be used to discretize a region enables a variety of meshes to be considered. Furthermore, when testing the success of the solution technique by increasing the mesh refinement of a flow problem the meshing program will reduce the effort considerably, enabling a thorough numerical study to be made; see chapter five.

In this chapter a brief description of the mesh program is presented. Subsequently the extensive work required in interfacing the generator and the fluid flow program is explained showing a special treatment of the no-slip and free-slip boundaries. Finally the need to produce highly regularised meshes is discussed and it is then shown how this is carried out by special data description.

4.2 The High Level Language

In the mesh program the use of a high-level or fortran-extended language to provide information to the program is exploited. A set of simple commands has been developed to represent a complex string of operations used in producing a (F.E) mesh.

The running of the mesh generator and the subsequent running of the solution program are carried out through these high level commands. For an outline of the relevant commands refer to Nelson [31].

4.3 Supervisory Calls

Once the mesh has been generated it is necessary to transfer the problem data from the mesh program to the solver. This occurs by means of a fortran extended command execute. When this occurs a subroutine 'USRPRG' is called which now replaces the main (F.E) program. This is the starting routine of the (F.E) solver and it is here that the interface between the two programs is made.

It is first necessary to transfer the problem data into the solution program and this is carried out by a series of supervisory calls., again refer [31].

The program terminates when the subroutine FPSTOP(n) is called if n is zero it stops in the normal way. If n is non-zero this abort number is printed out, thus indicating why and where the program has stopped. A set of abort numbers has been created related to the interface section of the program , see appendix C for the current list of these numbers. With the use of the supervisory commands the problem data can be transferred to the solution program. Subsequently the program runs in the normal way.

4.4 The Interface between Mesh Program and the Solution Program

In order to combine the mesh program and the (F.E) program an interface is developed to suit the particular needs of the fluid flow problem. In this section the interface development is explained.

So far this mesh generator has been demonstrated in successfully discretizing two dimensional domains of many different shapes, without any concern about the quality of the mesh and the

subsequent results produced from them. The purpose of this research is to model real fluid flow problems, consequently this program has to be geared to generate suitable mesh discretizations. The solution program is dealing with two separate unknowns, i.e. stream function and vorticity, in conjunction the no-slip boundary condition is applied in a non-standard manner. As a consequence the variety of boundary types is greater than in most cases. In order to handle the transfer of these boundary conditions successfully a suitable interface between the two programs is created.

The input subroutine which reads in the data directly is replaced by a series of supervisory calls to transfer data from the mesh generator instead.

The basic problem parameters, nodal coordinates and element connectivity are obtained directly by implementing the relevant supervisory calls. The problem of defining the boundary conditions is not so simple.

(i) To Transfer the Boundary Condition Data

The boundary conditions as described in section (2.3) are applied.

To recap, these are: the natural outflow condition; where the stream function and vorticity gradients are set to zero, this is applied in the matrix formulation by default. The no-slip boundary conditions where stream function is prescribed and vorticity is defined by a limiting equation, and finally the free-slip boundary where both stream function and vorticity are prescribed. In the interface section it is necessary to distinguish between the no-slip and the free-slip

boundary nodes.

The no-slip wall can be either moving or stationary, see section (3.4), and this velocity needs to be transferred. Normally the no-slip wall is stationary: however, in the case of a closed cavity for example the top wall is moving.

The boundary information needed for the solution program consists of the node number, the boundary type, the prescribed stream function value, the no-slip wall velocity and the prescribed vorticity. In most cases the prescribed vorticity is zero, but in the case of developed channel flow it is not; where the inlet velocity profile is of a parabolic form.

An interfacing subroutine is developed to assemble the boundary nodes in an adjacent order about the boundary with the free-slip and no-slip walls separated by dummy nodes.

The mesh generation scheme has been designed to deal with problems of many boundary configurations, enabling it to model a variety of flow problems.

(a) The first is the enclosed problem with a complete no-slip boundary; see figure 4.1(a). This fully enclosed configuration may be useful in solving the flow within a square cavity induced by a moving wall.

(b) The second consists of two boundaries of a no-slip and a free-slip type; see figure 4.1(b), with the outlet defined by default. Note that the inlet has the same variable configuration as the free-slip boundary. This boundary distribution can be applied to the solution of flow past a plate, for example.

(c) the third problem contains two no-slip boundaries separated by a free-slip boundary, i.e. the inlet, see figure 4.1(c). This boundary type maybe used to model flow within a channel, e.g. a channel containing a downstream step.

(d) This case is similar to (b) with two boundary types. However; here there is an obstruction of a no-slip boundary type surrounded by three free-slip boundaries describing the inflow and two side boundaries with an outflow boundary downstream; see figure 4.1(d).

This configuration is useful when modelling the flow past any bluff body,e.g. a circular cyclinder in parallel flow.

(e) This is an extension of type (d) where a set of obstructions of no-slip boundary types are surrounded by three free-slip boundaries as in (d), see figure 4.1(e). This is useful in modelling the interaction between a set of obstructions in a flow regime, e.g. two or more cylinders in a parallel flow field.

In the forthcoming chapters some of these boundary configurations are used to solve some practical flow problems.

With this list of problem configurations the program can model a wide variety of flow conditions. It must be remembered that any extension to this collection may be made by a simple addition to the particular interfacing routine.

(ii) To Check the Number of Nodes on the No-Slip Boundary

The limiting vorticity boundary condition is applied in such a manner that any element can have a maximum of two nodes on the no-slip boundary, i.e. a boundary element can have a maximum of one boundary

side.

The mesh generation program can produce elements containing three wall nodes. especially at a corner of a region, see figure 4.2(a), as it is not designed to make such a distinction.

An interfacing routine is first employed to locate such elements and subsequently to change the element configuration to ensure that this does not occur; see figure 4.2(b).

(iii) The Use of Disc Files to Store Mesh Data

When generating a large mesh the computer time taken becomes significant. In order to reduce the overall run time it is necessary to set up a disk file of the mesh data and for subsequent running of the problem this data is read directly into the solver. As these flow problems are highly non-linear several program runs may be needed to achieve a reasonable solution, this feature can reduce the C.P.U time considerably.

When a mesh is initially generated and found to be suitable for numerical analysis the nodal coordinates, element connectivity and boundary arrays are written to a data set.

(iv) The Optimization of the Node Numbering

The mesh program provides a mesh that has been optimized; however, preliminary work has shown that an improvement can be made to this optimization scheme.

With increasing refinement of the mesh discretization the need to achieve a more efficient node numbering scheme becomes apparent. This is more acute here since the system matricies are non-symmetric

and both their upper and lower diagonal parts have to be stored, thus doubling the amount of space normally required for a symmetric problem. A renumbering subroutine is included at the interface stage. It assumes the y - axis to be the shortest and thus numbers sequentially up this axis along a constant x line, beginning at the lowest x and y nodal point, see figure 4.3.

The assumption that the y - axis is the shortest is reasonable for all the problems considered here since the mainstream velocity is usually taken to be in the longitudinal x direction.

(v) The Problem Data Graphics Package

The set of interface routines described above is designed to produce the mesh data from the mesh generation program to suit the particular needs of the solution program.

The solution program requires a set of arrays which stores both boundary nodes and elements in a particular order about each boundary. To ensure this is occuring correctly each time a new mesh is produced, these need to be checked.

A graphics program has been developed which plots the complete mesh and these relevant nodal and element arrays. In this way a quick and safe visual check of the problem data can be made, before the mesh is chosen to carry out numerical analysis.

With the addition of these features at the interface stage a suitable optimized mesh is generated with the minimum of data definition and CPU time.

4.5 A Preprocessor for Internal Node Generation

In non-linear flow problems the quality of the region discretization is critical to the success of the solution obtained. This can also be said for structural problems: however, it is more pronounced in fluid mechanics where the non-linearities of flow can cause great problems. If the distribution of nodes within the region is poor or the element connectivity is irregular, i.e. many elements attached to one node, the results appear to be unstable and inaccurate, as the element discretization inadequately describes the flow problem.

It is found that the automatic internal node generator used in the mesh program, does not produce an adequate distribution of internal nodes. Instead it is necessary to specify the internal nodes directly. Even when defining the internal nodes in this manner with a regular spacing between them the element pattern is irregular, although they are of a constant size.

Figure 4.4 illustrates the discretization of an 11x11 square mesh; where the internal nodes have been defined as above. The mesh discretization displays this irregular element distribution mentioned.

In order to improve the element distribution a full understanding of the meshing algorithm is needed.

It first considers two nodes as the current base line. It then scans all the remaining nodes and the most suitable one is taken to create the next element. The most suitable node is the one producing the smallest circle with these two base nodes, see figure 4.5(a).

In the special case where the nodes are regularly spaced there are obviously two of equal suitability: then the meshing routine

chooses the first one it reaches, which is not necessarily the correct one to ensure a regular element distribution. To ensure that the correct node is chosen the position of each internal node may be adjusted slightly,; see figure 4.5(b).

A preprocessor is developed to produce the adjusted nodal positions which will ensure that a regular mesh is created. Figure 4.6(a) shows how the nodes are adjusted to generate this regular symmetric mesh for a square domain. Figure 4.6(b) shows an 9x9 square symmetric mesh produced in this manner.

Once the mesh is computed, a routine is inserted at the interface stage of the program to readjust the nodes to their correct positions.

Similar preprocessor routines are developed to produce a suitable displacement of internal nodes for other flow configurations.

In this chapter the mesh generating program has been introduced to reduce the effort required in producing problem data. This user-orientated scheme is designed to be interfaced with the fluid flow program. Since a large part of this work has involved the development of a successful interface between the two programs it has been necessary to devote a complete chapter to its description.

A series of subroutines is produced to ensure the smooth transfer of data from the generator to the solver. In conjunction with this a suite of preprocessor programs is developed to produce the correct nodal data to ensure regular mesh discretization. Having adopted this mesh program the production of suitable and compact problem data is now possible. A variety of flow problems can now be

modelled with much reduced effort. In chapter five this is clearly demonstrated when the complete system is used to model some laminar flow examples.

In section 4.4 the solution system is shown to be capable of dealing with a wide variety of flow conditions. Obviously it is beyond the scope of this work to try all of them: however, some problems are attempted for which existing work is available.

CHAPTER FIVE

A STUDY OF LAMINAR FLUID FLOW

5.A Study of Laminar Flow

5.1 Introduction

The mesh generation system has been interfaced with the (F.E) flow program. It is now possible to solve various flow problems without the need for tedious manual data processing.

In this chapter some flow examples are modelled and extensive comparison is made with earlier numerical and experimental work, if available.

There are three main aims of this chapter:

(i) To evaluate and demonstrate the effectivness of the mesh generating scheme,

(ii) To assess the value of the solution technique, and

(iii) To gain further enlightenment about various flow conditions.

5.2 Square cavity flow

5.2.1 Introduction

In this section recirculating flow within a square cavity induced by the motion of a top 'moving lid' is solved for various flow conditions. The solution of this example can shed light on more complicated separated flows, for example the wake behind a cylinder.

For this reason extensive numerical work has been carried out on this problem. Moreover, owing to its simple geometry, (F.E) and (F.D) discretization is straightforward. In this problem increasing

the mesh refinement requires little additional effort, and so a full test of the solution technique can be made.

As the flow problem is of a closed form and all the boundaries are of an explicit nature a solution is achieved with relative ease. Furthermore, fluid flow within a confined region remains steady throughout a wider range of Re than that of open flow.

The walls of the cavity are all of a no-slip type, with the top wall moving horizontally as a 'lid', see section 3.4. Figure 5.1 illustrates the problem and the boundary conditions applied.

A preprocessor is used to compute the internal nodes suitable for regular square mesh discretization: see section 4.5. Using this process a series of meshes is produced with increasing refinement, i.e. 11x11, 17x17, 21x21 and 31x31. By increasing the mesh refinement a better model of the flow is expected.

A study of the fluid flow within the cavity is obtained at Re of 10^{-4}, 100 and 400. Initially the vorticity is set to zero for the starting flow of $Re=10^{-4}$. For subsequent increases of Re the initial vorticity is taken from the previous solution.

The Reynolds Number is defined as, $Re=dU/\nu$. Contour plots of the solution variables of stream function and vorticity are produced using a graphic postprocessor. The variable contour plots are normalized; where $\psi'=\psi/Ud$ and $\omega'=-\omega d/U$,

Where:

U - is the mainstream velocity

d - is the characteristic length, i.e. the dimension of the cavity

Extensive (F.E) and (F.D) work is available for comparison. Here the (F.D) results of Burggraf [11] are used. He presents a (F.D) solution adopting a stream function vorticity approach supported by an analytical solution at low Re. In addition a (F.E) work by Tuann and Olson [32] is quoted. In this case a solution is obtained for the stream function based on the momentum equation written in terms of stream function alone. As this produces a fourth order equation a unique quintic triangular discretization of the domain has been introduced.

As in the current study, Tuann and Olson produced a series of results using four mesh discretizations. The results taken for comparison are obtained using the most refined mesh, i.e. the 8x8 quintic mesh.

The work by Burggraf is used to compare the two different numerical techniques. Conversely the work of Tuann provides a comparison between two different approaches of the (F.E) technique. Both ensure a rigorous test of the current solution scheme.

5.2.2 Results

Here contour plots of stream function and vorticity are presented, see figures 5.2 - 5.7. Each figure contains the plots of one variable at a particular Re. The figures (a) - (d) show results of the current work with increased mesh refinement, and (e) and (f) show the earlier (F.D) work of Burggraf and the (F.E) work of Tuann and Olson respectively.

(i) $Re=10^{-4}$

Solutions for the square cavity problem at a Re of 10-- are

obtained for the four meshes mentioned above.

This is a slow creeping flow condition and has a limiting solution similar to the biharmonic equation of plate bending. As this limiting condition is reached the inertial effects become negligible and the solution becomes symmetric.

Figures 5.2 and 5.3 show plots of stream function and vorticity respectively. Both sets of results display the expected symmetry comparing well with previous work. The accuracy of the flow solution is shown to improve with increased mesh refinement.

In the stream function plots the flow structure is well defined, consisting of a main central vortex core and two secondary vortices at both lower corners.

All current results show the inner core stream function value to be too high, as the inner streamline of level 0.1 is a point in the centre of the vortex for both the earlier solutions. This streamline however appears to converge to the centre of the vortex as the mesh is refined. The discrepancy is also due to the limiting vorticity solution from which the stream function is derived.

The secondary vortices at both lower corners are too large and produce some fluctuation of the streamline, see figure 5.2(d).

The vorticity results all display this similar converging distribution, with these two secondary vortices occuring at the lower corners. These results converge with mesh refinement to compare very well with Burggraf; see figures 5.3(d) and 5.3(e). However, a comparison with Tuann is not so good; see figure 5.3(f).

The secondary vortices of the most refined solution, see figure 5.3(d), appear as a combination of three smaller vortices about each corner. This is due to the limited resolution of the elements in this region close to the corner. In the local region about a corner the variation of the unknowns is large, in order to describe this accurately a large amount of local mesh refinement is needed when using linear elements. It is these vortices which cause the fluctuations in the streamline plots as shown in figure 5.2(d).

In the (F.E) technique of Tuann the vorticity is obtained from the approximate solution of stream function. Conversely here the stream function is retrieved from a solution of vorticity. The leading variables in both (F.E) schemes, i.e. the stream function of Tuann and the vorticity here, display good comparison with the (F.D) work, whereas the retrieved results display some error.

(ii) Re=100

Using the vorticity results from (i) as the initial values a solution at Re=100 is computed.

Figures 5.4 and 5.5 present the stream function and vorticity results obtained at this Re.

Increasing the Re the inertial effects are now large enough to become significant. The result has been to shift the main vortex centre to the left, causing the flow to lose symmerty. Again the overall structure is the same as above, consisting of a main central core and two secondary vortices at both lower corners. Here the left-hand vortex has enlarged compared to the right-hand one : see figure 5.4(d).

As in (i) the inner part of the main vortex core has a larger value of stream function then that of the previous solutions; as illustrated in figures 5.4(d),(e) and (f). The secondary vortices are similarly too large, displaying the same streamline fluctuations.

Again the vorticity results compare most accurately with Burggraf . The secondary vortices are again defined as a combination of three small vortices about each corner; see figure 5.5(d).

As before both sets of results presented display improved accuracy with increased mesh refinement. Due to the increased inertial effects this improvement is more pronounced as the non-linearities of the problem increase; compare figure 5.5(a) with 5.5(d).

(iii) Re=400

Using the vorticity results of (ii) as the initial flow conditions the solution at a Re=400 is obtained. With increasing inertial effects the non-linear terms become larger and the flow configuration is more unstable.

Figures 5.6 and 5.7 display the stream function and vorticity plots along with the comparative work of Burggraff and Tuann.

The shape of the streamline plots is consistent with the earlier work. Again the inner core region displays values of stream function that are too high. Similarly the work of Tuann shows the same trend, with the main vortex stream function value large compared to that of Burggraf; see figures 5.6(e) and 5.6(f)..

The outer streamline of the main vortex displays a point of inflection at the top right-hand corner; this is consistent with both

earlier (F.D) and (F.E) results.

Comparing these results with the solution at Re=100; the main vortex has moved slightly right, back towards the centre of the cavity and downwards. The left-hand secondary vortex has grown vertically restricting the size of the main vortex, thus pushing it back towards the centre. The right-hand vortex has now extended into the centre of the cavity.

These vorticity plots, see figure 5.7, illustrate how unstable the flow regime has become due to the increased inertial effects. Only the finest mesh can now achieve a smooth distribution of vorticity, see figure 5.7(d).

This result compares reasonably well with the work of Burggraf: however, the central region of the main vortex is different, figure 5.7(e). Greater similarity is now shown with the work of Tuann, see figure 5.7(f). Along the outer boundary of the main core the three meshes display good agreement. Within the main core the (F.D) solution differs from both (F.E) solutions, displaying lower values of vorticity.

Similarly the vorticity contour level of -1.0 on the left-hand side of the cavity attaches itself to the bottom wall in both (F.E) solutions. Conversely in the (F.D) solution this contour level is split into two separate regions indicating that the vortex movement is more developed in the (F.E) results.

At a Re=400 the inertial effects have become so large that they produce great non-linearities in the flow . They manifest themselves as an unstable vorticity distribution within the flow region; see

figures 5.7(a) - (b). In the past mixed success has been met for results at Re greater then 400. It seems reasonable to assume that with the current methods available the solution limit has been reached at about this Re. Any attempt to increase the Re beyond this point has proved to be speculative.

When the limits of the solution are reached both (F.E) solutions display similar behaviour. They both differ from the (F.D) solution, which indicates a consistent distinction between the two techniques.

5.2.3 Conclusion

Four mesh discretizations are used to model flow within a square cavity at Re of 10^{-4}, 100 and 400. Contour plots of stream function and vorticity illustrate how the solution improves with increased mesh discretization.

A full comparison with earlier (F.E) and (F.D) results has been carried out. It is found that the vorticity solution is more accurate then that of stream function when compared to the (F.D) solution. The reverse is the case for the (F.E) solution of Tuann and Olson, where the stream function results compare better then those of vorticity. It is concluded that in general the results for the leading variables are good, whereas the retrieved results are subject to some inaccuracy.

The two secondary vortices of the finest mesh are described as a combination of three smaller vortices. This is due to the limited resolution of the linear elements in a region of large vorticity gradient and results in a fluctuating streamline at both lower corners.

At a Re=400 the limits of the solution technique are approached for the cavity problem. Only the finest mesh discretization provides a smooth vorticity distribution. At this Re both (F.E) solutions are similar, with the (F.D) work producing a less developed vorticity distribution. At the upper limit the (F.D) solution is proving less accurate when compared to both (F.E) solutions. The (F.E) solutions are similar and so the discrepancy cannot be due to the limiting resolution of the linear elements as displayed by the corner vortices. Instead it must be due to a fundamental difference between both numerical techniques. It is more likely that the range of the (F.D) technique is exceeded at Re=400.

The above study displays a rigorous test of the solution technique. By making extensive comparisons with two sets of reliable numerical results and refining the mesh to illustrate its convergence capabilities, much information about the solution scheme has been gained. These results provide the standard by which the quality of more difficult flow problems may be anticipated. Consequently it is now desirable to extend this research to other flow configurations where an informed judgement can be made of the computed results.

5.3 Flow Over a Downstream Step

5.3.1 Introduction

In the previous section the flow within a square cavity generated by a top moving wall is presented. The results obtained are shown to compare well with previous numerical work. This enclosed problem lends itself easily to solution, since the boundary conditions are well defined and its shape is easy to handle.

In order to test the program more fully, it is necessary to extend the model to other flow problems; preferably of a more practical nature. The flow over a downstream facing step is of considerable importance and so is to be investigated next.

This problem can also be considered as a sudden expansion in a channel and its solution is important in many fluid applications. It may be necessary to compute for instance the energy loss caused by such expansions. This would be vital when calculating the pressure gradient required to pump water through a network of channels.

It may be desirable to calculate the shear stress on the walls of the channel, especially in the recirculation region behind the step. This is useful to the civil engineer who may be concerned with the rate of scour in either a natural or a man-made environment.

Owning to its wide application, considerable work has been carried out to solve this problem. In particular, there exists a set of reliable experimental results gathered by Denham and Patrick [33]. The velocity measurements were obtained using a newly developed directionally sensitive laser anemometer.

As a consequence of this work a (F.D) solution to the step problem was presented by Atkins et al [34]. Using stream function and vorticity as the dependent variables a solution is obtained applying both central differencing and directional differencing schemes in the laminar and turbulent range of flow.

Work by Hutton et al [35] has produced a solution to this problem using the (F.E.M). Solving the flow in terms of velocity and pressure :with the introduction of a special wall element successful

results have been achieved.

More recently a paper by Thomas; C.E. et al [36] presents further (F.E) results for this problem. In this paper, a solution is computed in terms of velocity and pressure again for both the laminar and turbulent problem. The instabilities of the problem are by passed by introducing upwinding weighting functions.

Here, there is the unique opportunity to model a problem and make comparison with reliable experimental and numerical data.

In addition, it allows the author to demonstrate the ability of the solution scheme in modelling a variety of boundary conditions. This step example may be considered an example of a general class of channel problems; see section 4.4(i).

5.3.2 The Problem Discription

Figure 5.8 illustrates the boundary conditions of the step problem, with the flow moving from right to left.

The top and bottom boundaries are both no-slip walls, where the stream function is prescribed and the vorticity is described by the limiting boundary condition.

On the left-hand side or inlet boundary the stream function and vorticity are perscribed such that the velocity profile is of a fully developed form within a channel. This profile takes the form of a parabola and may be expressed by:

$$u_1 = \frac{2u_m}{D}\left[Z - \frac{Z^2}{2D}\right] \qquad (5.3.1)$$

$Z = x_2 - h$

h - step height

u_m - the centre line velocity

D - the half channel width

When using a primitive variable scheme the velocity variation is simply prescribed along the inlet boundary. In this case as the dependent variables are stream function and vorticity it is necessary to prescribe the equivalent stream function and vorticity values.

From section 2.3 the stream function is defined as:

$$\frac{\partial\psi}{\partial x_2} = \frac{\partial\psi}{\partial Z} = u_1 \qquad (5.3.2)$$

Taking the integral of equation (5.3.1), within the channel width a cubic variation of the stream function is obtained:

$$\psi = \frac{2u_m}{D}\left[\frac{Z^2}{2} - \frac{Z^3}{6D} + C_1\right] \qquad (5.3.3)$$

By defining the datum stream function value to be zero and assuming the centre line velocity to be unity, the equation becomes:

$$\psi = \frac{Z^2}{D} - \frac{Z^3}{3D^2} \qquad (5.3.4)$$

The stream function may now be prescribed as a function of

position along the inflow boundary.

As the inflowing velocity is not parallel the vorticity of the boundary is non-trivial. By considering this physically, it can be seen that some rotation of the fluid must exist to produce a parabolic velocity profile.

From section 2.3 the vorticity is defined as:

$$\omega = \frac{\partial u_2}{\partial x_1} - \frac{\partial u_1}{\partial x_2}$$

The velocity normal to the direction of main flow is considered minimal and so:

$$\omega = - \frac{\partial u_1}{\partial x_2} = - \frac{\partial u_1}{\partial Z} \qquad (5.3.5)$$

where:

$$u_1 = \frac{2A}{D} - \frac{Z^2}{D^2}$$

and so:

$$\omega = - \frac{2}{D} + \frac{2Z}{D^2} \qquad (5.3.6)$$

The vorticity along the inlet boundary can now be prescribed as a function of position.

If the vorticity is assumed to be zero along the inlet boundary, and equation (5.3.4) is used to prescribe the stream function, a conflict between the two conditions will occur. The former

is applying a parallel velocity condition and the latter a parabolic velocity condition. The resultant flow would be some combined condition.

Referring to figure 5.8 again, on the right hand side or outflowing boundary, the natural conditions are applied. There is some doubt as to its precise location with respect to the step. In theory, it should be positioned far enough downstream, so that the effect of the step on the flow has diminished.

As in the case of the square cavity problem, a small preprocessor is written to compute the nodal data of the step domain automatically. Similarly, these nodes are adjusted to ensure a regular mesh discretization.

In this case it is necessary to describe local regions within the domain by a varying mesh discretization. In the cavity problem adequate results are obtained without this extra complication.

The step is an open type problem, containing both an inflow and an outflow boundary. This means that there are large differences in flow behaviour within the domain, from the large variations of the unknowns due to recirculation behind the step, to the small variations further downstream. In order to discretize the problem efficiently it is necessary to have local variations of nodal distribution.

In truth, the discretization of the cavity can also be made more efficient, however, the problem is not so acute in this enclosed case.

Initially, the step domain was split into two distinct regions. In the area downstream of the step including the recirculation zone,

there are large variations of the unknowns, requiring a fine nodal resolution. In the region above the step, from the inflow to the outflow boundary, the nodal discretization need not be so fine. Figure 5.9a shows the type of mesh produced in this manner. A series of such meshes was produced, but the results computed from them proved to be very unstable.

It is concluded that the region about the top corner of the step is very sensitive to the quality of the local discretization. From figure 5.9(a) it can be seen that the zone coincides with the interface of the two mesh regions. What is needed is a regular discretization tracing the bottom wall from the left hand boundary to the right hand boundary.

This is achieved by introducing a different nodal distribution scheme. Now the variation of nodal concentration is split orthogonally, parallel to the direction of flow and along the normal to it across the channel. For a particular point in the domain the nodal distribution in either direction depends upon its location in that direction. The nodal concentration is zoned with increasing fineness as the step is approached, from either direction.

Since the variation of the unknowns is highly orthogonal due to the character of the problem it is possible to define a suitable discretization of the domain by applying such a scheme.

Figure (5.9b) illustrates the step domain discretized in this manner . The region near the top wall is discretized using a coarse distribution. Since there is no recirculation at this wall, it is considered to be adequate.

It can be seen from figure 5.9(b) that care is needed in the orthogonal zoning scheme to ensure that the discretization of the region about the top corner of the step is regular. This is found to reduce the instability of the results.

5.3.3 Results

Using this mesh generation scheme the step problem is computed at, Re=73,125 and 191, at which there already exist both experimental and numerical results. To be consistent with earlier work; $Re=hU_o/\nu$, where, h is the step height, U_o is the mean inlet velocity. These results are presented in terms of velocity profiles at various positions along the channel. In addition, to ensure consistency with earlier work the ratio of the inlet channel width to the outlet channel width is equal to 2.

Here, the velocity at positions along the channel is calculated from the stream function solution, and is plotted so that a direct comparison can be made with earlier work. In conjunction, equivorticity and streamline plots are also presented.

From the velocity values measured by Denham and Patrick, the stream function throughout the channel was computed at Re=73. In order to make a direct comparison with this result the contour levels are adjusted; $\psi'=\psi/\psi_{max}$; where ψ' are the plotted values and ψ_{max} the maximum stream function value along the top wall.

Although there are no vorticity results available in the literature for comparison, it is still important to present them for the benefit of future work. The equivorticity levels are normalised, $\omega'=-\omega h/U_{max}$, where ω' are the plotted levels and U_{max} the maximum

upstream velocity.

Two meshes are chosen to model the problem, a coarse one already presented in figure 5.9b, and a finer mesh; shown in figure 5.9c.

As in the case of the square cavity problem, inital conditions equivalent to orthogonal flow are applied, i.e. the vorticity in the domain is set to zero. A solution at Re=73 is first found, then subsequent solutions at higher Re are obtained by applying the vorticity of the previous solution as the initial flow conditions.

Below the results for this problem are presented:

(i) Re=73

Figures 5.(10,11 and 12) show the equivorticity plots the streamline plots and the velocity profiles at Re=73 respectively.

Considering the vorticity; figure 5.10(a) is a solution from the coarse mesh while figure 5.10(b) shows a solution using the fine mesh. In the case of one-dimensional channel flow the vorticity represents the gradient of the velocity. Along a channel without an expansion the equivorticity lines would be straight and parallel to the channel walls. Figure 5.10 shows the vorticity lines running parallel to the walls both upstream of the disturbance and further downstream as the effect of the step diminshes. Note also that these lines are closer together upstream and gradually spread out downstream with the velocity diminishing as the channel expands.

In the recirculation zone behind the step the vorticity pattern is not as regular and more difficult to predict. It is shown to be an

area of large variations of vorticity, especially close to the step where both meshes have difficulty in describing the flow. The finer mesh produces a better plot especially in this region. In addition , downstrean of the mesh the vorticity spreads out in a more symmetrical fashion about the centreline of flow when compared to the coarse mesh.

Figures 5.11(a) and 5.11(b) show the streamline plots for the coarse and fine mesh respectively. In figure 5.11(c) a streamline plot presented by Denham and Patrick, derived from velocity measurements, is also presented.

Good comparision is displayed between the numerical solutions and the experimental solution, especially in the region away from the step. All three plots display a similar wake region, with the zero streamline marking its outline. The fine mesh result shows a wake region which is in closer agreement with that of Denham et al.

Within the recirculation zone the variation of the stream function is at its largest. The fine mesh displays a marked improvement over the coarse mesh for this region. Close to the step, however, the gradients are too large due to the sharp change in geometry. This produces a corner condition similar to that of the square cavity problem.

Figures 5.12(a) and 5.12(b) present the velocity profiles along the channel for both meshes in conjunction with experimental results obtained by Denham et al. Figure 5.12(c) presents the earlier (F.E) results of Hutton [35] and (F.D) work of Atkins [34] compared with the experimental results.

These velocity profiles illustrate clearly the effect of the

step on the flow. Upstream a parabolic velocity profile exists as prescribed. Behind the step the flow is recirculating, this is illustrated by the negative components within the wake region. Further downstream beyond the wake region the recirculation effects diminish as the parabolic velocity profile returns. Obviously, the maximum centre-line velocity downstream is less then that upstream, due to the expanded width of the channel.

Both the coarse and fine mesh solutions compare adequately with the experimental measurements. There is a distinct improvement in the solution of the fine mesh compared to that of the coarse one.

From figure 5.12(c) it is possible to compare the current results with existing numerical work. Both the work of Hutton et al and Atkins et al compare favourably with the current results. This clearly shows the scheme's ability to model such flow problems.

There is however some error, notably near the top wall for both meshes; where the discretization could be improved to describe the prescribed veloctiy distribution along the inlet boundary more accurately. Furthermore, the actual input velocity of the experimental work is not quite of a parabolic nature. Consequently, the results could be improved if the exact experimental profile was prescribed along the inlet boundary. Both these improvements are necessary in order to reproduce to experimental results exactly. However, it is felt that the current results adequately represent the problem and what is needed is to test the existing problem at a higher Re.

(ii) Re=125

Figures 5.13(a) and (b) display the vorticity plots for both

meshes at Re=125. Again the lines run parallel to the channel wall both upstream and downstream of the step. The recirculating vorticity levels have extended further downstream due to the increased Re of flow. However there is a distinct difference in the lengths of this zone which must be due to the difference in mesh discretization.

The additional inertial effects caused by increasing the Re make the flow problem more difficult to solve. This is clearly illustrated by the oscillating vorticity lines in the upstream region. These oscillations are greater in the coarse mesh solution. There is some oscillation of the vorticity in this region at Re=73, however, it has much increased here.

Figures 5.14(a) and 5.14(b) present the streamline plots for both meshes at Re=125. Again a similar flow pattern exists as in the previous case with a smooth channel flow upstream and downstream with recirculation in between caused by the step.

Due to the increased Re of flow the wake extends downstream for both solutions. As in the vorticity results the fine mesh produces a longer wake then the coarse one. Again the problem of defining the flow in the corner region is illustrated near the bottom corner of the step.

Figures 5.15(a) and (b) present the velocity profiles for both solutions at this Re. Again a good comparison is made with the work of Denham and Patrick. Clearly a better model of the flow is made by the finer mesh. As already mentioned the wake extends further downstream ; this is displayed here by negative velocity components occuring further downstream.

As at Re=73 there is an error in the velocity distribution along the top wall. This is due to coarse discretization of the domain locally. As the Re is increased this error should also increase. Furthermore, the downstream outflow boundary is now close enough to the wake to influence the last velocity profile and produce an error with the experimental results. This can be overcome by positioning the outflow boundary further downstream.

(iii) Re=191

Figures 15.16(a) and (b) show the vorticity results for both meshes at this Re. Both display the same vorticity field as before with the recirculation zone moving even further downstream.

Due to the increased non-linearity of the problem the inlet oscillations have grown. As a result the solution has become very unstable and great care is necessary to find a solution. As in the previous case the vorticity lines in the step region are close together due to the recirculation of the flow there. There is some improvement in the solution of the fine mesh compared to the coarse mesh with the flow vorticity distribution being smoother.

The streamline plots, see figures 15.17(a) and (b), illustrate clearly how the wake region extends further downstream. The fine mesh produces a better solution especially in the recirculation zone.

The velocity plots are presented in figures 5.18 (a) and (b) for both meshes. In addition figure 5.18(c) shows the results of (F.E) work by Hutton et al compared with the experimental measurements.

Both meshes produce a reasonable comparison with the work of Denham and Patrick with the finer mesh producing closer agreement. The

errors in the top half of the channel and downstream of the step are apparent as before.

A good comparison can be seen with the (F.E) results of Hutton which again show the current technique to be a reasonable method of solving this problem.

Owing to the large oscillations existing in the vorticity solution the problem at this Re is very unstable, consequently a better domain discretization is needed to extend the solution to higher Re.

It is decided to conclude the problem here since adequate results have been obtained. Following on from this an attempt to model the more elaborate problem of flow past a cylinder is presented, again combining the solution technique and the mesh generation program.

5.3.4 Conclusions to the Step Problem

In the section above a comprehensive solution to the problem of flow over a downstream facing step is presented. Extensive comparision with earlier experimental and numerical work is carried out.

It is concluded that adequate success is achieved when using this stream function vorticity approach.

In order to improve these results further a number of possibilities are available. Failure to completely model the quadratic velocity variation along the top wall of the channel suggests an improved mesh discretization in this region is required.

As the Re is increased and the wake extends further downstream it approaches the downstream boundary. The result is that this boundary begins to influence the flow in a region where the step

disturbances are still significant. To combat this the boundary may be positioned further downstream

As already mentioned the inlet velocity of the experimental problem is not exactly of a parabolic form. In the earlier (F.E) work both the theoretical and experimental inlet velocity profiles are prescribed. It is expected that an improvement in the velocity results would occur if the actual experimental profiles were prescribed.

In the (F.D) work of Atkins it is found that a better description of the problem is achieved if the prescribed conditions on the inlet boundary are replaced by less restrictive conditions. He reports that using the prescribed conditions the vorticity perpendicular to the flow is undefined, and the resulting streamlines drop immediately after the step. This particular phenomonon is not found here where the inlet conditions are applied in a similar manner.

The oscillations of the vorticity which occur in the inlet region are well known to numerical engineers. Using the primitive variables similar oscillations occur for velocity results.

Leone and Gresho [37] describe them as wriggles, and suggest that they may be caused by a combination of singularities at the inlet and constraining effects at the outlet. Some people have found it necessary to introduce upwinding weighting functions in order to achieve a stable solution.

There is much discussion as to the reliability of such upwinding schemes. The critics claim that it introduces false diffusion effects, and the solution achieved is not that required. However, there is some work available showing that upwinding can be

successful for certain cases. For example the (F.E) results obtained by Thomas et al use such a scheme.

As can be seen from the above discussion much work is still needed before a complete solution is achieved to this step problem. Certain improvements can be made to the current scheme in order to produce better and more stable results.

It is not the purpose of this research to devote itself entirely to a study of the step problem. Instead it has been used to display successfully the solution scheme's capability. Now it is necessary to apply the scheme to another flow problem.

5.4 The Flow Past a Circular Cylinder

5.4.1 Introduction

The (F.E) solution scheme based on a stream function vorticity formulation has been used to model flow within a square cavity and flow over a downstream facing step. The results obtained compare well with available experimental and numerical work.

In this section the problem of flow past a cylinder is modelled using the same solution scheme. This is a prototype of the general problem of flow past any bluff body. From the early drawings of the vortex flow past a bridge pier by Leonardo da Vinci, man has endeavoured to obtain a better understanding of this problem. The solution of bluff body problems has a wide relevance to the engineering world as a whole. Consequently, much attention has been given to its analysis both in the numerical and the experimental field.

It is true to say that the desire to model this problem more

than any other has had the greatest influence on the development of numerical techniques for viscous fluid flow.

For example as far back as 1933 pioneer work by Thom [1] produced a solution to the cylinder problem in terms of difference equations at Re=10 and 20. Extending this work Kawaguti [2] produced a (F.D) solution at Re=40.

This (F.D) work was further extended, with the advent of computational methods, by Allen and Southwell [38], and Apelt [3] for the steady state case and by Payne [28] and Kawaguti and Jain [39] for the time dependent problem.

An interesting development was presented by Thoman and Szewczk [40] who extended the central difference scheme to directional differencing for the convective terms. It is claimed that the errors caused by this upwinding may be minimized if careful choice of the (F.D) cell structure is made. Using this scheme a solution has been achieved up to $Re=3x10^5$.

A good solution of the steady state problem using the (F.D.T) was later developed by Dennis and Chang [41] up to Re=100. This technique differs from others in that a solution of the stream function is expressed in terms of a Fourier series thus simplifying the relation between stream function and vorticity. The steady state solution to the cylinder problem at Re=5 to 100 is presented in terms of streamline and equivorticity plots. These results are used for comparative purposes below.

At about the same time work by Takami and Keller [42] reported a solution to this problem for Re=1 to 60. Here again a solution is

achieved by the (F.D.T) for the steady state equations. The problem is solved iteratively and convergence of the drag coefficient is monitered. Again results are presented in terms of streamline and equivorticity plots and shall be quoted below.

More recently, a successful solution to this problem has been achieved by Nieustadt and Keller [43] up to Re=40. Extending the work of Dennis and Chang both the stream function and the vorticity are expressed in terms of Fourier series. The resultant system of second order ordinary equations has been solved by the (F.D.T).

All this numerical work has been supported by experimental work, see Taneda [44], Acrivos et al [45] and more recently by Coutanceau and Bouard [27] to name but a few. The numerical solutions chosen for comparison here have been shown to compare well with this experimental work.

Resulting from this large amount of (F.D) research certain guidelines have evolved. The solution of the governing equations in terms of stream function and vorticity as the dependent variables is clearly favoured; in fact none of the solutions quoted above uses the primitive variable approach. The steady state solution is preferred to the time-dependent one for problems in the steady range of flow.

Most of these techniques have adopted a transformation of the coordinates in order to improve the cell structure about the cylinder; thus reducing the errors caused by the discretization of the domain.

The distinct advantages of the (F.E.M) in solving problems of an irregular domain are clearly important in this example. Along with the other advantages it provides an attractive alternative to the well

tried (F.D.T). Withstanding this not much work has been carried out using the (F.E.M). As a result the relative merits of the different approaches are not so clear.

Work by Taylor and Hood [6] has produced some steady state solutions to the flow past a cylinder using pressure and velocity as the dependent variables. A more comprehensive solution was presented by Tuann and Olson [46] using stream function alone as the dependent variable, as reported in the square cavity example. The results are presented in terms of plots of stream function and vorticity for Re=1 to 100, and shall be used below for comparative purposes. Smith [14] used a similar technique to produce some predictive solutions to the unsteady flow case. However, no extensive comparison was made with other numerical work for the steady state case.

5.4.2 The Problem Description

The boundary conditions describing the bluff body problem are presented in figure 5.19. The vorticity and stream function are prescribed on the inflow boundary to ensure parallel flow.

The cylindrical obstruction is defined as a no-slip boundary where the stream function is constant and the vorticity is described by the limiting constraint. Along the side boundaries both the vorticity and stream function are prescribed. This is a free-slip wall and defines the limits of the influence of the obstruction on the flow latterly. The stream function is constant as the wall runs parallel to the flow and the vorticity is zero since it is assumed that the fluid rotation has diminished to a minimum in this region.

The outlet is described by natural boundary conditions as in

the previous examples. This and the side boundaries are positioned far enough away from the obstruction to ensure they have no influence on the flow.

Since the velocity along the inlet boundary is constant the variation of stream function along it is linear with the gradient representing the value of the velocity. In addition, the vorticity is zero on this boundary since there is no rotation of the fluid.

As in the case of the two previous examples above, a preprocessor is developed to generate the internal nodes of the cylinder domain automatically. These are routed directly to the mesh generating scheme. This preprocessor enables the discretization of the domain with a certain degree of flexibility built in, in order to increase mesh refinement where desired.

The mesh is divided into two regions, the first being about the cylinder and the second downstream of the cylinder. In the first a completely symmetric nodal distribution is described. It is defined by a set of concentric rings of nodes about the cylinder. Figure 5.20 illustrates this nodal distribution clearly for a cylinder described by 16 nodes. It can be seen that the width of each ring of elements increases with distance from the obstruction. This is reasonable since the variable gradients decrease with distance from the body.

This figure also shows that each ring of nodes is rotated about the axis of the cylinder so that every node is positioned between two nodes of both adjacent inner and outer rings. This has been done to ensure a good triangular discretization in this region. This is more clearly illustrated in figure 5.21(a) and (b); where the mesh discretization about the cylinder is presented for both a fine and a

coarse mesh.

The boundary of the region is defined by a square centred about the cylinder described by the same number of nodes as each ring. This boundary is placed far enough away from the obstruction so that it is not expected to influence the flow about the cylinder.

Quite obviously, this is not the case downstream where the presence of the wake, especially at high Re, makes it necessary to enlarge the flow domain. The second part of the domain is discretized symmetrically about the centre line of the flow. Again the element width is increased with distance from the obstruction. Figure 5.22 shows the discretization of the entire domain including this downstream region. The symmetry of the region is ensured by applying the adjustment technique discussed in section 4.5.

The method of discretizing the cylinder domain has been outlined above. In the step problem some speculation is needed before a suitable mesh discretization is achieved. As there are no sharp corners here such problems are unlikely. Moreover, research into the cylinder problem has been more extensive; consequently a better knowledge of the flow behaviour is available, thus reducing the amount of speculation required.

5.4.3 Results

Using the nodal distribution scheme outlined in the previous section a steady solution of flow past a cylinder up to Re=40 is computed.

Two meshes are used with figures 5.21(a) and (b) showing the coarse and fine mesh discretization for the region about the

obstruction. The coarse mesh has 16 nodes describing the cylinder while the fine mesh has 32 nodes describing the cylinder.

The results are presented in terms of streamline and equivorticity plots about the cylinder. Both contour levels are normalised; with $\psi'=\psi/Ua$ and $\omega'=-\omega a/U$, where U is the inlet velocity and a is the cylinder radius. The Reynolds number is taken as; $Re=2aU/\nu$.

These results are compared directly with the comprehensive (F.E) work of Tuann and Olson along with other (F.D) solutions where available. Each figure contains four plots, where (a) and (b) are the current solution for the coarse and fine mesh respectively while (c) and (d) are the results of earlier (F.E) and (F.D) work respectively. Since all the results are found to be symmetrical about the axis of flow only one half of the flow is presented.

(i) Re=1

Figures 5.23 and 5.24 show the streamline and vorticity plots respectively. The (F.D) work of Takami and Keller is used here for comparative purposes.

The streamline results compare well with both earlier works. They show the slow motion of the fluid without any separation on the downstream side of the body. The finer mesh produces a smoother distribution of stream function when compared to that of the coarse mesh.

This is also the case for the vorticity plots: see figure 5.24. The (F.D) results show a vorticity distribution which is closer to the obstruction compared with both (F.E) solutions; however, all four plots are in good agreement with each other. They show the vorticity to be

a maximum close to the body , decreasing with distance away from it. It must be remarked that as the flow is so low that the vorticity is also nearly symmertical about an axis perpendicular to the flow through the centre of the cylinder.

In addition figure 5.35(a) shows a plot of vorticity about the cylinder. This displays the vorticity increasing steadily from the downstream stagnation point, reaching a maximum at an angle of about 109° and decreasing to zero at the upstream stagnation point.

(ii) Re=5.

Figures 5.25 and 5.26 present the streamline and equivorticity plots for this Re. Again the (F.D) work of Takami and Keller is used for comparison.

In the streamline plots all four results are in good agreement in the region away from the cylinder. Closer to the cylinder, however, both the coarse and fine meshes display a small separation zone which does not exist in either earlier work. There is a distinct decrease in length of the separation regions as the mesh is refined, indicating that this error is due to the limitation of linear element discretization in the region of the wake where large gradients of the unknowns exist. It is quite common to find the wake length varying with mesh refinement.

As the Re increases the vorticity effects are pushed further downstream . Both the fine and the coarse mesh illustrate this clearly, with the former producing a more developed flow pattern. No (F.D) work is available at this Re; however, a good comparison with the work of Tuann and Olson can be seen.

Figure 5.35(b) shows the distribution of the wall vorticity with angle about the cylinder, where a comparison with the work of Tuann and Olson and the (F.D) work of Dennis and Chang is made.

The vorticity distribution is similar to that at Re=1.0. Due to the increase in the Re the maximum vorticity value increases and its position moves upstream towards the inlet. Moreover, in the region about the downstream stagnation point for $\theta=0^{o}$ to 15^{o} the wall vorticity is zero.

When compared to earlier work the wall vorticity for both meshes is larger then that of the earlier work, with the (F.E) work of Tuann producing closer agreement then that of Dennis and Chang. The position of the maximum is coincident for all the solutions at $\theta=123^{o}$, except for the crude mesh which is positioned slightly downstream of this.

The fine mesh produces a reduced wall distribution which is closer to both the previous solutions. Indicating how the solution is converging as the mesh is refined.

(iii) Re=7.

The streamline plots of figure 5.27 take a similar form to those of the previous Re. In the region away from the body the flow appears to be in close agreement with the earlier work. The (F.D) results quoted here are from Dennis and Chang.

In the region close to the body and especially in the downstream section the comparison is not so good. All four solutions display some separation downstream of the cylinder; however; both current results produce a larger separation zone then the earlier work.

The work of Tuann and Olson shows closer agreement with the current work.

All four vorticity solutions are in good agreement showing how its influence extends further downstream as the Re increases, see figure 5.28c. Again the fine mesh produces a better overall distribution then the coarse one. The solution presented by Tuann is somewhat unstable extending further downstream then the others.

The wall vorticity plot, see figure 5.35(c), is of a similar shape to the last Re. As the Re increases the maximum vorticity on the wall also increases. There is a region close to the downstream stagnation point, from $\theta=0^{o}$ to 23^{o}, where the vorticity has become negative. This is indicitive of the growth of a separation zone, i.e a region where the fluid is rotating in the reverse direction.

(iv) Re=10.0

Figure 5.29 presents the streamline plots which display a continuing trend as the separation zone behind the obstruction grows with increasing Re. Again the results show greater separation when compared to earlier (F.E) and (F.D) solutions. The (F.D) results are taken from Dennis and Chang.

The vorticity solutions are more favourable where all four plots show good agreement, see figure 5.30. Again the work of Tuann shows greater instability with the vorticity effecting the fluid further downstream then any of the other solutions.

The wall vorticity plot,figure 5.35(d) shows the maximum wall value to have increased and the negative region about the downstream stagnation point to have enlarged, from $\theta=0^{o}$ to 34^{o}.

(v) Re=20.0

The streamline plot at Re=20.0 again show an enlarged wake due to the increased Re, see figure 5.31. Similarly the current results fail to compare well with the earlier work in the region close to the body, however, the fine mesh shows an improvement. The (F.D) results qouted here are again taken from Dennis and Chang.

The vorticity plots shown in figure 5.32 are in good agreement, the vorticity having influenced the flow further downstream as the Re increases. The work of Tuann is again unstable and extends further downstream when compared to the other solutions.

The wall vorticity distribution figure 5.35(e) shows an increased maximum and minimum value with the negative region extending from $\theta=0^{o}$ to 45^{o}. This plot shows the coarse results to be shifted downstream slightly when compared to the other results. The fine mesh produces a similar distribution to the previous results, although the actual values are again too high.

(vi) Re=40.0

The streamline plots again show an extended separation zone,see figure 5.33. The coarse mesh results look unstable as the inertial terms become very significant. The finer mesh produces a more reasonable result. It must be noted that both results display a wake whose width extends above the top of the cylinder, this is consistent with both previous results.

Turning to the vorticity plots, see figure 5.34, the coarse mesh produces a very unstable solution, however, good agreement is seen

between all four solutions. The work of Tuann again presents an unstable solution. The fine mesh plot shows some small oscillations of the contours upstream of the obstruction, these are generally associated with excessive inertial effects for the mesh discretization used.

The wall vorticity distribution has grown as expected , see figure 5.35(f), with the maximum and minimum vorticity values increasing and the negative vorticity region extending from $\theta=0^{o}$ to 56^{o}.

(iv) The Development of the Wake

Above, the results are presented and successful comparison with earlier work is made. Here a discussion of the development of the flow with increasing Re is explained.

At Re=1 the flow is slow and creeping with the viscous terms dominant, producing a nearly symmertical pattern between the upstream and downstream part of the obstruction.

By increasing the Re to 5 the inertial effects become more significant. The flow becomes assymetric as the vorticity begins to influence the flow downstream of the body. The wall vorticity graphs help to illustrate this assymetry as the position of the maximum value moves towards the upstream stagnation point.

At about Re=7. separation of the fluid occurs in the downstream region of the cylinder. This phenomenon of separation is well known in viscous fluid flow and can be clearly explained using the cylinder problem as an example.

Various experiments have been carried out bearing the

conclusion that separation can only occur in a fluid flow environment containing a negative pressure gradient.

The pressure distribution on the obstruction is crucial to the fluid behaviour about it. Starting at the upstream stagnation point the pressure applied to the wall is a maximum. Moving along the wall downstream to the top of the cylinder, the fluid speed increases and the pressure drops to a minimum, thus producing a positive pressure gradient along this section of the wall. Moving further downstream towards the downstream stagnation point the fluid velocity decreases again, producing a negative pressure gradient in this region.

If the frictional effects are large enough the fluid fails to reach the downstream stagnation point before its velocity becomes zero and so separation occurs producing a negative velocity recirculation zone in this part of the cylinder. As the fluid flow direction in this zone is opposite to the main direction of flow it is reasonable to expect the fluid to be rotating in a negative direction to the external region.

Increasing the Re further the pattern continues with the vorticity influencing the fluid further downstream from the obstruction. In conjunction, the separation point creeps upstream along the wall extending the region of separation behind the body. As the negative gradient rises the fluid flow in this region is retarded sooner thus causing separation to occur closer to the top of the cylinder.

As mentioned above at Re=40.0 the wake region becomes wider than the cylinder diameter, although the point of separation is still below the top of the cylinder. This means that the wake region is no

longer completely screened from the oncoming flow by the cylinder. It is speculated that this is the reason for the unsteady vortex shedding. For if the Re is increased above 40 regular oscillatory vortex shedding occurs alternatively from the top and the bottom of the cylinder. Such a study is not included here, however, extensive work on this subject has been presented by Smith.

5.4.4 Conclusions

The solution of flow past a cylinder is presented for the steady state case at a Re of 1 to 40. Good comparison is made with earlier numerical work.

The streamline solution shows the poorest comparison with earlier work in the region close to the body. Conversely, the vorticity solution provides a reasonable comparison up to a Re of 40, although at this Re the coarse mesh contour lines display large oscillations.

In truth this mesh is inadequate when modelling flows at high values of Re. However, it provides a guide to the lower limit capabilities of the solution scheme. The fine mesh produces a good vorticity distribution, however, at Re=40 there are small oscillations in the contour lines upstream of the obstruction. This indicates the presence of excessive inertial effects.

The wall vorticity results show the current solution to be converging towards that obtained by earlier numerical work as the domain mesh is refined. The vorticity about the body for the fine mesh is still somewhat larger than in the earlier solutions.

This underlines the limitations of the use of linear element

discretization when modelling flow close to the no-slip wall. Here the cylindrical obstruction has been described by a polygon of sixteen sides for the coarse mesh and thirty-two sides for the fine mesh. Increasing the number of sides on the polygon will obviously improve this approximation. Since there are large variations of the flow close to the obstruction, this region is very sensitive to any change in wall shape. In experimental work great care is needed to ensure that the obstruction is free from any uneveness, as they are found to alter the resultant flow considerably. Such uneveness can reduce the upper limit of steady state flow, for example the uneven surface of a golf ball encourages the development of a turbulent wake improving its flight through the air. The unsmooth shape of the fine mesh, even using 32 nodes, is causing a similar effect of the vorticity close to the wall.

In order to combat this a greater mesh refinement can be carried out. In the steady case the problem may be halved by considering just the top part of the problem with an axis of symmetry running from the inlet to the outlet boundary .

A further improvement to the description of the no-slip wall boundary may be made if the local wall elements are replaced by superparametric elements with the boundary side described by a curve.

The stream function is poorer then the vorticity since it is calculated using the approximate solution of vorticity. This has been disussed in detail in section 5.2 in the case of the square cavity problem. In that section the (F.E) work of Tuann and Olson produced better results for stream function then vorticity. Here for the cylinder problem this is also the case as the vorticity plots of Tuann produce erratic contour levels, especially at the higher Re. The

reasons for this are the same, with the flow being solved in terms of stream function and vorticity being computed once convergence has been achieved.

The problem of flow past a cylinder is modelled using the (F.E.M) in terms of stream function and vorticity, with the use of the mesh generation scheme to discretize the region.

The results are compared with earlier numerical work and reasonable agreement is achieved. These results also demonstrate the ease with which the system can model a bluff body problem. Consequently, the scheme could quite easily be adapted to study the flow past an aerofoil shaped body for example. Such predictive work is beyond the scope of this current research.

Three flow problems are presented here. Earlier numerical work and experimental work is used in order to assess the results. A reasonable comparison is found, however improvements can be made to each problem studied.

In conjunction, the scheme is demonstrated to correctly discretize three general cases of flow problem automatically, i.e enclosed flow, channel flow and bluff body flow. This list may be extended; however, such a study is beyond the limits of this work.

With the laminar flow case having been extensively studied the emphasis shall now turn to the solution of turbulent flow conditions. In the following chapter the way in which this is done is presented. By modifying the existing program it is possible to extend the scope of this work to the mechanisms of turbulence.

CHAPTER SIX

TURBULENT FLOW

6.1 Introduction

In the previous chapters the solution of fluid flow for the laminar case is studied. Here the concepts of turbulent flow are introduced and the methods of solution are discussed.

In laminar flow the fluid moves in a series of layers with no momentum transfer between them. In turbulent flow, however, although the overall flow is in one direction, superimposed on this is an irregular transverse motion. The distinction between the two types of flow was made by Reynolds in 1883 while tracing the flow of fluid in a circular pipe using a dye.

Clearly as there are two mechanisms of flow a different solutions approach is required for both. However, the set of (N.S) equations govern the flow of a fluid whatever its mechanism, but in the case of turbulent flow the equations have to be written in a more suitable form. If the existing equations are solved within the turbulent range of flow the results obtained will change with discrete intervals of time. These values have no overall meaning, since they represent random fluctuatations of the flow with respect to time.

If the equations are written in terms of time averaged values the results obtained are of a more practical nature. When dealing with turbulent flow conditions the time averaged values of the unknowns have more practical relevance then the discrete fluctuating ones.

When the equations are written in terms of time averaged velocity and pressure extra terms exist in the momentum equation. This is due to the transfer of momentum across the shear layers and is called the turbulent or Reynolds stress.

The problem arises when expressing this stress in terms of solvable unknowns in order to achieve closure of the set of equations. Work by Boussinesq in 1877 attempted to write the Reynolds stress in a form similar to the viscous stresses by introducing the concept of apparent viscosity. Although the idea of relating fluctuating stress to mean time averaged velocity has physical limitations, it has proved to be most successful in practice.

The apparent viscosity approach was later extended by Prandtl in 1925. Basing his ideas on the molecular theory of gases he developed a relation for this viscosity in terms of a mixing length and time averaged velocity. It is now possible to shed some light on the physical meaning of the mixing length. It is similar to the mean free path in molecular theory and represents the distance travelled by a lump of fluid before it changes its momentum.

For some flow conditions the mixing length has been measured and is found in most cases to be of the order of the boundary layer thickness; see Escudier [47]. With some knowledge of the size of the mixing length closure of the governing equations is possible for certain turbulent flow conditions.

Before the development of computational methods sophisticated analytical techniques were used to solve these problems, where the partial differential equations are integrated into ordinary differential equations and solved. In order to solve such equations crucial assumptions about the flow behaviour had to be made. At the Stanford conference in 1968 all the various techniques for predicting turbulent layer flow were assessed. The overall conclusion of the conference was that the numerical technique, particularily the (F.D.T)

at the time, proved to be more accurate and more general when compared to the best integral method; see Reynolds; W.C [48] for a review of this conference. This conference was very much a watershed for the solution of turbulent boundary layer problems and heralded the future potential of the numerical approach. As a result much work has been carried out to achieve (F.D) solutions for this problem in terms of time averaged unknowns.

Cebeci and Smith [17] developed a solution technique where closure was obtained by using the apparent or eddy viscosity concept. Work by Patankar and Spalding [18] developed a similar procedure and obtained closure to the equations by the use of Prandtl's mixing length.

Gosman et al [4] solved the problem in terms of the time averaged stream function and vorticity, again defining the Reynolds stress by the use of mixing length. A further (F.D) solution in terms of stream function and vorticity as the dependent variables was presented by Richman and Azad [49] for flow through a circular pipe. Here again Prandtl's mixing length concept is employed.

More recently work at Swansea has been carried out to develop a (F.E) solution scheme based on mean value primitive variables and again the mixing length idea has been adopted; see Hughes [19]. Here a variety of flow conditions has been modelled, from the axysymmetric flow through a pipe to the two-dimensional flow of a mixing layer.

It must be noted that although the mixing length concept has shown a wide success, it is based on major assumptions about the mechanisms of turbulent mixing. Attempts have also been made to define the Reynolds stress directly by introducing separate differential

equations. Such schemes are very complicated and have proved to be computationally costly without any marked improvement in accuracy. For a comparison of both approaches see Birch [50].

Below the mixing length concept is explained more fully, with its adaptation to the stream function vorticity equations presented.

6.2 The Equations of Turbulent Flow

The two equations governing fluid flow are:

continuity:

$$\frac{\partial u_i}{\partial x_i} = 0$$

momentum:

$$\frac{du_i}{dt} + u_j \frac{\partial u_i}{\partial x_j} = - \frac{1}{\rho} \frac{dP}{dx_i} + \nu \frac{\partial}{\partial x_j} \left(\frac{\partial u_i}{\partial x_j} \right)$$

Again assuming that molecular viscosity and fluid density remain constant.

Considering an arbitrary variable a:

$$a = A + a'$$

where:

$$A = \frac{1}{T} \int_0^T a(t + \tau) \, d\tau$$

where T is large compared to the time scale of turbulent flow.

Where A is the time averaged value and a is the fluctuating value of the variable a. Similarly the variables velocity and pressure are defined in the same manner:

$$u_i = U_i + u_i'$$

$$P = \overline{P} + p' \qquad (6.2.1)$$

Fitting into the above equations of motion to obtain:

$$\frac{\partial U_i}{\partial x_i} = 0 \qquad (6.2.2)$$

$$\frac{dU_i}{dt} + U_j \frac{\partial U_i}{\partial x_j} = -\frac{1}{\rho}\frac{d\overline{P}}{dx_i} + \nu \frac{\partial}{\partial x_j}\left(\frac{\partial U_i}{\partial x_j} + \frac{\partial U_j}{\partial x_i}\right) - \frac{\partial}{\partial x_j}\left(\overline{u_i' u_j'}\right)$$

(6.2.3)

The term caused by the fluctuating velocity may be considered as an extra component of stress in addition to viscous stresses and the direct pressure.

The complete stress effect may now be expressed as:

$$\sigma_{ij} = -\overline{P}\,\delta_{ij} + \mu\,\overline{D}_{ij} - \rho\,\overline{u_i' u_j'}$$

$\overline{D}_{ij}$ - the time averaged deformation tensor

$\rho\,\overline{u_i' u_j'}$ - the Reynolds stress

It can be readily seen that the Reynolds stress is of a tensor form, similar to the viscous stresses. It was for this reason that Boussinesq interpreted them to be proportional to the mean velocity gradient, thus introducing the idea of turbulent viscosity.

The stress tensor may be defined accordingly:

$$\sigma_{ij} = -\bar{P}\,\delta_{ij} + (\mu + \rho\,\varepsilon_m)\,\overline{D_{ij}}$$

where

$$-\overline{u_i' u_j'} = \varepsilon_m\,\overline{D_{ij}} = \varepsilon_m \left(\frac{\partial U_i}{\partial x_j} + \frac{\partial U_j}{\partial x_i}\right)$$

ε_m - turbulent viscosity

This may be envisiged physically as an additional viscosity caused by the transverse motion of turbulent flow. A distinction must now be made between molecular viscosity and this apparent viscosity . The former is a property of the fluid, while the latter is a property of the fluid motion and disappears when the turbulent mechanisms diminsh.

The introduction of the turbulent viscosity is a simple way of relating the fluctuating terms of the Reynolds stress to the mean flow velocity.

Few people have actually used the equations in this precise form, since a direct definition of turbulent viscosity is difficult to predict.

Consequently, Prandtl devised a relation for the turbulent viscosity based on the classical concepts of molecular viscosity. The molecular viscosity is caused by the diffusive nature of the molecules. Here the turbulent effects are considered to be caused by the diffusive nature of lumps of fluid. Considering the transport of a scalar a across a plane perpendicular to x_2. The transport per unit area and time is:

$$\tau_a = \rho \overline{u_2' L} \frac{\partial a}{\partial x_2}$$

L - the mean length over which a lump of fluid travels

Refer to Hinze [51] for a more extensive discussion of the mixing length concept.

Let a be the x_1 component of momentum per unit mass of fluid per unit area in unit time.

$$\tau_m = \overline{\rho u_2' L_m} \frac{\partial (\rho U_1)}{\partial x_2} \qquad (6.2.5)$$

defining the turbulent stress components as follows:

$$\sigma_{12} = -\tau_m = -\rho \overline{u_2' L_m} \frac{\partial U_1}{\partial x_2}$$

where the eddy viscosity becomes

$$\varepsilon_m = -\overline{u_2' L_m} \qquad (6.2.6)$$

Assuming that the component u_1' is the difference in mean velocity between two adjacent layers of fluid; the fluctuating velocity may be expressed as:

$$u_1' = L \frac{\partial U_1}{\partial x_2}$$

equating the fluctuating velocities in orthogonal directions:

$$u_2' \doteq u_1' = L \left|\frac{\partial U_1}{\partial x_2}\right|$$

where the sign is defined by L.

Substituting this into equation (6.2.6) the turbulent viscosity becomes:

$$\varepsilon_m = - \overline{u_2 L_m} = \text{CONST.X } \overline{L_m^2} \left|\frac{\partial U_1}{\partial x_2}\right|$$

$$\varepsilon_m = \ell^2 \left|\frac{\partial U_1}{\partial x_2}\right| \qquad (6.2.7)$$

ℓ - is the mixing length

The turbulent stress component may now be expressed as:

$$\sigma_{12} = \rho\ \ell^2 \left|\frac{\partial U_1}{\partial x_2}\right| \frac{\partial U_1}{\partial x_2} \qquad (6.2.8)$$

Where ℓ is Prandtl's mixing length, and represents the distance travelled by a lump of fluid before losing its excess momentum. It is now possible to express the Reynolds stress in a form more suitable for solution in terms of time averaged unknowns:

$$\sigma_{ij} = - \rho \overline{u_i' u_j'} = \rho\ \ell^2 \left|\frac{\partial U_i}{\partial x_j}\right| \frac{\partial U_i}{\partial x_j} \qquad (6.2.9)$$

It can be readily seen from the above relationship that in its general form the turbulent viscosity is a second order tensor. For the

specific case of two-dimensional unidirectional flow this is simplified to a scalar, e.g. for channel flow.

The problem of solving turbulent flow has now been reduced to evaluating the mixing length. It is at this stage that empirical knowledge based on experimental investigation is sought.

6.3 The Mixing Length Model

It is now necessary to predict how the mixing length will vary within a turbulent region. Broadly speaking turbulence may be split into two types: free shear turbulence and wall turbulence.

Both pose two distinct problems when predicting the variation of turbulent effects within the region. To do this a knowledge of the way the fluid behaves in such regions is required.

(i) Free Shear Flows

This is classified as a turbulent flow without the presence of a solid wall. Examples of this are the wake behind a cylinder and the wake of a jet.

All these wakes display a slowly widening pattern, with a similarity of the velocity profile downstream of the original disturbance. The turbulent viscosity is constant throughout the wake and so the mixing length is similarly taken to be a constant; see Townsend [52].

The mixing length may be written:

$$\ell = K_1 \delta$$

δ - half width of the jet

K_1 - empirical constant

Where the flow is in the x_1 direction.

(ii) Wall Turbulence

There are two types of wall turbulence, that caused by the flow around rigid bodies and that by flow which is bounded within rigid walls. For both these conditions the behaviour near the wall is the same.

Here, the problem of flow past a flat plate with zero incidence to the flow direction is used to demonstrate the general concepts of wall turbulence.

The flow may be split into an external and an internal region. In the external region the fluid is unaffected by any disturbance whether viscous or turbulent, and may be considered inviscid. Conversely in the internal region the fluid is affected by both; as the wall is approached the viscous effects increase and the turbulent effects diminish until the flow becomes completely laminar adjacent to the wall. This dramatic change between the two regions was first proposed by Prandtl for the limiting case of reduced viscous effects with increasing Re. He concluded that no matter how large the Re there always exists a thin layer about the wall where the viscous effects are significant: this is called the turbulent boundary layer.

This layer can now be subdivided to obtain a fuller

understanding of the flow.

Close to the wall the viscous effects dominate with the turbulent effects becoming negligible; this is called the viscous sublayer, i.e. $x_2 < \delta_\ell$ see figure 6.1. Moving away from the wall the viscous effects decrease as the turbulent effects become more significant. At a certain point the turbulent effects begin to dominate, as the viscous effects tend to zero, i.e. at $x_2 = \delta_t$, this marks the start of the turbulent boundary layer. Between the end of the viscous sublayer and the start of the turbulent boundary layer there exists a transition region, where both effects are important, i.e. where $\delta_\ell < x_2 < \delta_t$.

The flow close to the wall is determined by assuming that the shear stress is constant throughout the viscous sublayer; producing a linear variation of velocity:

$$U_1 = \frac{\sigma_w}{\mu} x_2 \qquad x_2 < \delta_\ell \qquad (6.3.1)$$

σ_w - wall shear stress

The region of the turbulent boundary layer, i.e. $\delta_t < x_2$, is still sufficiently close to the wall for the shear stress to be assumed constant. Ignoring the viscous effects and assuming a linear variation of turbulent viscosity the velocity distribution is shown to be logarithmic:

$$U_1 = A \ \ell n \ x_2 + B \qquad x_2 > \delta_t \qquad (6.3.2)$$

Prandtl obtained the same logarithmic variation for velocity by

assuming a linear variation of the mixing length.

The region where the linear velocity variation and the logarithmic velocity variation hold is called the constant stress layer. There is however a large part of the turbulent boundary layer where the shear stress is not constant. In this region the flow behaviour is similar to the external region where the turbulent viscosity is constant.

No direct relation for the velocity profile is available in this non-constant stress region, however, there is a similarity of the velocity profiles in consecutive sections, which is described by the velocity defect law:

$$\frac{U_0 - U_1}{u^*} = \gamma\left(\frac{x_2}{\delta}\right) \qquad (6.3.3)$$

u^* - wall friction velocity, $u^* = \left(\frac{\sigma_w}{\rho}\right)^{\frac{1}{2}}$

$\gamma(\ )$ - arbitrary function

U_0 - free stream velocity

No further information is needed about the velocity in this region, since it has been found experimentally to coincide with the velocity variation in the constant stress region.

So far the equations describing the velocity variation in both the fully viscous and the fully turbulent region have been presented. It is now necessary to obtain a smooth transition between these two limiting cases. Many attempts have been made to do this. A most successful attempt to describe the entire region using a single relation has been developed by Van Driest [53].

(iii) Van Driest's Model of Wall Turbulence

Work by Van Driest produced a theoretical velocity variation for the entire boundary layer.

He bases his derivation on the diminishing amplitude of an oscillating fluid as a stationary wall is approached. The amplitude is found to increase by the factor $[1-\exp(-x_2/A)]$ with distance from the wall.

From equations (6.2.4) and (6.2.8) the total shear stress may be defined as:

$$\tau = \mu \left(\frac{\partial U_1}{\partial x_2}\right) + \rho \ \ell^2 \left|\frac{\partial U_1}{\partial x_2}\right| \frac{\partial U_1}{\partial x_2} \qquad (6.3.4)$$

As the wall is approached the turbulent effects are diminished and the viscous effects will dominate. In the turbulent boundary region Prandtl proposed that the mixing length varied linearly with distance from the wall.

$$\ell = \kappa \ x_2$$

κ - universal mixing constant

Van Driest assumes that the turbulent effects behave in a fashion similar to oscillations in the fluid and so derives a relationship for the mixing length over the entire boundary.

$$\ell = \left[1 - \exp\left(-\frac{x_2}{A}\right)\right] \kappa \ x_2 \qquad (6.3.5)$$

substituting this into equation (6.3.4) produces:

$$\tau_{nw} = \mu \left(\frac{\partial U_1}{\partial x_2}\right) +$$

$$\rho\, \kappa^2\, x_2^2 \left[1 - \exp\left(-\frac{x_2}{A}\right)\right]^2 \left|\frac{\partial U_1}{\partial x_2}\right| \left(\frac{\partial U_1}{\partial x_2}\right) \qquad (6.3.6)$$

A - Van Driest's damping parameter

κ - the universal mixing constant

τ_{nw} - shear stress near the wall

From this a formula for the velocity in the boundary layer was derived and found to match for all the three regions of the layer.

Consequently it is possible to describe the full boundary region using the mixing length of Prandtl in conjunction with this model. However, some empirical knowledge is still required in order to evaluate the damping constant A and the universal mixing constant κ. Furthermore, moving away from the wall, the turbulent stresses increase. At a certain point the wall no longer influences the transport of turbulence and the turbulent viscosity becomes constant. Consequently, it is also nesessary to define this cut-off point before a solution can be made.

The mixing length for turbulent flow near a wall may now be expressed:

$$\ell = \left[1 - \exp\left(-\frac{x_2}{A}\right)\right] \kappa\, x_2 \qquad x_2 < x_c$$

$$\ell = \ell_{(x_2 = x_c)} \qquad x_2 \geq x_c \qquad (6.3.7)$$

The choice of cut-off point x_c beyond which the turbulent effects are assumed constant is dependent upon the problem to be solved and is the subject of certain speculation.

To summarize, closure of the time averaged equations is achieved by describing the Reynolds stress in terms of the mean gradient of flow and the turbulent viscosity. This apparent viscosity is subsequently defined in terms of mixing length, for which an empirical relation is presented.

It is now necessary to express these equations in terms of stream function and vorticity, for which there already exists a (F.E) solution program.

6.4 The Turbulent Equations in Terms of Stream Function and Vorticity

As in section (6.2) above, the equations may be expressed in terms of their respective time averaged unknowns:

$$\psi = \Psi + \psi' \qquad (6.4.1)$$
$$\omega = \Omega + \omega'$$

The relationship between stream function and vorticity see equation (2.3.4), becomes:

$$\frac{\partial^2 \Psi}{\partial x_j^2} = -\Omega \qquad (6.4.2)$$

Considering the vorticity as a scalar, the turbulent transport may be obtained quite simply, where the source term is taken to be

zero:

$$\frac{D\Omega}{Dt} = \nu\frac{\partial^2\Omega}{\partial x_j^2} - \frac{\partial(\overline{u_i' \omega'})}{\partial x_j} \qquad (6.4.3)$$

This equation is of a similar form to equation (2.3.3) with the extra term representing the turbulent transport effect caused by the fluctuation of the velocity and the vorticity in the fluid.

Applying Boussinesq's concept of turbulent viscosity this may be rewritten:

$$-\overline{u_i' \omega'} = \varepsilon_\omega \frac{\partial\Omega}{\partial x_j}$$

ε_ω - the turbulent vorticity viscosity

Applying Prandlt's mixing length hypothesis the turbulent viscosity may be expressed as:

$$(\varepsilon_\omega)_{ij} = \ell_\omega^2 \left|\frac{\partial U_i}{\partial x_j}\right|$$

The value of the mixing length is not necessarily of the same form as that of momentum; however, in this case, as in many, it is taken to be so.

The transport of vorticity for two-dimensional unidirectional turbulent flow may now be written as:

$$\frac{D\Omega}{Dt} = \nu\frac{\partial^2\Omega}{\partial x_j^2} + \frac{\partial}{\partial x_j}\left(\ell_\omega^2 \left|\frac{\partial U_1}{\partial x_2}\right| \frac{\partial\Omega}{\partial x_j}\right) \qquad (6.4.4)$$

This equation may also be derived by taking the curl of the two-dimensional momentum equation. This leaves residual terms which are not significant in the flow problem modelled here. The (F.D) work of Richman and Azad found the effect of including these terms to be minimal, a similar conclusion was reported by Gosman.

An algebraic closure to the governing equations has been achieved. Subsequently the solution of developing flow in a channel is presented.

The shortcomings of this particular model are well known and many efforts have been made to improve on it. A major criticism of this approach is that it only accounts for the local influences of turbulence.

In order to improve this Prandtl and Kolmogorov proposed that the turbulent stresses be related to the time averaged kinetic energy. This requires the solution of an extra differential equation for the kinetic energy: such a scheme is called the one-equation method.

This was later extended to a two equation method, where the mixing length distribution is obtained by an additional differential equation. For a background of these models see; Launder and Spalding[54].

Both these models are beyond the scope of this work, but are necessary avenues of research when solving flows of a more complex nature.

6.5 The Finite Element Implementation

So far closure of the governing equations describing turbulent flow is achieved by the introduction of apparent or turbulent viscosity. In the previous section these ideas have been applied to the existing vorticity transport equation and now the existing (F.E) program is extended to deal with certain turbulent cases.

The total viscosity may be expressed as the sum of the molecular viscosity ν and the apparent viscosity ν_a.

$$\nu_t = \nu + \nu_a \qquad (6.5.1)$$

This may be defined more specifically:

$$\nu_t = \nu + \kappa^2 x_2^2 \left[1 - \exp\left(-\frac{x_2}{A}\right)\right]^2 \left|\frac{\partial U_1}{\partial x_2}\right| \qquad (6.5.2)$$

Since the total viscosity is no longer constant throughout the fluid domain the turbulent vorticity transport equation may be rewritten as:

$$\frac{D\Omega}{Dt} = \frac{\partial}{\partial x_j}\left[\frac{\partial}{\partial x_j}(\nu_t \Omega)\right] \qquad (6.5.3)$$

This may be expanded to give:

$$\frac{D\Omega}{Dt} = \frac{\partial^2 \nu_t}{\partial x_j^2}\Omega + 2\frac{\partial \nu_t}{\partial x_j}\frac{\partial \Omega}{\partial x_j} + \nu_t \frac{\partial^2 \Omega}{\partial x_j^2} \qquad (6.5.4)$$

Comparing this equation with the original laminar vorticity transport equation (2.3.3) extra terms on the right-hand side have to be included in the existing (F.E) formulation.

Consequently applying the weighted residual technique in the same manner as before, as in section (3.2).

$$\int_A \left[\frac{D\Omega}{Dt} - \frac{\partial^2 \nu_t}{\partial x_j^2}\,\Omega - 2\,\frac{\partial \nu_t}{\partial x_j}\,\frac{\partial \Omega}{\partial x_j} - \nu_t\,\frac{\partial^2 \Omega}{\partial x_j^2}\right]\,\delta\,\Omega\,dA$$

$$-\int_{S_{\omega_2}} \nu_t\,(\bar{g}_\Omega - \frac{\partial \Omega}{\partial n})\,\delta\,\Omega\,dS = 0 \qquad (6.5.5)$$

The boundary conditions applied are identical to those used previously. Similarly the finite element equations are expressed using linear interpolation. The total viscosity values integrated over an element or its side may therefore be expressed as an average.

By comparing the above formulation with the original one, see equation (3.2.4a), it can be seen that all but the second and third terms of the integral statement have already been derived.

Considering these two terms alone:

$$-\int_A \left[\frac{\partial^2 \nu_t}{\partial x_j^2}\,\Omega\,\delta\,\Omega + 2\,\frac{\partial \nu_t}{\partial x_j}\,\frac{\partial \Omega}{\partial x_j}\,\delta\,\Omega\right]\,d\Omega$$

As in the case of the stream function and vorticity, for the benifit of expressing these terms the variation of the total vorticity is taken to be linear within each element. Consequently in order to express the first term it is necessary to integrate it by parts to

reduce its order.

$$- \int_A \left[\frac{\partial^2 \nu_t}{\partial x_j^2} \Omega \delta \Omega\right] dA = - \int_{S_{\omega_2}} \frac{\partial \nu_t}{\partial n} \delta \Omega \Omega \, dS$$

$$+ \int_A \left[\frac{\partial \nu_t}{\partial x_j} \frac{\partial}{\partial x_j} (\delta \Omega \Omega)\right] dA =$$

$$- \int_{S_{\omega_2}} \frac{\partial \nu_t}{\partial n} \delta \Omega \Omega \, dS + \int_A \frac{\partial \nu_t}{\partial x_j} \frac{\partial (\delta\Omega)}{\partial x_j} \Omega \, dA +$$

$$\int_A \frac{\partial \nu_t}{\partial x_j} \frac{\partial \Omega}{\partial x_j} \delta \Omega \, dA$$

The additional terms may now be expressed as:

$$\int_A \left[\frac{\partial \nu_t}{\partial x_j} \frac{\partial (\delta\Omega)}{\partial x_j} \Omega - \frac{\partial \nu_t}{\partial x_j} \frac{\partial \Omega}{\partial x_j} \delta \Omega\right] dA - \int_{S_{\omega_2}} \frac{\partial \nu_t}{\partial n} \Omega \delta \Omega \quad (6.5.6)$$

The domain is again discretized and the unknowns are expressed in terms of discrete nodal values:

$$\Omega = \sum_{n=1}^{n=NE} \underline{\phi}_j^T \underline{\Omega}_j \; ; \; \Psi = \sum_{n=1}^{n=NE} \underline{\phi}_j^T \underline{\Psi}_j \quad (6.5.7)$$

$$\nu_t = \sum_{n=1}^{n=NE} \underline{\phi}_j^T \underline{\nu}_j$$

where:

$$t_1 = \frac{\partial \nu_t}{\partial x_j} \int_a \phi_j \frac{\partial \phi_j}{\partial x_j} \, da$$

$$t_2 = \frac{\partial \nu_t}{\partial x_j} \int_a \frac{\partial \phi_j}{\partial x_j} \phi_j^T \, da \qquad (6.5.8)$$

$$s = \frac{\partial \nu_t}{\partial n} \int_s \phi_j \, \phi_j^T \, ds$$

ω_2

Consequently the complete element formulation is expressed as:

$$\Sigma \underline{m} \, \dot{\underline{\Omega}}^n + \underline{a}(\underline{\psi}^n) \, \underline{\Omega}^n + \nu_{av} \, \underline{k} \quad \underline{\Omega}^n$$

$$- \underline{t}_1 \, \underline{\Omega}^n + \underline{t}_2 \, \underline{\Omega}^n - \underline{s} \, \underline{\Omega}^n = \nu_{av} \, \underline{b}_\omega \qquad (6.5.9)$$

ν_{av} - average total viscosity on an element

The element effects are again summed together and the global form of the finite element formulation is obtained.

$$\underline{M} \, \dot{\underline{\Omega}} + \underline{A} \, (\underline{\psi}) \, \underline{\Omega} + \nu_{av} \, \underline{K} \, \underline{\Omega} - \underline{T}_1 \, \underline{\Omega} + \underline{T}_2 \, \underline{\Omega} - \underline{S} \, \underline{\Omega} = \nu_{av} \, \underline{B}_\omega \qquad (6.5.10)$$

The relationship between the time averaged stream function and the vorticity is similar to the laminar case; see equation (6.4.2). The boundary conditions are also the same. Subsequently the global form of the equations may be expressed as:

$$\underline{K} \, \underline{\Psi} - \underline{M} \, \underline{\Omega} = \underline{B}_\psi \qquad (6.5.11)$$

The set of matrix equations have been presented; it is now necessary to arrange them in a suitable form in order to integrate -through time.

6.6 The Solution Technique

As the fractional step technique is shown to produce successful results for many laminar problems, it is reasonable to extend its use to solving flow in the turbulent range.

Adopting this solution scheme as before it is necessary to express the solution equations in terms of time averaged variables and include the extra matrices.

The solution scheme may now be described:

(i) Input initial values of vorticity, $\underline{\Omega}_t$, and obtain values for stream function, see equation (3.3.2):

$$\underline{K}\ \underline{\Psi}_t = \underline{M}\ \underline{\Omega}_t \qquad (6.6.1)$$

(ii) An increment of stream function is now computed; see equation (3.3.3)

$$\left[\frac{\underline{K}}{\Delta t} - \underline{A}\ (\underline{\Omega}_t)\right]\ \underline{\Delta}\ \underline{\Psi} = \left[-\underline{A}(\underline{\Psi}_t)\ \underline{\Omega}_t - \nu_{av}\ \underline{K}\ \underline{\Omega}_t + T_1\ \underline{\Omega}_t - T_2\ \underline{\Omega}_t + S\ \underline{\Omega}_t\right] \qquad (6.6.2)$$

(iii) Writing the momentum formulation in terms of, $\underline{\Omega}_t$ and $\underline{\Psi}_{t+\Delta t}$ an increment of vorticity is computed, see equation (3.3.4).

$$\underline{M}\ \Delta\ \underline{\Omega} = -\Delta t\left[\underline{A}\ (\underline{\Psi}_{t+\Delta t})\ \underline{\Omega}_t + \nu_{av}\ \underline{K}\ \underline{\Omega}_t\right.$$

$$\left. - \underline{T}_1\ \underline{\Omega}_t + \underline{T}_2\ \underline{\Omega}_t - \underline{S}\ \underline{\Omega}_t - \nu_{av}\ \underline{F}_1\ \underline{\Psi}_{t+\Delta t} - \nu_a\ \underline{F}_2\ \underline{\Omega}_t\right] \quad (6.6.3)$$

(iv) By writing the momentum formulation in terms of $\underline{\Omega}_{t+2\Delta t}$ and $\Psi_{t+\Delta t}$ a futher increment of vorticity is obtained; see equation (3.3.5).

$$\left[\frac{\underline{M}}{\Delta t} + \underline{A}\ (\underline{\Psi}_{t+\Delta t}) + \nu_{av}\ \underline{K} - \underline{T}_1 + \underline{T}_2\right.$$

$$\left. - \underline{S} - \nu_{av}\ \underline{F}_2\right]\ \underline{\Delta}\ \underline{\Omega} = -\left[\underline{A}\ (\underline{\Psi}_{t+\Delta t}) + \nu_a\ \underline{K}\right.$$

$$\left. - \underline{T}_1 + \underline{T}_2 - \underline{S} - \nu_{av}\ \underline{F}_2\right]\ \underline{\Omega}_{t+\Delta t} + \nu_{av}\ \underline{F}_1\ \Psi_{t+\Delta t} \quad (6.6.4)$$

(v) Finally the stream function is updated by solving the Poisson formulation again.

$$\underline{K}\ \underline{\Psi}_{t+2\Delta t} = \underline{M\Omega}_{t+2\Delta t}$$

At this stage the turbulent viscosity is updated using the algebraic relation and the cycle starts again at step (ii). It must be remembered that although the problem is time dependent, as the unknowns are time averaged, the solution is expected to be steady for most turbulent flows. It is only in some special cases that the time averaged solution of a turbulent flow is unsteady.

In this chapter the problem of modelling turbulent flow is discussed. The implementation of a suitable solution approach is presented, based on the mixing length concept.

This is introduced to the existing (F.E) program in order to permit the solution of some turbulent problems. Finally the fractional step time integration scheme is adopted to solve these equations. Below the unidirectional flow within a two-dimensional channel is presented, starting with the laminar case and finally extending the solution to turbulent conditions.

6.7 The Developing Flow in a Channel

In the previous sections the methods of solving turbulent fluid flow problems are discussed with particular reference to the mixing length approach. Later this concept is applied to the existing laminar flow program.

Here the suitability of this model is assessed by calculating the developing flow in a two-dimensional channel. This may be considered a prototype of a wide range of more complex wall shear problems. Owing to its comparative simplicity it may be used as a test problem for any two-dimensional turbulent solution scheme.

In the developing flow of a channel the flow changes from a boundary type at the entrance to a fully developed type at some distance downstream. The boundary layer grows from zero at the entrance until it reaches the centre line of the channel at which point the freestream is completely screened.

Early methods of solving such flow problems involved suitable integral techniques. The assumptions made in order to permit such a

solution restrict their validity to the region where the freestream still has an influence, i.e. $0.0<x/A<15$, where A is the channel width.

Leading on from this a (F.D) solution of developing flow in a pipe was computed by solving the full time averaged stream function vorticity equations using the eddy viscosity concept to achieve closure of the equations, see Richman ad Azad [49].

More recently a (F.E) solution of the problem was reported by Hughes [19] employing the same closure techniques in terms of time averaged velocity and pressure.

Here the (F.E.M) is extended to solve the equivalent two-dimensional flow problem in terms of stream function and vorticity.

An identical comparison between developing pipe flow and channel flow is not expected. However similarities in the flow behaviour are expected.

(i) The Problem Description

Figure 6.2 illustrates the boundary distribution for developing flow in a channel. On the left hand or inlet boundary the vorticity is zero and the stream function is prescribed to be linear, thus providing a free stream parallel flow condition at the channel entrance.

The bottom longitudinal boundary is a no-slip wall. On the top boundary the stream function and the vorticity are both prescribed, this free-slip wall describes the centre line axis of symmetry of the channel. The downstream or outlet boundary is described in the usual way.

As the problem region is a rectangle the mesh discretization

may be simply described in terms of two arrays, the first containing the location of the nodes along the channel and the second containing the location of the nodes across the channel. Obviously the lateral variation of the flow variables is greatest close to the no-slip wall. Consequently the nodes across the channel must be placed closer together as the wall is approached. Similarly in the region adjacent to the entrance of the channel the lengthwise variations of flow are largest as the boundary layer grows. It is therefore necessary to position these nodes closer together in the entrance region.

It must be remembered that there is a singularity at the bottom left hand corner where the inlet boundary and the solid wall join. Here a drastic change in the flow field occurs, from the freestream velocity of the adjacent inlet node to the zero velocity condition on the no-slip wall. Consequently a fine discretization of this region is required.

Two meshes are used to solve this problem, where the longitudinal nodes are positioned at; 0.0,0.05,0.1,0.2,0.3,0.5, 0.75,1.0,1.5,3.0,5.0,10.0,20.0,30.0,40.0,60.0,80.0,100.0,120.0,140.0, 160.0,180.0,200.0. The nodal positions across the channel are; 0.0,0.01,0.025,0.05,0.075,0.1,0.15,0.2,0.3,0.4,0.5,0.6,0.7,0.8,0.9,1.0.

The second mesh has the same distribution of nodes along the channel but a finer distribution of nodes across it. This distribution is the same as that used by Richman and Azad, where the width of the channel is divided into twenty equal spaces. The first eighteen are retained with a further twelve nodes between the no-slip wall and the node at y=0.1, a geometric progression of 1:1.4 is used.

Since the (F.E) model assumes only a linear variation of the

unknowns a fine discretization of the domain is needed to describe the large flow variable gradients which prevail in turbulent flow conditions.

As a preliminary to solving the turbulent flow case and to provide suitable initial conditions for this problem the laminar case is computed.

(ii) The Laminar Flow Case

Implementing the original solution program as used in chapter five the channel problem is solved for Re=10,100,200,2500.

Finally the vorticity results obtained at Re=2500 are used as the initial values of the turbulent flow. It is known that the transition from laminar to turbulent flow occurs at about this Re.

The behaviour of developing flow can be described as the transition from the boundary layer at the entrance to a fully developed profile some distance downstream. In the case of laminar flow the fully developed velocity profile takes the form of a quadratic variation, as discussed in section 5.3. Results show this quadratic profile to exist, being described here by a cubic variation of stream function and a linear variation of vorticity across the channel in the fully developed region.

This pattern exists whatever the Re. However, by increasing it the developing region extends further into the channel as the fully developed region is pushed downstream. The Re is defined as $Re=AU/\nu$, where A is the channel width and U is the inlet velocity.

Figures 6.3 to 6.6 show the stream function and the vorticity

plots for the developing region at Re=10,100,200 and 2500. The contour levels are normalized; $\psi'=\psi/UA$ and $\omega'=-A\omega/U$.

At Re=10 the vorticity and stream function plots show a small transition region from the entrance to the fully developed flow region where both fields show contour lines running parallel to the flow direction, see figure 6.3. The vorticity results highlight the singular point at the lower left hand corner where even at such a low Re the gradients are large.

As the Re is increased the transition region extends further downstream and the fully developed region of flow is pushed further away from the entrance.

At the same time the large variations caused by the singularity also grow downstream. Finally at Re=2500 the vorticity plots look very unstable since it seems likely at this stage that the flow mechanisms are changing from laminar to turbulent, see figure 6.6.

A (F.E) solution of this problem was reported by Baker [12] using a stream function vorticity approach. Current results compare well with this work.

Figure 6.7 compares the velocity profiles in the developing region of flow for Re =200 and 2500 respectively. This illustrates how the fully developed region is forced downstream as the Re is increased. At Re=200 fully developed flow starts at approximately between x/A=1.5 to 2.5, whereas at Re=2500 it starts at between x/A=5.0 to 10.0.

Finally figure 6.8 shows the axial velocity along the channel at different distances across the channel at Re=2500. This clearly shows how the free stream velocity is diffused in the entrance region

resulting finally in a fully developed flow condition.

(iii) The Turbulent Case

Using the laminar vorticity field from the solution at Re=2500 as the initial conditions of the turbulent solution is obtained at this Re.

An algebraic closure of the equations is achieved where; κ=0.38 and A=26.0. The cut-off point for Van Driest's damping condition is at:

$$y_1 = \frac{\lambda}{\kappa}$$

$$\lambda = 0.09$$

κ - the universal mixing constant

These parameters are taken from a (F.D) solution by Oliver [55]. Where a solution to developing flow within a pipe is solved using a stream function vorticity approach. He introduced two different algebraic models one in terms of a variable mixing length throughout the boundary layer and another in terms of a variable viscosity throughout the layer. Little difference was found when comparing both methods.

Two meshes are used here to model the turbulent conditions. Figures 6.9 and 6.10 show the velocity profiles and the axial plots for both these meshes respectively.

Both results illustrate a marked change in the velocity distribution throughout the channel. The laminar velocity profile has now been replaced by a flatter profile across the channel. This is clearly displayed in figure 6.10 where the axial velocity is higher close to the wall and the centre line velocity is retarded.

Both the meshes produce similar flow configurations, with the coarse mesh producing a more diffused flow field. Also the finer mesh produces a smoother velocity field in the developing flow region.

This change is consistent with the theoretical mechanisms of turbulence. Where the transfer of momentum lateral to the flow direction results in a better distribution of the time averaged velocity across the channel.

This result is borne out by the velocity distribution obtained for flow in a circular pipe. A difference between the two types of flow occur close to the wall where the axial velocity at y=0.022 is markedly lower for the channel then for the pipe.

Since the solution of the turbulent equations invokes different flow mechanisms the stability requirement needs to be reconsidered. Preliminary tests show the existing time step to be inappropriate.

A lower time step is introduced, however it is beyond the bounds of this work to optimize this. Instead a reduced time step is used and a solution of the turbulent problem is computed initially with the coarser mesh.

When using the finer mesh the time step has become very small indeed. This is due to the size of the elements close to the wall coupled with the reduced stability of the turbulent mechanisms. It is necessary to by pass the inordinate amount of C.P.U time necessary to achieve a solution when using this fine mesh.

This is achieved by setting up the initial flow vorticity at each node of the mesh from the turbulent vorticity results obtained with the coarse one. A simple interpolation is employed to evaluate

each nodal point.

Finally this composed vorticity solution is iterated until the full resolution of the mesh is achieved.

The solution of this problem is very difficult owing to the reduced stability of the scheme. The above results however show a turbulent solution to be possible. It is very much at the upper limits of the solution scheme, since the C.P.U. time required for a solution is becoming large.

(iv) Conclusions to the Channel Problem

In this chapter the solution of developing flow in a two-dimensional channel is solved. Initially under laminar conditions and finally under turbulent conditions.

The laminar results comply with the expected behaviour with the flow starting as a boundary layer growth near the entrance and finally reaching a fully developed state some distance downstream. This displays the predicted parabolic velocity profile across the channel.

The turbulent solution is subsequently obtained using the laminar results as the initial conditions. Here the velocity profiles show a distinct contrast to the laminar case.

Owing to the reduced stability of the turbulent scheme it is necessary to compose initial flow values for the fine mesh solution. Any increase in the Re is ruled out owing to the large amount of C.P.U time required to achieve a solution.

It is felt that an adequate demonstration of the different effects of both flow mechanisms is presented and so the study is

concluded.

CHAPTER SEVEN

CONCLUSIONS

7.1 Conclusions

In this work a solution of te Navier-Stokes equations is obtained by the finite element method with the stream function and the vorticity taken as the dependent variables. Here the fluid is assumed to be incompressible and to have constant molecular viscosity.

In chapter three the solution scheme is presented for the time dependent non-linear equations. The fractional step technique applied to the uncoupled equations is adopted owing to its stability at high Re.

The problem of describing the vorticity behaviour on the no-slip wall is overcome by applying a limiting solution locally in the finite element formulation.

It became clear that although the finite element method has distinct advantages over the finite difference technique, the mesh discretization required to model a flow problem at a reasonable Re becomes intolerably fine close to the no-slip boundary. Consequently a mesh generation scheme is incorporated into the program in order to provide suitable mesh discretization with the minimum of effort.

Chapter four outlines how this user- orientated scheme works and later it explains how this scheme is adjusted to suit the particular needs of fluid flow conditions. For all the flow cases solved in this work a mesh generator is used to discretize the domain.

In chapter five three fluid flow problems are modelled for the laminar steady state range. Extensive comparison is made with earlier work, which highlights the strengths and weaknesses of the solution scheme.

In chapter six the problem of turbulent flow is discussed. The various methods by which closure of the time-averaged turbulent equations is achieved are mentioned here. Finally an algebraic form of the mixing length method is presented and a one dimensional turbulent flow in a channel is modelled by extending the original program.

To model a steady state problem by solving the time-dependent equations is considered, by finite difference workers in any case, to be less efficient then solving the steady state equations. It is found that considerably more iterations of the program are needed before an adequate result is achieved.

In the finite element method most of the numerical solutions quoted for comparative purposes adopt a solution of the steady state equations by the Newton-Raphson Method. The (N.R.M) is known to have a quadratic rate of convergence and is obviously likely to be more efficient when compared to the monotonic convergence of the linear time integration scheme, as is used here.

The disadvantage of the (N.R.M) is that the final solution is completely dependent upon the initial flow conditions applied. Consequently the scheme is prone to producing diverging solutions if care is not taken when defining the initial flow conditions. On the other hand the time-dependent scheme is not so sensitive to this and should not diverge, providing the time step does not exceed a certain value. This is a distinct advantage in very unstable problems where the possibilities of divergence are greater, e.g the flow over a step. As long as the time step is small enough the solution will converge.

An empirical formula is used to define the upper limit of the

required time step. A distinction must be made between any converging solution and a correct converging solution. As the Re increases the upper limit of the time step also increases and at some point this exceeds the time step limit required to model any flow condition for that particular mesh.

In order to speed up the solution scheme a variety of time step schemes have been tried to model the flow within a square cavity. The time step during the program run is taken to be a function of the gradient of the vorticity with time at the current cycle. Various functions are used, it is thought that when the gradient is small the time step can increase, and when it is large the time step must be reduced.

The result of this work is very inconsistent: however, in some cases the problem converged with as much as a 50% reduction in the number of iterations. No overall guidelines are obtained since the results appeared not only to be mesh dependent but they also varied as the flow conditions changed.

Leading on from this work efforts to try to improve the time integration scheme using a constant time step were tried. Instead of the fully implicit integration scheme adopted in the fractional step technique, a parital integration can be carried out by introducing a coefficient - to the matrix equation. In some cases this is considered to provide a better integration technique. Here again the square cavity problem is run with $\gamma=2/3$ the Galerkin technique and $\gamma=1/2$ the Crank-Nicholson technique. No significant change in the rate of convergence is found by using either scheme.

Finally the Runge-Kutta integration scheme is adopted. Here

four values of the preceeding increment of the unknown are computed and the actual increment is taken as the sum of the four values weighted separately. As this scheme computes a better estimate of the next increment when compared to the Eulerian scheme it is hoped that the time step may be enlarged. However, results show that the time step could not be increased significantly before the solution diverged. As the Eulerian scheme is much faster over each iterarion it is used in preference. However, the Runge-Kutta scheme may still be useful for particularily unstable problems where a more accurate integration scheme is needed to obtain a converging result.

It is concluded that more knowledge is required about the mechanisms of time-integration for such non-linear problems. This is demonstrated by the inconsistent results reported above. These mechanisms are obviously more complicated than first thought. In order to improve the existing time integration scheme a fuller understanding of them is required. This is obviously a worthwhile area of further research.

In some preliminary work using the fractional step technique the solution of flow past a cylinder is computed using double precision variables. Since the problem is non-linear it is important to ensure that the numerical errors accumulated over a succession of iterations do not significantly effect the resultant flow. All the computation is carried out on the IBM 360/195 machine at Rutherford: since a real variable has only four bytes per word this is a reasonable consideration.

The double precision results compared well with those of the single precision, and so the possible numerical errors are small.

However, it is important to note that this double pecision run required about 20% fewer cycles to reach convergence. This indicates that the numerical errors resulting when using single precision only have the effect of delaying the convergence. It would be ideal to run all the examples in double precision: however, since this drastically increases the size of the problem the single precision is used instead.

The description of the vorticity along the no-slip boundary, as described in chapter three, is shown to produce successful results. As this is not a prescribed condition it is non-linear and its effect converges as the solution is achieved. Different methods of applying this condition are tested in order to improve the description of the flow behaviour in this region.

Various methods of implementing the natural boundary conditions using the limiting equation as defined by Gosman are applied when solving the flow within a square cavity. As a result the implementation as outlined in chapter three provides the best description of the limiting equation along the no-slip wall.

Recent work has been reported where the flow problem is solved in terms of stream function and vorticity with the no-slip vorticity condition being applied more directly.

Work by Campion-Renson and Crochet [56] redefined the uncoupled Galerkin formulations of the governing equations. In this way the need to provide a vorticity condition on the no-slip boundary is by-passed and the gradient of the stream function w.r.t the normal is applied along the boundary. A successful solution to flow within a square cavity is obtained using this approach.

Secondly, work by Dhatt, Bonaventure and Bourque [57] produced a solution scheme in terms of vorticity and stream function for the steady state problem. Using the coupled equations the vorticity no-slip boundary condition has again been by-passed in a more direct manner. This time the normal gradient of the stream function is employed to determine the boundary value of vorticity. Again successful results of the square cavity problem are obtained.

Both techniques apply the no-slip condition directly: consequently the convergence of the problem is fast. There is little difference between the two schemes reported here: obviously the coupled scheme is a more direct application. The improvement of the no-slip vorticity condition is necessary in order to speed up the rate of convergence of the solution scheme. Such direct methods outlined above provide a good line for further research.

Having carried out a series of tests applying different time integration schemes and no-slip boundary applications, the scheme presented in chapter three is finally adopted.

The first problem of flow within a square cavity produced good agreement with earlier numerical solutions. In solving this enclosed example the problem of describing the flow about a corner comes to light. These corner points are considered to be areas where the flow is singular. In any numerical calculation such regions are discretized very finely, thus endeavouring to keep the errors caused by the singularity localised. In a recent paper by Gupta and Manohar [58] the errors caused by the local discretization about these corner points have been studied. The conclusion is that greater inaccuracies occur in a corner where two stationary walls meet compared to a corner where

one wall is moving, i.e. the top corners of the cavity. This conclusion is borne out by the results presented here. Similar inaccuracies occur in both the bottom corners of the cavity and also in the corners of the downstream step problem.

This corner problem is well known in the general field of continuum mechanics. In structural problems elaborate techniques have been developed, by the introduction of double nodes for example, to overcome the abrupt change in direction of the boundary. Such methods could also be applied to the fluid problem. The problem of approximating the flow about a singular point is aggravated here where a linear variation of the unknowns has been chosen over each element.

The second problem considered is the flow over a downstream facing step. Here good agreement is found with both earlier numerical and experimental results. This is a particularly unstable problem owing to the presence of two corner regions. Further improvement of the present results is possible if the exact experimental inlet velocity profiles are prescribed. In conjunction a finer mesh discretization of the top region is required to deal with the parabolic flow.

The third problem chosen is the flow past a circular cylinder. The solution encompasses the steady state solution from the slow Stokesian flow through separation and up to the beginning of the unsteady state. The linear elements are causing some advance in the flow conditions due to describing an uneven cylinder wall.

The solution of all these examples has underlined the limitations of the linear element solution scheme. However, they show that good agreement can be achieved if a fine discretization of the

domain is used. In order to improve the quality of the results further it is felt that more sophisticated elements must be introduced. This is demonstrated in the cylinder problem where the vorticity solution could be improved by the introduction of superparametric elements along the cylinder boundary. This would improve the integration about the boundary, since each element side would describe a curve instead of a straight line.

The solution could be further improved by introducing quadratic elements, then the cylinder boundary could be described by isoparametric elements.

Work at Swansea has reported the use of elements about the no-slip wall which assume a logarithmic variation of the unknowns. The solution of flow problems at large Re has proved to be much simpler with the use of such sophisticated elements.

The introduction of upwinding weighting functions has found favour with some as a means of overcoming the problems which occur when the inertial effects become significant. This technique, which is similar to the directional differencing technique in finite difference, has been the subject of much controversy: however: some favourable results have been produced with it.

The solution of vorticity has consistently been in better agreement with earlier results then the solution of stream function. This is clearly seen in the contour levels of flow past a cylinder. A similar trend occurs for the finite element solution of Tuann and Olson. However in this case the stream function results are considerably better then the vorticity.

It is postulated that both discrepancies occur for similar reasons. In Tuann the flow is solved in terms of stream function and the vorticity is calculated from it once the stream function solution has reached convergence. Here the equations are solved in an uncoupled form with the vorticity as the leading variable and the stream function being updated periodically. The solution of stream function relies exclusively on the quality of the approximate vorticity solution. This is a major criticism of the uncoupled approach since the solution achieved has a staggered nature. The advantage of the uncoupled approach is that the number of unknowns is reduced, halved in this case, consequently reducing the size of the system matricies and the computer time per cycle for the same mesh. This can be very significant when a linear discretization is adopted since a large number of nodes are required to describe a flow problem.

In chapter six the existing solution program is extended to model wall turbulence by means of an algebraic closure of the time averaged equations. The solution of developing flow in a channel is presented.

Initially a laminar solution is obtained and the resulting flow is consistent with previous work. Leading on from this a turbulent solution is produced which shows a different flow distribution. There is a marked reduction in stability of the scheme due to the introduction of these turbulent terms.

This result illustrates how the complicated three-dimensional mechanisms may be reduced to simple localized effects. Obviously in general this is a gross simplification of the problem however it proves reasonable in this specific case.

In order to pursue this study an improvement of the solution scheme is required. The introduction of a logarithmic variation of the flow variables in the near wall region would clearly reduce the number of elements required close to the wall.

Conversley a technique has been applied by Oliver [55] and latterly by Hughes [19] where the near wall region is described by the law of the wall equations directly. This means that only the region away from the wall need be solved numerically. This again reduces the overall size of the mesh required. Moreover these suggestions will increase the size of the elements as a consequence the time step for solution would be larger.

As can be seen from the above discussion the solution of fluid flow problems by numerical methods is by no means complete. Many avenues of reseach are still left open.

In this research a variety of flow problems has been solved by numerical methods. The scheme developed is designed to describe the problem, solve it, and finally to process the results completely automatically.

Below a list of recommendations of further work resulting from this study is presented.

7.2 Recommendations

(i) The introduction of a direct application of the no-slip boundary. This will have the effect of improving the rate of convergence.

(ii) The development of a steady state solution of the equivalent coupled equations. By employing the Newton-Raphson

technique the rate of convergence would improve.

(iii) Increase the order of the interpolation functions.

A quadratic interpolation within each element would provide a better description of the near wall region. (N.B.: The mesh generating system can also produce triangles containing six nodes).

(iv) The introduction of special wall elements for the no-slip boundary. Since the variation of unknowns in this region is large, more sophisticated elements would provide a better description of the flow.

(v) The development of the equivalent axisymmetric scheme, this would enable the modelling of a variety of pipe flow problems. Many solutions are available for pipe flow especially in the turbulent range.

(vi) The investigation of the mechanisms behind the development of time integration solutions. This work would enable the introduction of a reliable variable time step scheme which would make the solution faster.

REFERENCES

[1] Thom ,A. 'Flow Past a Circular Cylinder at Low Speeds'. Proc. Royal Society London a141 (1933) pp.651-669.

[2] Kawaguti, M. ' Numerical Solution of the Navier-Stokes Equations for the Flow Around a Circular Cylinder at Reynolds Number of 40'. J. Physical Soc. Japan 8 No.6 (1953) pp.747-757.

[3] Apelt, C.J. ' The Steady Flow of a Viscous Fluid Past a Circular Cylinder at Reynolds Numbers 40 and 44 '. Tech. Report of the Aeronautical Research Council: Report and Memorandum No. 3175 96 Voll pp.1-15. (1958)

[4] Gosman, A.D.; Pun, W.M.; Runchal, A.K; Spalding, D.B. and Wolfshtein, M. ' Heat and Mass Transfer in Recirculating Flows '. Academic Press (1969).

[5] Zienkiewicz, O.C. and Godhole, P.N. ' Viscous Incompressible Flow with Special Reference to Non-Newtonian (Plastic) Fluids '. ' Finite Elements in Fluids 1 - Viscous Flow and Hydrodynamics '. edited by Gallagher, R.H. et al John Wiley and sons (1975).

[6] Taylor, C. and Hood, P. ' A Numerical Solution of the Navier-Stokes Equations Using the Finite Element Technique'. Computers and Fluids 1 (1973) pp.73-100.

[7] Kawahara, M.; Yoshimura, N.; Nakagawa, K. and Ohsaka, H. ' Steady and Unsteady Finite Element Analysis of Incompressible Viscous Fluid '. Int. J. Num. Meth. Engng., 10 (1976) pp.437-456.

[8] Nickell, R.E.; Tanner, R.I. and Caswell, B. ' The Solution of Viscous Incompressible Jet and Free-Surface Flows Using Finite Element Methods'. J. Fluid Mech. 65 pt.1 (1974) pp. 189-206.

[9] Fortin, M. ' Approximation des Fonctions a Divergence Nulle par la Methode des Elementes Finis '. Proc. 3rd Int. Conf. on Numerical Methods in Fluid Mechanics, 1 (1972) Ed. Cabannes, H. and Temam, R.

[10] Tuann, S. and Olson, M.D. ' A Study of Various Finite Element Solution Methods for the Navier-Stokes Equations'. The University of British Colombia, The Dept. Civil Eng. Structural Report Series No.14 (1976)

[11] Burggraf, O.D. ' Analytical and Numerical Studies of the Structure of Steady Separated Flows'. j. Fluid Mech. 24 pt.1 pp.113-151 (1966)

[12] Baker, A.J. ' Finite Element Solution Algorithm for Viscous Incompressible Fluid Dynamics'. Int. J. Num Meth Engng. 6 pp.89-101 (1973)

[13] Cheng, R.T. 'Numerical Solution of the Navier-Stokes Equations by the Finite Element Method'. The Physics of Fluids 15 No.12 pp. 2098-2105 (1972)

[14] Smith, S.L. ' Solution of the Navier-Stokes Equations for Transient Two-Dimensional Incompressible Flow by the Finite Element Method'. Ph.D. Thesis Southampton Univ. (1977)

[15] Nelson, J. ' An Interpertive Finite Element Problem Orientated Language for Hydraulic Engineering'. Ph.D. Thesis Southampton Univ. (1977)

[16] Prandtl, L. ' Bericht uber Untersuchungen zur Ausgebildeten Turbulenz'. ZAMM 5 p.136-139 (1925)

[17] Cebeci, T. and Smith, A.M.O. ' A Finite Difference Solution of the Incompressible Turbulent Boundary Layer Equations by an Eddy Viscosity Concept'. Proc. Computation of Turbulent Boundary Layers - 1968', AFOSR-IFP Stanford Conf. Stanford Univ. Dept. Mech. Eng. pp.346-355 (1968)

[18] Patankar, S.V. and Spalding, D.B. ' Heat and Mass Transfer in Boundary Layers'. 2nd. Edition, Intertext Books London (1970)

[19] Hughes, T.G. ' An Investigation of Turbulent Flow Models Using the Finite Element Method'. Ph.D. Thesis Swansea Univ. (1978)

[20] Malvern, L.E. ' Introduction to the Mechanics of a Continuous Fluid'. Prentice Hall (1969)

[21] Gallagher, R.H.; Oden, J.T.; Taylor, C. and Zeinkiewicz, O.C. ' Finite Elements in Fluids'. John Wiley and Sons London (1975)

[22] Brebbia, C.A. and Connors, J.J. ' Fundamentals of Finite Element Techniques for Structural Engineers'. Butterworths, London (1973)

[23] Zienkiewicz, O.C. ' The Finite Element Method'. McGraw Hill (UK) 3rd Edition (1977) 3rd. Edition (1977)

[24] Finlayson, B.A. and Scriven, L.E. ' On the Search for Variational Principles'. Int. J. Heat Mass Transfer 10 pp.799-821 (1964)

[25] Finlayson, B.A. and Scriven, L.E. ' The Method of Weighted Residuals - A Review'. Applied Mechanics Review 19, No.9 pp. 735-748 (1966)

[26] Brebbia, C.A. and Ferrante, A.J. ' Computationnal Methods for the Solution of Engineering Problems'. Pentech Press 2nd. Edition (1979)

[27] Coutanceau, M. and Bouard, R. ' Experimental Determination of the Main Features of the Viscous Flow in the Wake of a Circular Cylinder in a Uniform Translation. Part 1: Steady Flow'. J. Fluid Mech. 79 pt.2 pp.231-256 (1977)

[28] Payne, R.B. ' Calculation of Unsteady Viscous Flow Past a Circular Cylinder'. J. Fluid Mech. 4 pp.81-86 (1957)

[29] Ingham, D.B. ' Note on the Numerical Solution for Unsteady Viscous Flow Past a Circular Cylinder'. J. Fluid Mech. 31 pp.815-818 (1968)

[30] Hutton, A.G. ' Incompressible Viscous Flow Modelling by the Method of Finite Elements'. CEGB Report No. RD/B/N4209 (1977)

[31] Nelson, J.M. ' Fehpol User's Guide'. Internal Report Dept. of Civil Eng. Univ. Southampton (1977)

[32] Tuann, S. and Olson,M.D. ' Studies of Rectangular Cavity Flow with Reynolds Number by a Finite Element Method'. The Univ. of British Colombia, Dept. of Civil Eng. Structural Research Series Report No.19 (1977)

[33] Denham, M.K. and Patrick, M.A. ' Laminar Flow over a Downstream Facing Step in a Two-Dimensional Channel'. Trans. Instn Chem. Engnrs. 52 pp.361-367 (1974).

[34] Atkins, D.J.; Maskell, S.J. and Patrick, M.A. ' Numerical Prediction of Separated Flows'. Int. J. Numer. Meth. Engng. 15 pp.129-144 (1980)

[35] Hutton, A.G. and Smith, R.M. ' The Prediction of Laminar Flow over a Downstream Facing Step by the Finite Element Method'. CEGB Report No. RD/B/N3660 (1979)

[36] Thomas, C.E.; Morgan, K. and Taylor, C. ' A Finite Element Analysis of Flow Over a Backward Facing Step'. Computers and Fluids 9 pp.265-278 (1981)

[37] Leone, J.M. and Gresho, P.M. ' Finite Element Simulations of Two-Dimensional Viscous Incompressible Flow over a Step'. J. Comp. Physics 41 pp.167-191 (1981)

[38] Allen, D.N. and Southwell, R.V. ' Relaxation Methods Applied to Determine the Motion in Two-Dimensions of a Viscous Fluid Past a Fixed Cylinder'. Quart. J. Mech. Appl. Math. 8 pp.129-145 (1955)

[39] Kawaguti, M. and Jain, P. ' Numerical Study of a Viscous Fluid Flow Past a Circular Cylinder'. J. Physical Soc. Japan 21 pp.2055-2062 (1966)

[40] Thoman, D.C. and Szewczyk, A.A. 'Time Dependent Viscous Flow over a Circular Cylinder'. Physics of Fluid Suppl.II 12 pp.76-87 (1969)

[41] Dennis, S.C.R. and Chang, G. ' Numerical Solutions for Steady Flow Past a Circular Cylinder at Reynolds Number up to 100'. J. Fluid Mech. 42 pp.471-489 (1970)

[42] Takami, H. and Keller, H.B. ' Steady Two-Dimensional Viscous Flow of an Incompressible Fluid Past a Circular Cylinder'. Physics of Fluids Suppl.II 12 pp.51-56 (1969)

[43] Nieuwstadt,F. and Keller, H.B. ' Viscous Flow Past Circular Cylinders'. Computors and Fluids 1 pp.59-71 (1973)

[44] Taneda, S. ' Experimental Investigation of the Wakes Behind Cylinders and Plates at Low Reynolds Number'. J of Phys. Soc. Japan 11 pp.302=307 (1956)

[45] Acrivos, A.; Leal, L.G.; Snowden, D.D. and Pan, F. ' Further Experiments on Steady Separated Flow Past Bluff Objects', J. Fluid Mech. 34 pp.25-48 (1968)

[46] Tuann, S. and Olson, M.D. ' Numerical Studies of the Flow Around a Circular Cylinder by a Finite Element Method'. The Univ. of British Columbia, Dept. of Civil Eng., Structural Research Series, Report No.16 (1976)

[47] Escudier, M.P. ' The Distribution of the Mixing Length in Turbulent Flows near Walls'. Imperial Collage, Dept. of Mech. Eng. TWF/TN/1 (1965)

[48] Reynolds, W.C. ' Computation of Turbulent Flows -State-of-the -Art'. Stanford Univ., Dept. Mech. Eng., Thermosciences Division Report MD-27 (1970)

[49] Richman, J.W. and Azad, R.S. ' Developing Turbulent Flow in Smooth Pipes'. Appl. Sci. Res. 28 pp.419-441 (1973)

[50] Birch, S.F. ' Turbulent Length Scales in Non-Equilibrium Flow'. Proc. 1st. Int. Conf. ' Numerical Methods in Laminar and Turbulent Flow', Univ. Coll. Swansea (1978)

[51] Hinze, J.O. ' Turbulence, an Introduction to its Mechanism and Theory'. McGraw-Hill (1959)

[52] Townsend, A.A. ' The Structure of Turbulent Shear Flow' Cambridge Univ. Press (1956)

[53] Van Driest, E.R. ' On Turbulent Flow Near a Wall'.
J. Aeronaut. Sciences 23 pp.1007-1011 (1956)

[54] Launder, B.E and Spalding, D.B. ' Mathematical Models
of Turbulence'. Academic Press (1972)

[55] Oliver, A.J. ' An Analysis of Developing Turbulent Flow in a Tube
- A Comparison of Two Turbulence Models'. CERL RD/L/N 105/72 (1972)

[56] Campion - Renson, A. and Crochet, M.J. ' On the Stream Function
- Vorticity Finite Element Solution of Navier - Stokes Equations'.
Int. J. Num. Meth. Engng. 12 pp.1809-1818 (1978)

[57] Dhatt, G.; Bonaventure, K.F. and Bourque, G. ' A (ψ,ω) Finite
Element Formulation for the Navier Stokes Equations'. Int. J. Num.
Meth. Engng. 17 pp.199-212 (1981)

[58] Gupta, M.M. and Manohar, R.P. ' The Nature of Viscous Flow Near
Sharp Corners'. Computers and Fluids 9 pp.379-388 (1981)

B I B L I O G R A P H Y

(1) Batchelor, G.K. ' An Introduction to Fluid Mechanics'. Cambridge Univ. Press, (1967)

(2) Bradshaw, P. ' The Use of Transport Equations for Reynolds Stress'. Internal Report Dept. of Aeronautics Imperial Collage

(3) Bradshaw, P. ' The Understanding and Prediction of Turbulent Flow '. Aeronaut. J. 6 p. 403 (1972)

(4) Bradshaw, P. ' Turbulence '. Topics in Applied Physics 12 Springer-Verlag (1976)

(5) Castro, I.P. and Robins, A.G. ' The Flow around a Surface-Mounted Cube in Uniform and Turbulent Streams'. J. Fluid Mechs. 79 II pp. 307-335 (1977)

(6) Cebeci, T. and Smith, A.M.O. ' Analysis of Turbulent Boundary Layers'. Applied Mathematics and Mechanics 15 Academic Press (1974)

(7) Connors, J. and Brebbia, C.A. ' Finite Element Techniques for Fluid Flow'. Newnes-Butterworth London 1976

(8) Douglas, J. and Dupont, T. ' Galerkin Methods for Parabolic Equations '. SIAM J. Num. Anal 7 pp. 575-626 (1970)

(9) Finlayson, B.A. and Scriven, L.E. 'The Method of Weighted Residuals and its Relation to Certain Variational Principles for the Analysis of Transport Processes'. Chem. Engng. Sci. 20 pp. 395-404 (1965)

(10) Goldstein, S. ' Modern Developments in Fluid Dynamics'. Oxford Univ. Press (1938)

(11) Gresho, P.M.; Lee, R.L.; Sani, R.L and Stullich, T.W. ' On the Time-Dependent FEM Solution of the Incompressible Navier-Stokes Equation in Two and Three-Dimensions'. Lawrence Livemore Laboratory Preprint UCRL-81323 (1978)

(12) Gresho, P.M.; Lee, R.L. and Sani, R.L. ' On the Time-Dependent Solution of the Incompressible Navier-Stokes Equations in Two and Three-Dimensions'. Lawrence Livemore Laboratory Preprint UCRL-83282 (1978)

(13) Gupta, M.M. and Manohar, R.P. ' On the Use of Central Difference Scheme for Navier-Stokes Equations'. Int. J. Num. Meths. Engng. 15 pp.557-573 (1980)

(14) Hutton, A.G. ' A Survey of the Theory and Application of the Finite Element Method in the Analysis of Viscous Incompressible Newtonian Flow'. CEGB Report No. RD/B/N3049. (1974)

(15) Hussain, A.K. and Reynolds, W.C. ' Measurements in Fully Developed Turbulent Channel Flow'. Trans A.S.M.E. pp.568-580 (1975)

(16) Kreysig, E. 'Advanced Engineering Mathematics'. Wiley 4th Edition (1979)

(17) Lambe, H. ' Hydrodynamics'. Cambridge Univ. Press 6th Edition (1932)

(18) Massey, B.S. ' The Mechanics of Fluids'. Van Nostrand Reinhold 3rd Edition (1975)

(19) Milne-Thompson, L.M. ' Theoretical Hydrodynamics'. Macmillan Press Ltd. 5th Edition (1977)

(20) Morgan, K.; Hughes, T.G. and Taylor, C.' The Analysis of Turbulent, Free-Shear and Channel Flows by the Finite Element Method'. Computer Meth. Appl. Mechs.-Engng. 19 pp.117-125 (1979)

(21) Oden, J.T. 'Finite Element Methods of Non-Linear Continuae'. McGraw Hill (1972)

(22) Roache, P.J. ' Computational Fluid Dynamics'. Hermosa Press Albuquerque (1972)

(23) Schlichting, H. ' Boundary Layer Theory'. McGraw Hill (1968)

(24) Taylor, C; Hughes, T.G. and Morgan, K. ' A Numerical Analysis of Turbulent Flow in Pipes'. Computers and Fluids 5 pp. 191-204 (1977)

(25)Taylor, C.; Hughes, T.G. and Morgan, K. ' Finite Element Solution of One-Equation Models of Turbulent Flow'. J. Comp. Phys. 29 pp. 163-172 (1978)

(26) Taylor, C.; Morgan, K. and Brebbia, C. ' Numerical Numerical Methods Laminar and Turbulent Flow'. Proc. 1st Int. Conf. Swansea (1978)

(27) Tottenham, H. and Brebbia, C. ' Finite Element Techniques in Structural Mechanics'. Stress Analysis Publs. (1970)

(28) Tuann, S. and Olson, M.D. ' Computing Methods for Recirculating Flow'. J. Comp. Physics 29 pp. 1-19 (1978)

(29) Tuann, S. and Olson, M.D. ' A Transient Finite Element Solution Method for the Navier-Stokes Equations' Computers and Fluids 6 p. 141 (1978)

(30) Wootton, L.R.; Warner, M.H.; Sainsbury, R.N. and Cooper, D.H. ' Oscillations of Piles in Marine Structures - A Description of the Full-Scale Experiments at Immingham'. CIRIA Tech. Note 40 (1972)

(31) Wylie, C.R. ' Advanced Engineering Mathematics' McGraw Hill (1975)

(32) 'Modern Computing Methods'. Notes on Applied Science No. 16 Science No. 16 2nd Edition HMSO National Physics Laboratory

(33) ' Finite Element Methods in Flow Problems'. 2nd Int. Symp. Ligure, Italy (1976).

(34) ' Computation of Turbulent Boundary Layers '. AFOSR-IFP- Stanford Conference (1968) McGraw Hill (1972)

F I G U R E S

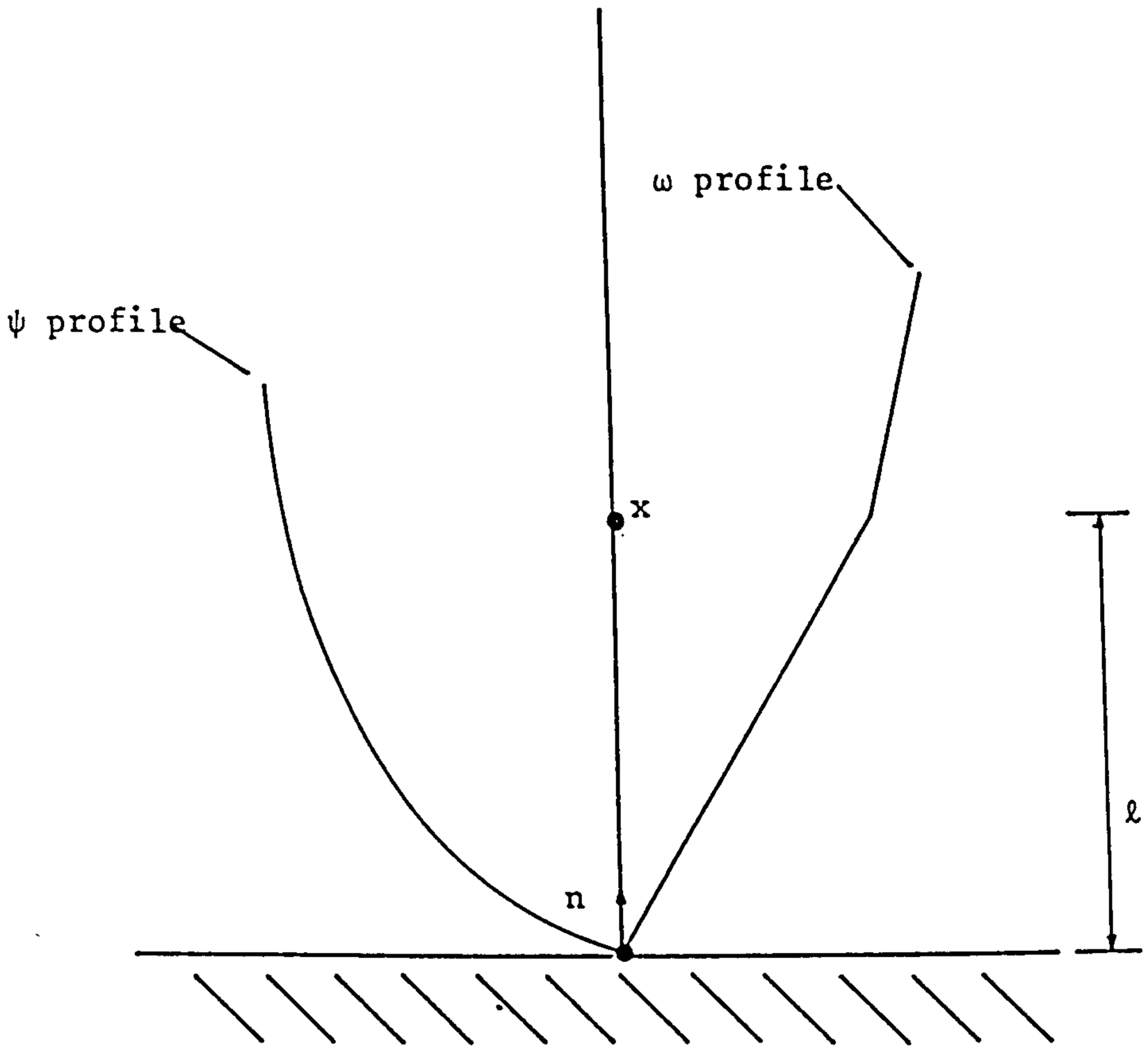

Figure 3.1 The No-slip Wall

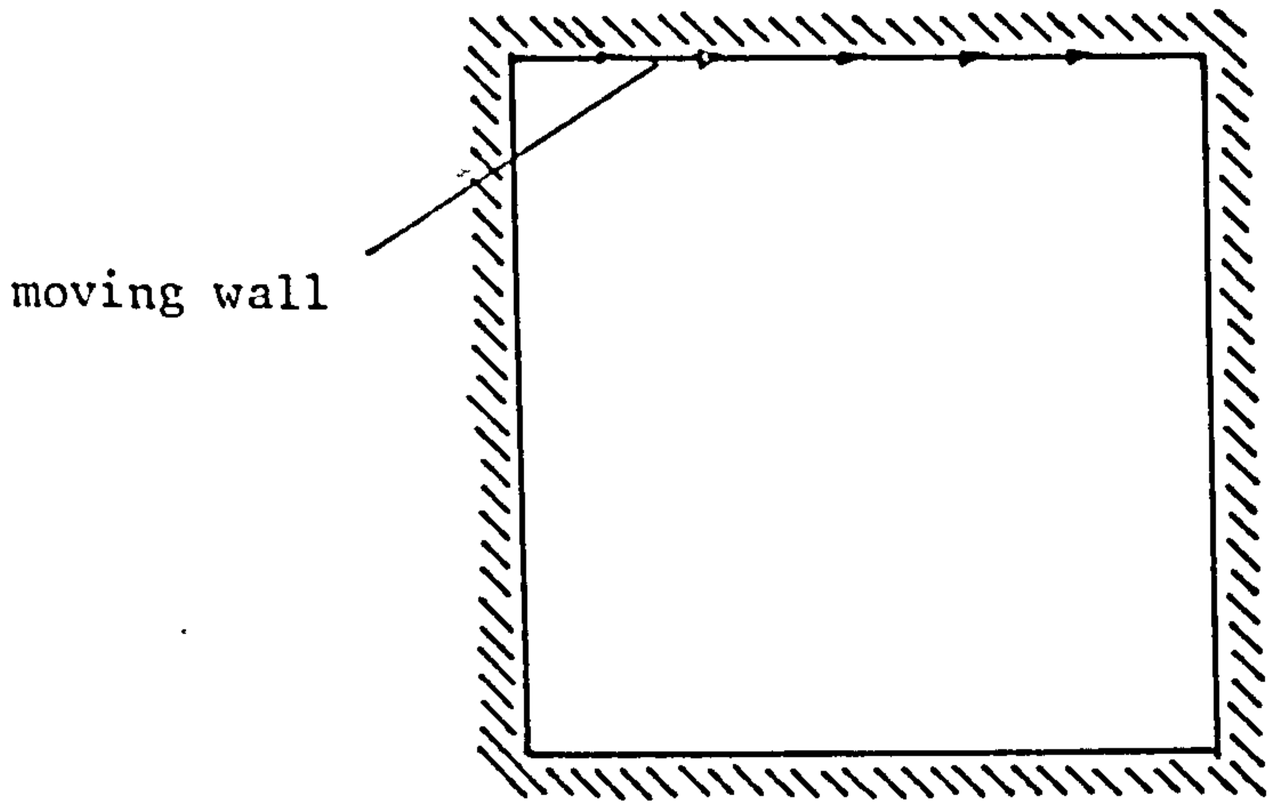

(a) An enclosed problem; the complete boundary is a no-slip wall

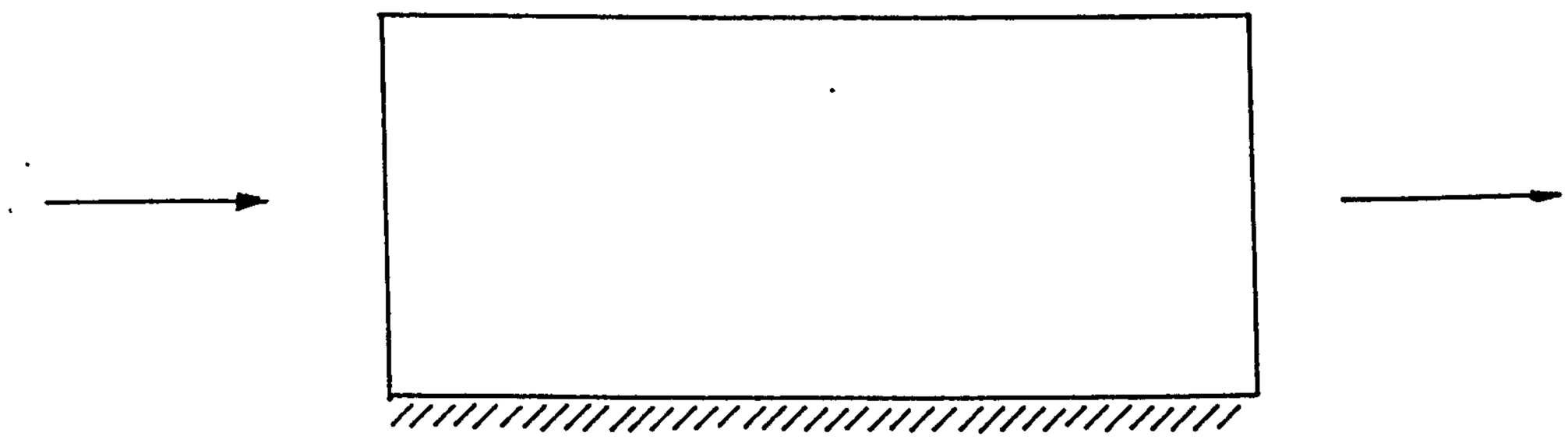

(b) An open problem, the bottom is a no-slip wall, the left-hand and top boundary is a free-slip wall and the right-hand boundary is an outlet.

Figure 4.1 List of Boundary Configurations

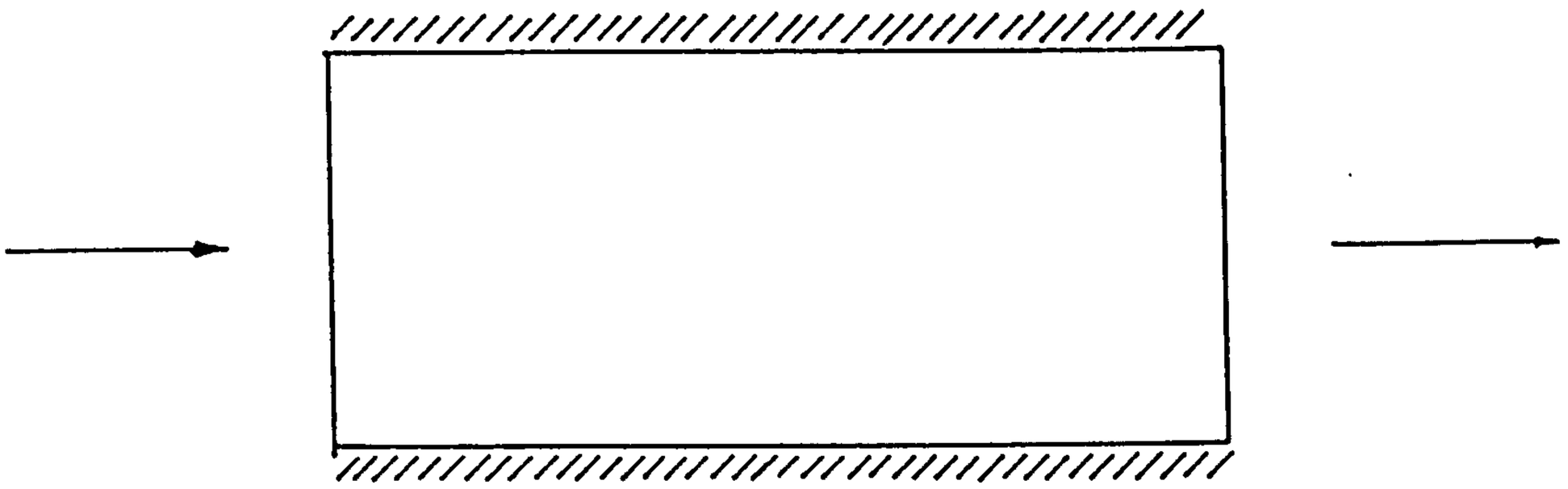

(c) A channel problem, both sides are no-slip boundaries, the left-hand side boundary is a free-slip and the right-hand boundary is an outlet.

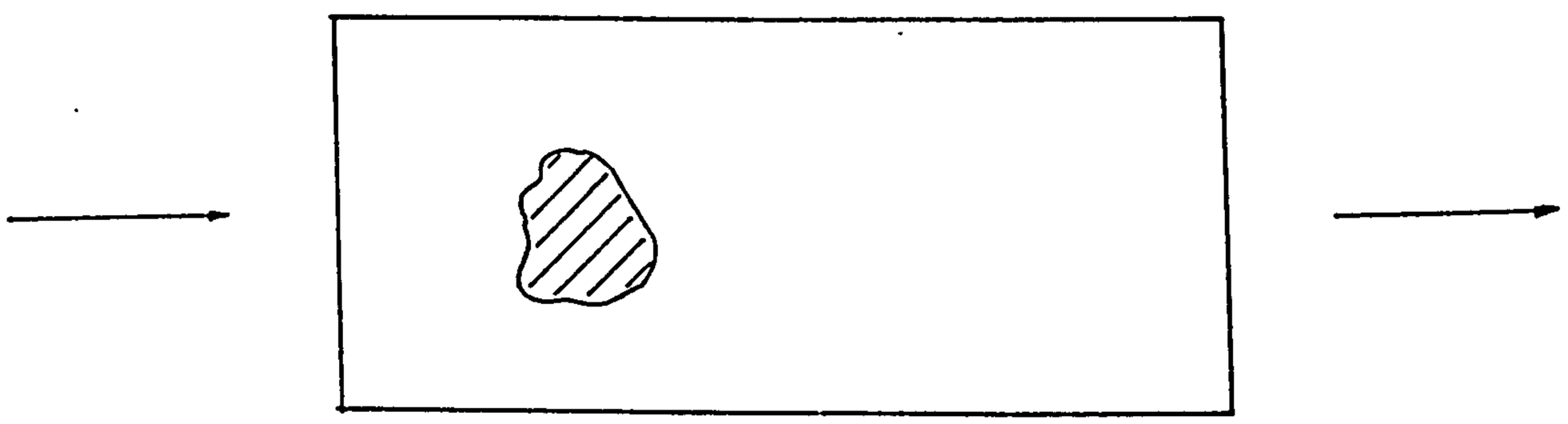

(d) a bluff body problem, the obstruction is no-slip, the two sides and the inlet boundary are free-slip and the right-hand boundary downstream is an outlet.

Figure 4.1 List of Boundary Configurations Continued

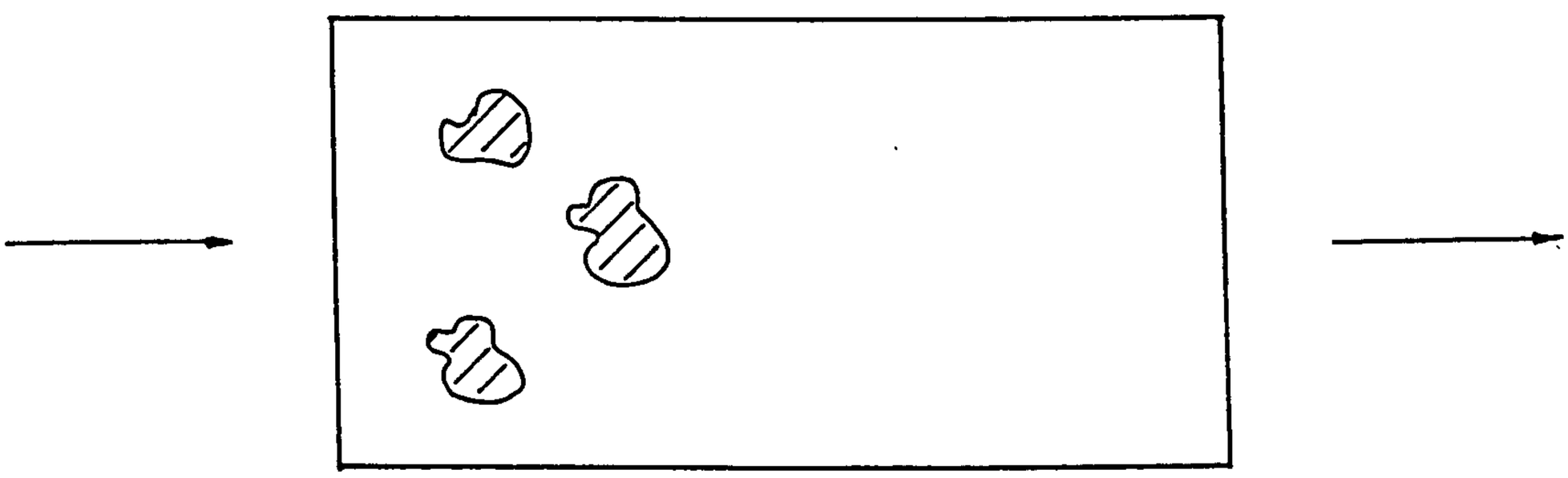

(e) As for (d) but with a multi-obstruction no-slip boundary.

Figure 4.1 List of Boundary Configurations Continued

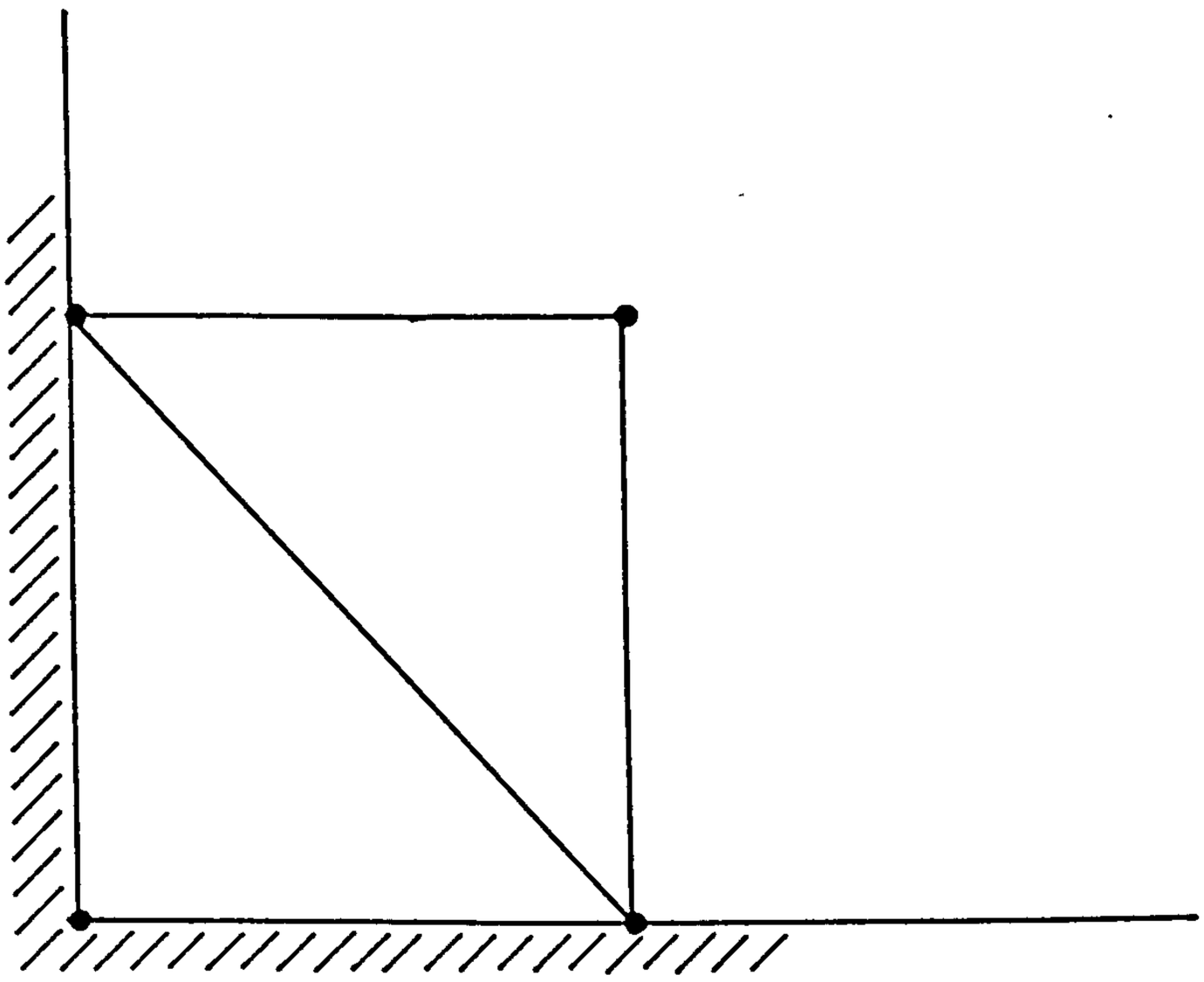

(a) Likely element distribution generated by mesh program.

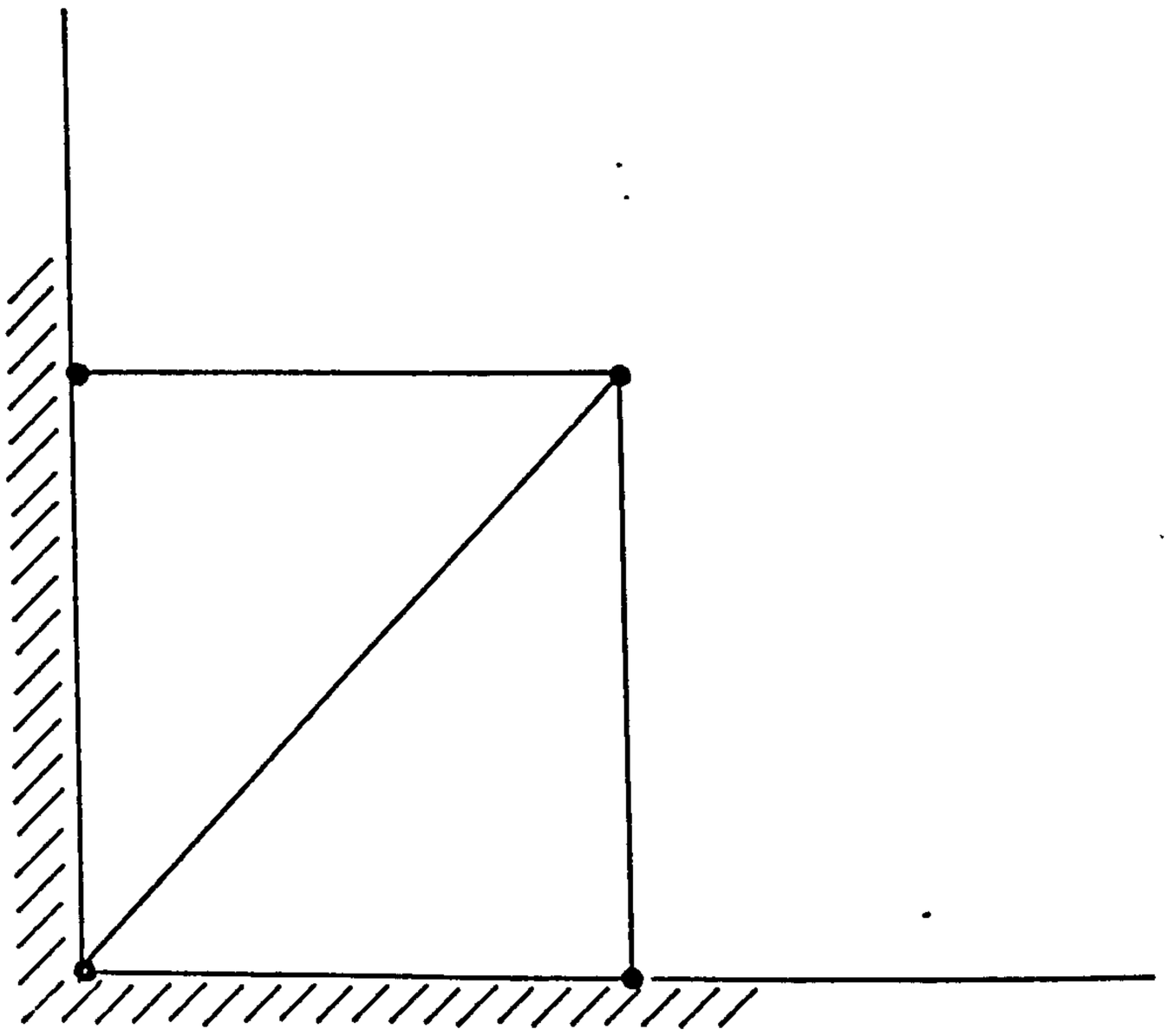

(b) Such elements need to be located and adjusted

Figure 4.2 Correcting the Corner Region Discretization

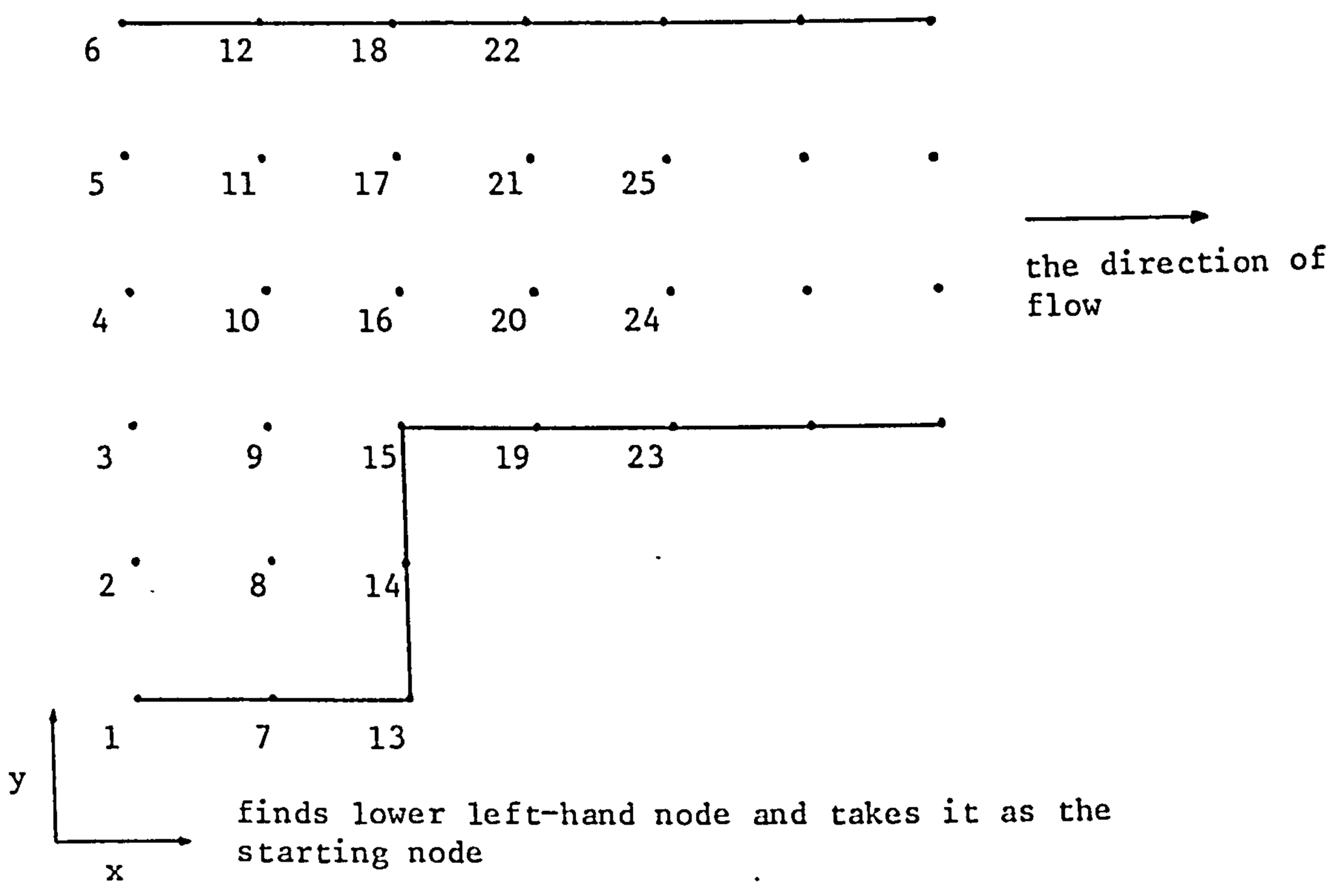

Figure 4.3 The Optimum Node Numbering Scheme for a Domain Describing Unidirectional Flow.

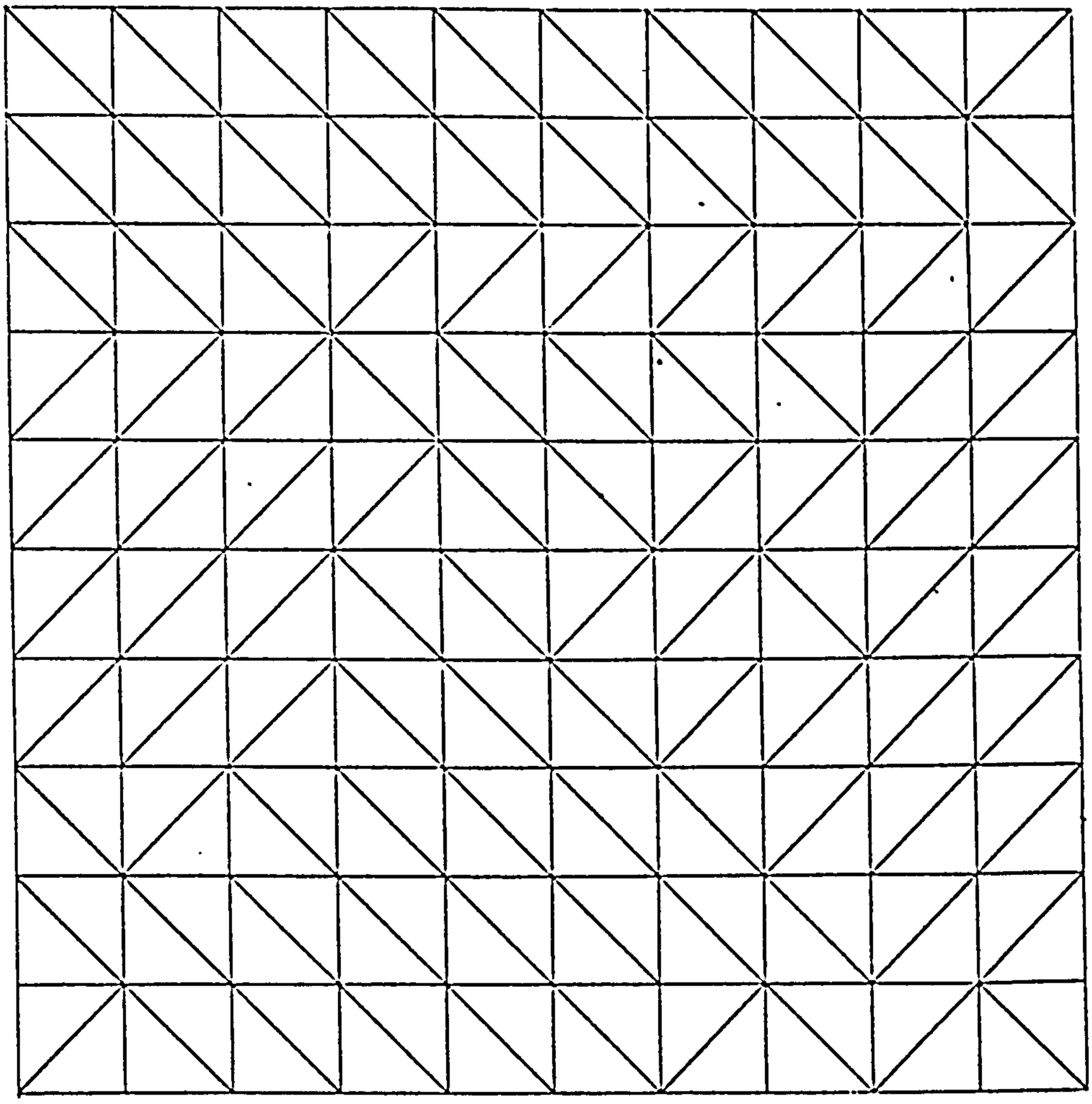

Figure 4.4 A Square 11 x 11 Mesh Generated using Regularly Spaced Nodes without any Adjustment

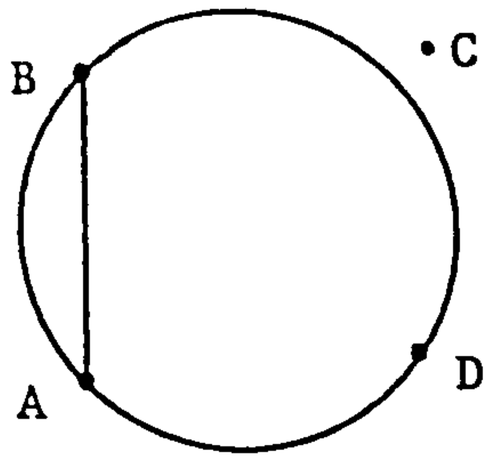

(a) A and B are the base nodes, D is closer to them and so is more suitable than C.

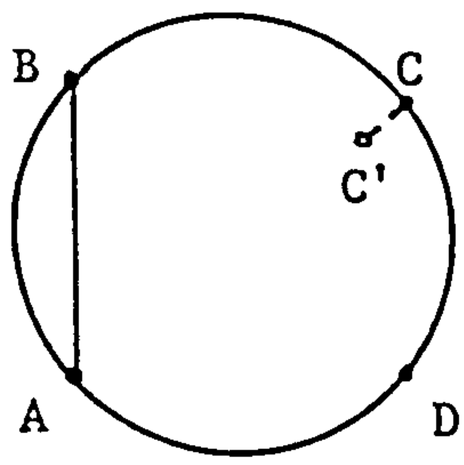

(b) Now both C and D are equally suitable to ensure that C is chosen move the node to C'.

Figure 4.5 Using the Mesh Generator to produce a Regular Mesh.

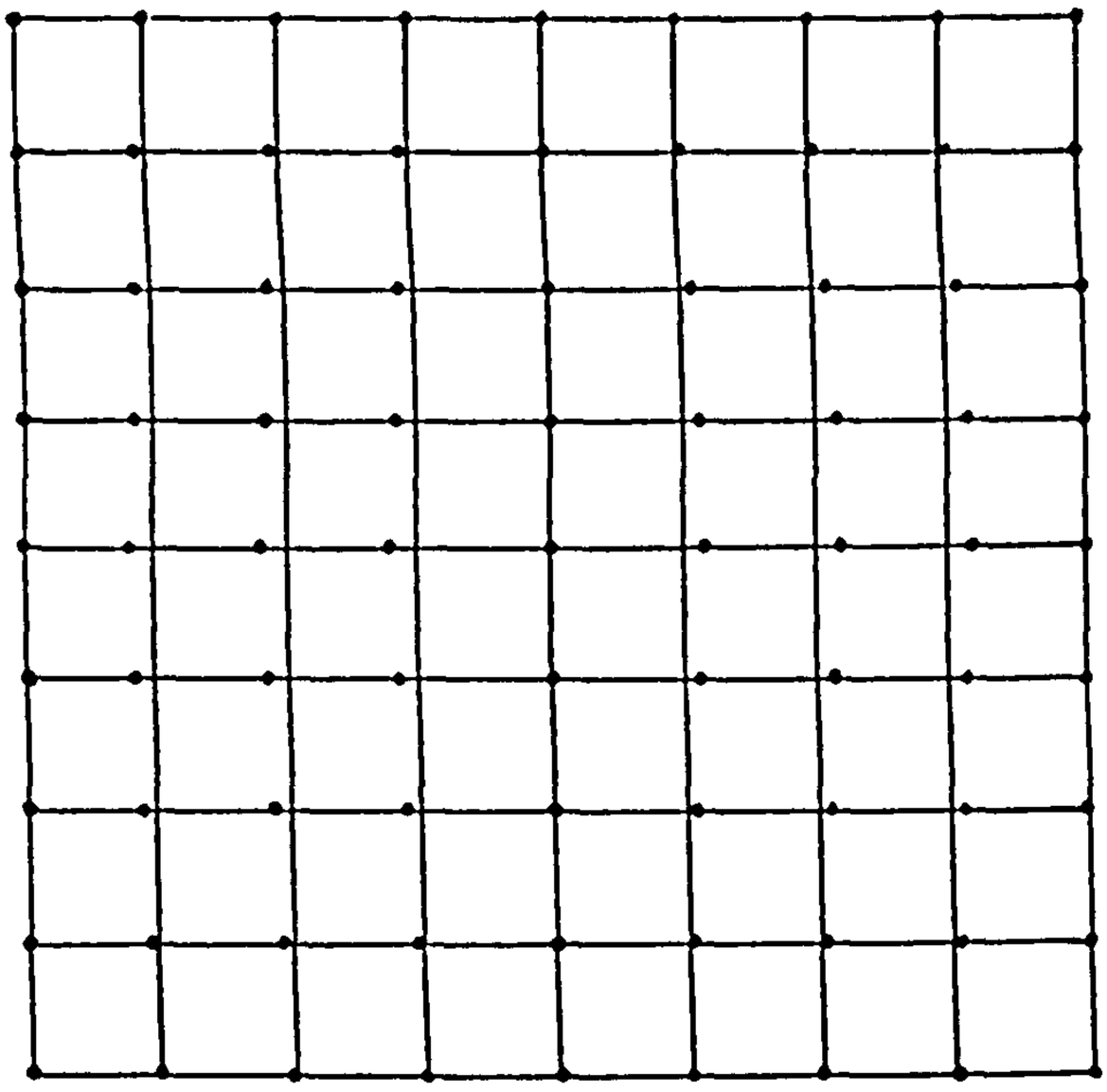

(a) The nodes are adjusted in order to ensure the generation of regular symmetric mesh.

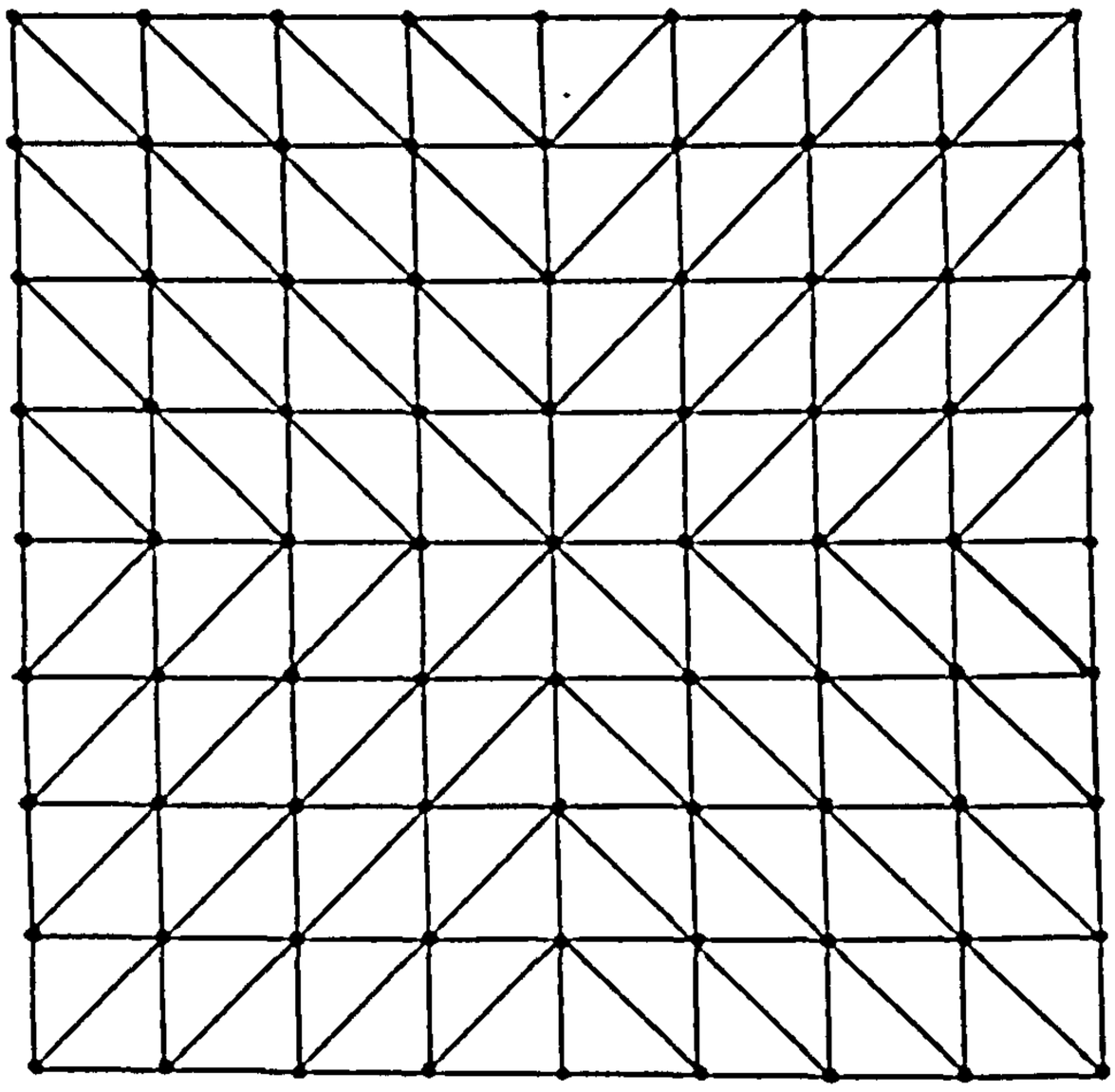

(b) A symmetric mesh resulting from the nodal adjustment

Figure 4.6 How the Nodes are Adjusted to Ensure a Regular Mesh Discretization.

$$\begin{cases} \omega = \omega_{NSB} \\ \psi = 0.0 \\ v_{mL} = 1.0 \end{cases}$$

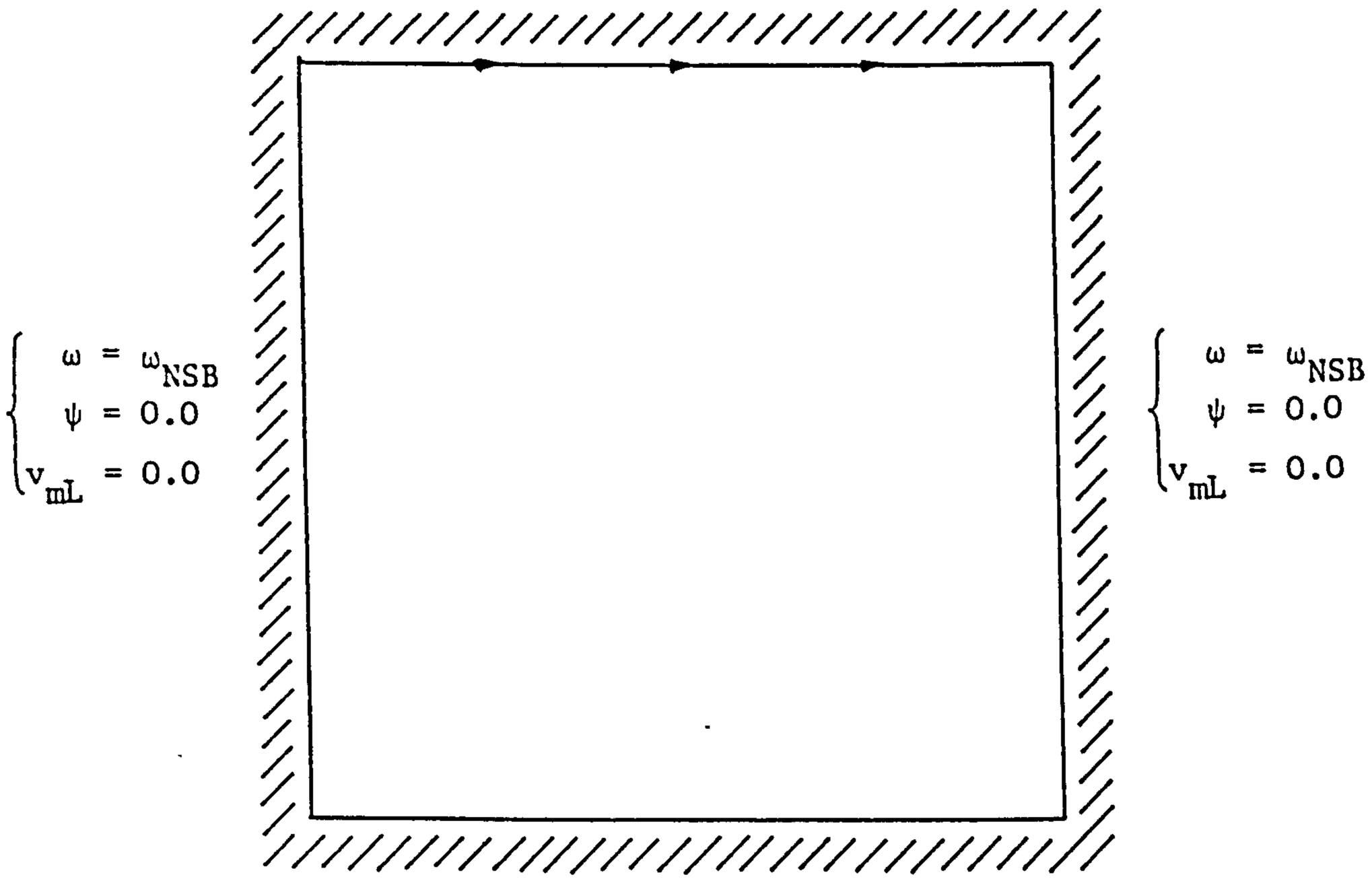

$$\begin{cases} \omega = \omega_{NSB} \\ \psi = 0.0 \\ v_{mL} = 0.0 \end{cases}$$

$$\begin{cases} \omega = \omega_{NSB} \\ \psi = 0.0 \\ v_{mL} = 0.0 \end{cases}$$

$$\begin{cases} \omega = \omega_{NSB} \\ \psi = 0.0 \\ v_{mL} = 0.0 \end{cases}$$

Figure 5.1 Flow Within a Square Cavity with a Top Moving Wall

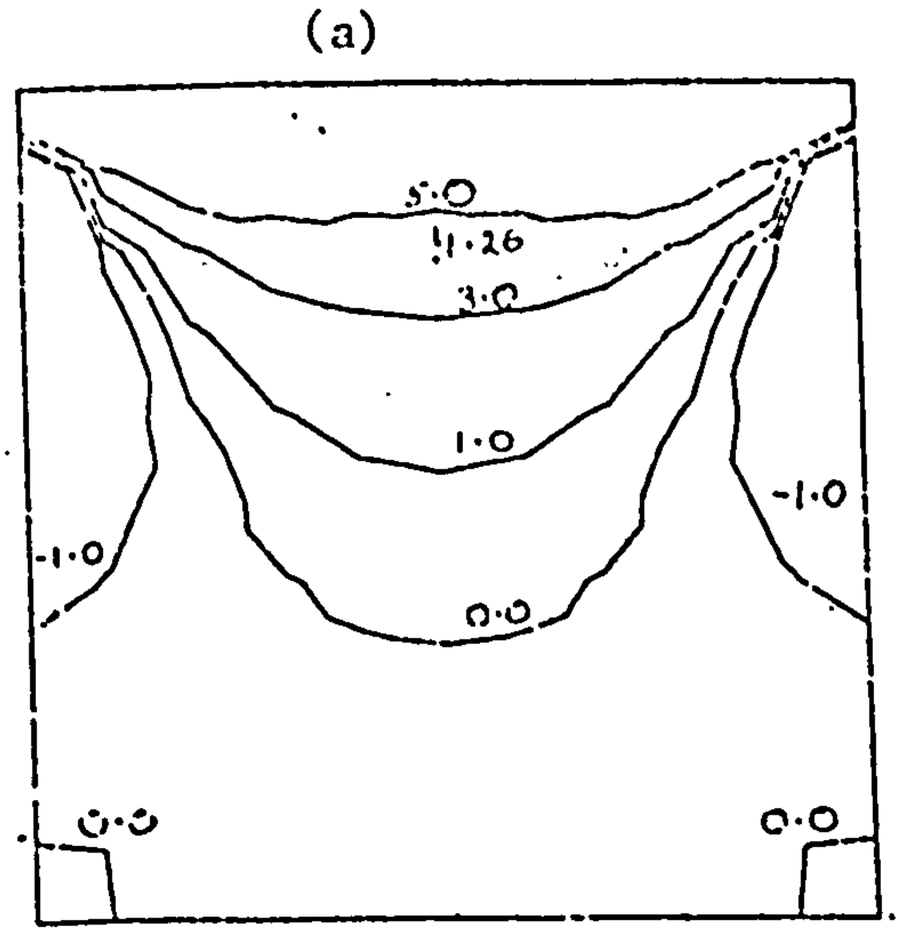

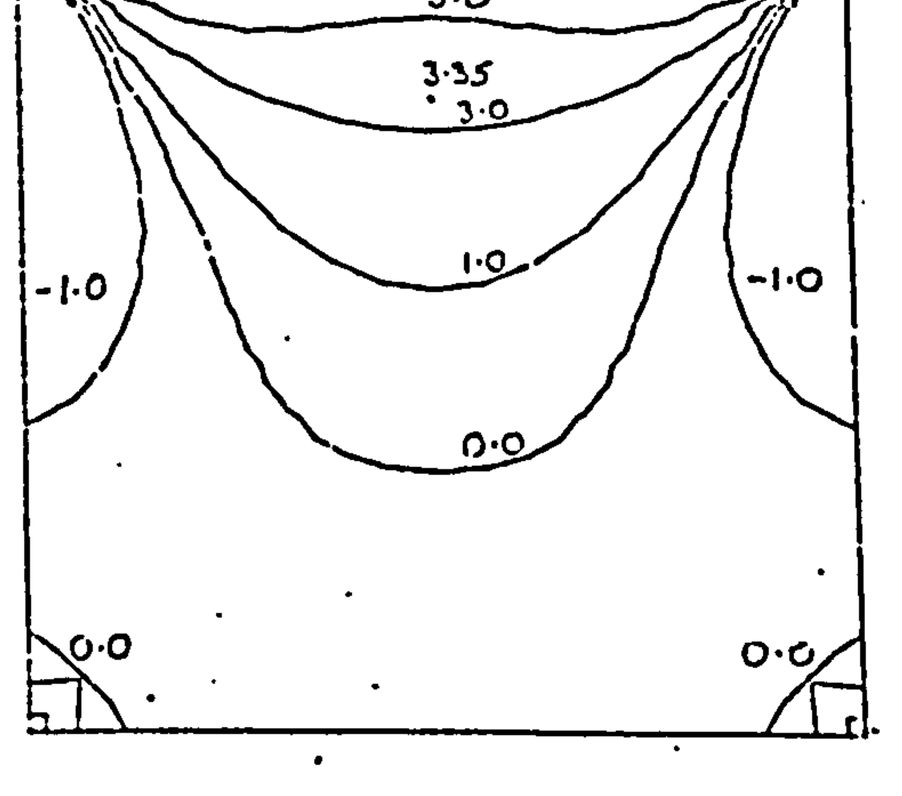

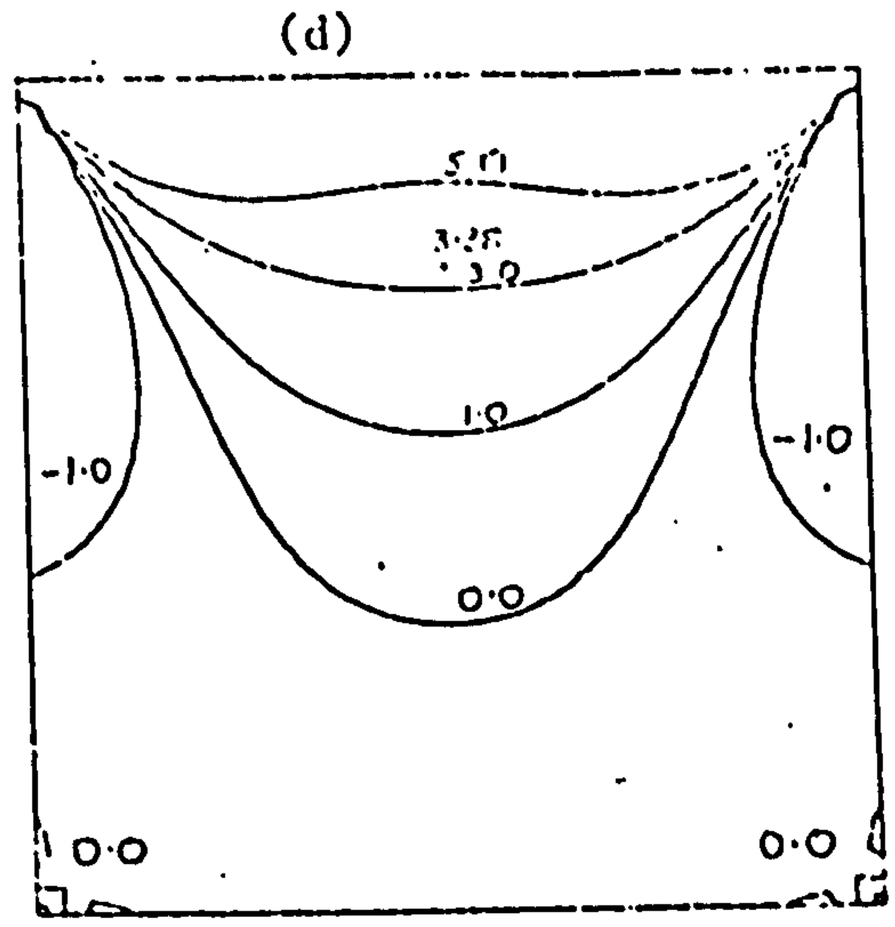

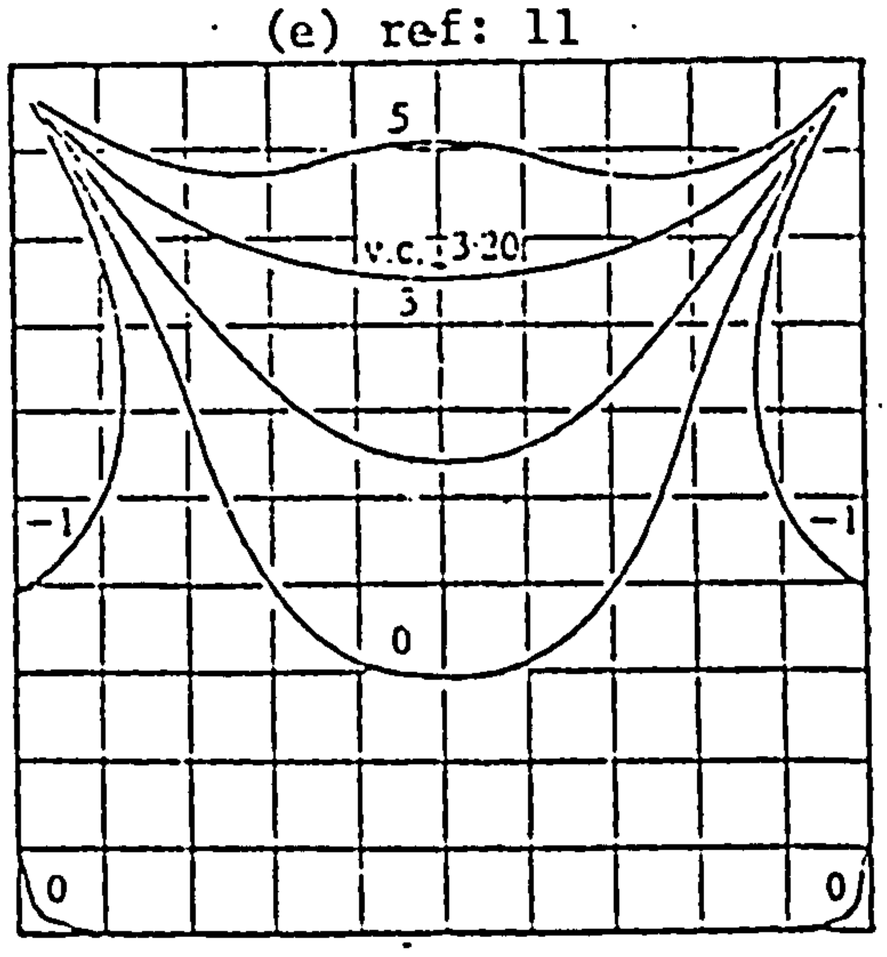

Figure 5.3 Vorticity at $R_e = 10^{-4}$

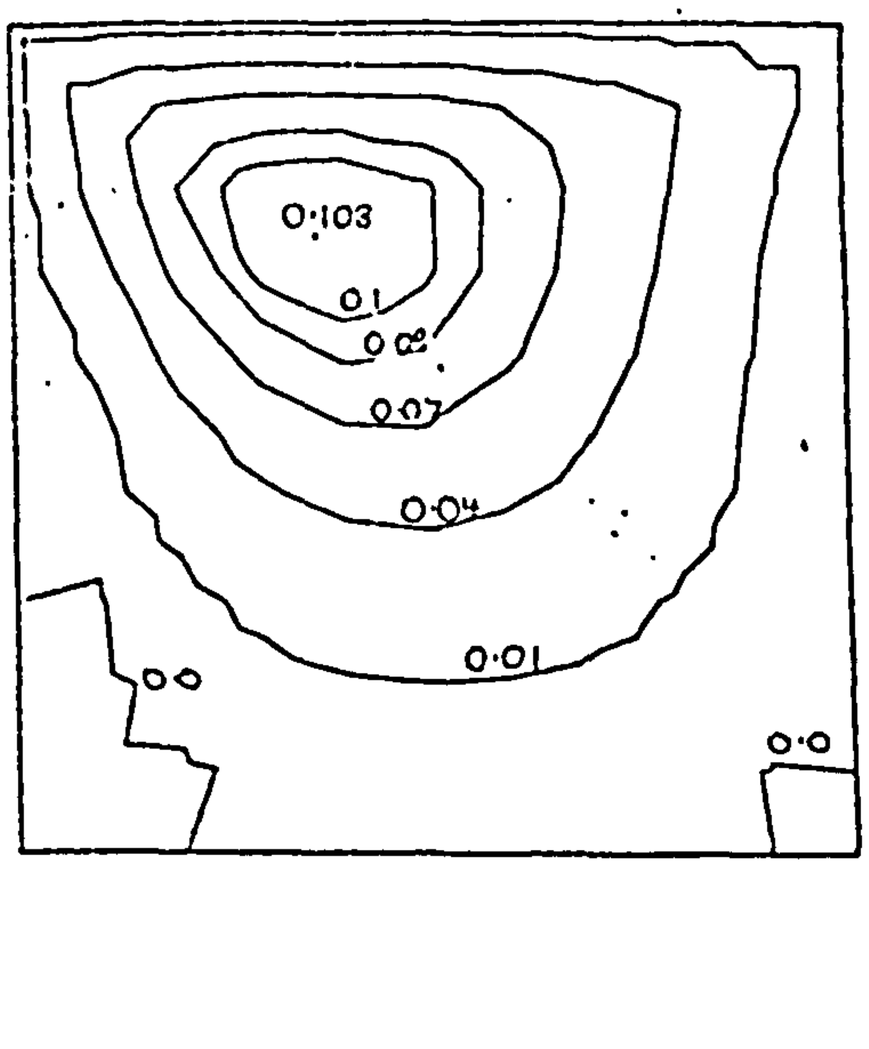

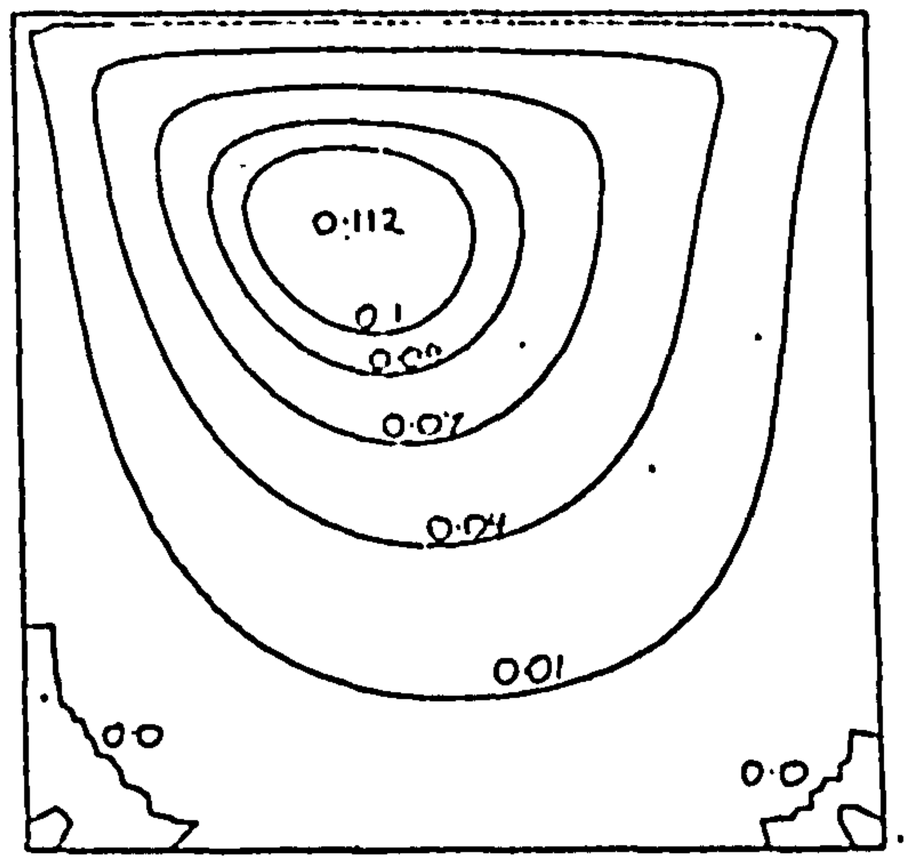

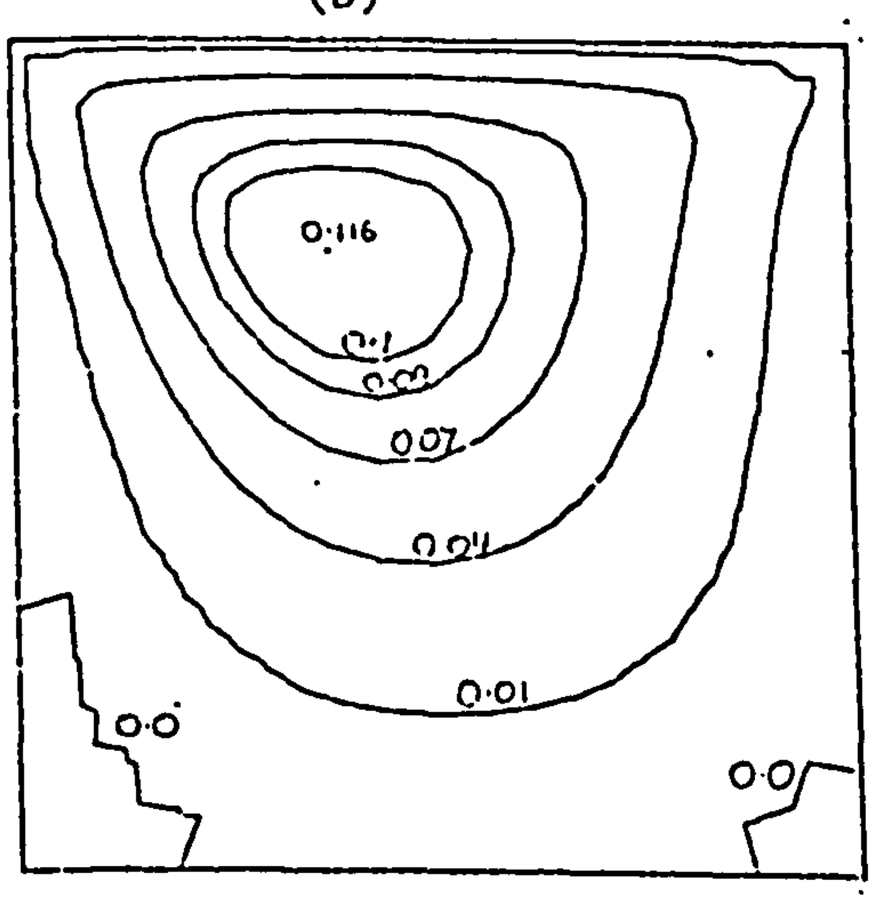

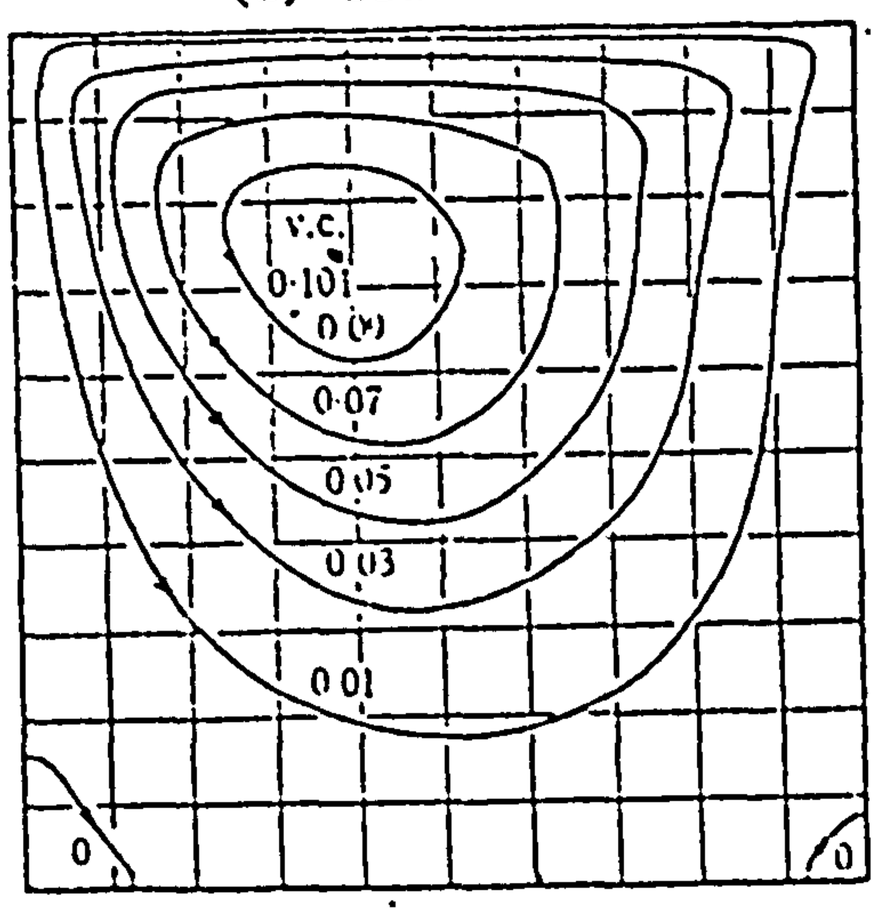

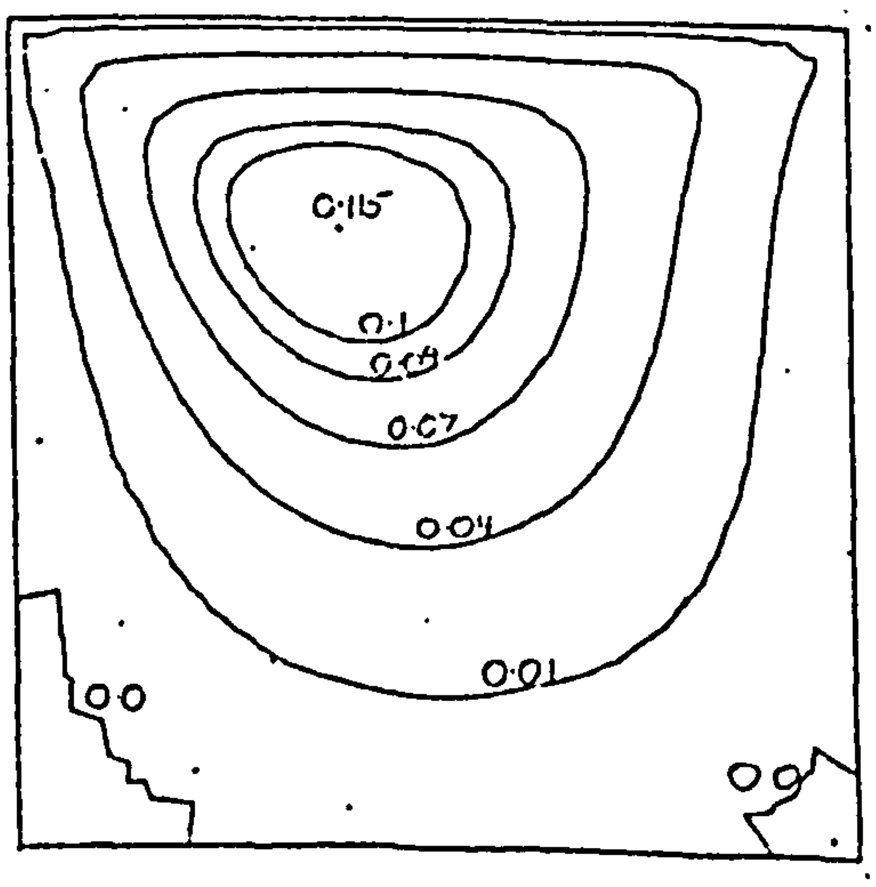

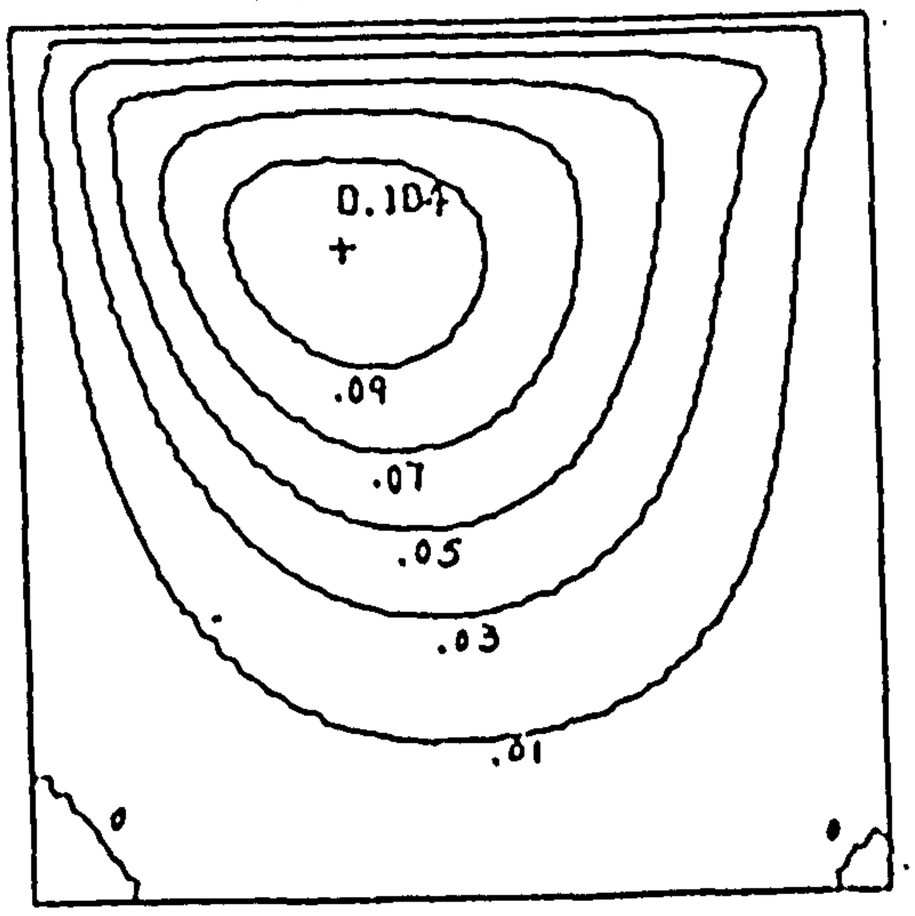

Figure 5.4 Stream Function at R_e = 100

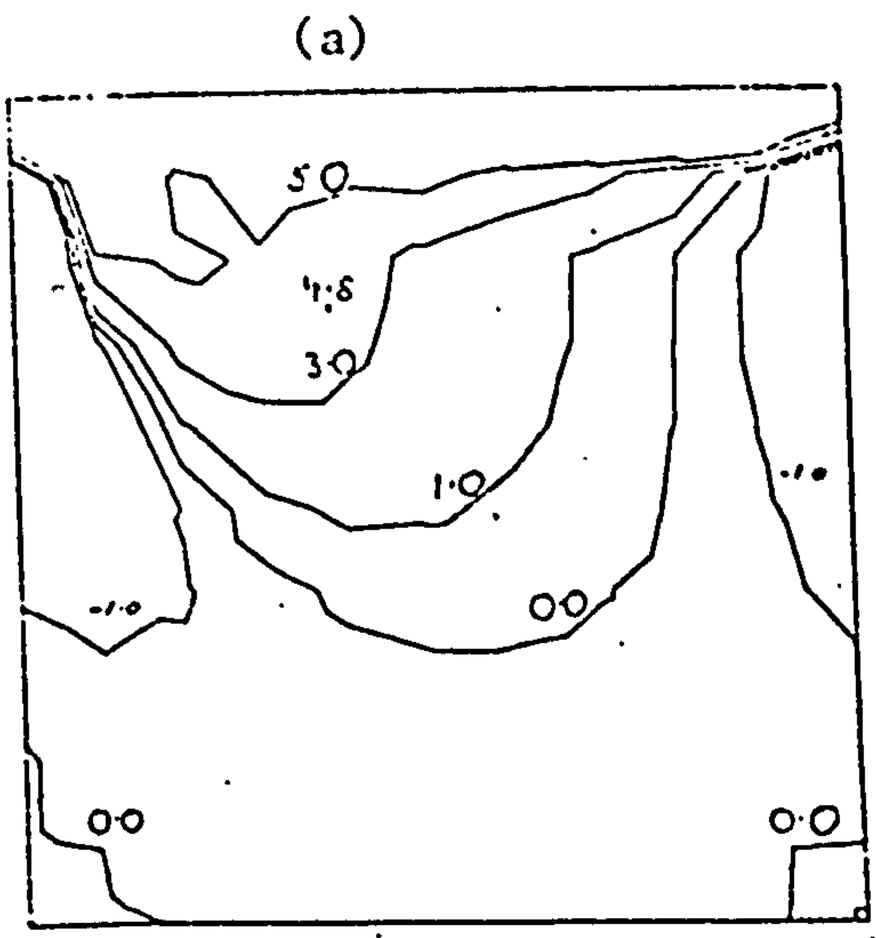

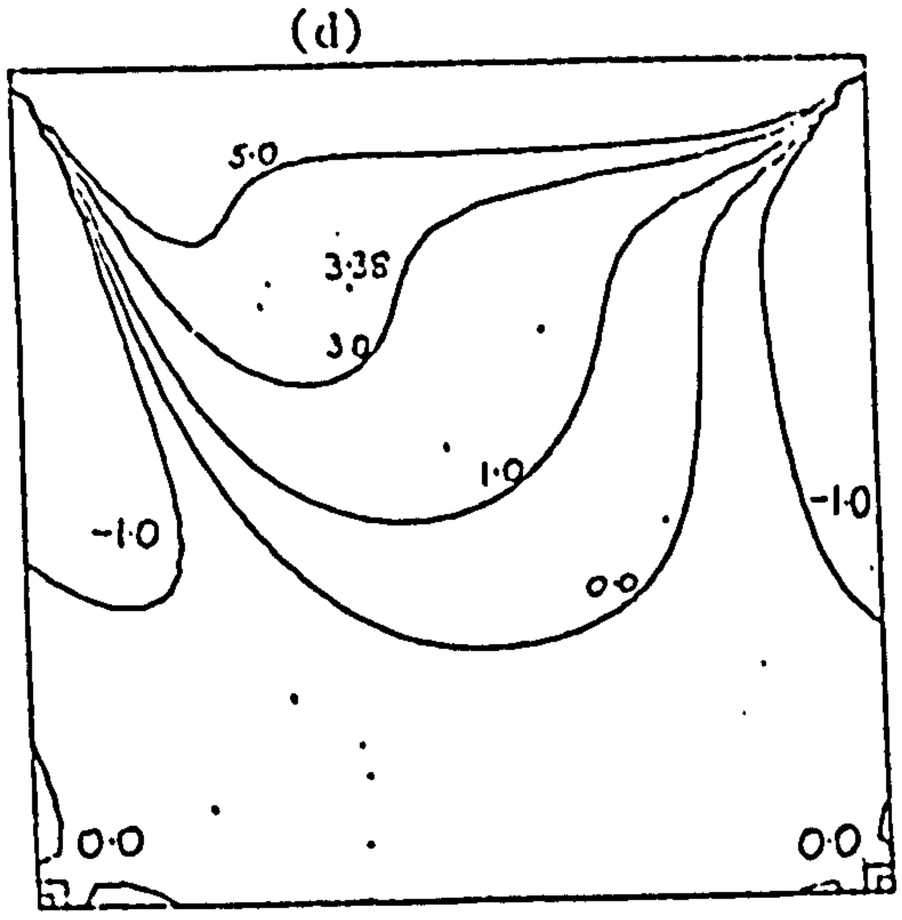

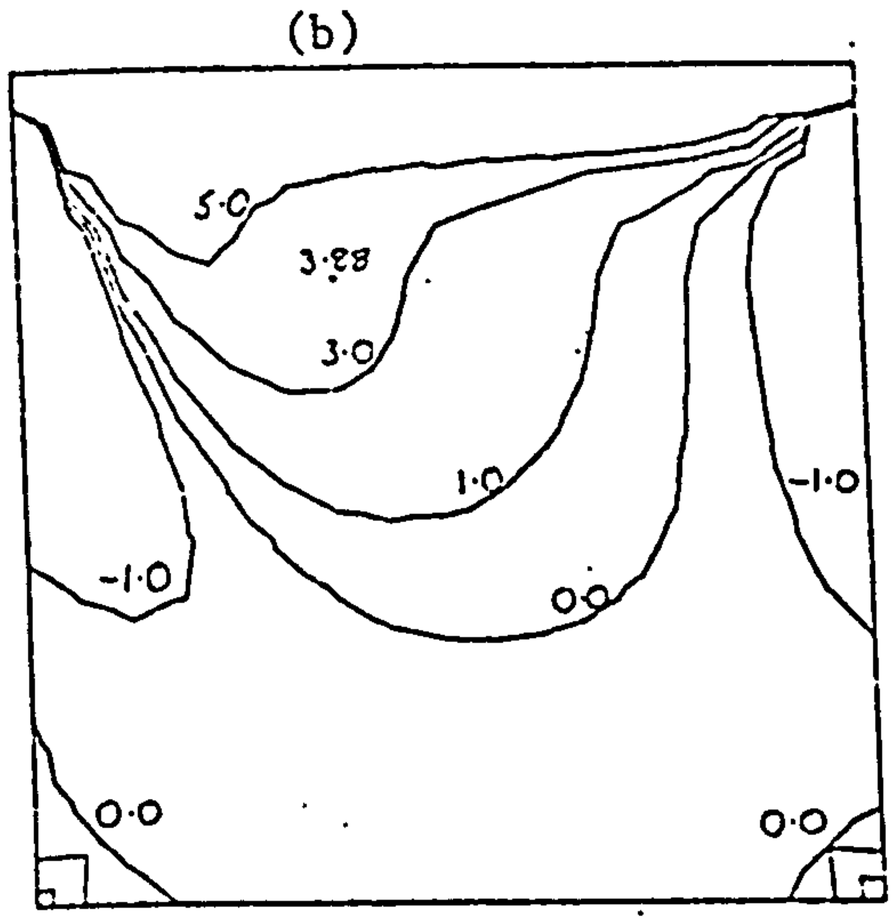

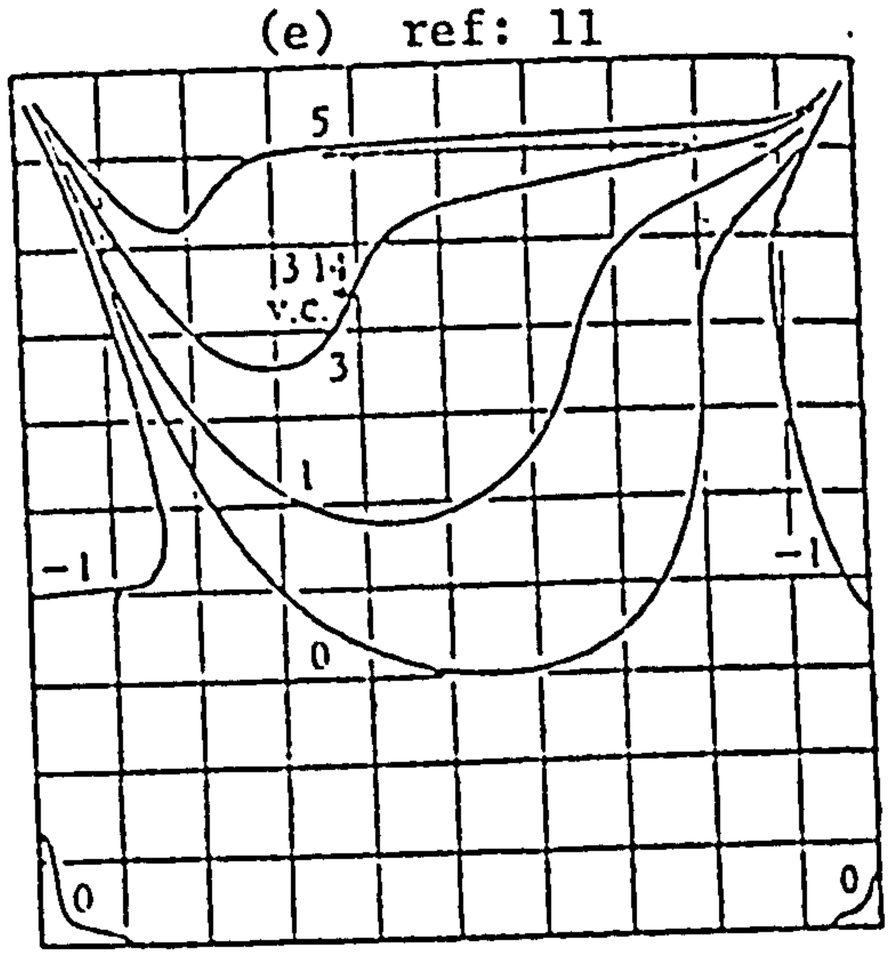

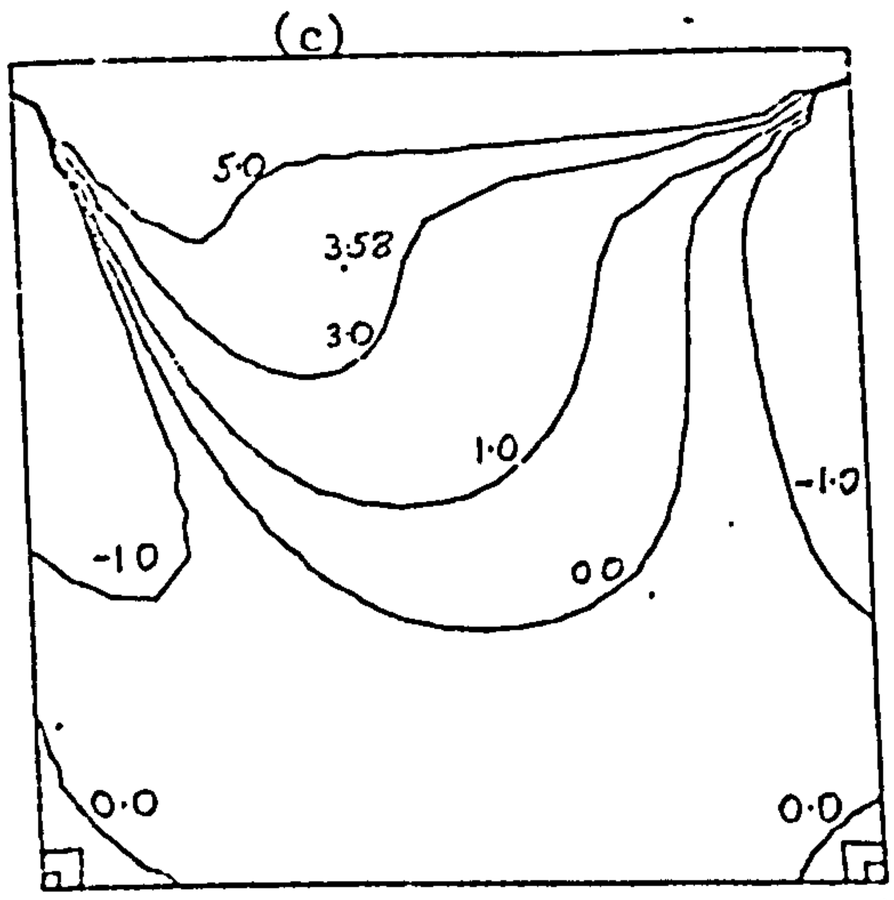

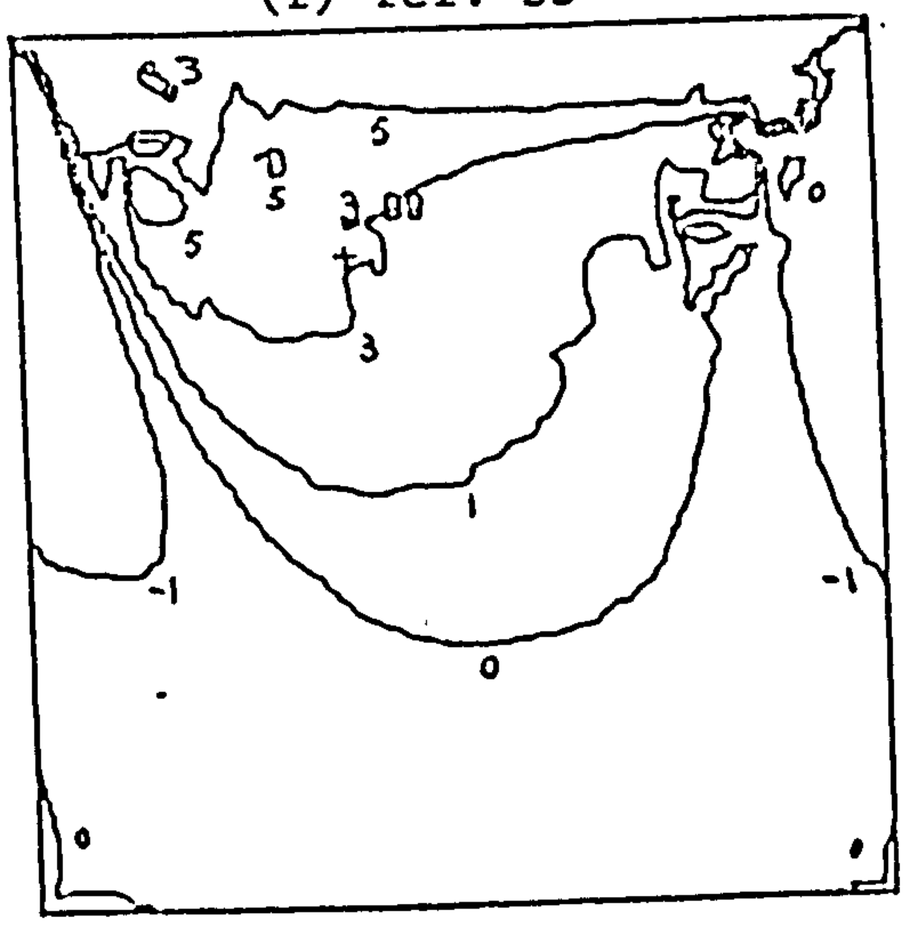

Figure 5.5 Vorticity at R_e = 100

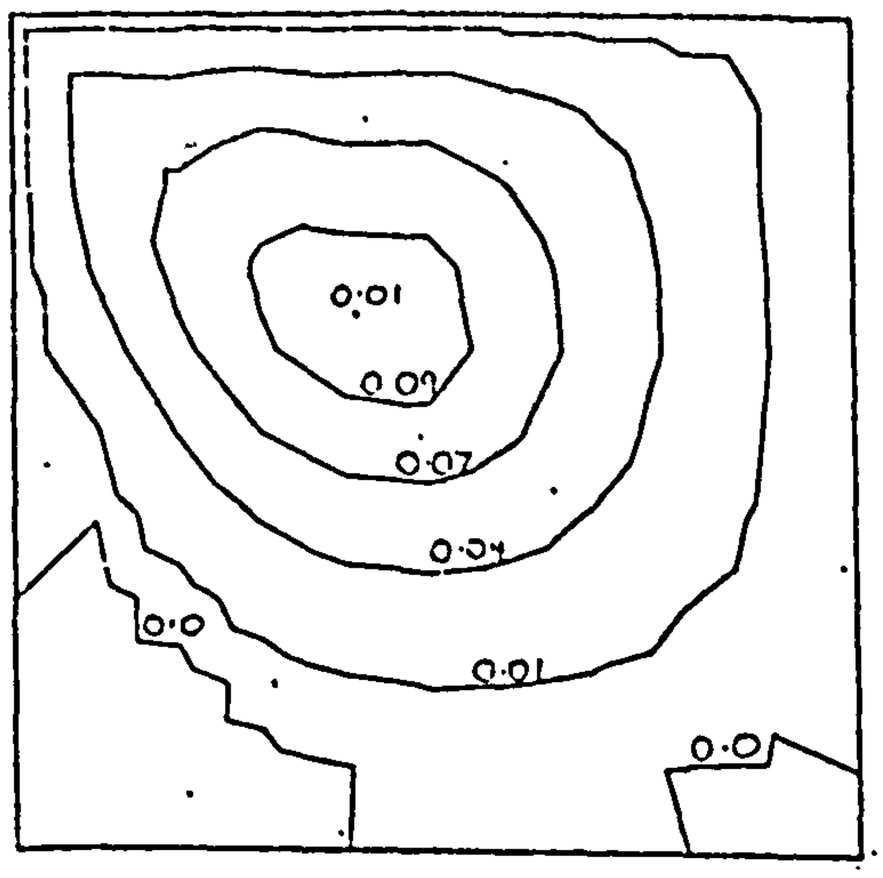

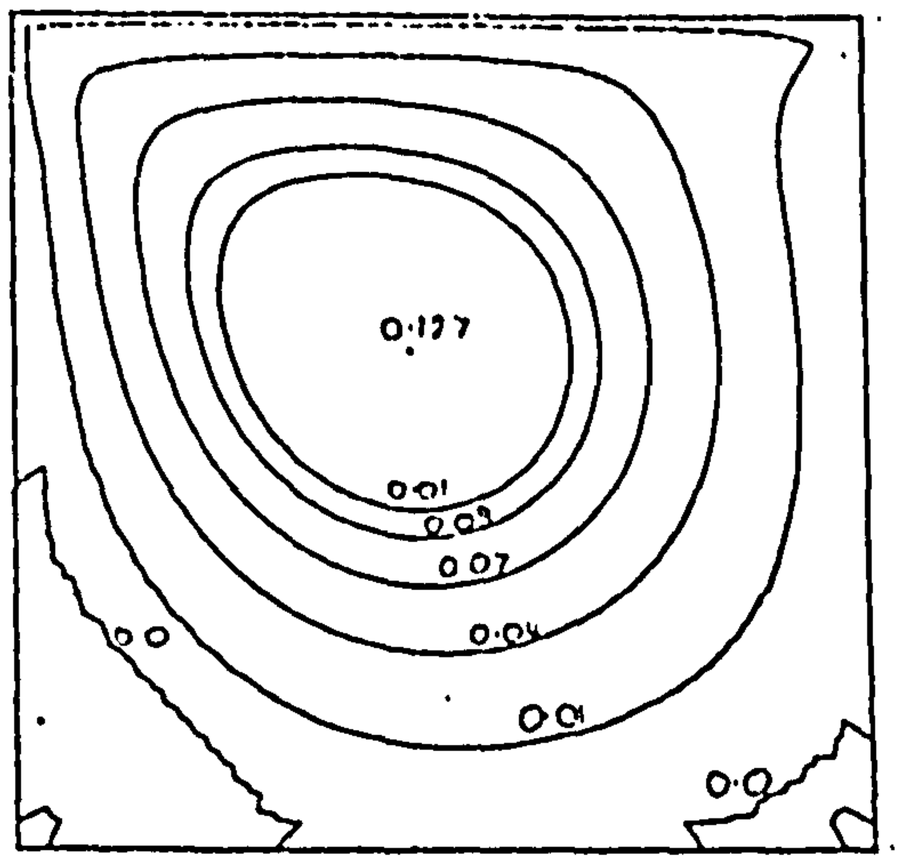

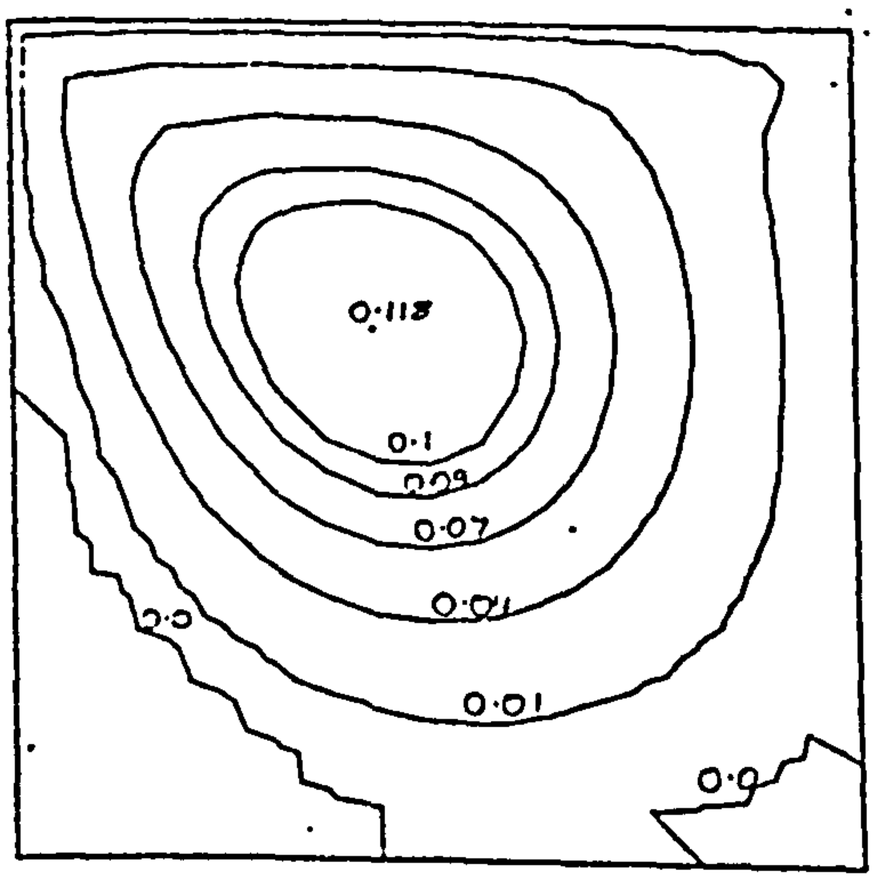

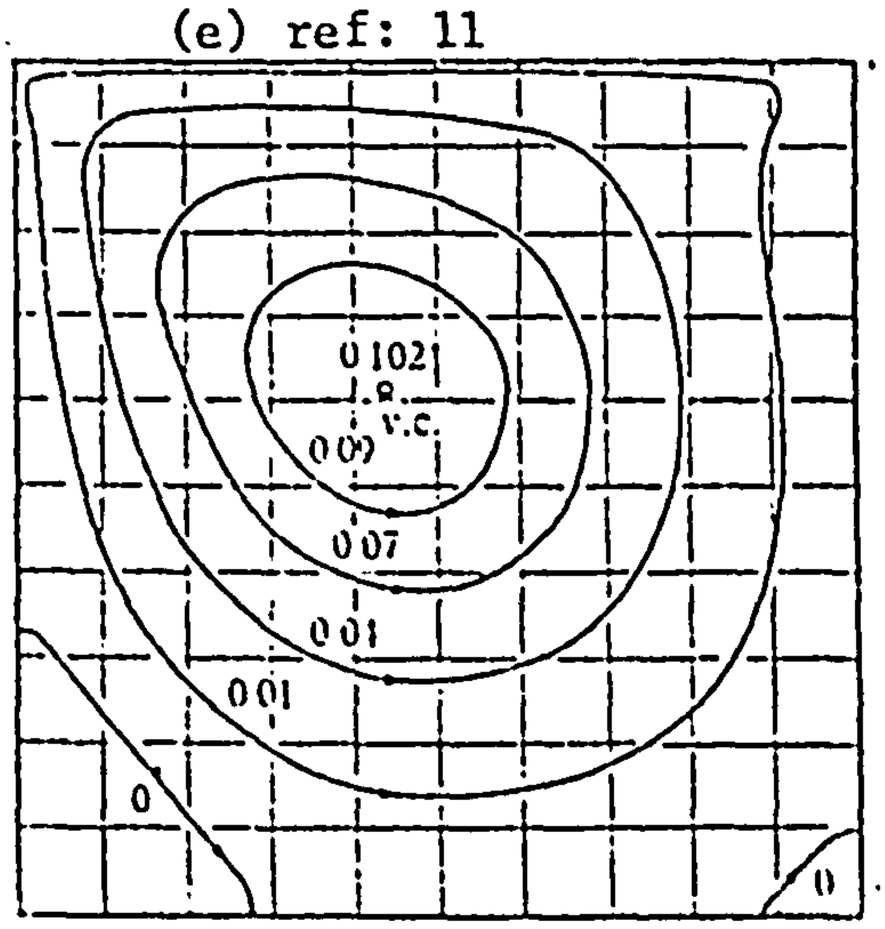

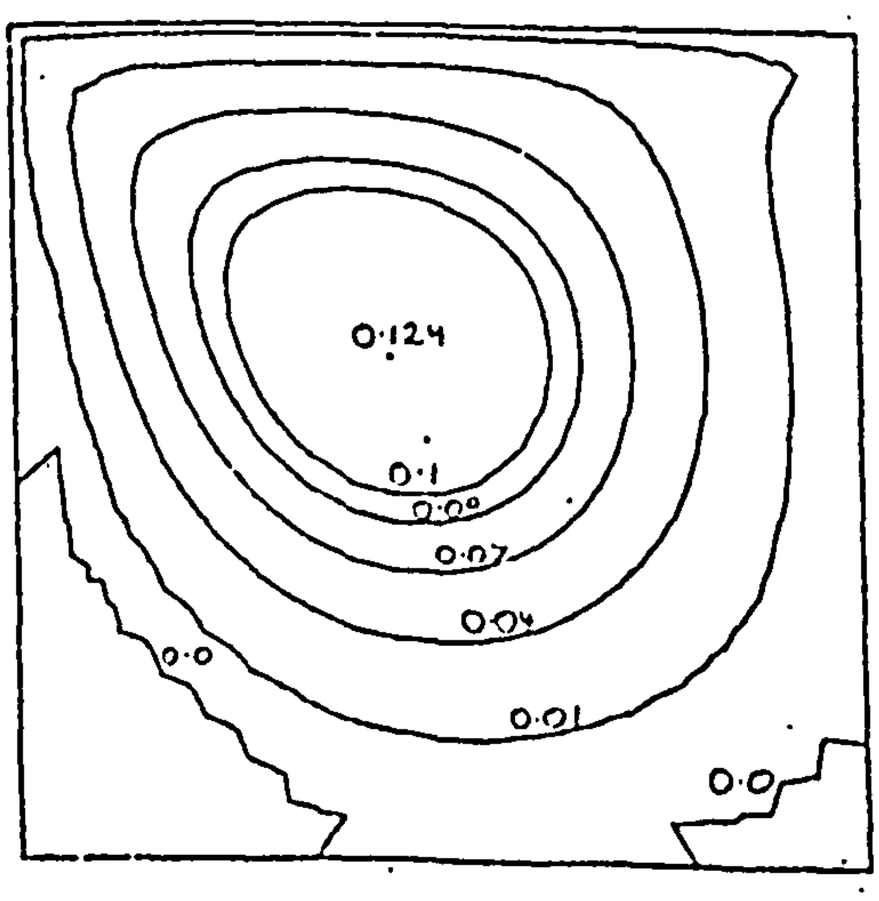

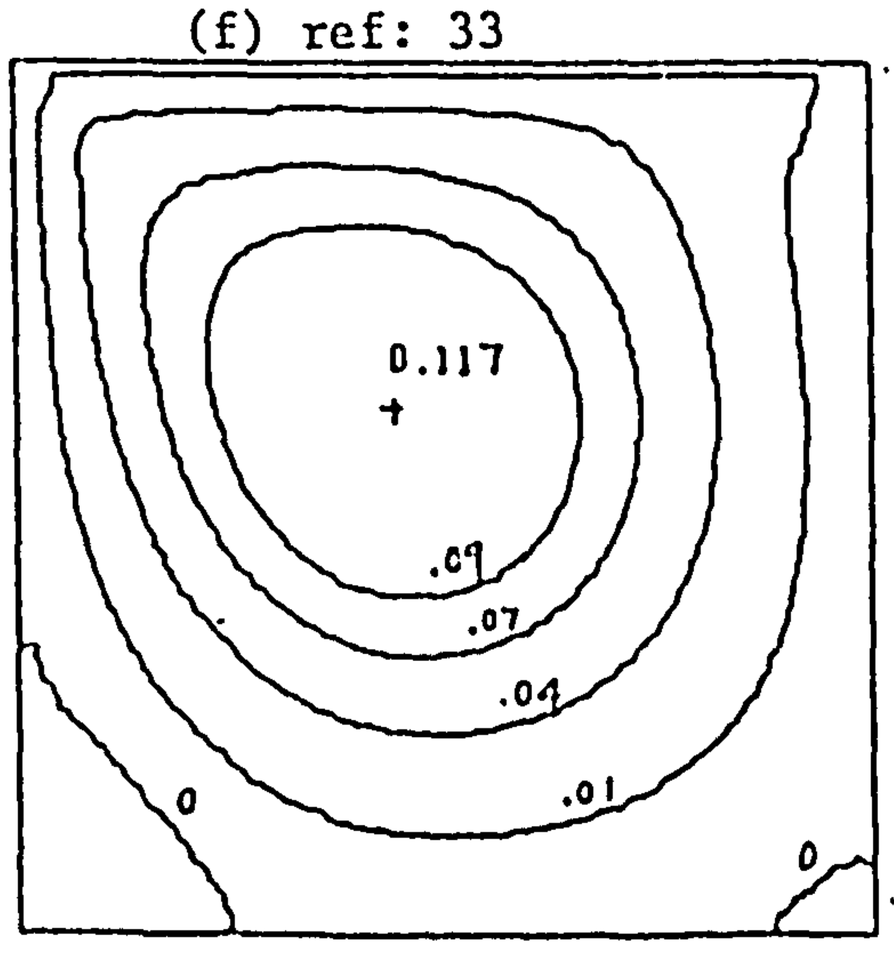

Figure 5.6 Stream Function at R_e = 400

(a)

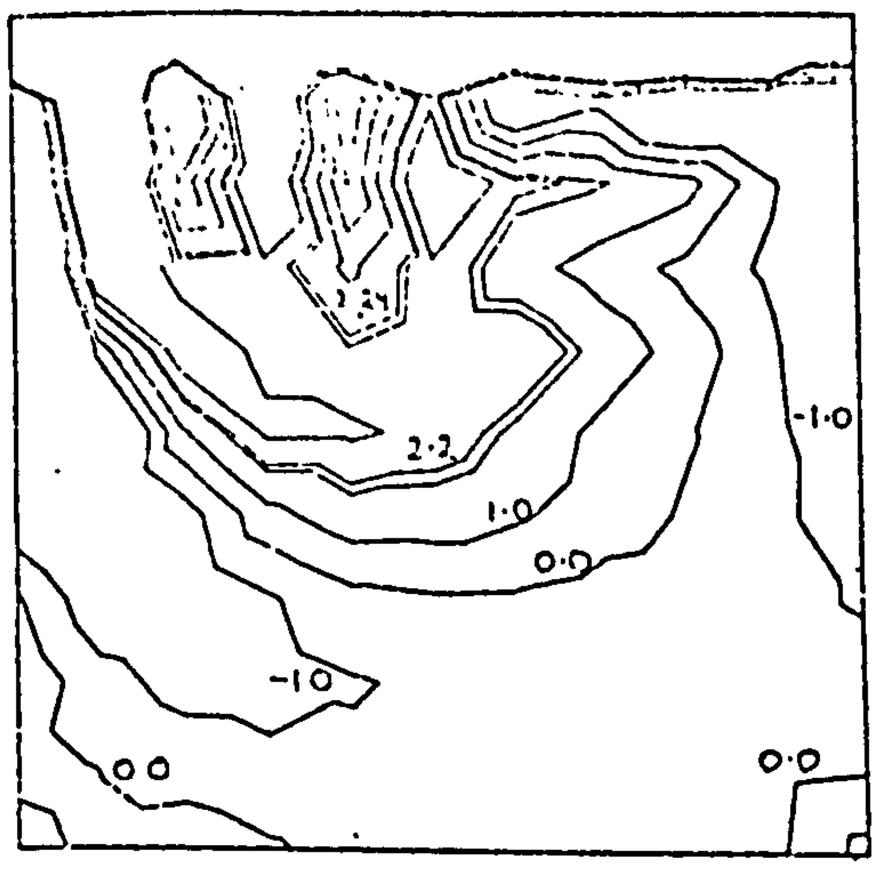

(b)

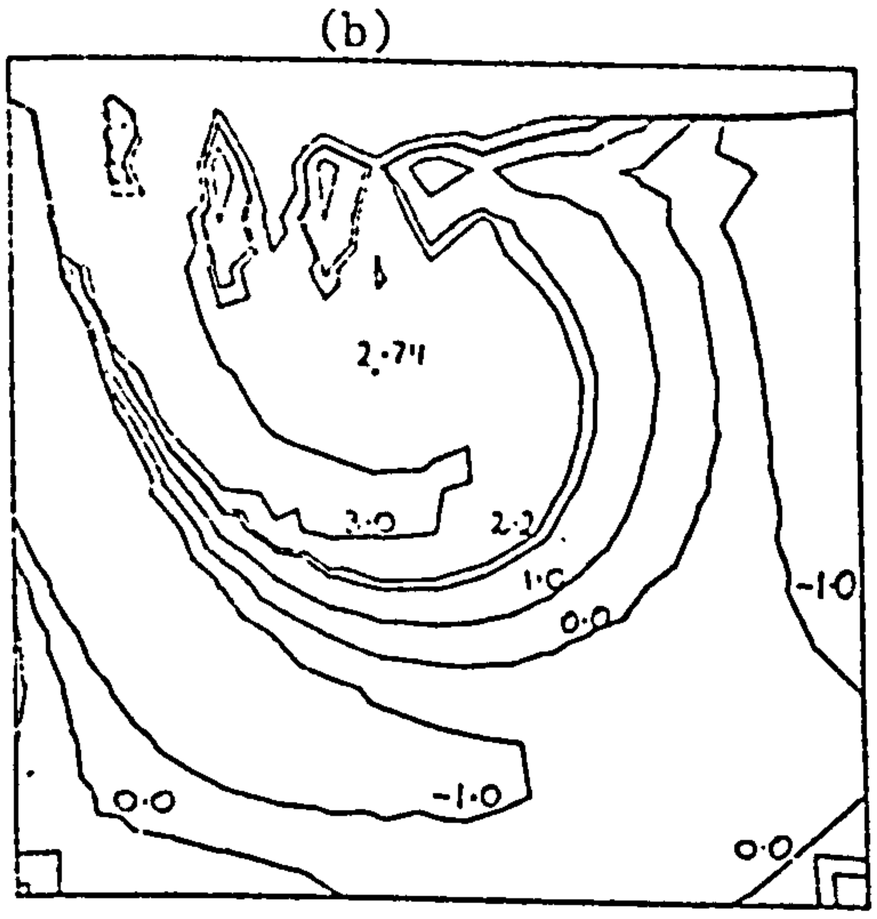

(c)

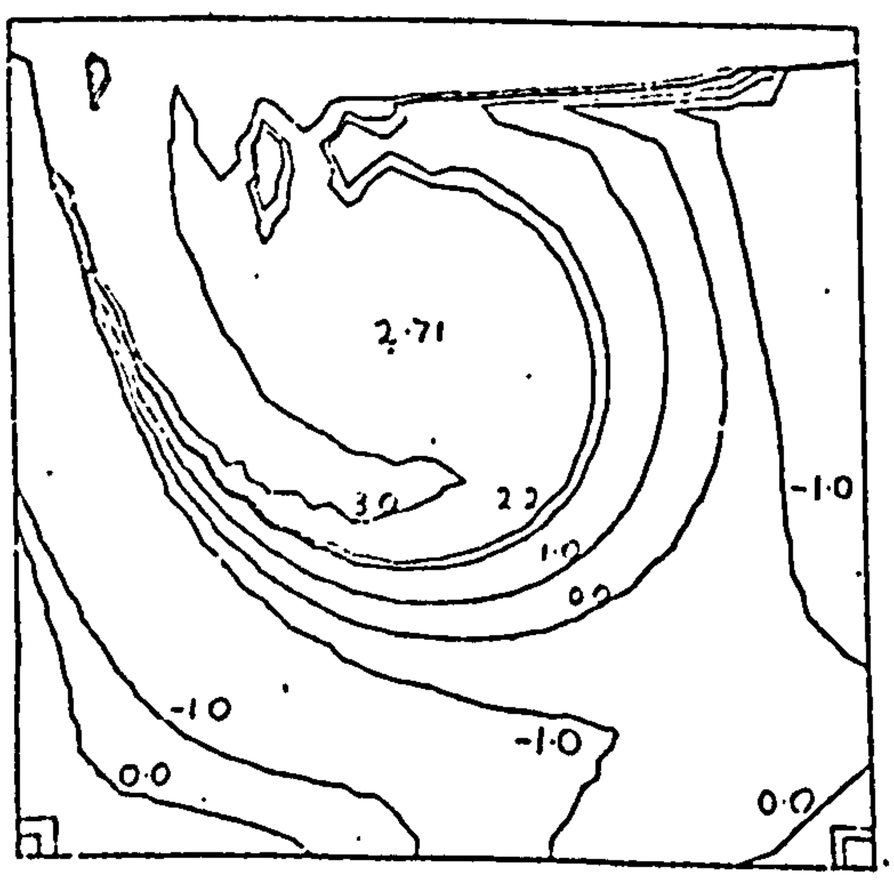

(d)

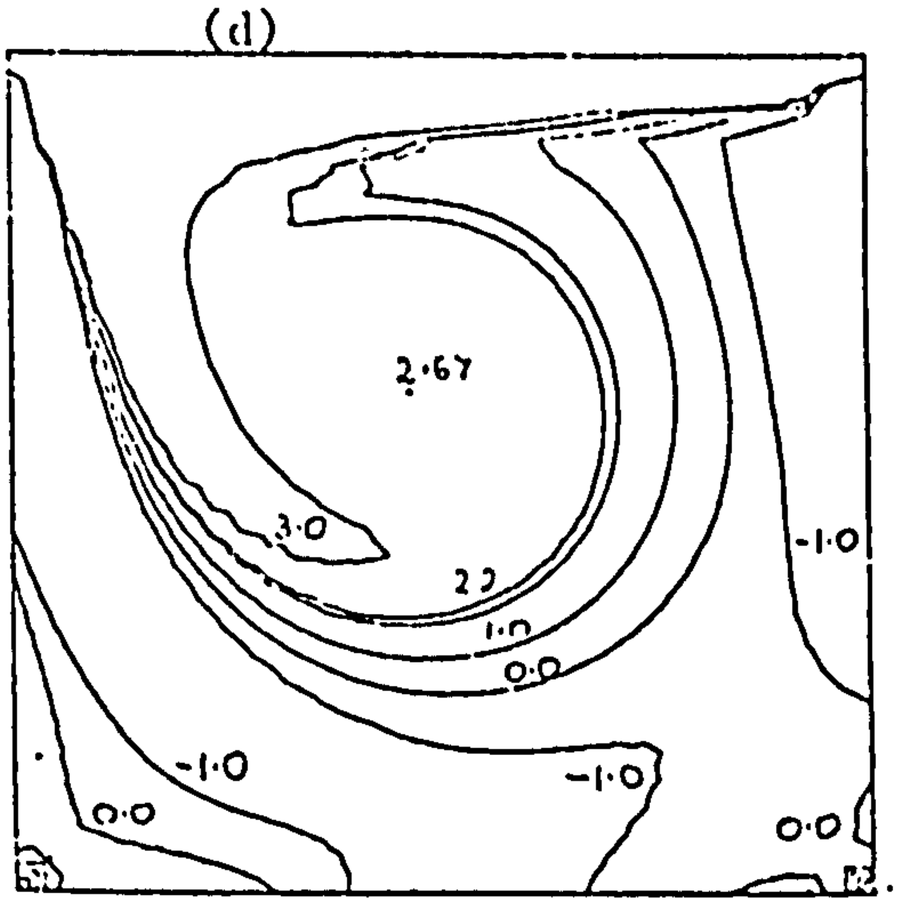

(e) ref: 11

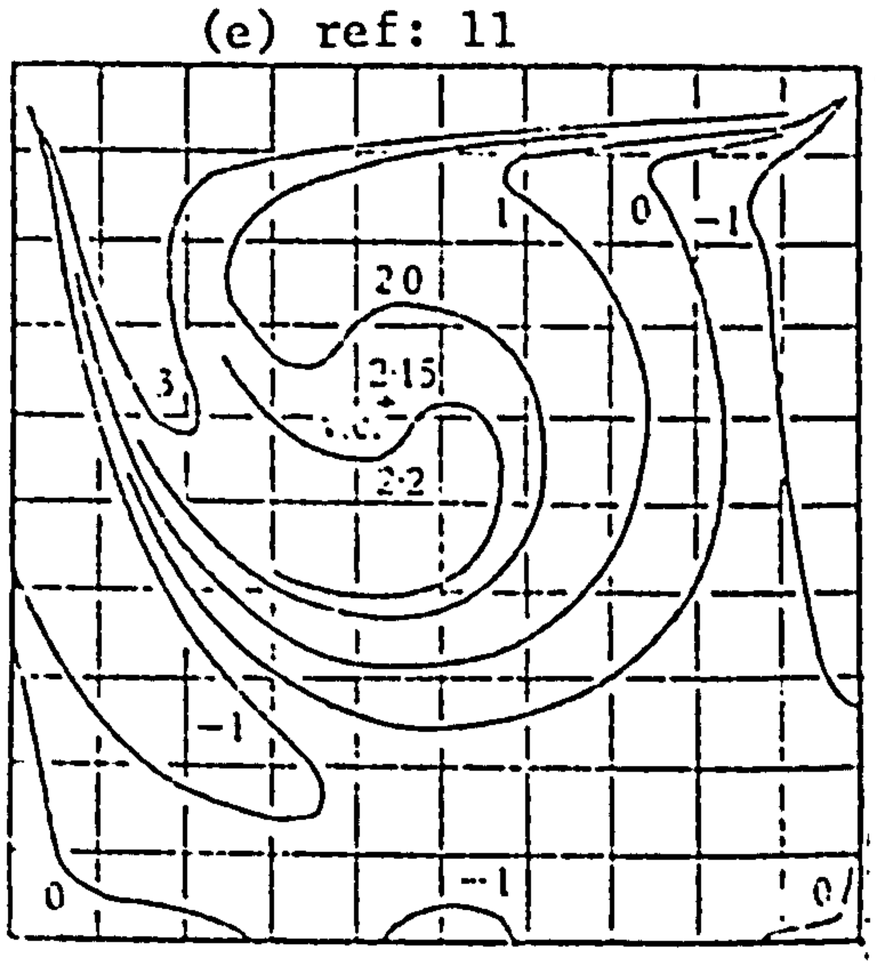

(f) ref: 33

Figure 5.7 Vorticity at R_e = 400

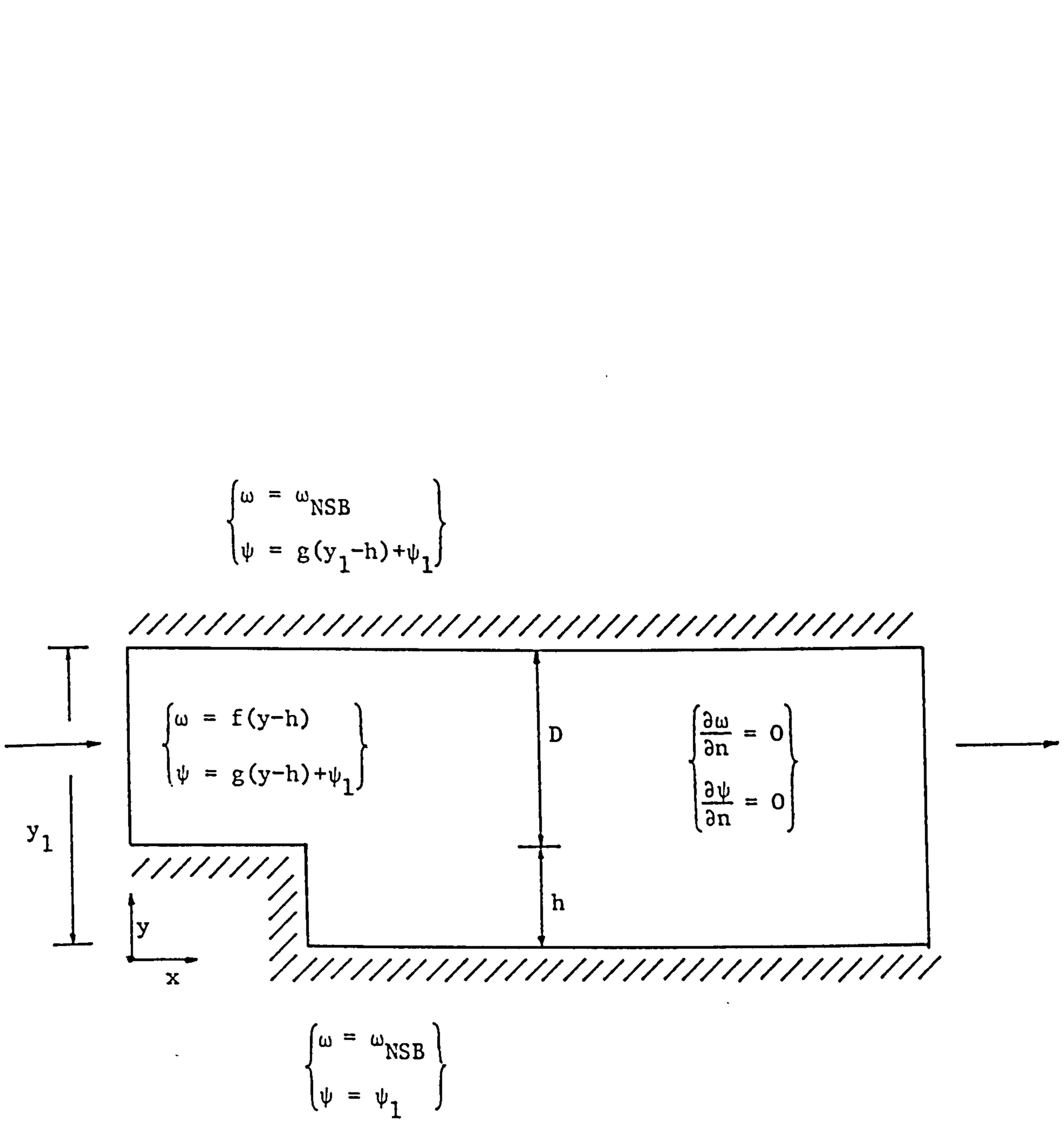

Figure 5.8 The Step Problem, f( ), and g( ) are polynomials used to Describe a Suitable Inlet Velocity Profile, e.g. A Parabolic Profile.

(a) Initial mesh

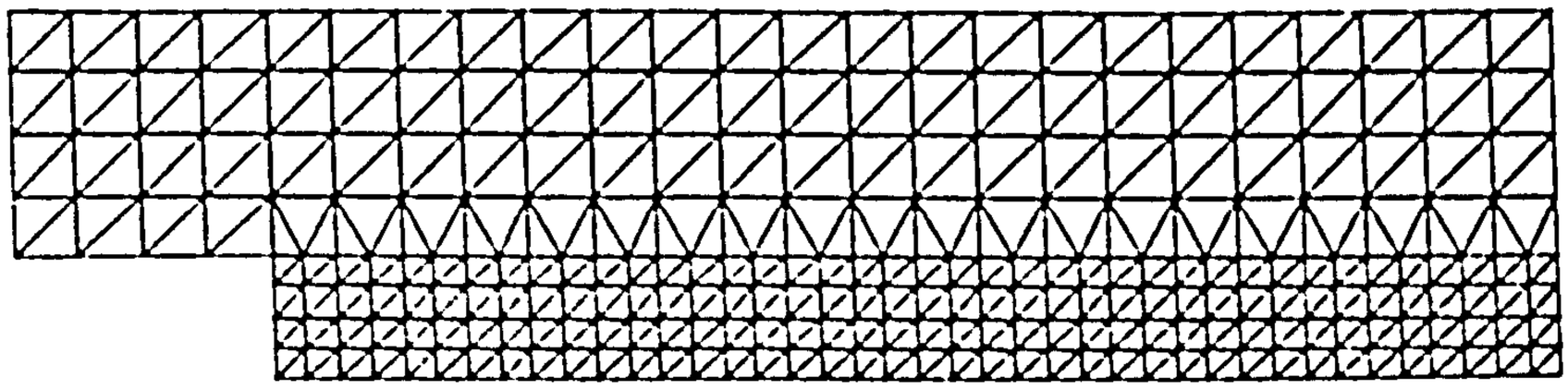

(b) Coarse mesh

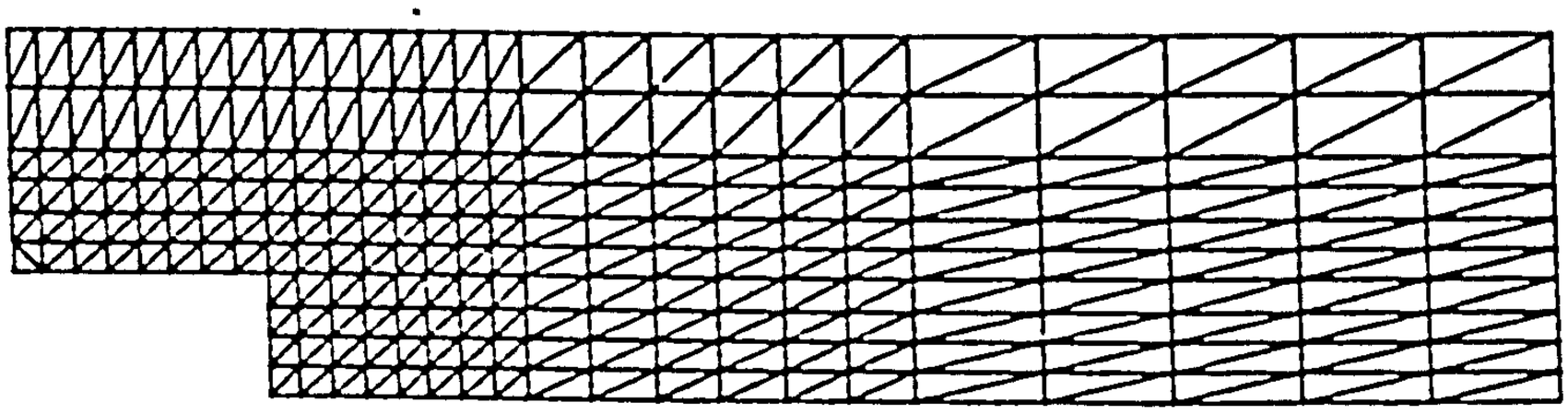

(c) Fine mesh

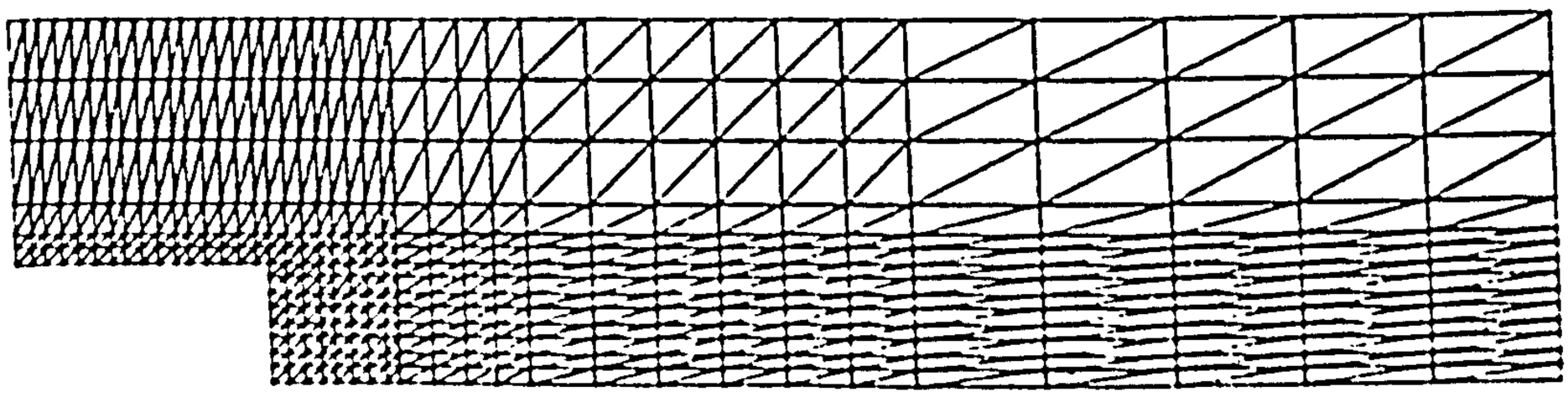

Figure 5.9 The Step Meshes

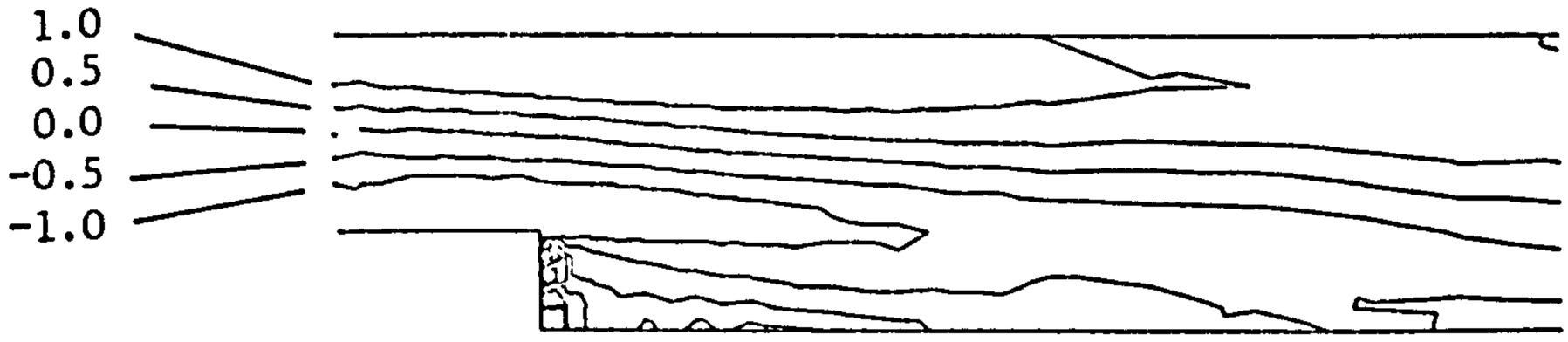

(a) Coarse results

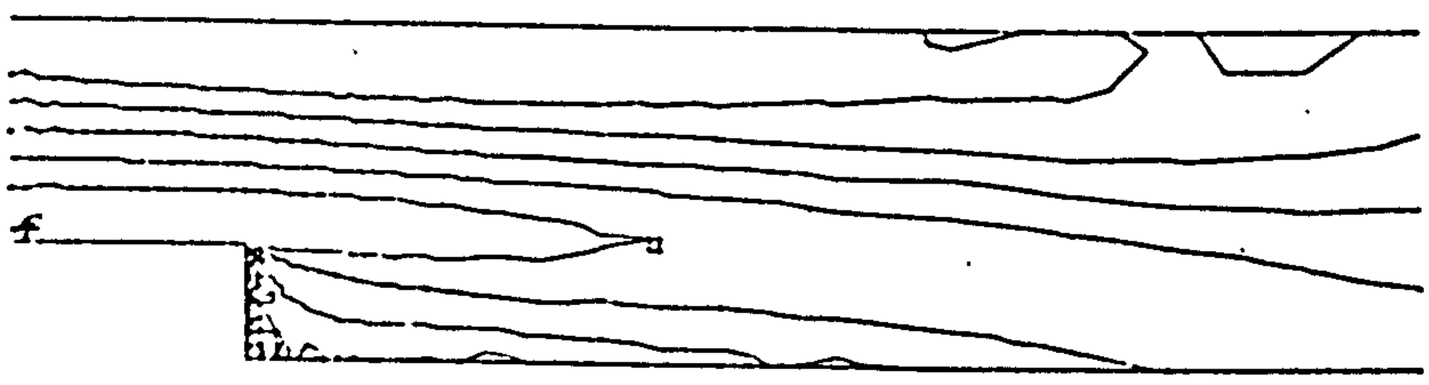

(b) Fine results

Figure 5.10 The Vorticity at R_e = 73

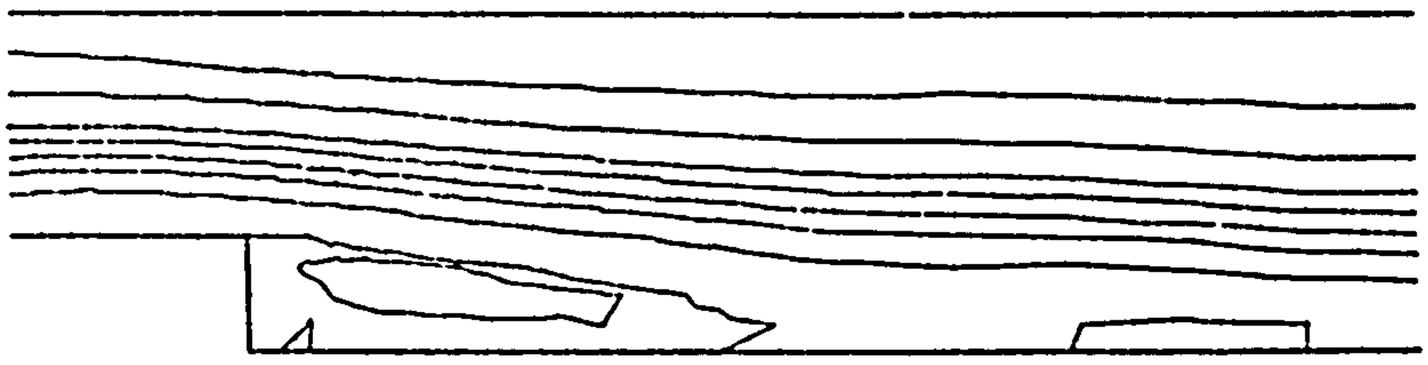

(a) Coarse results

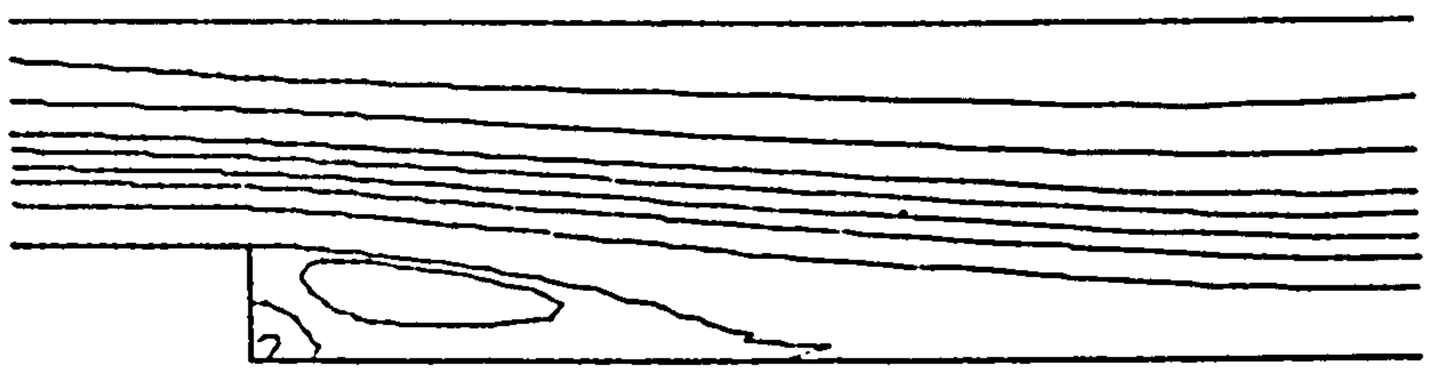

(b) Fine results

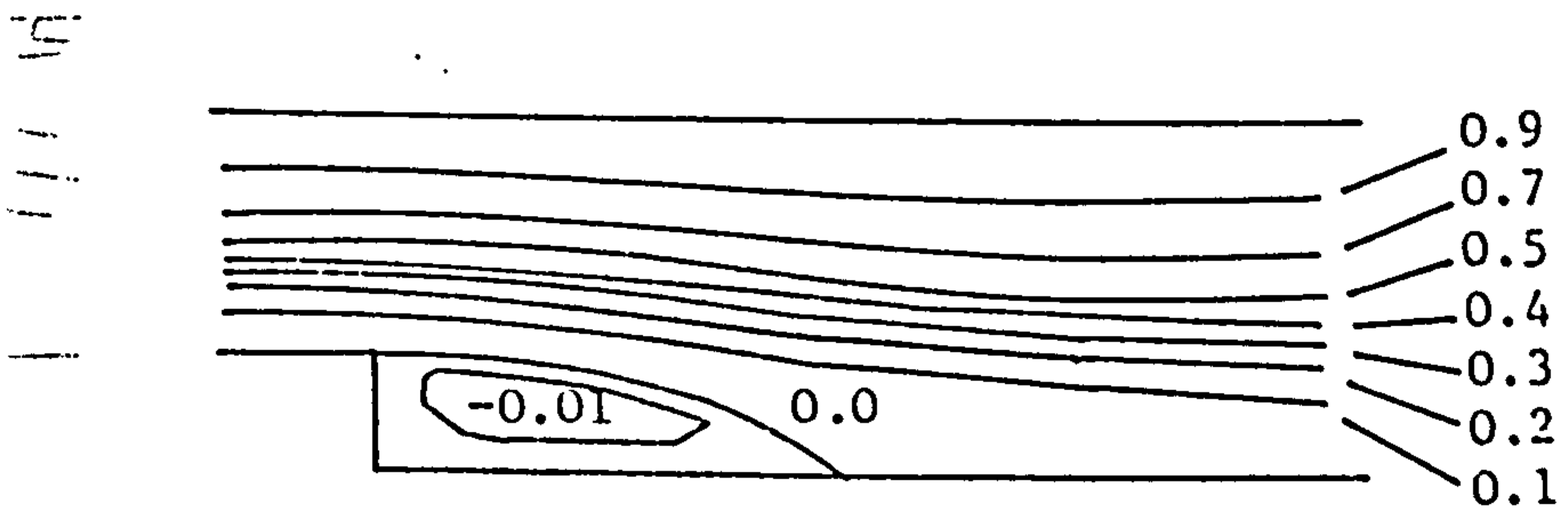

(c) Experimental results

Figure 5.11 The Stream Function at R_e = 73

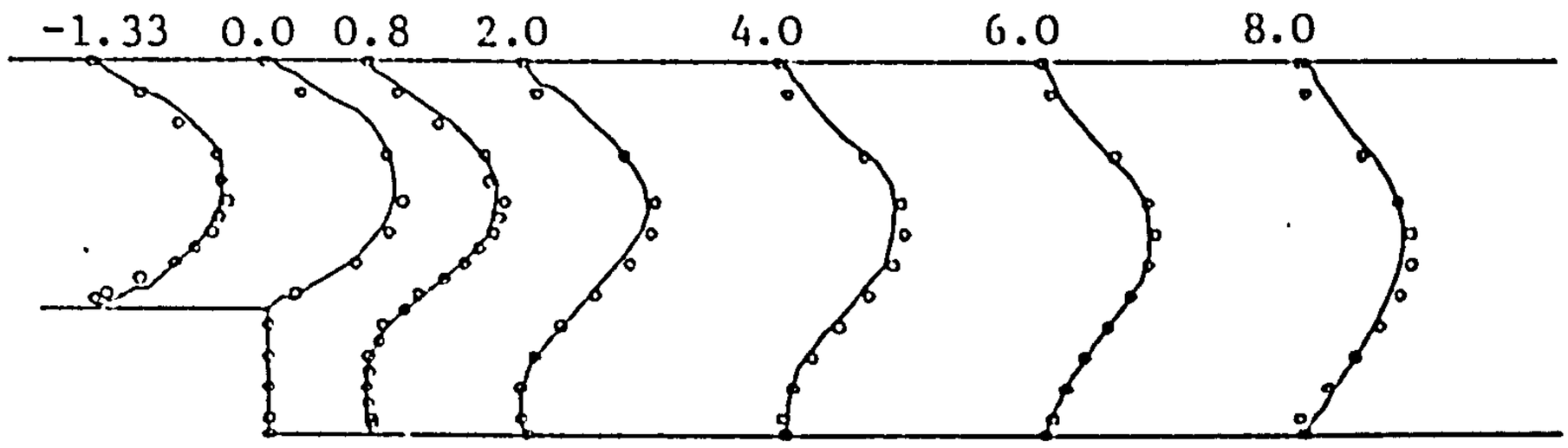

(a) Coarse results

—— Denham and Patrick

o Current work

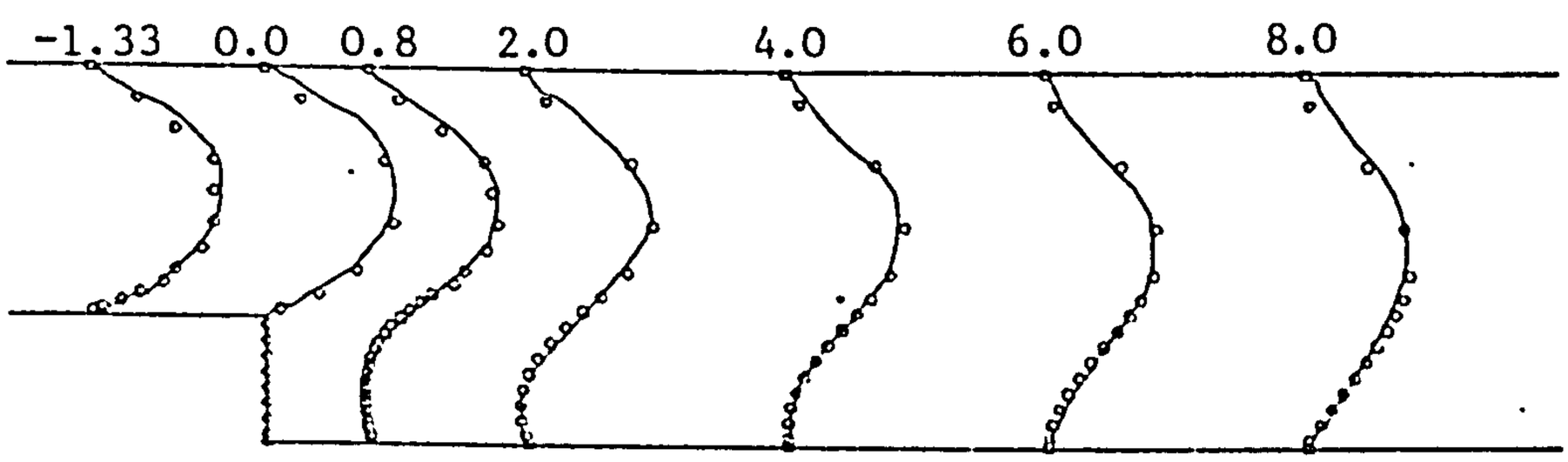

(b) Fine results

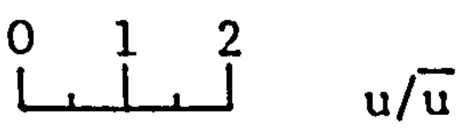

• Hutton

+ Atkin et al

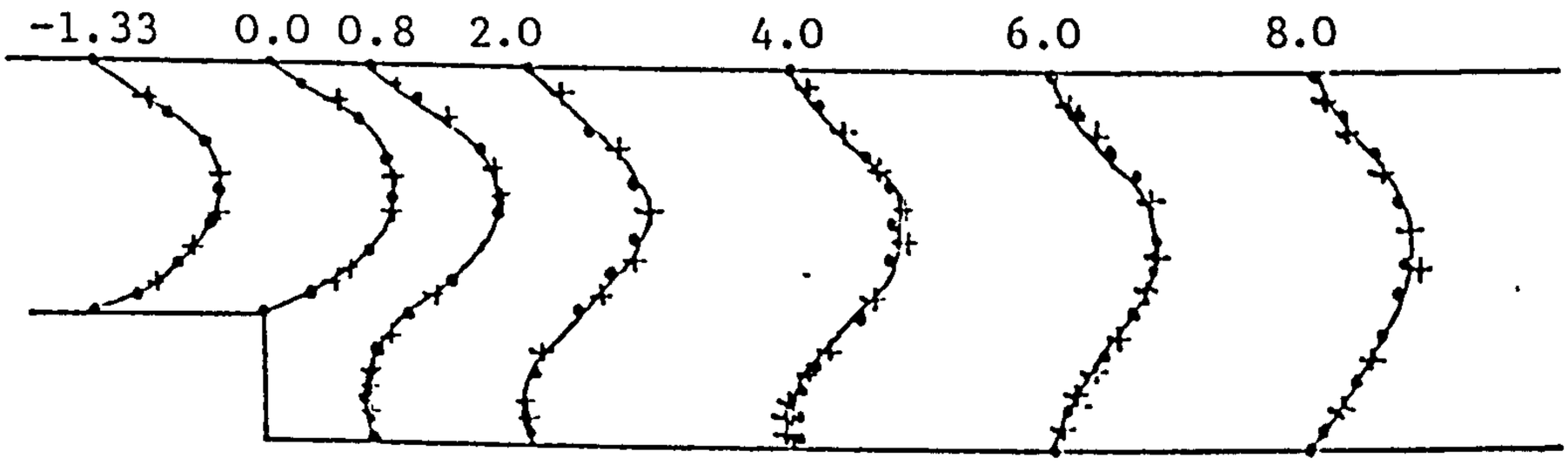

(c) Earlier results

Figure 5.12 The Velocity at R_e = 73

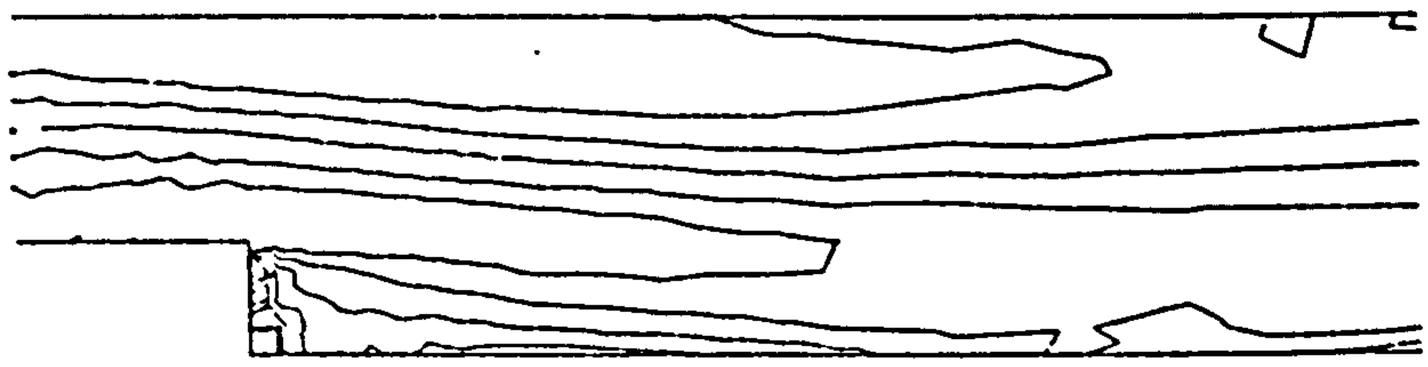

(a) Coarse results

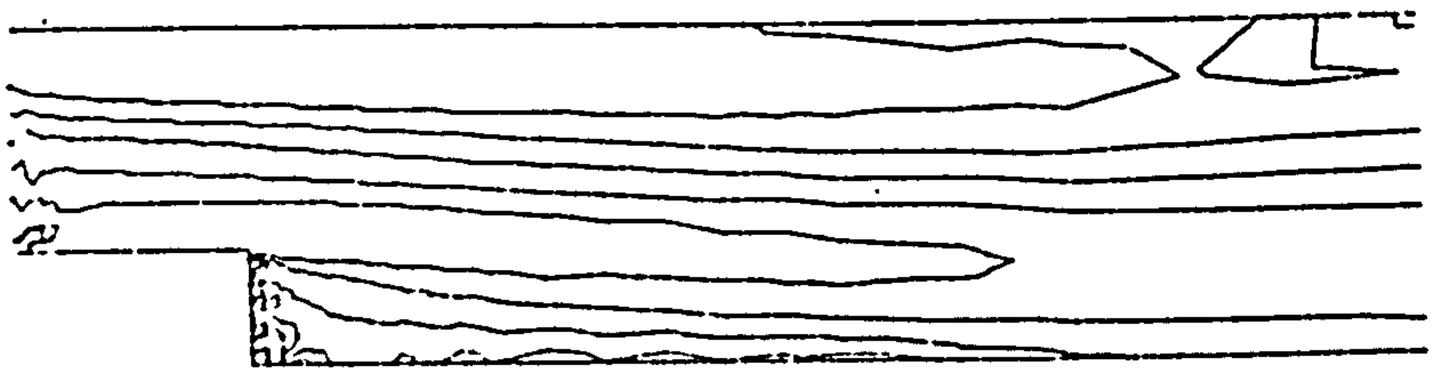

(b) Fine results

Figure 5.13 The Vorticity at R_e = 125

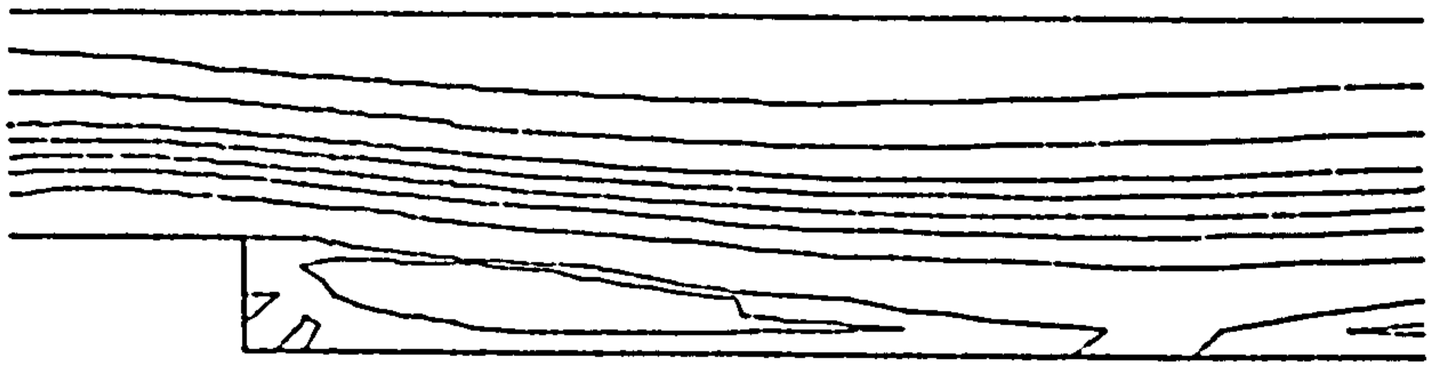

(a) Coarse results

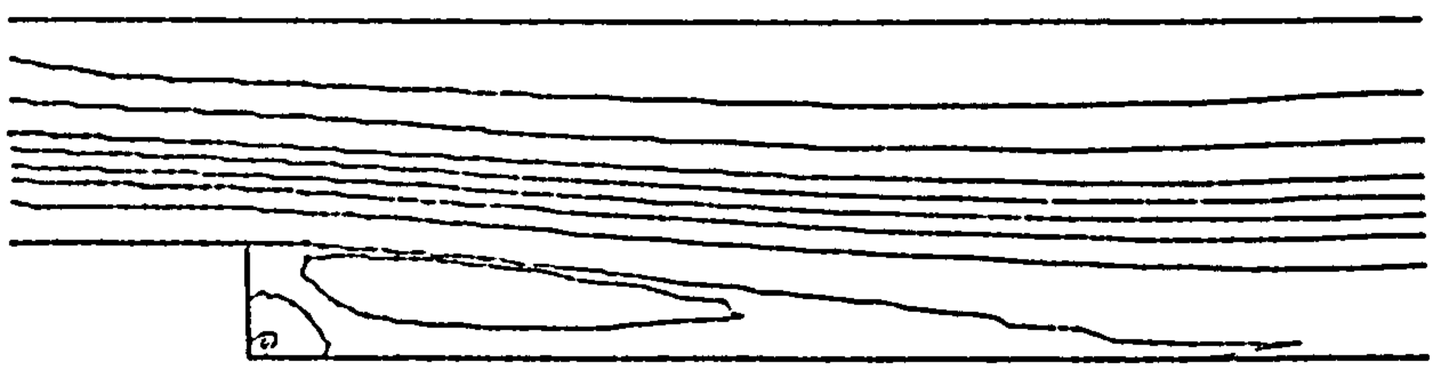

(b) Fine results

Figure 5.14 The Stream Function at R_e = 125

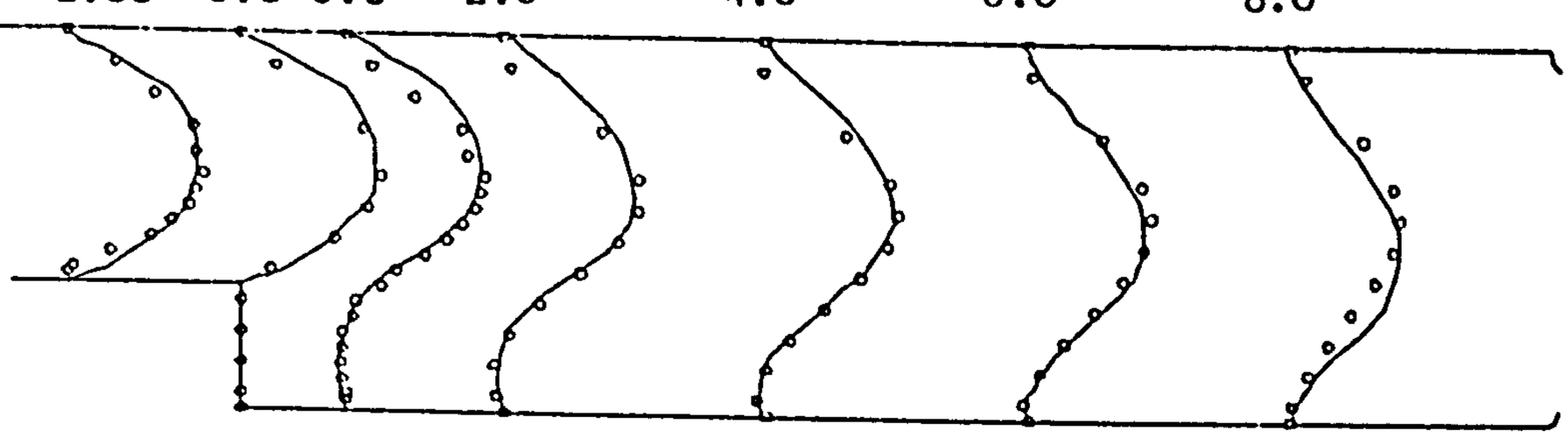

(a) Coarse results

—— Denham and Patrick

o Current results

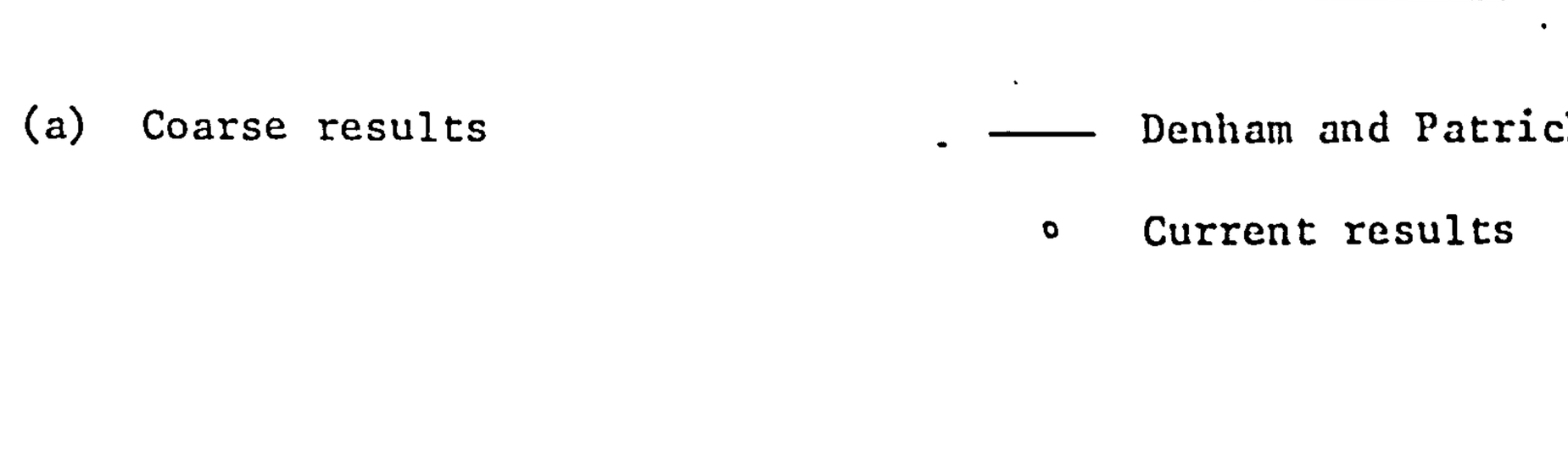

(b) Fine results

Figure 5.15 The Velocity at R_e = 125

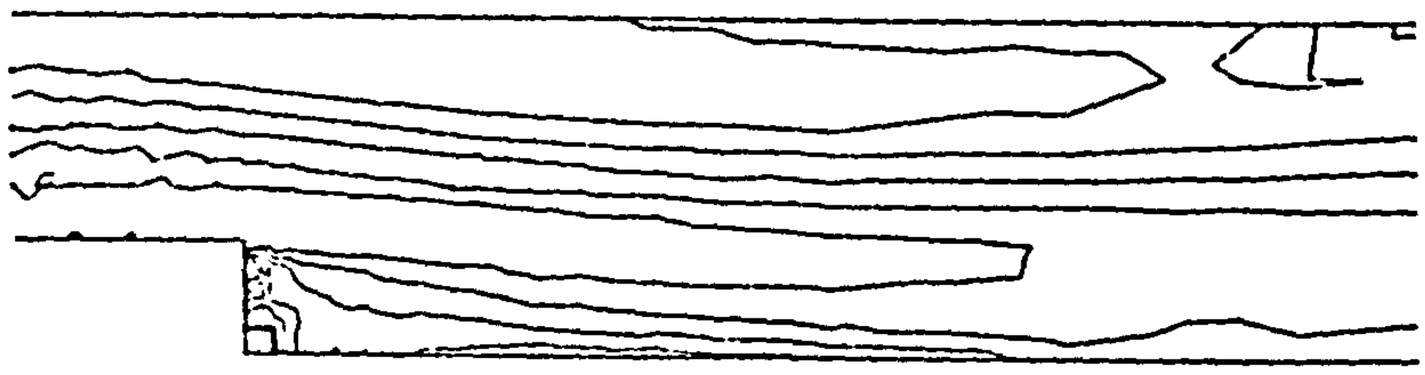

(a) Coarse results

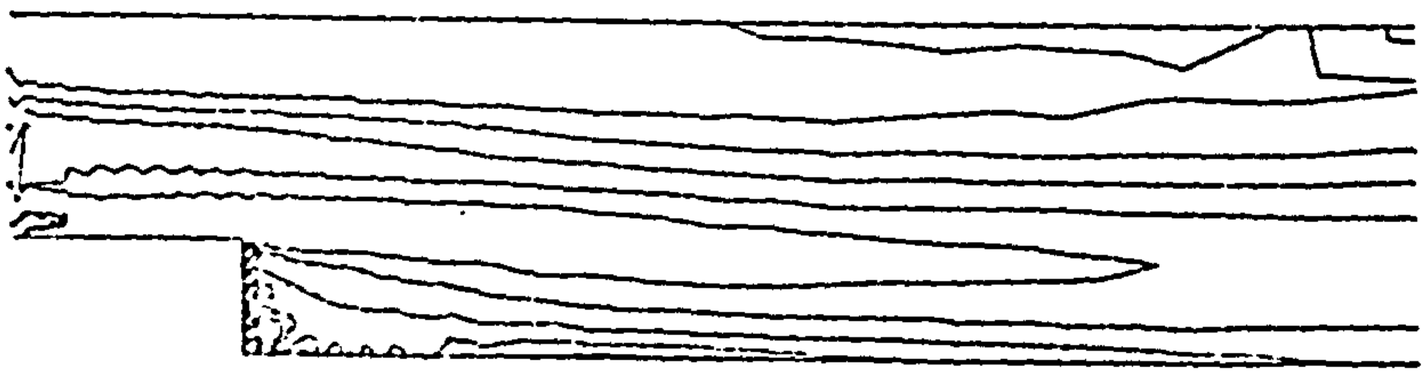

(b) Fine results

Figure 5.16 The Vorticity at R_c = 191

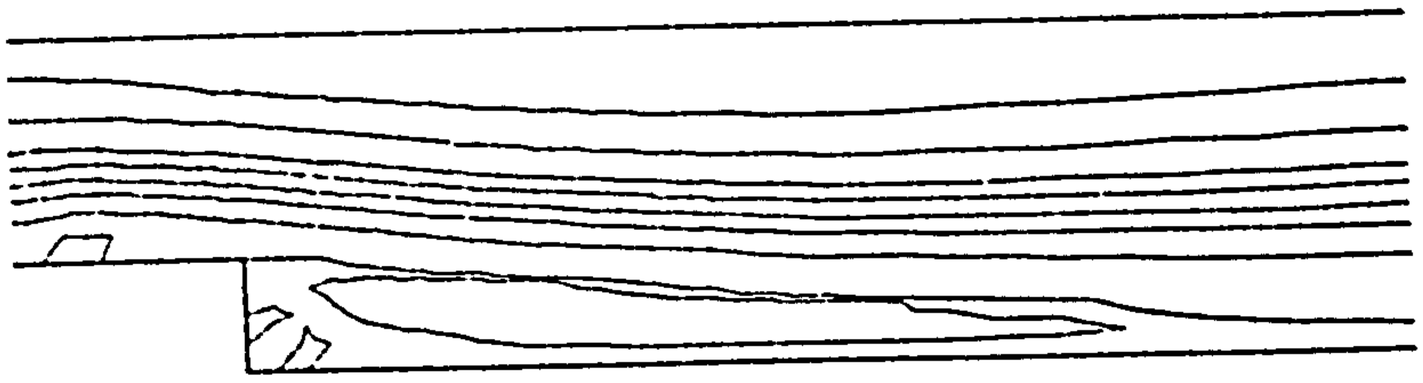

(a) Coarse results

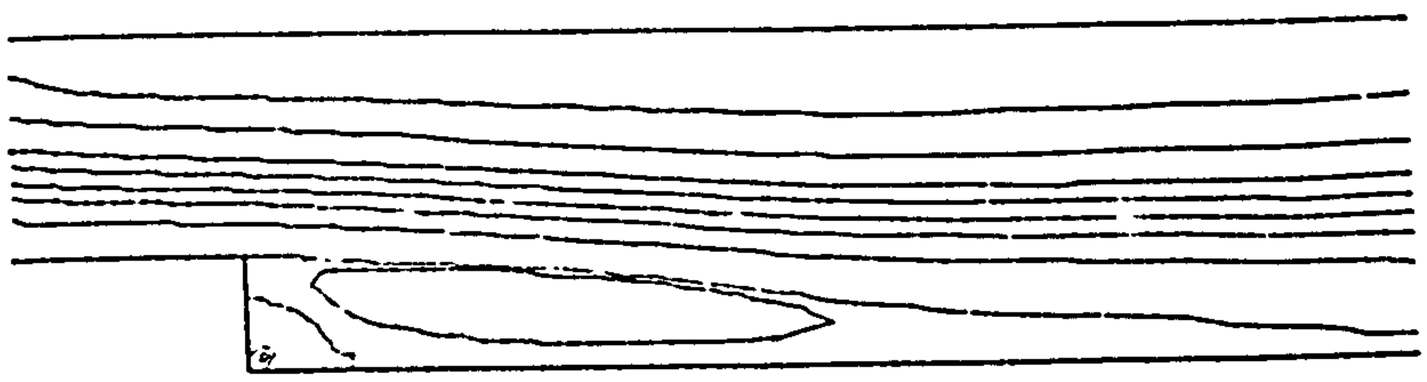

(b) Fine results

Figure 5.17 The Stream Function at R_e = 191

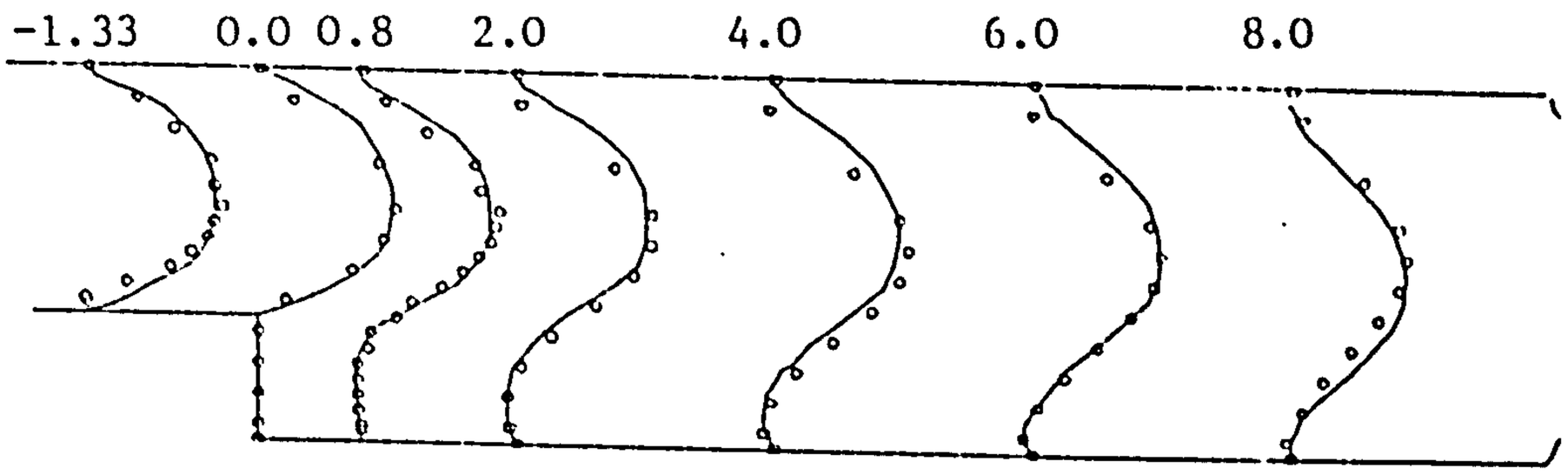

(a) Coarse results

—— Denham and Patrick

o Current results

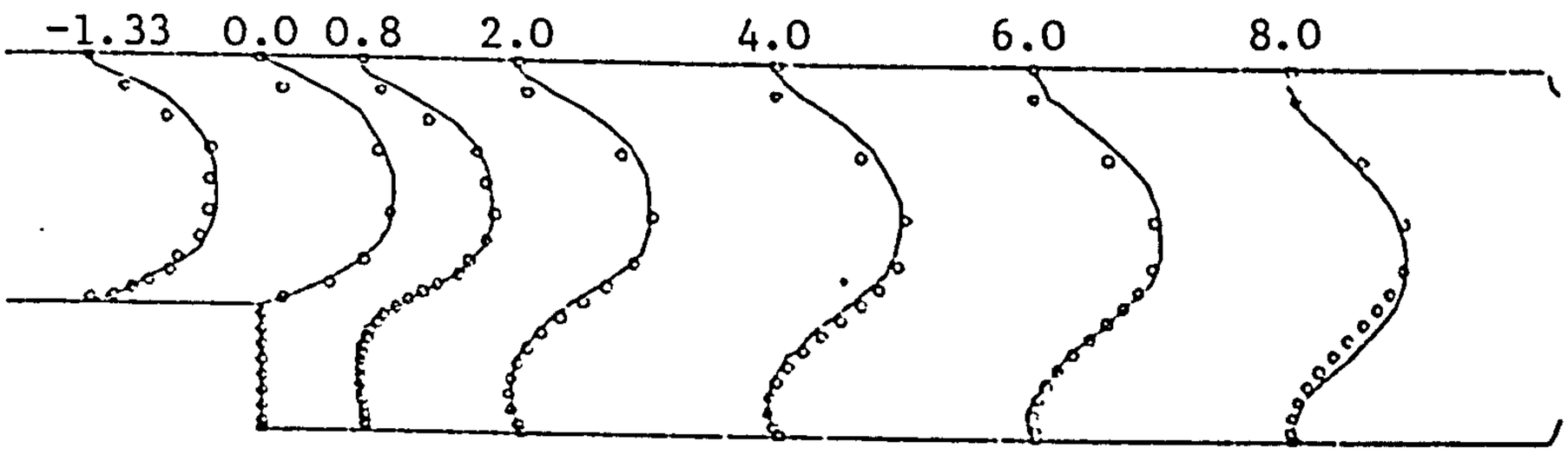

(b) Fine results

• Hutton

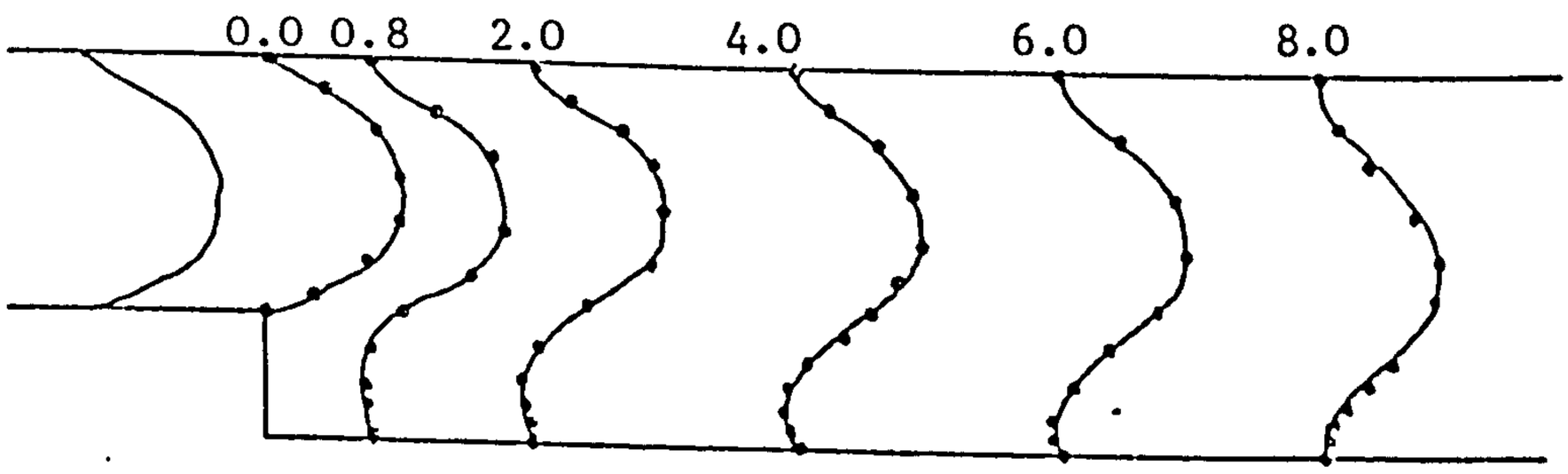

(c) Earlier results

Figure 5.18 The Velocity at R_c = 191

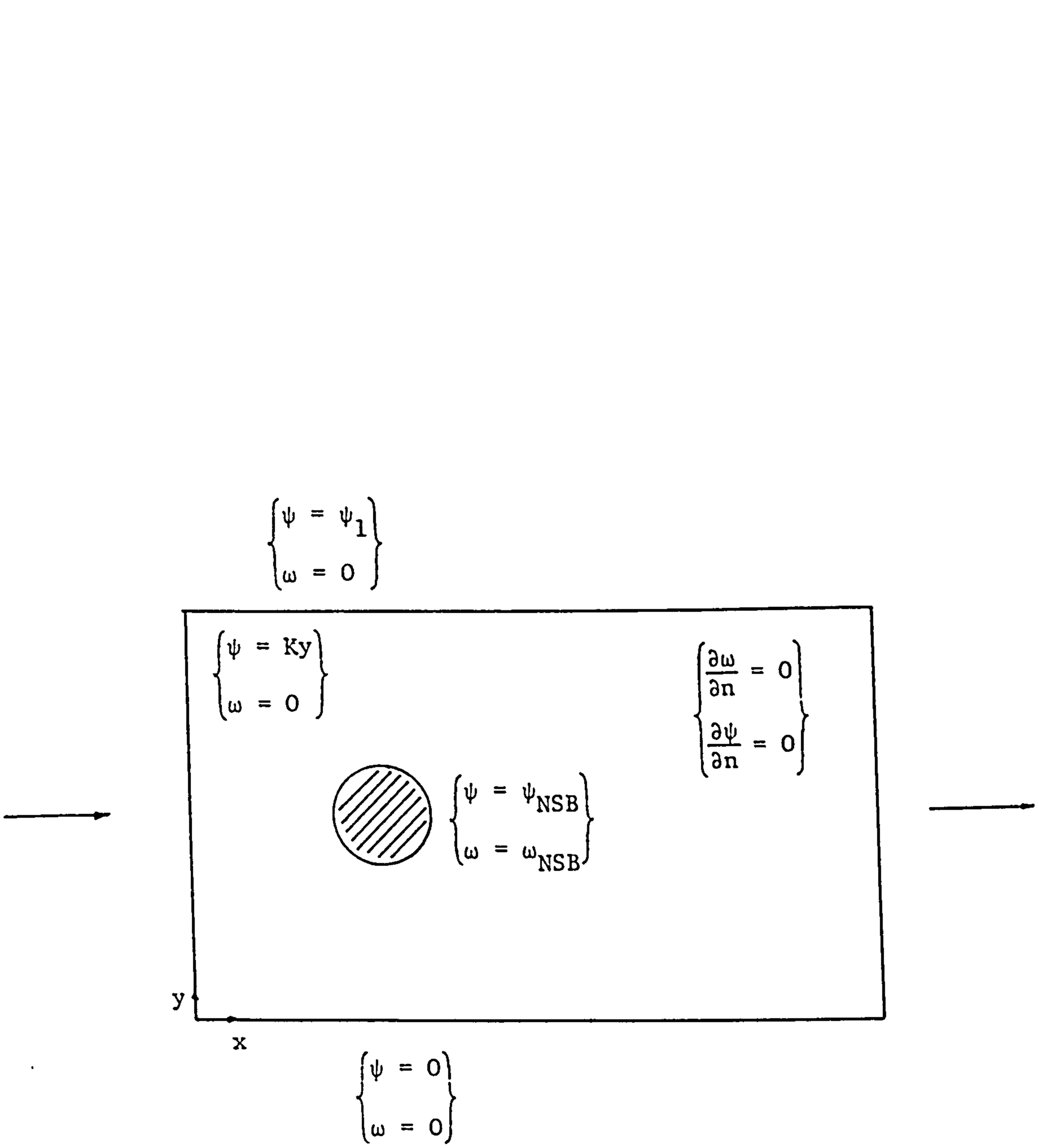

K - is the magnitude of the inlet velocity

Figure 5.19 The Flow Past a Circular Cylinder with the Inlet Flow Being Prescribed.Parallel.

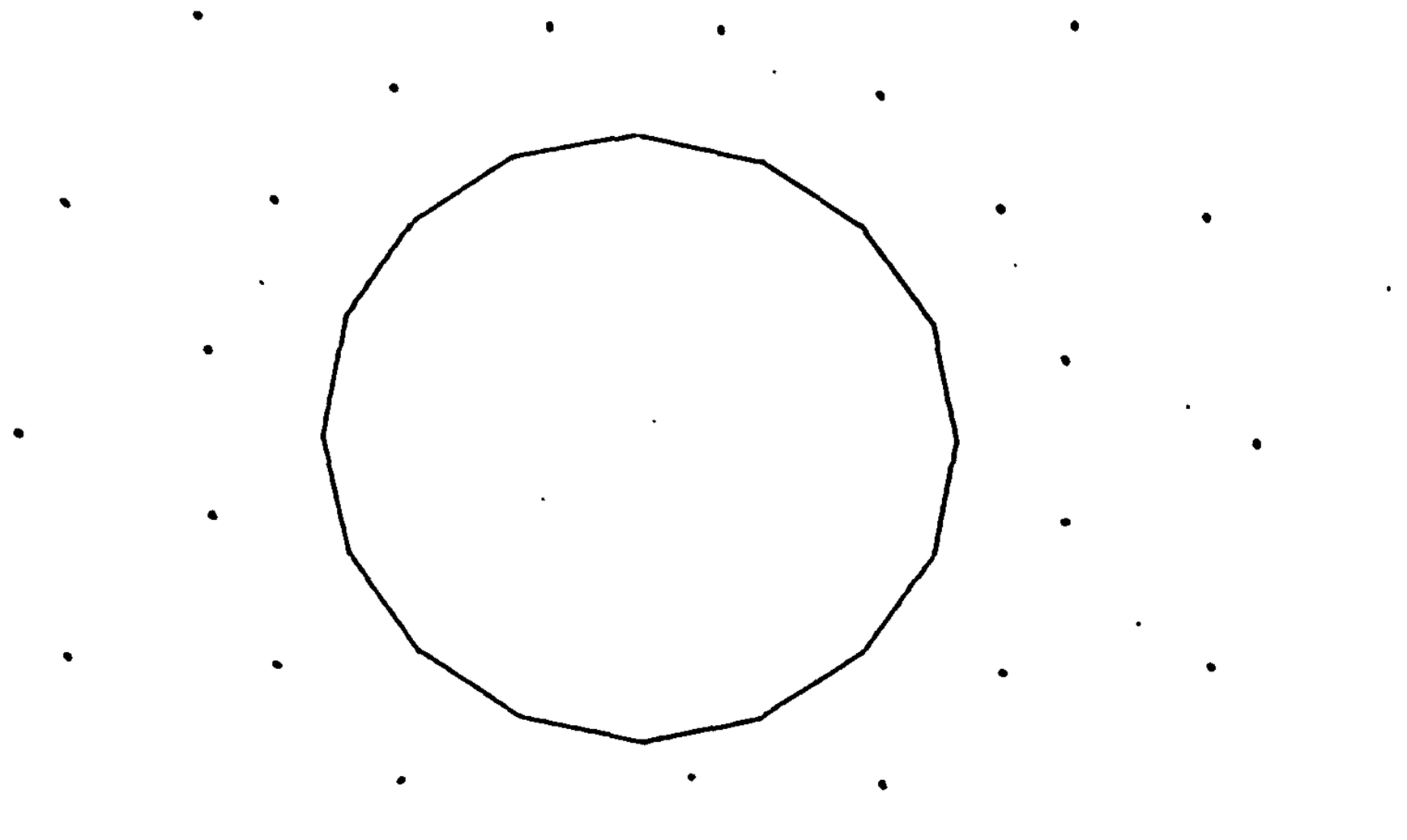

Figure 5.20 The Nodal Distributions about the Cylinder

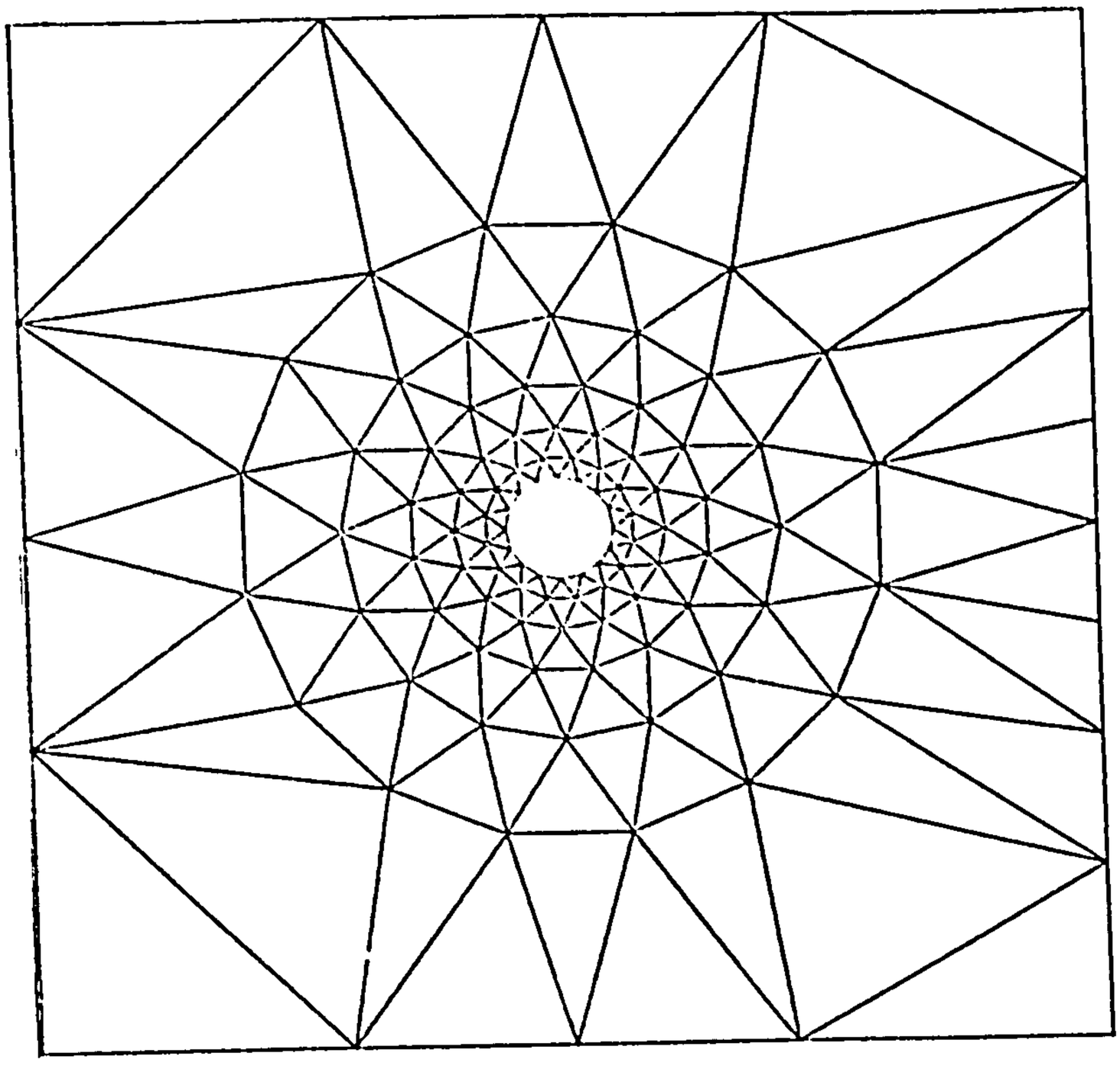

(a) Coarse mesh nodes = 16

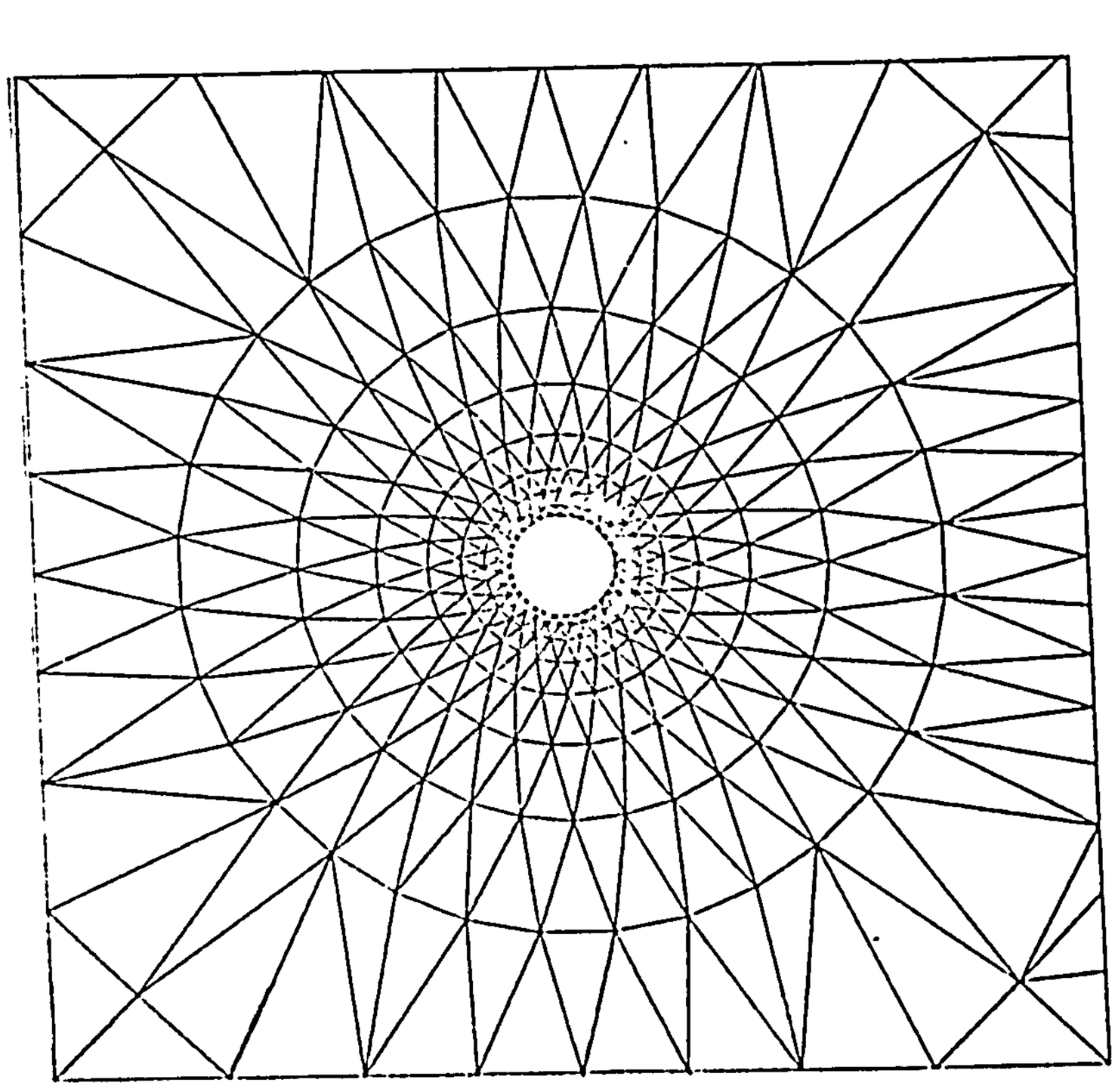

(b) Fine mesh nodes = 32

Figure 5.21 Element Distributions about the Cylinder

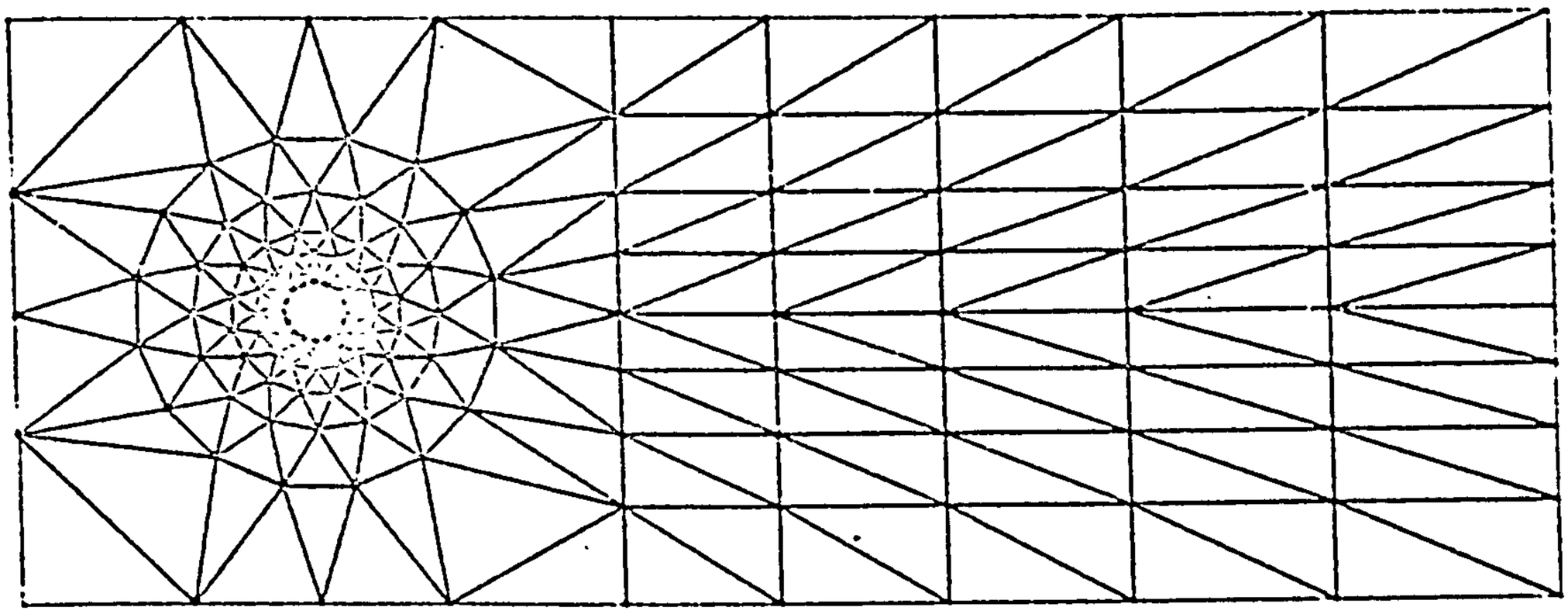

Figure 5.22 The Complete Mesh with 16 nodes Surrounding the Obstruction

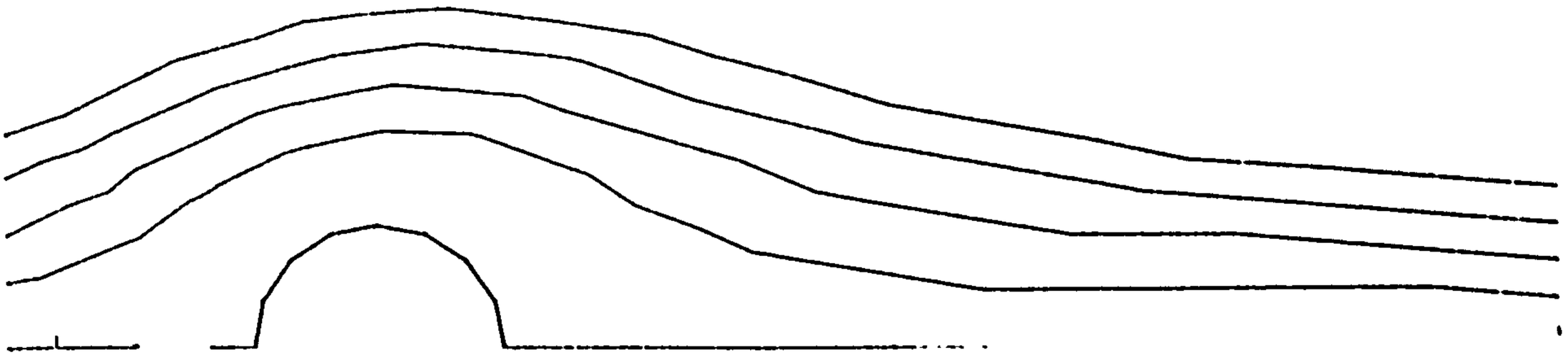

(a) Coarse results

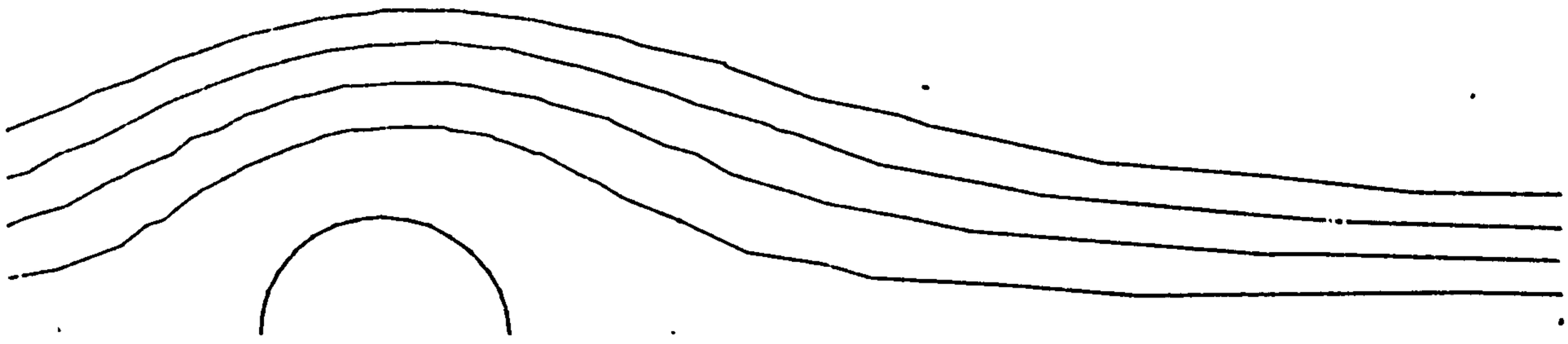

(b) Fine results

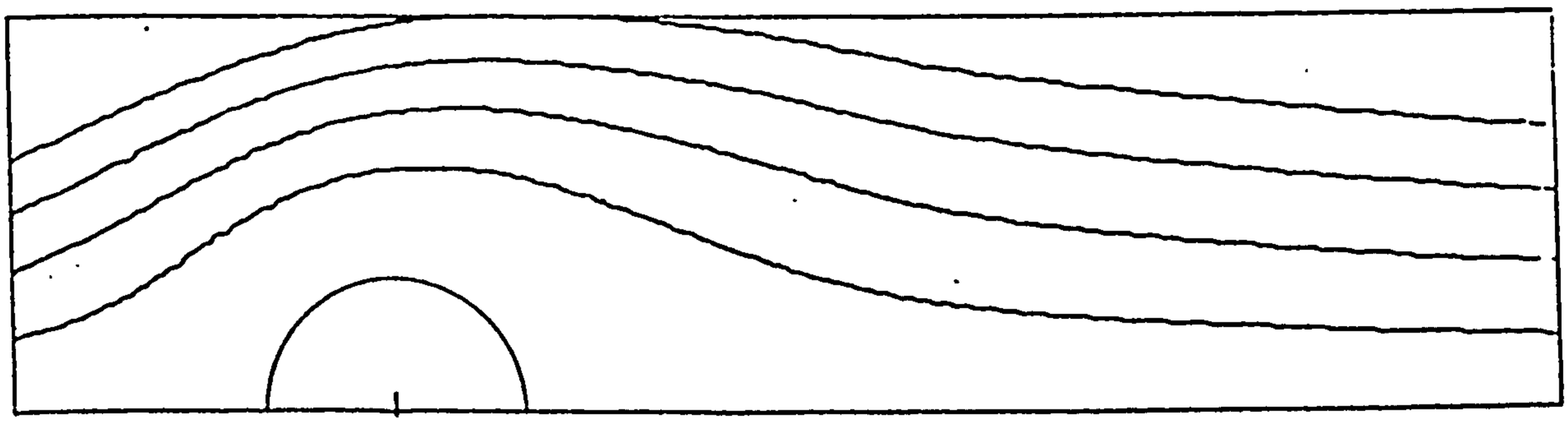

(c) ref: 48

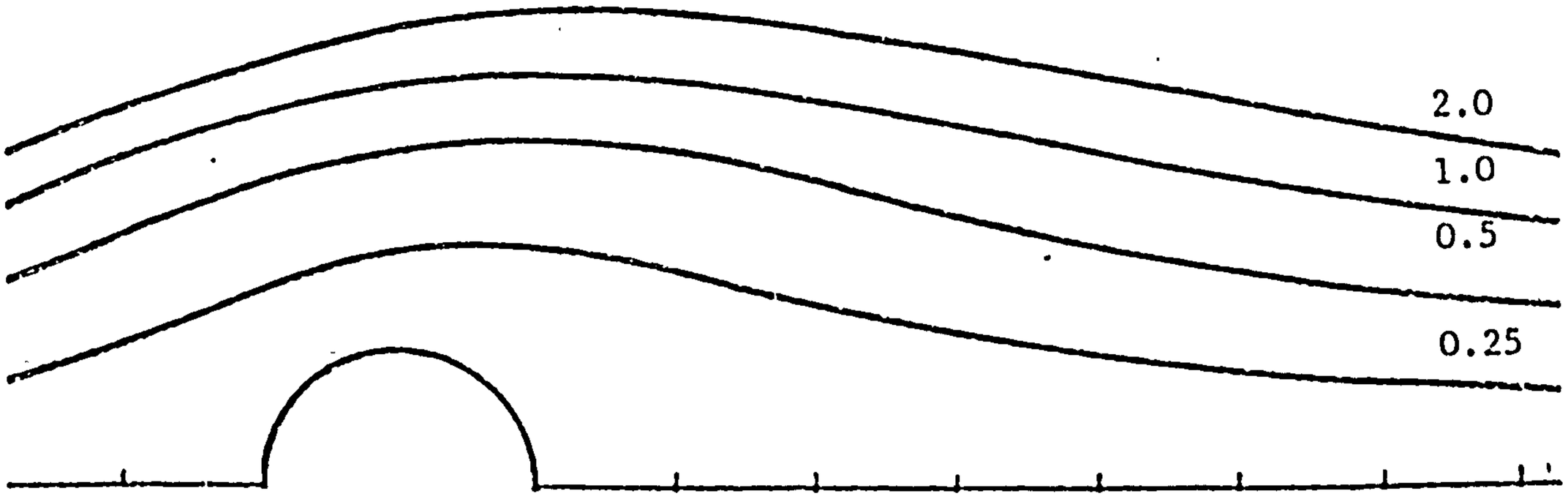

(d) ref: 44

Figure 5.23 The Stream Function at $R_e = 1$

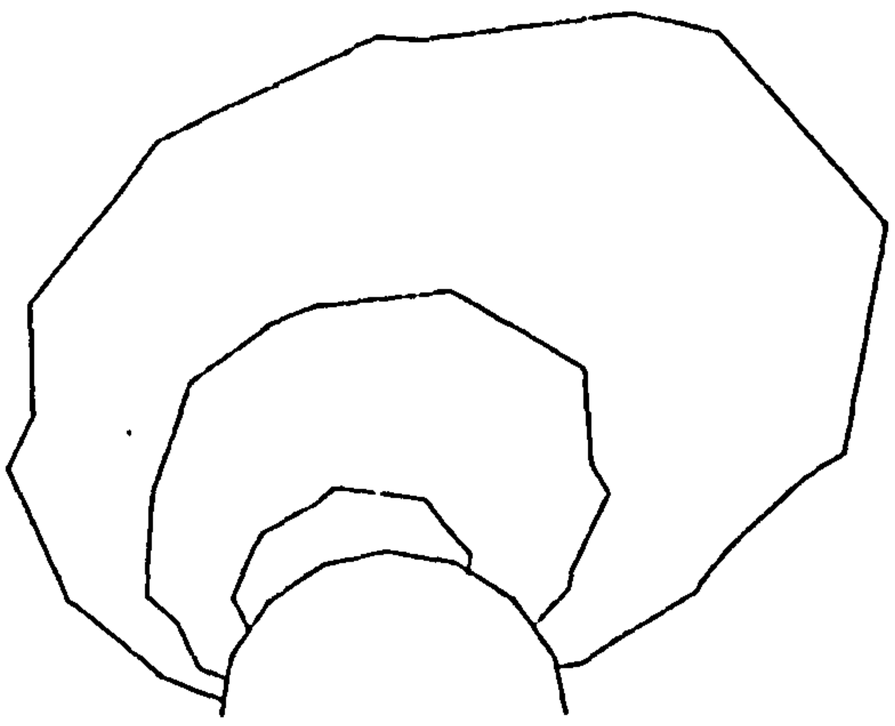

(a) Coarse results

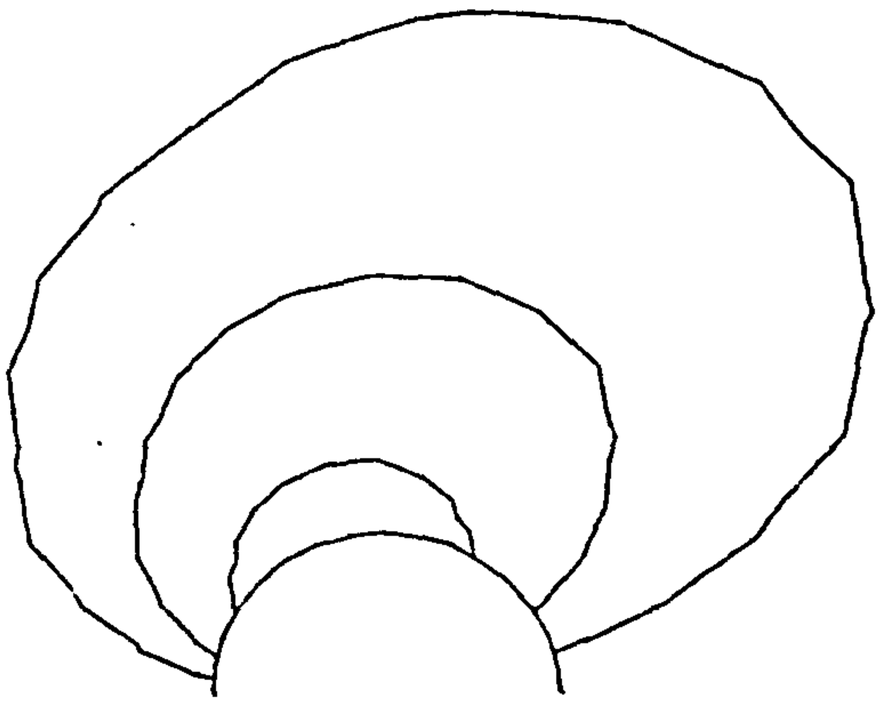

(b) Fine results

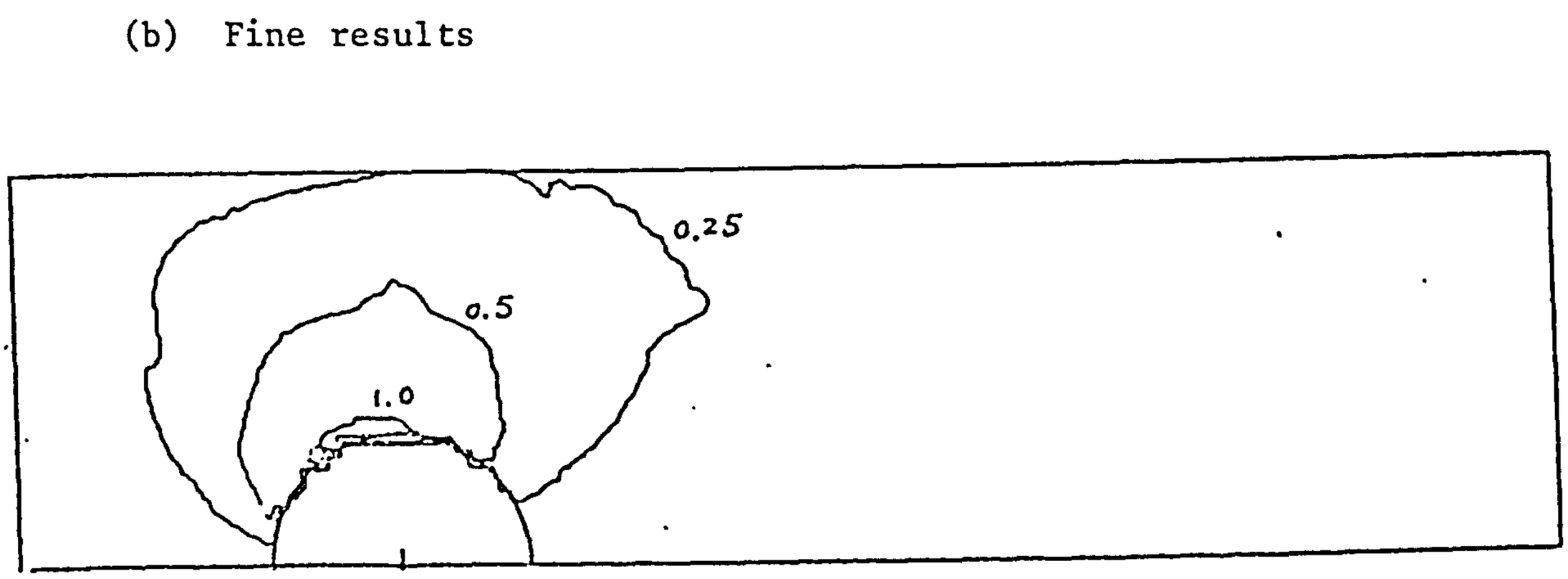

(c) ref: 48

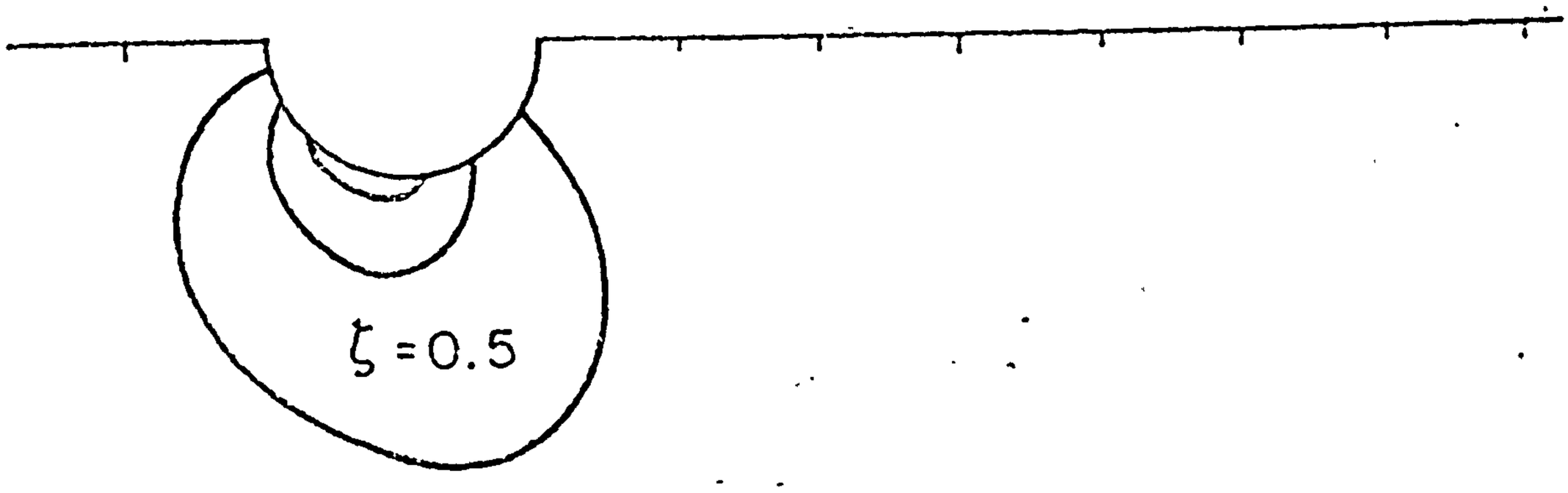

(d) ref: 44

Figure 5.24 The Vorticity at R_e = 1

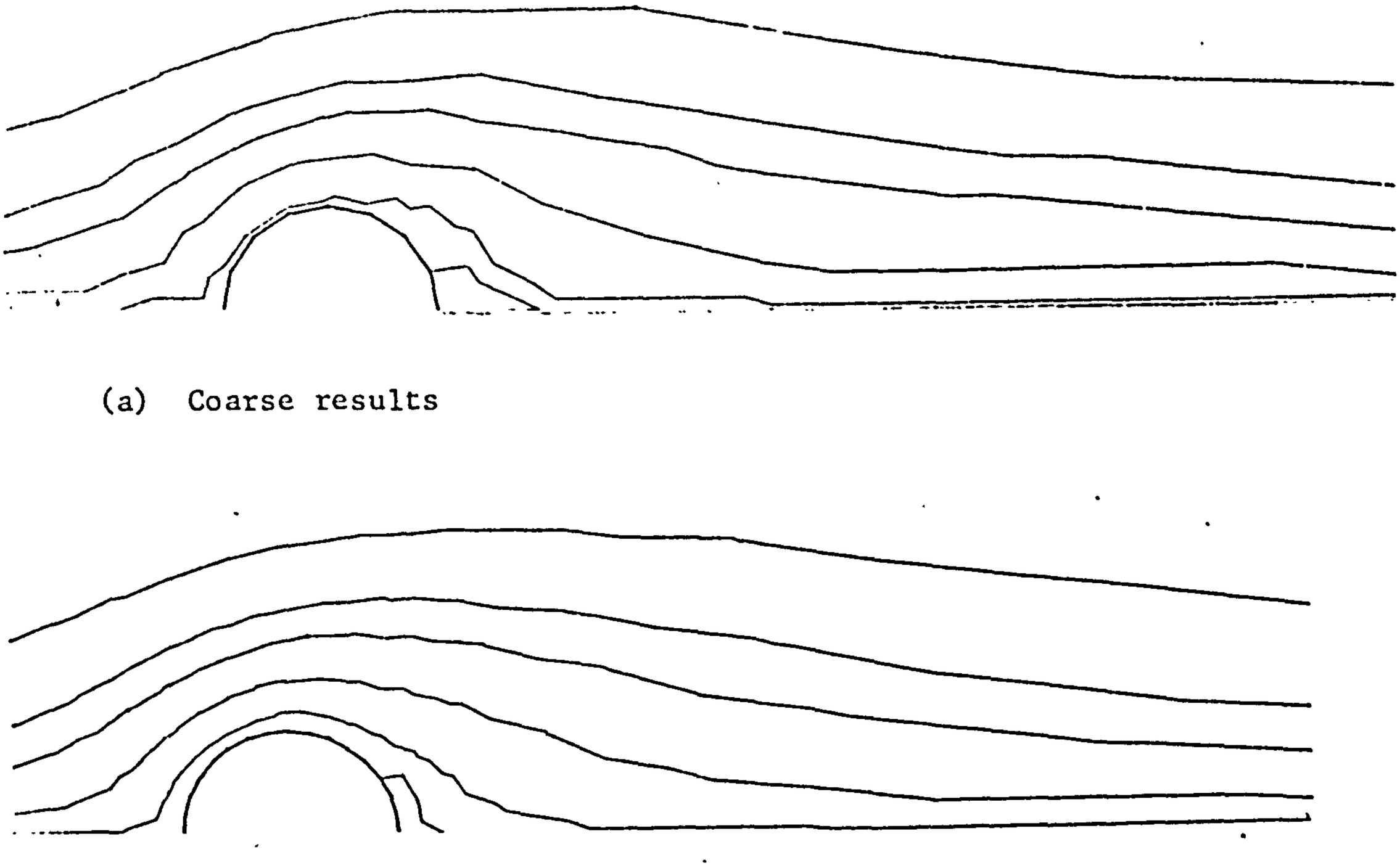

(a) Coarse results

(b) Fine results

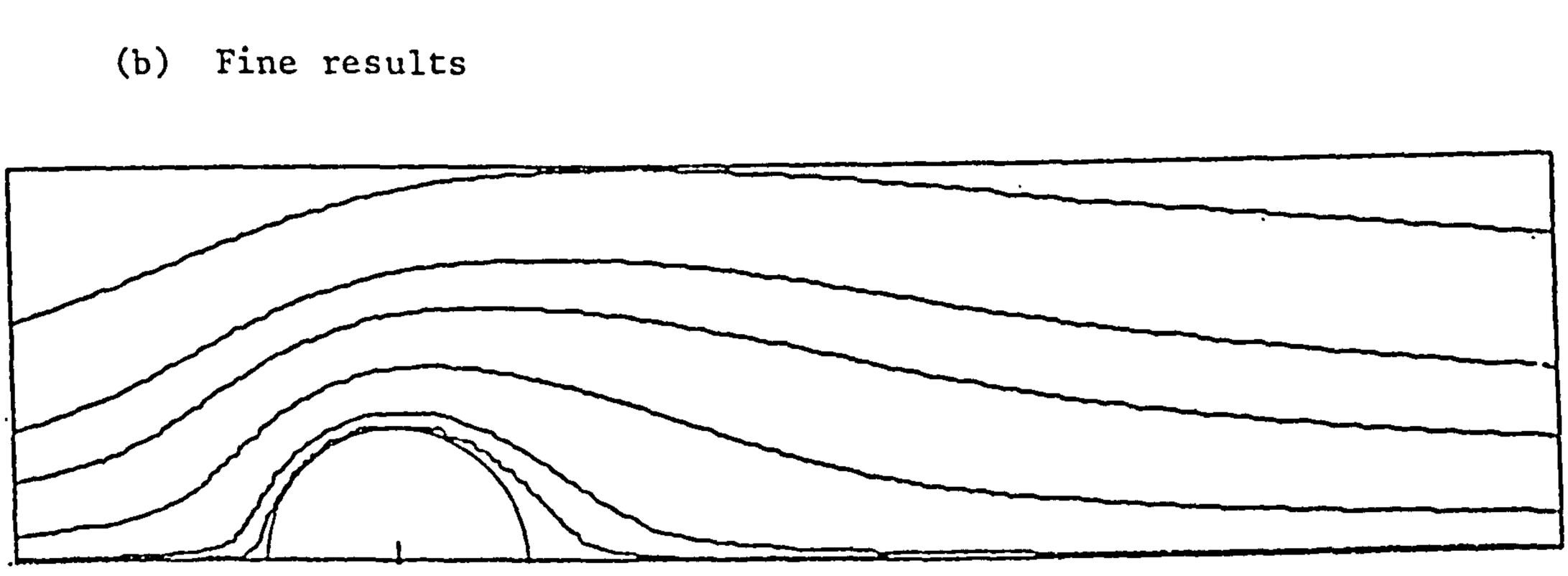

(c) ref: 48

(d) ref: 44

Figure 5.25 The Stream Function at $R_e = 5$

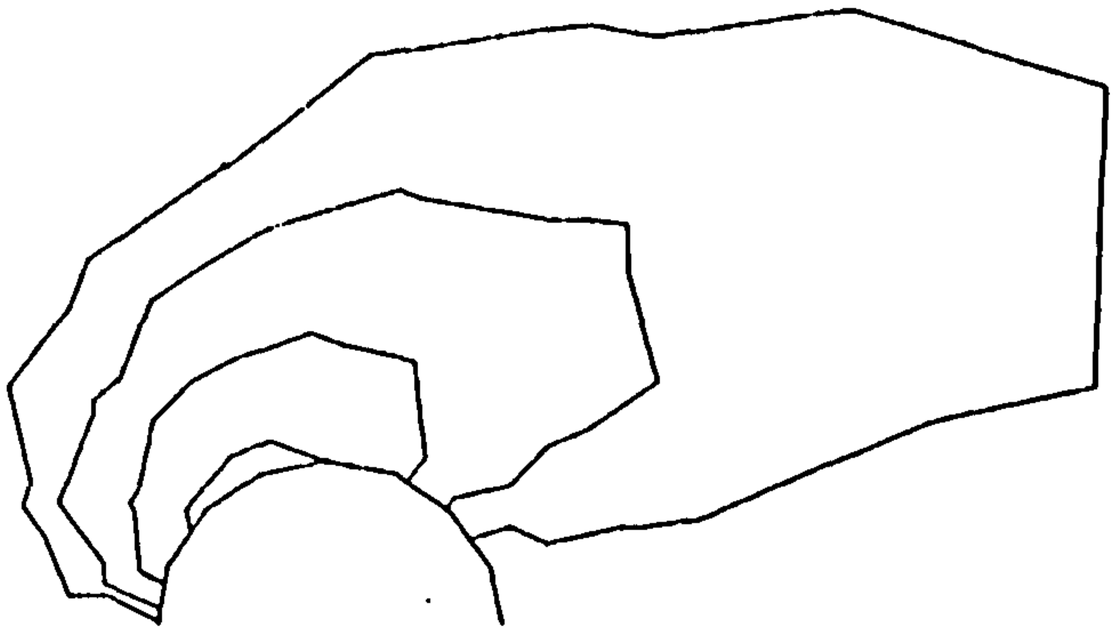

(a) Coarse results

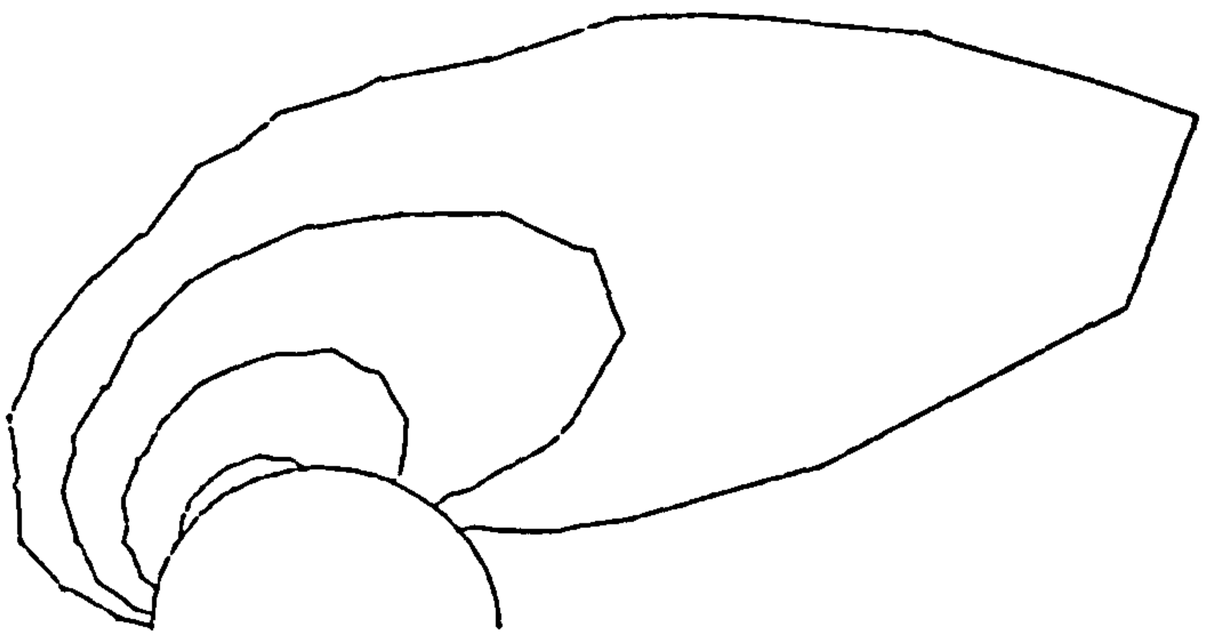

(b) Fine results

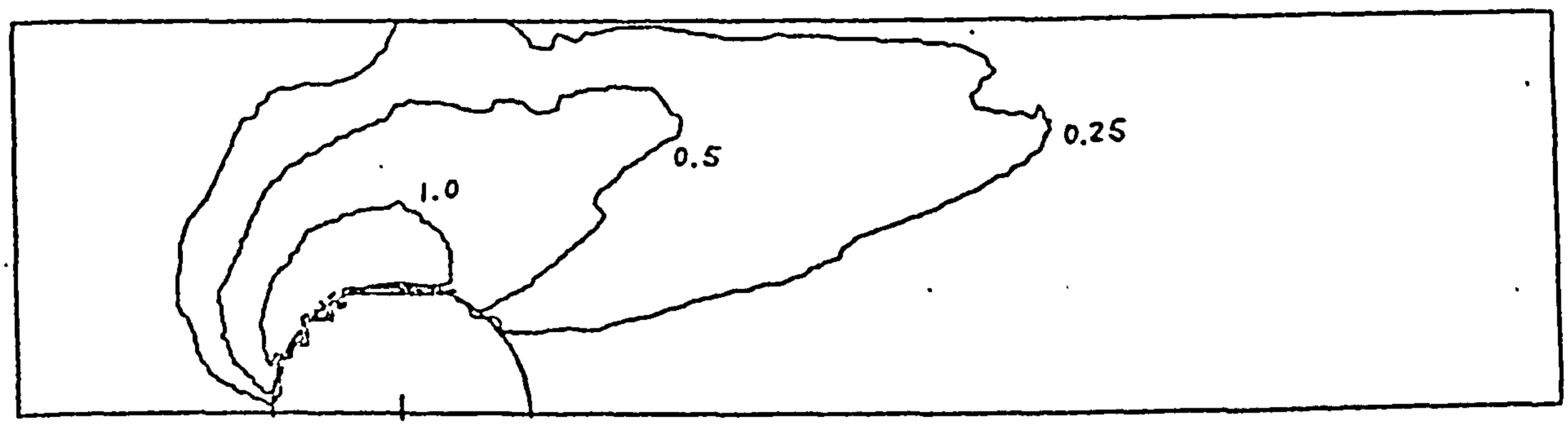

(c) ref: 48

Figure 5.26 The Vorticity At R_e = 5

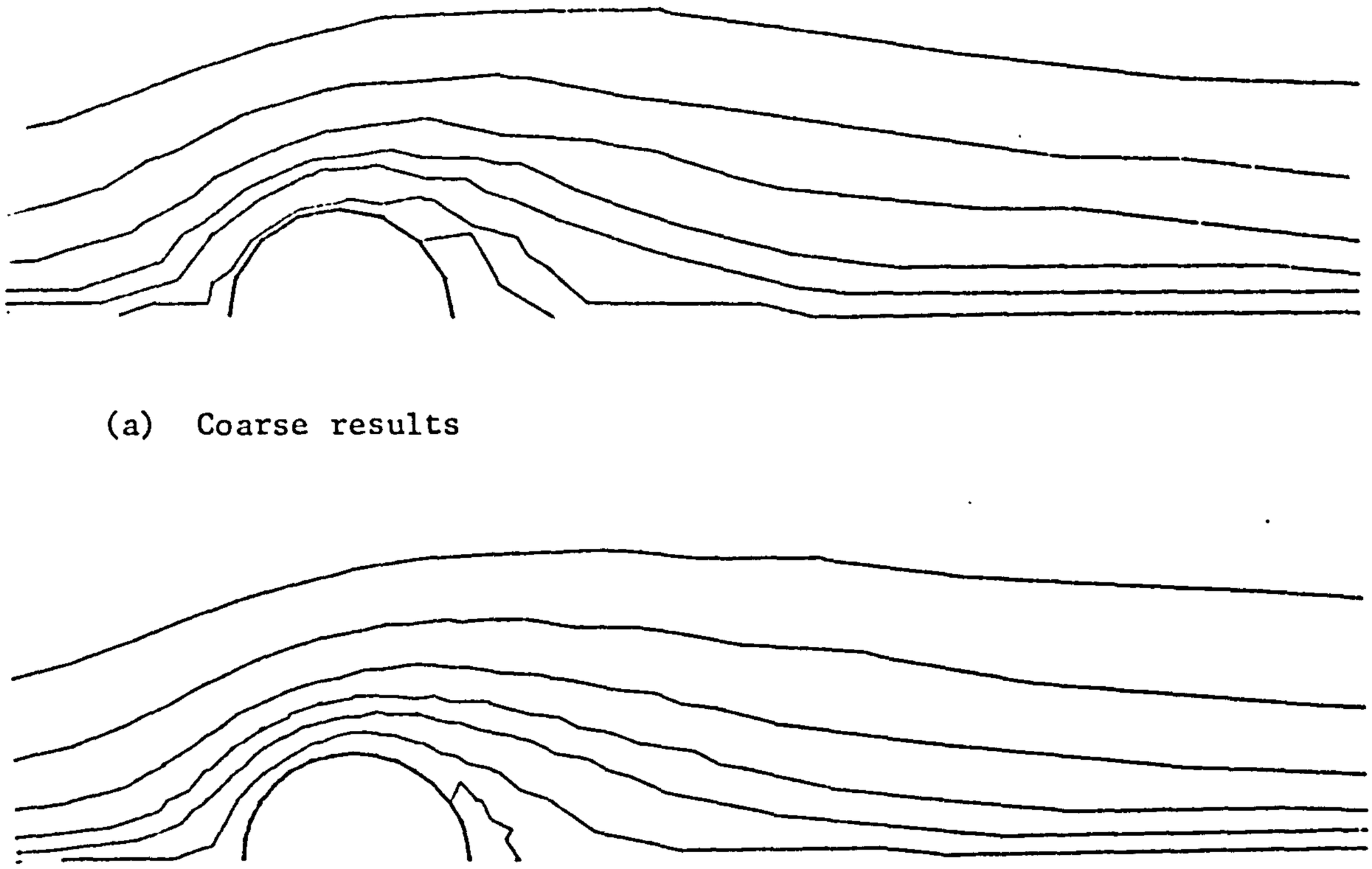

(a) Coarse results

(b) Fine results

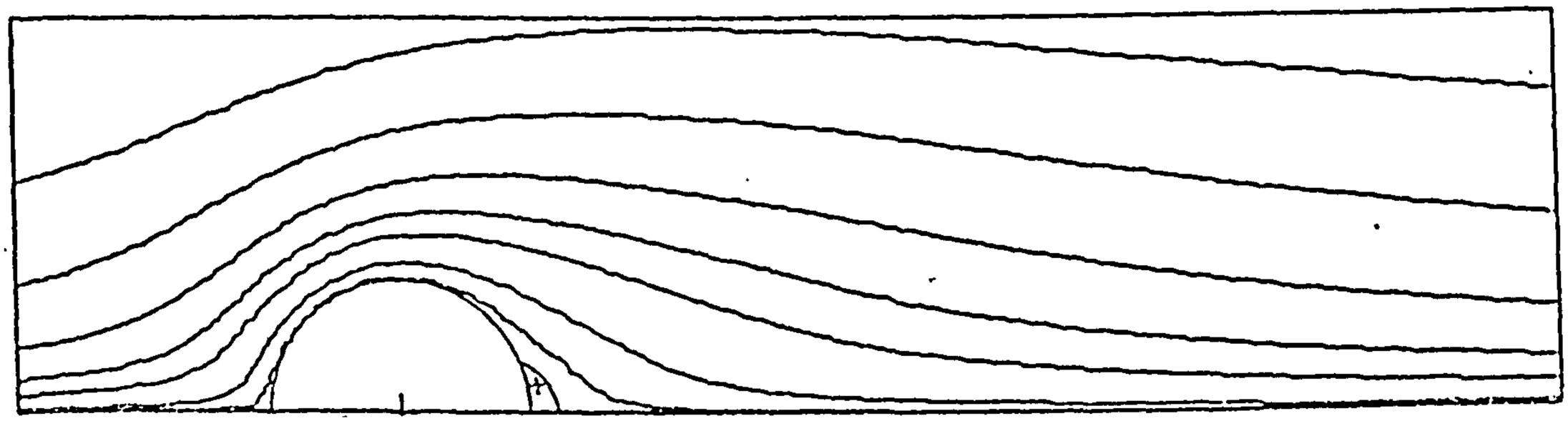

(c) ref: 48

(d) ref: 43

Figure 5.27 The Stream Function at $R_e = 7$

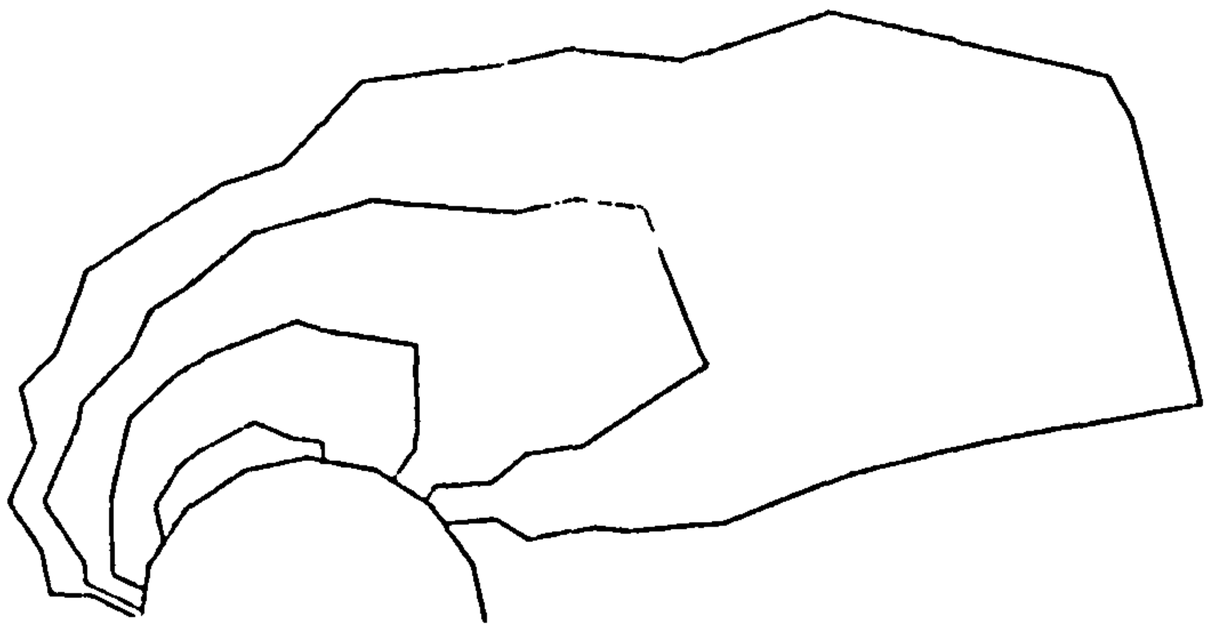

(a) Coarse results

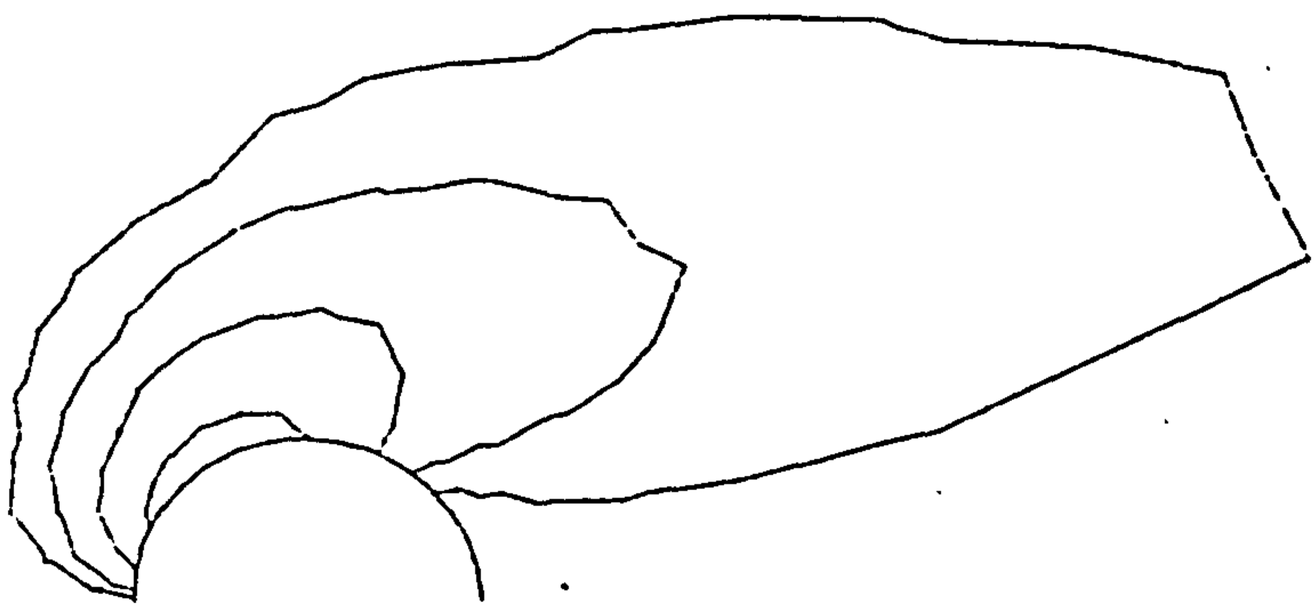

(b) Fine results

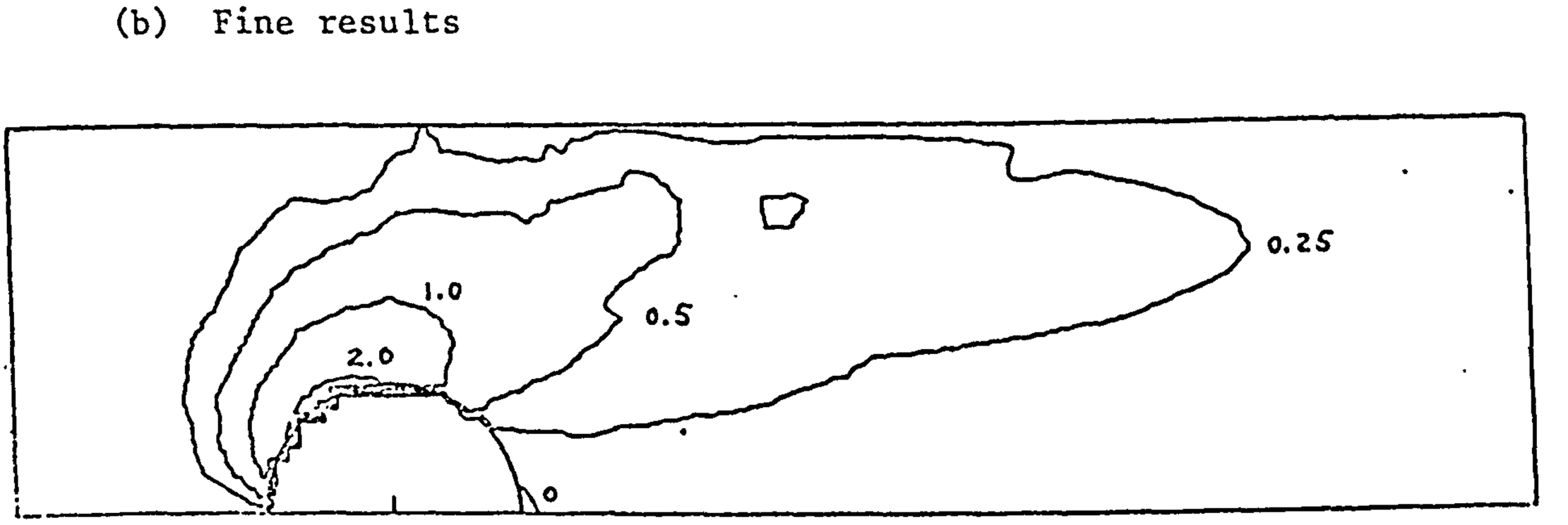

(c) ref: 48

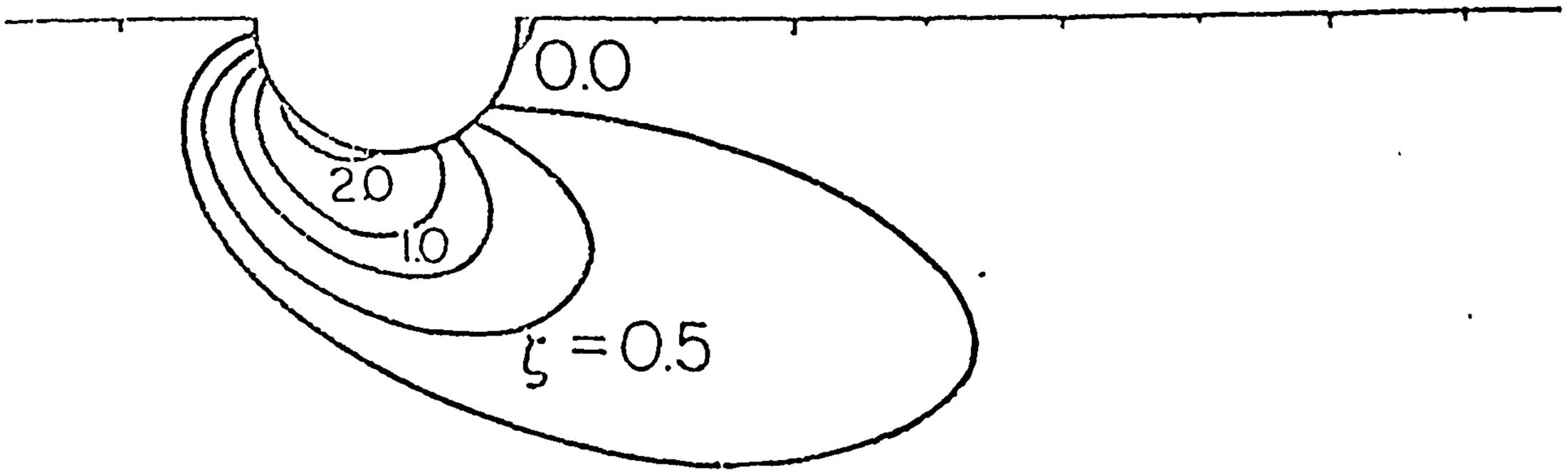

(d) ref: 43

Figure 5.28 The Vorticity at R_e = 7

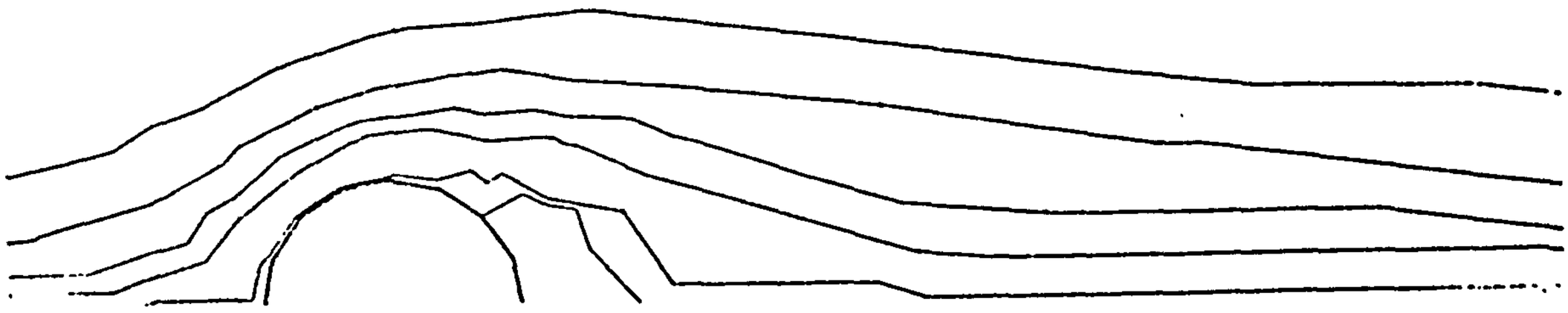

(a) Coarse results

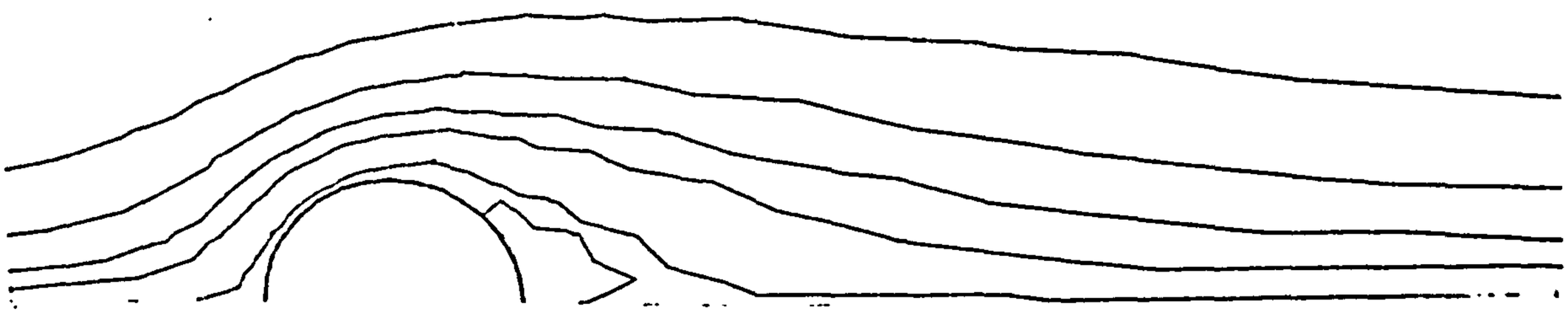

(b) Fine results

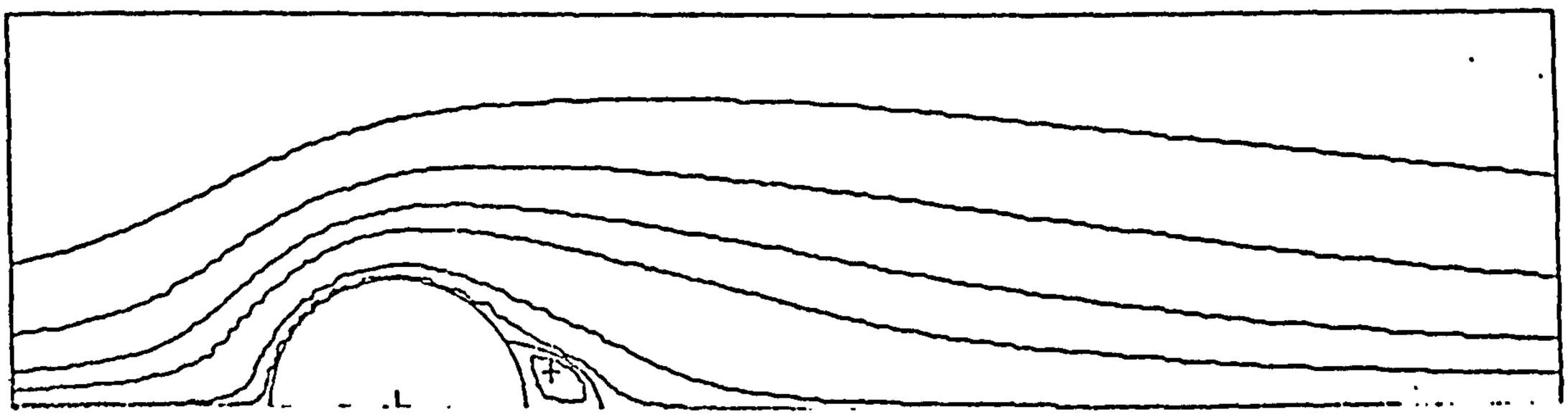

(c) ref: 48

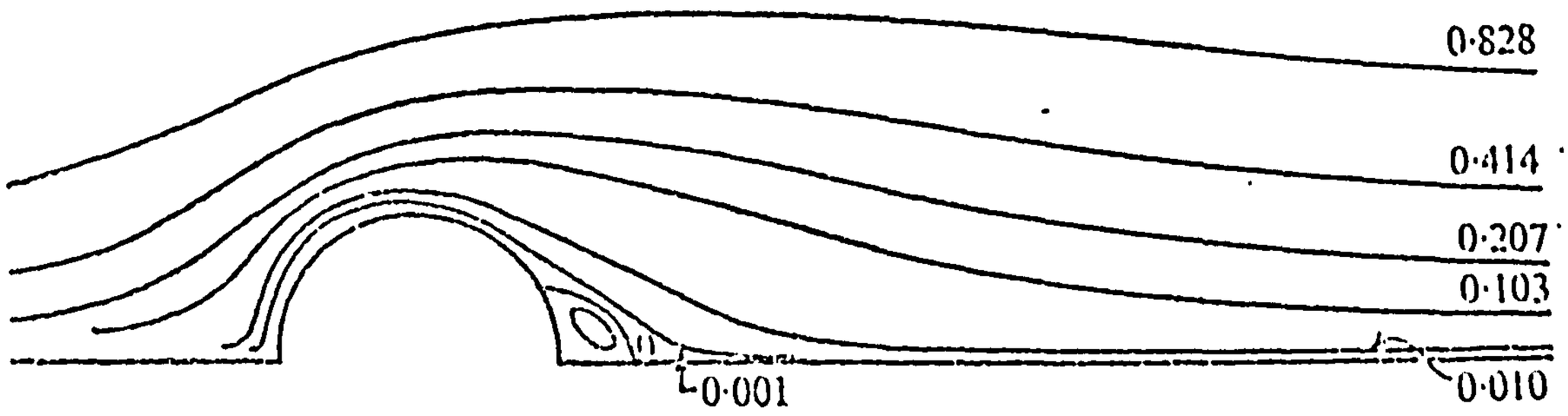

(d) ref: 43

Figure 5.29 The Stream Function at R_e = 10

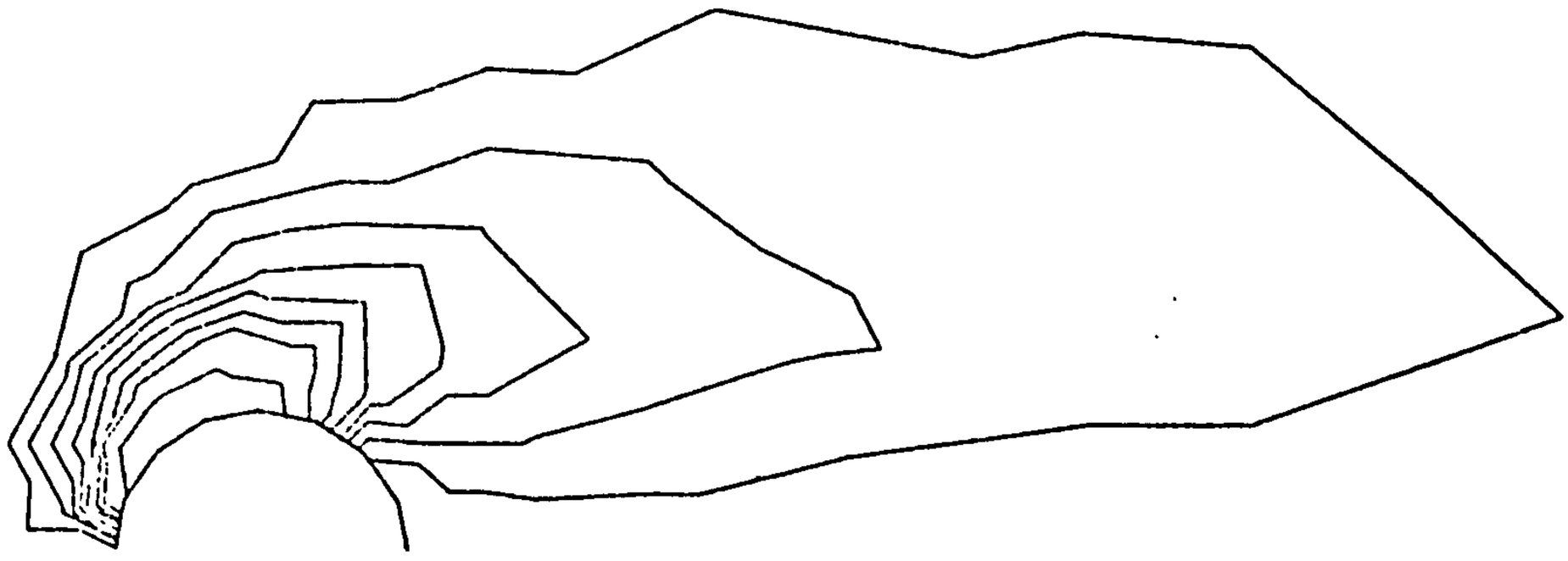

(a) Coarse results

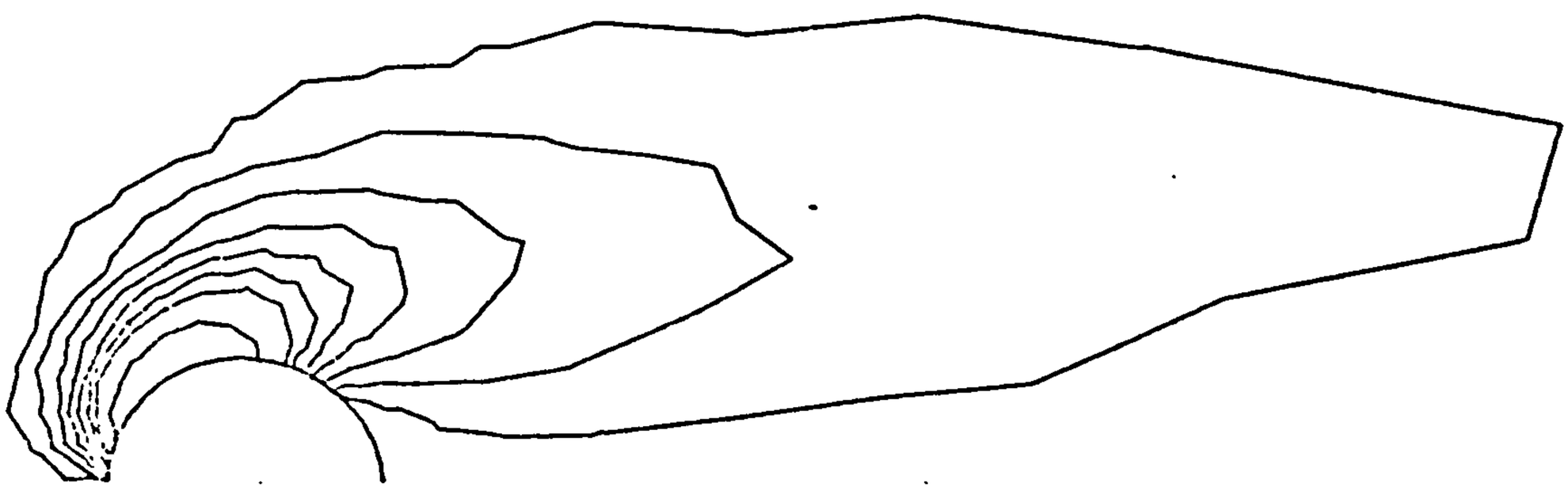

(b) Fine results

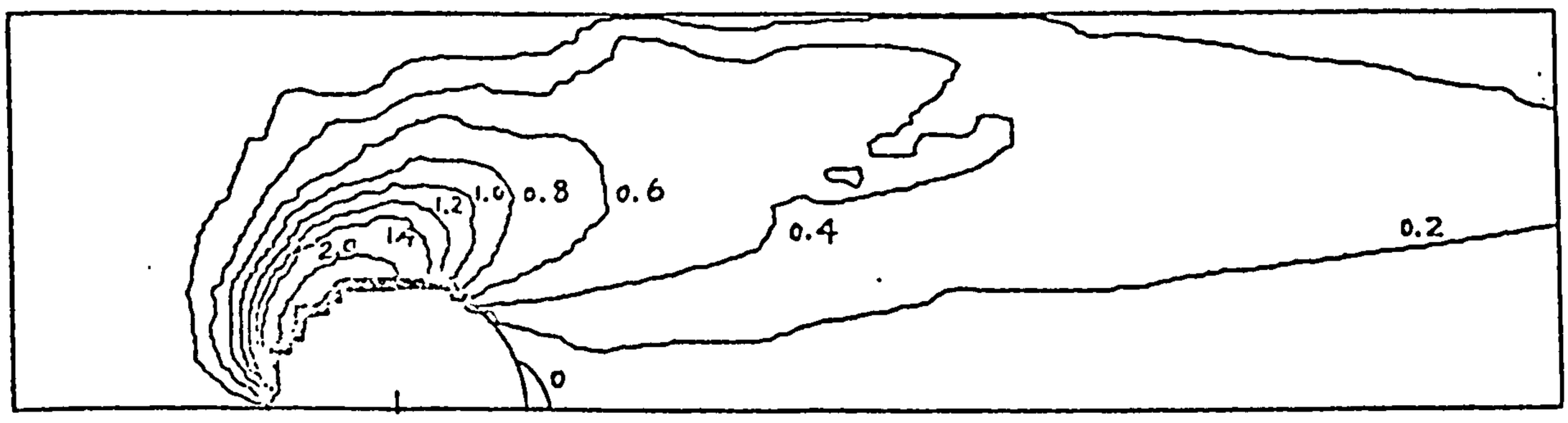

(c) ref: 48

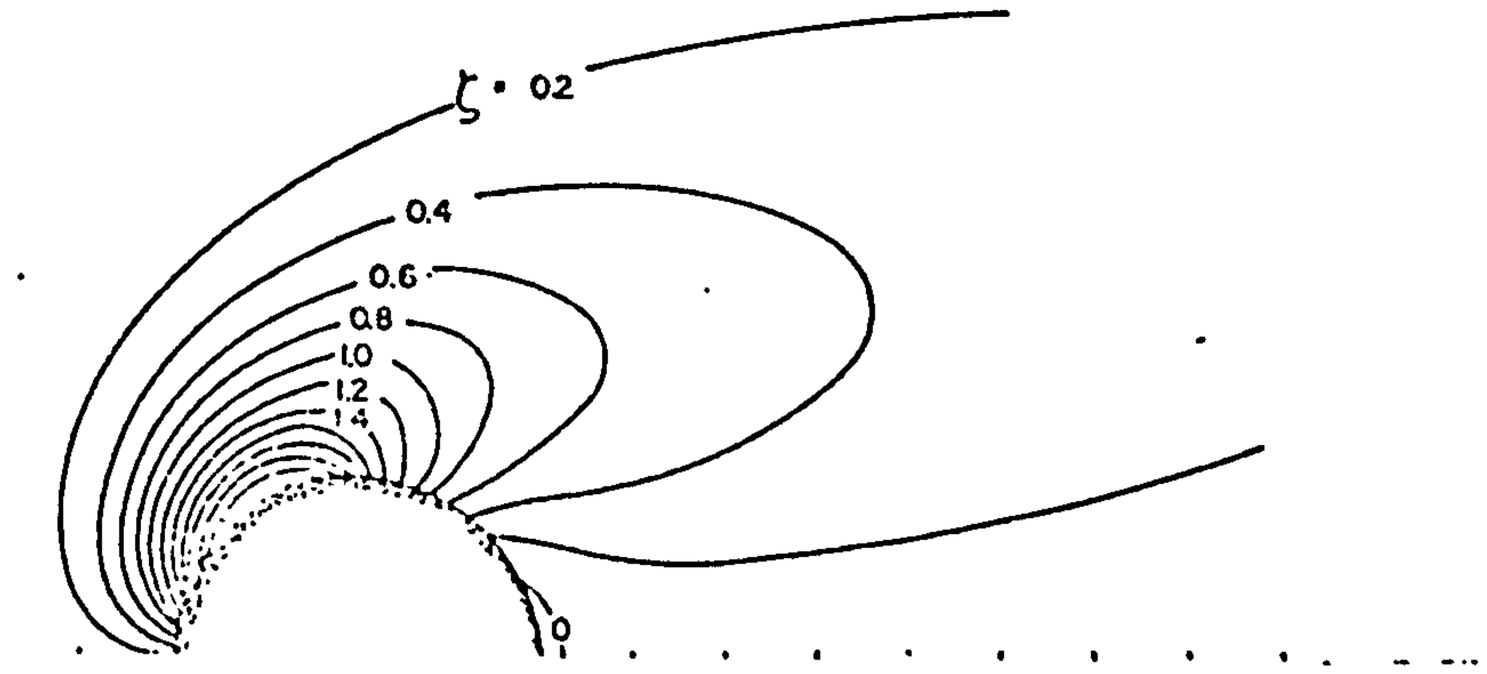

(d) ref: 43

Figure 5.30 The Vorticity at R_e = 10

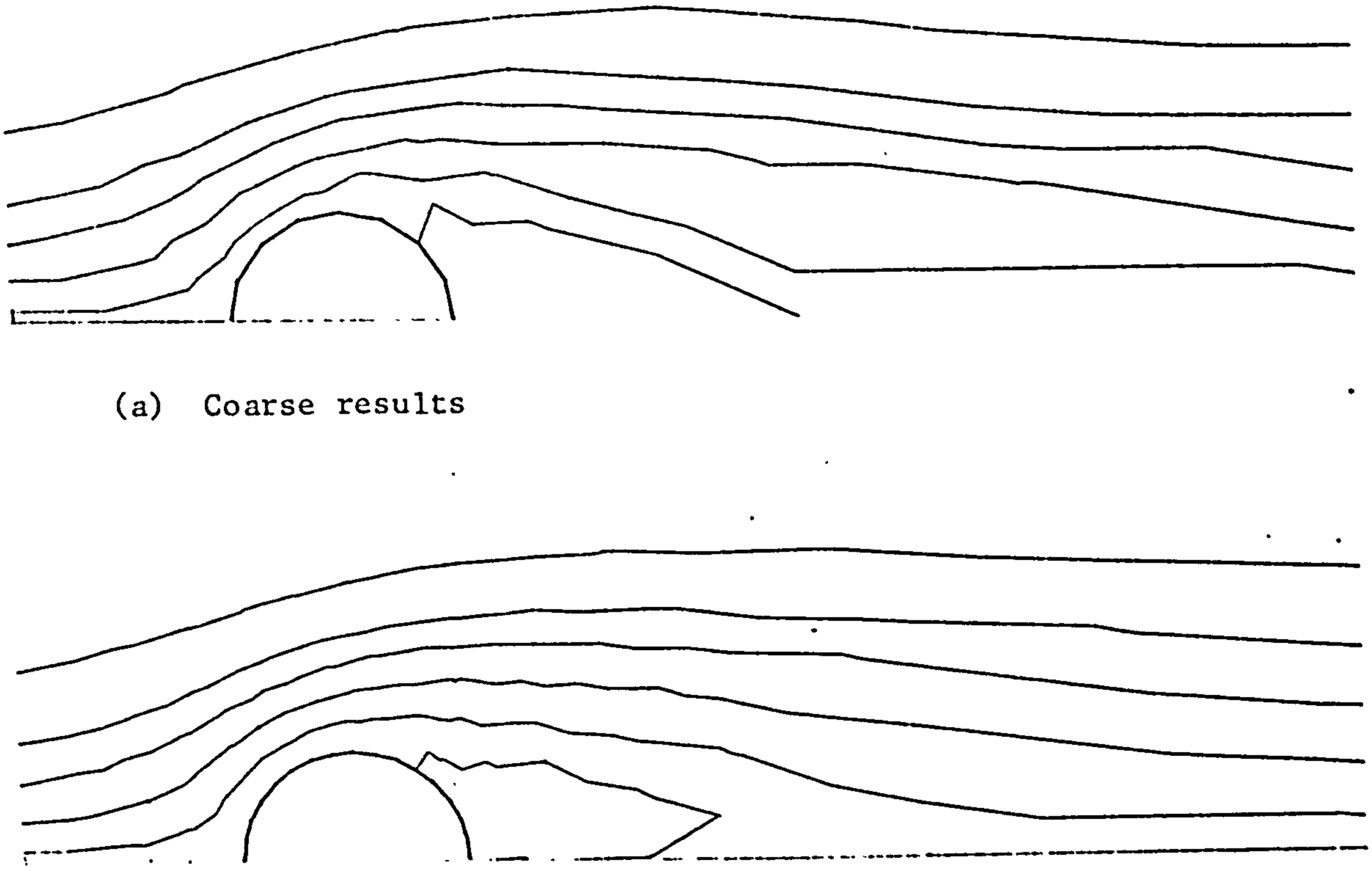

(a) Coarse results

(b) Fine results

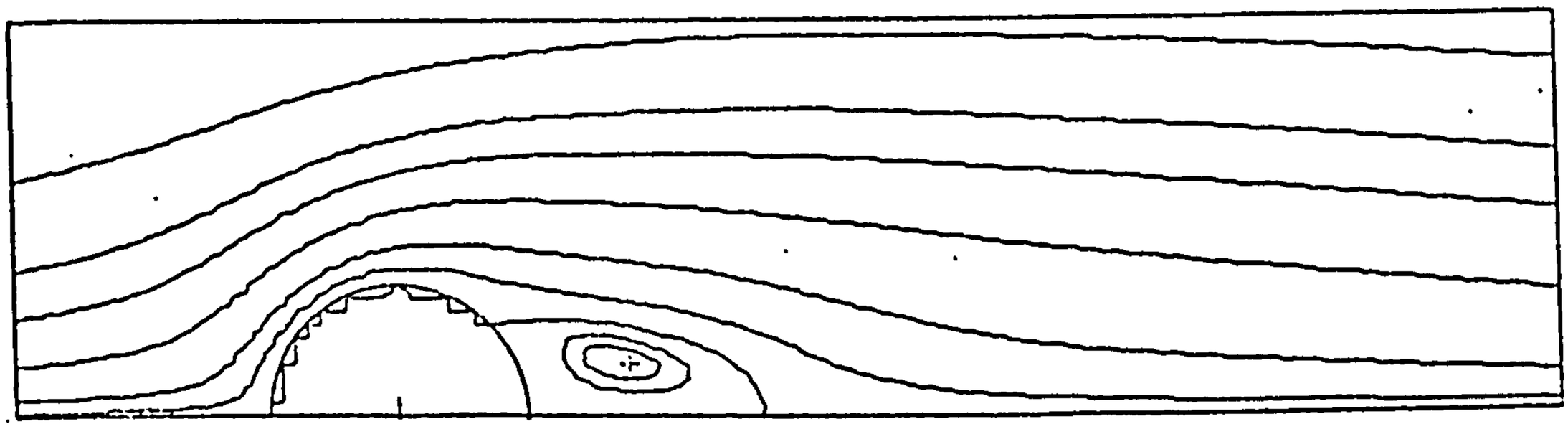

(c) ref: 48

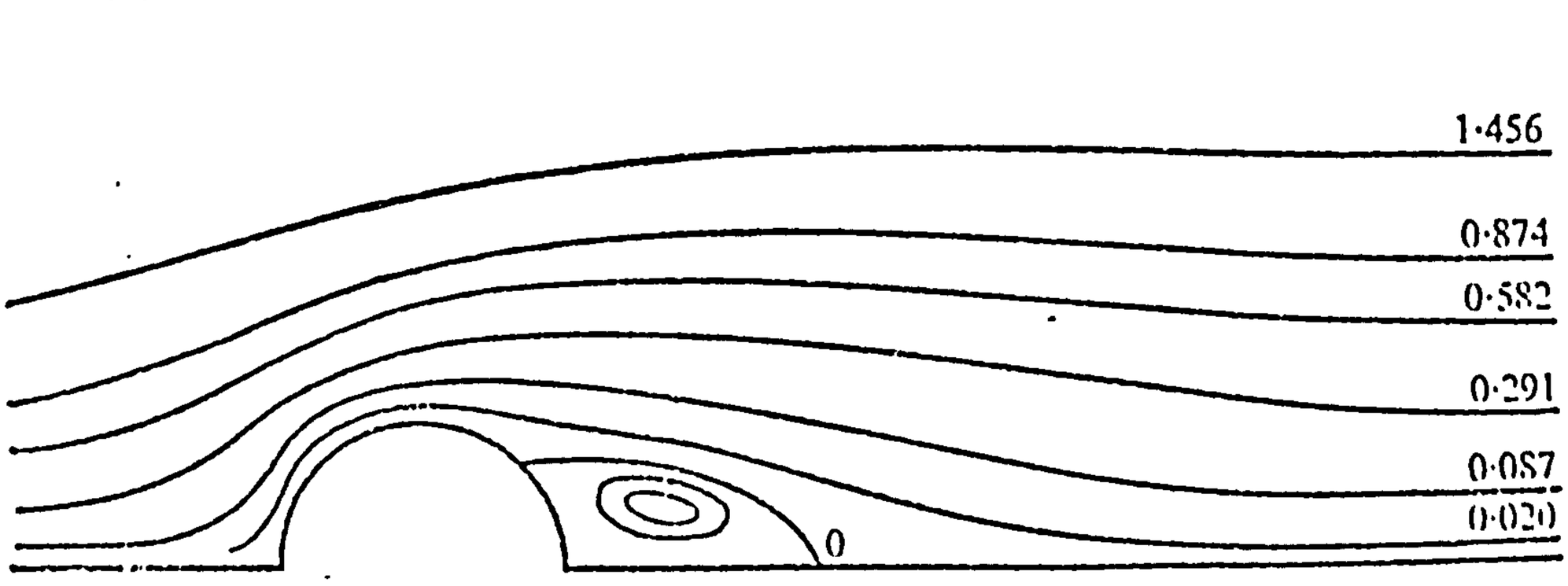

(d) ref: 43

Figure 5.31 The Stream Function at R_e = 20

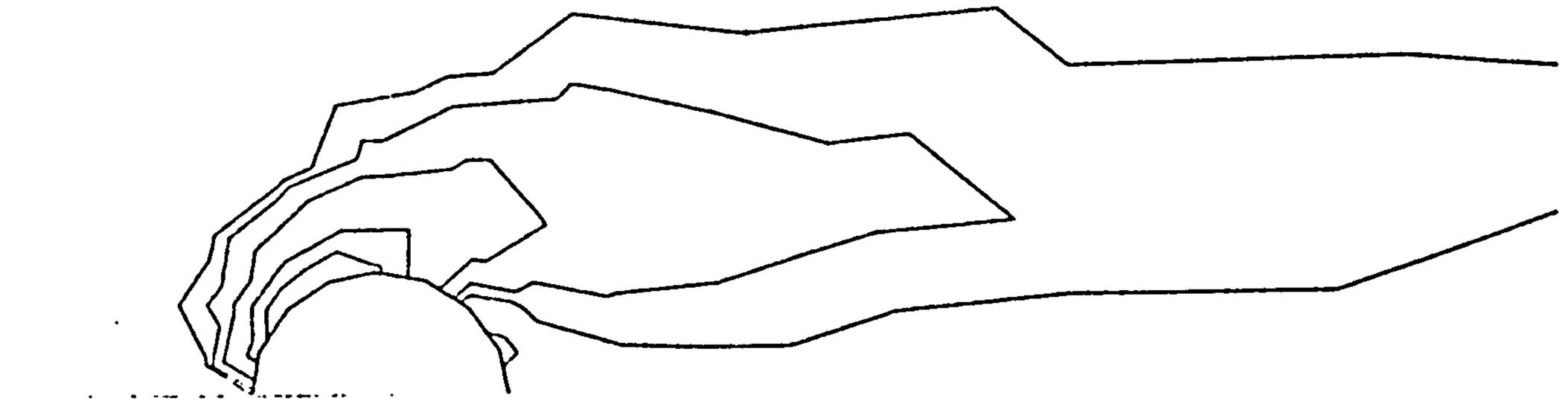

(a) Coarse results

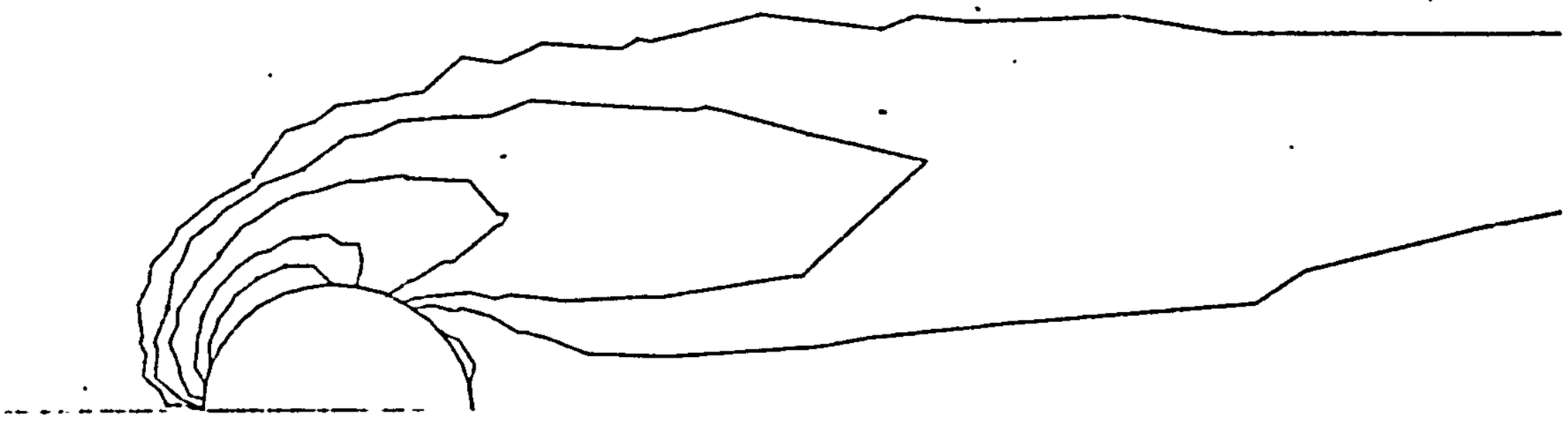

(b) Fine results

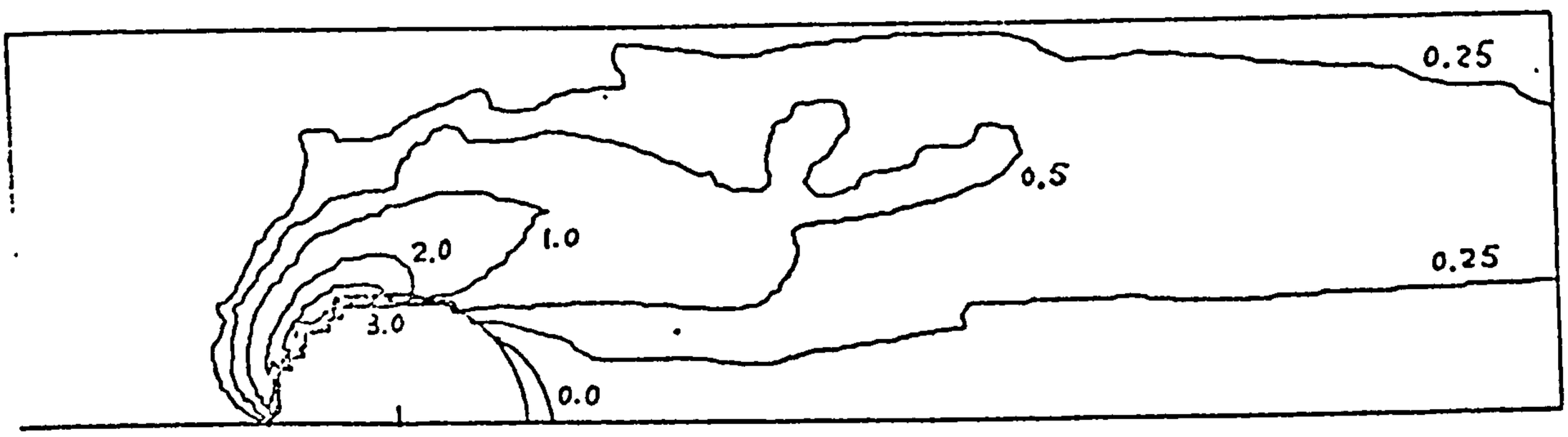

(c) ref: 48

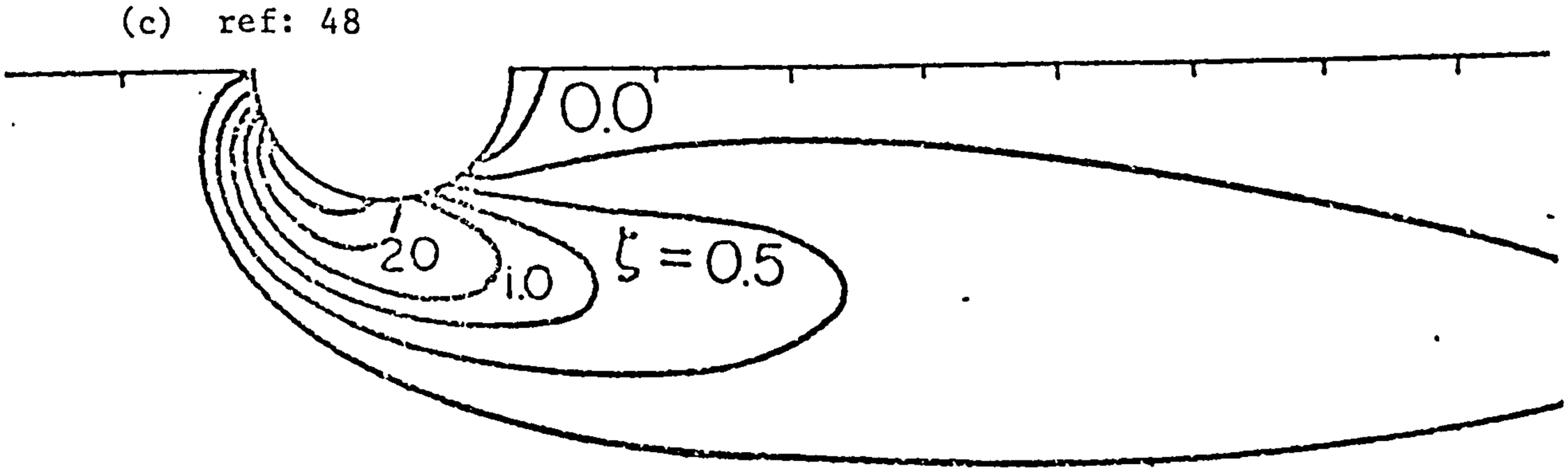

(d) ref: 43

Figure 5.32 The Vorticity at R_e = 20

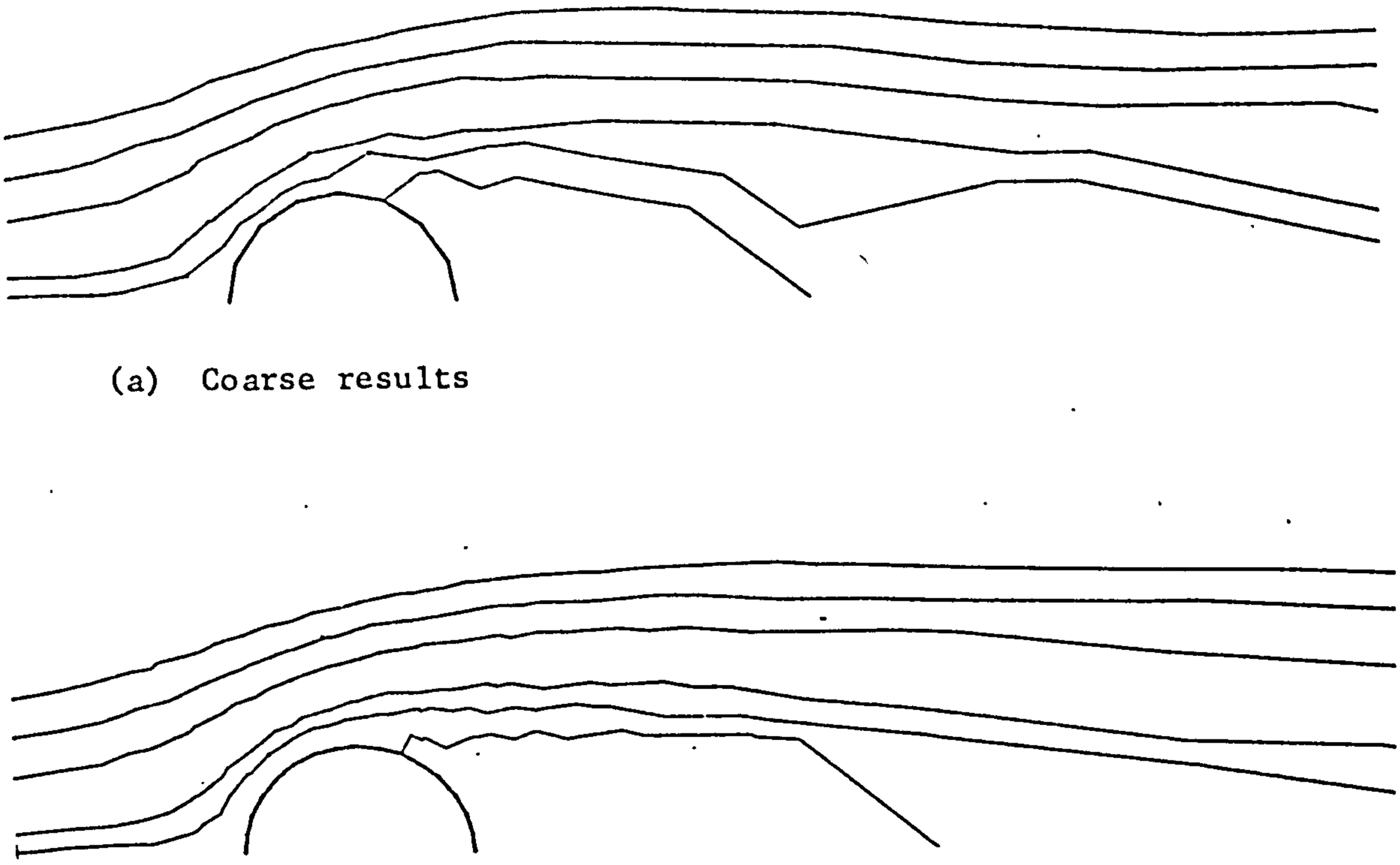

(a) Coarse results

(b) Fine results

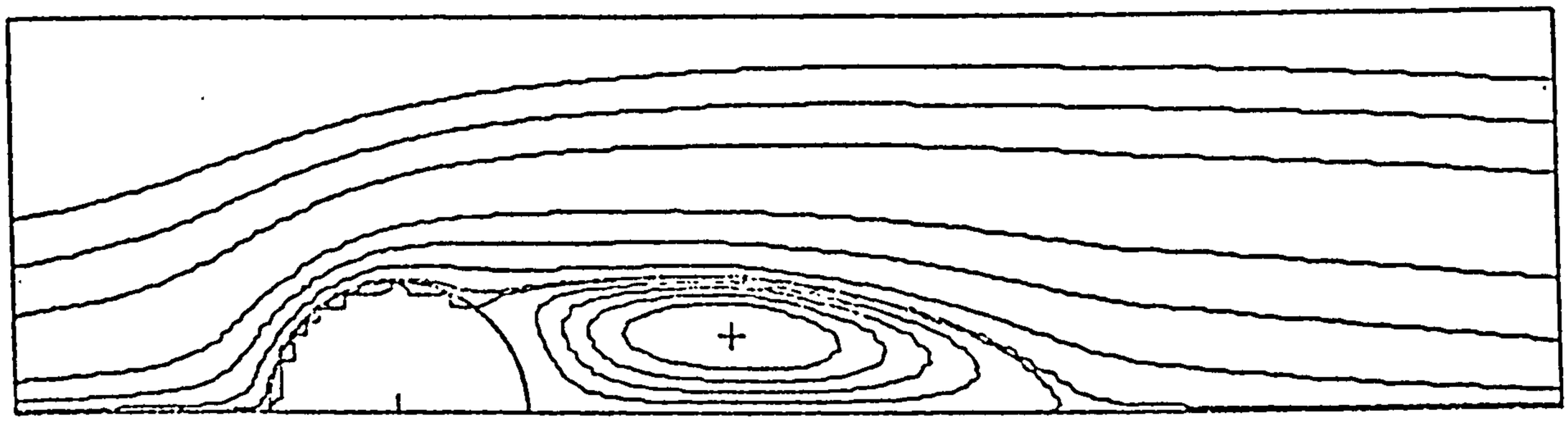

(c) ref: 48

(d) ref: 43

Figure 5.33 The Stream Function at R_e = 40

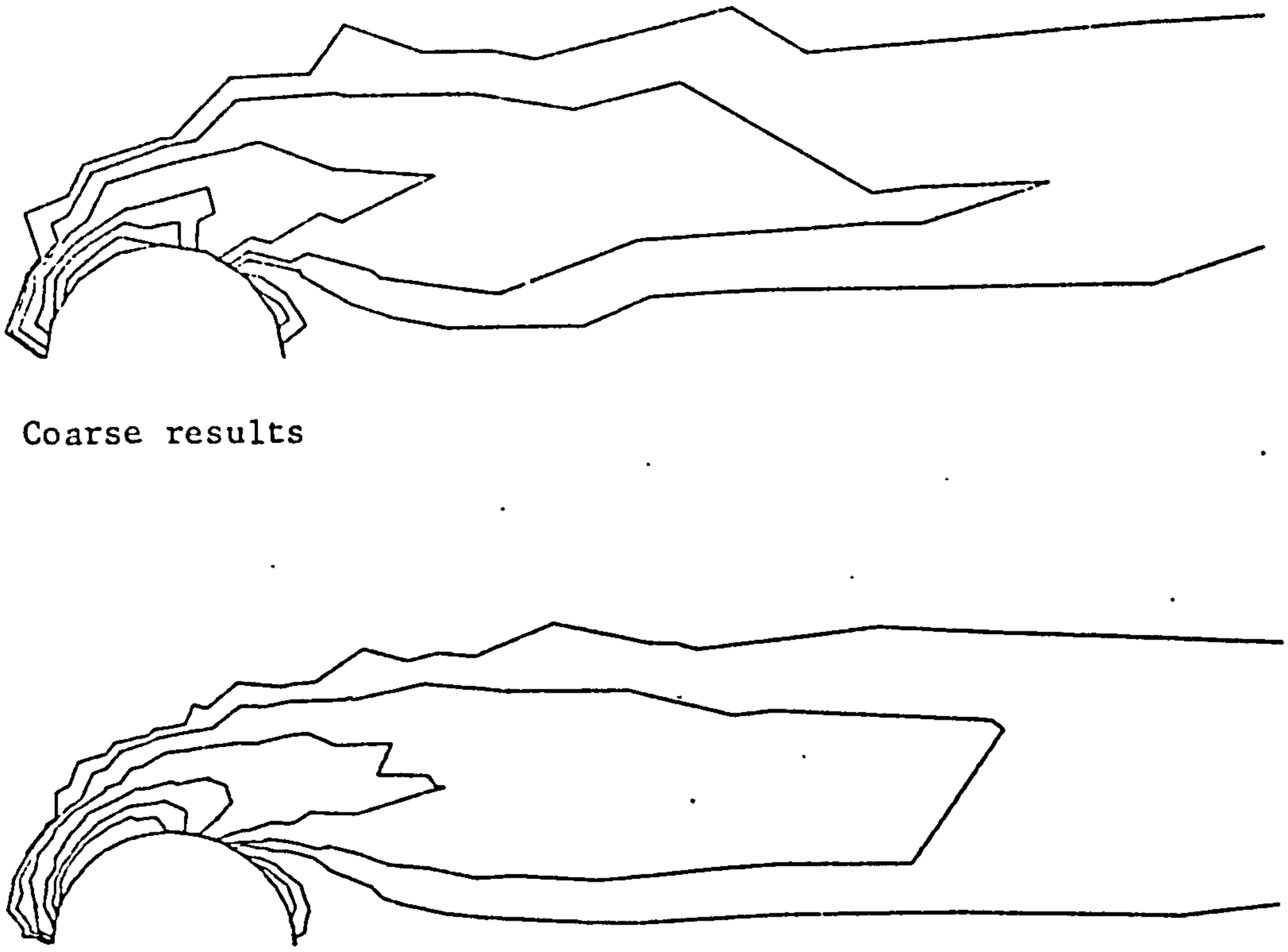

(a) Coarse results

(b) Fine results

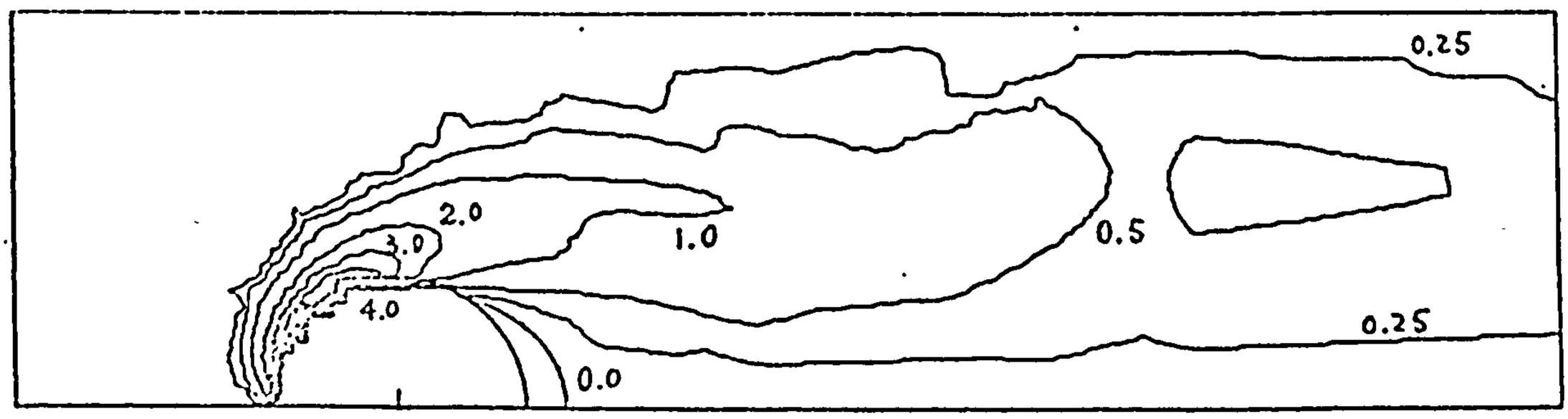

(c) ref: 48

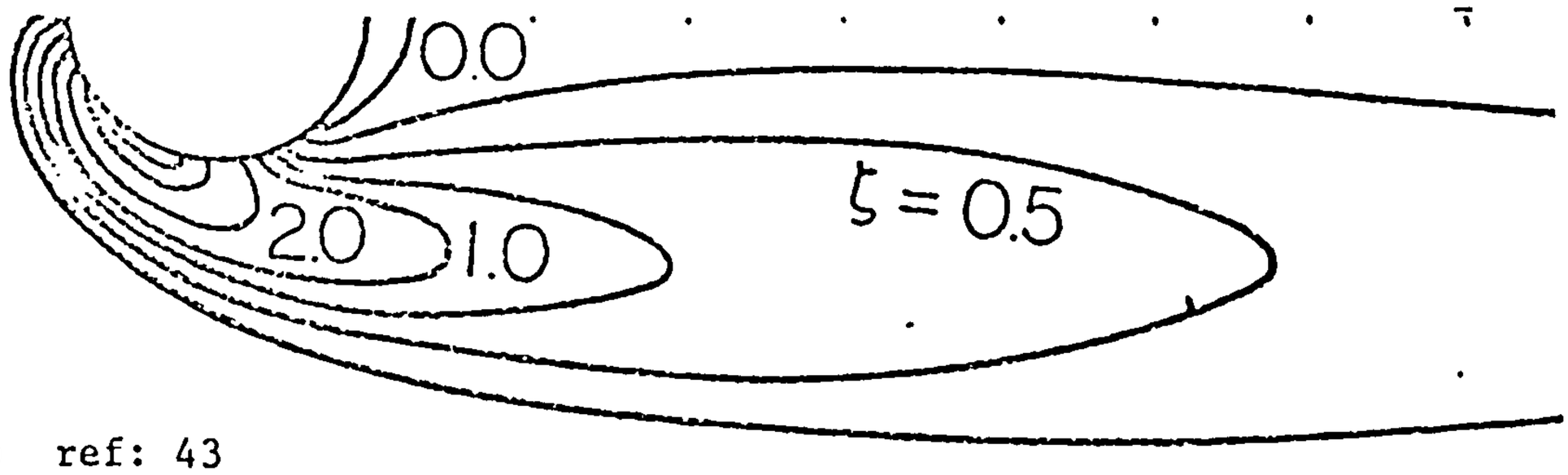

(d) ref: 43

Figure 5.34 The Vorticity at R_e = 40

(a) $R_e = 1$

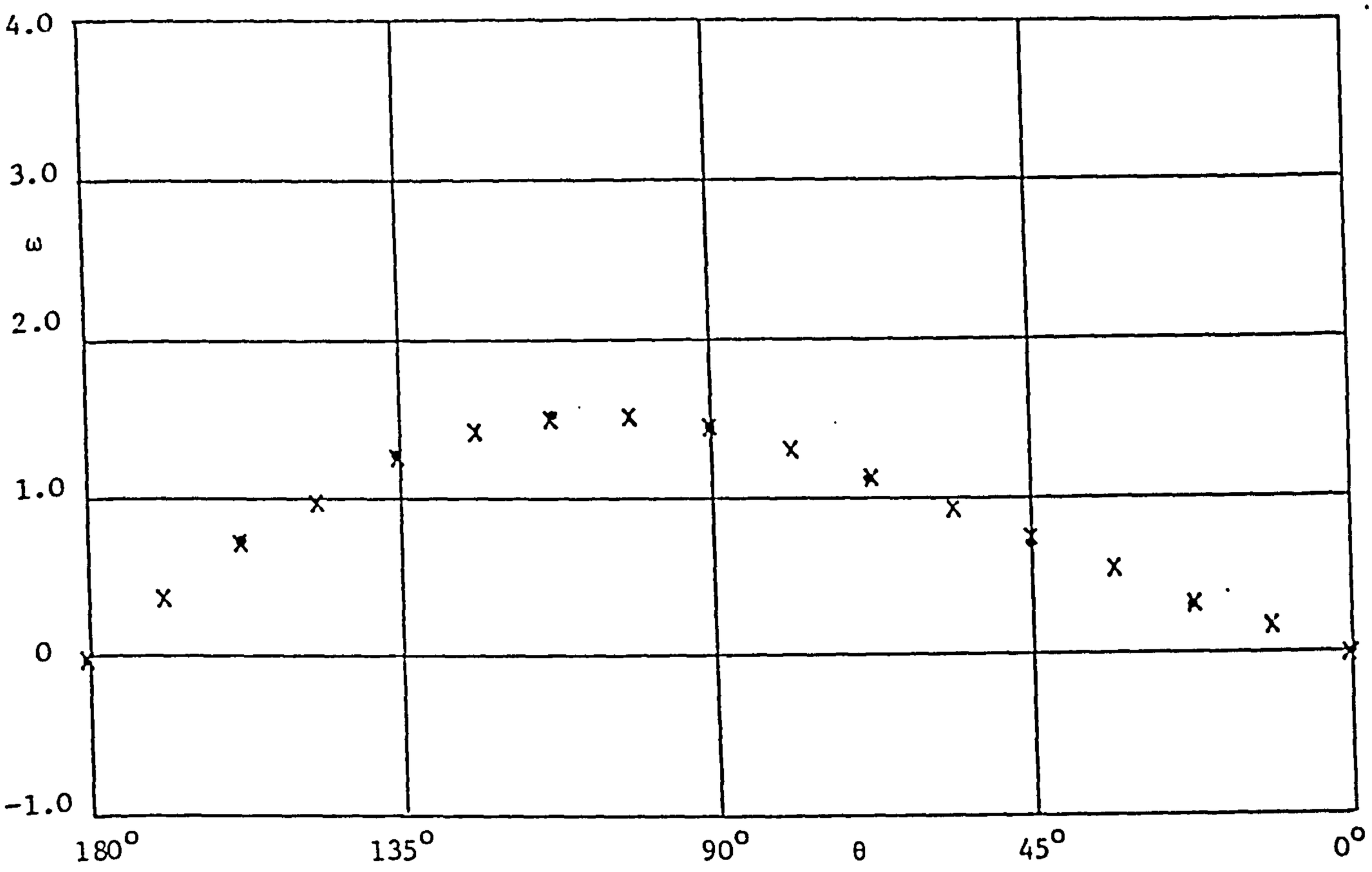

ref: 48 - 16 node mesh

ref: 43 - 32 node mesh

(b) $R_e = 5$

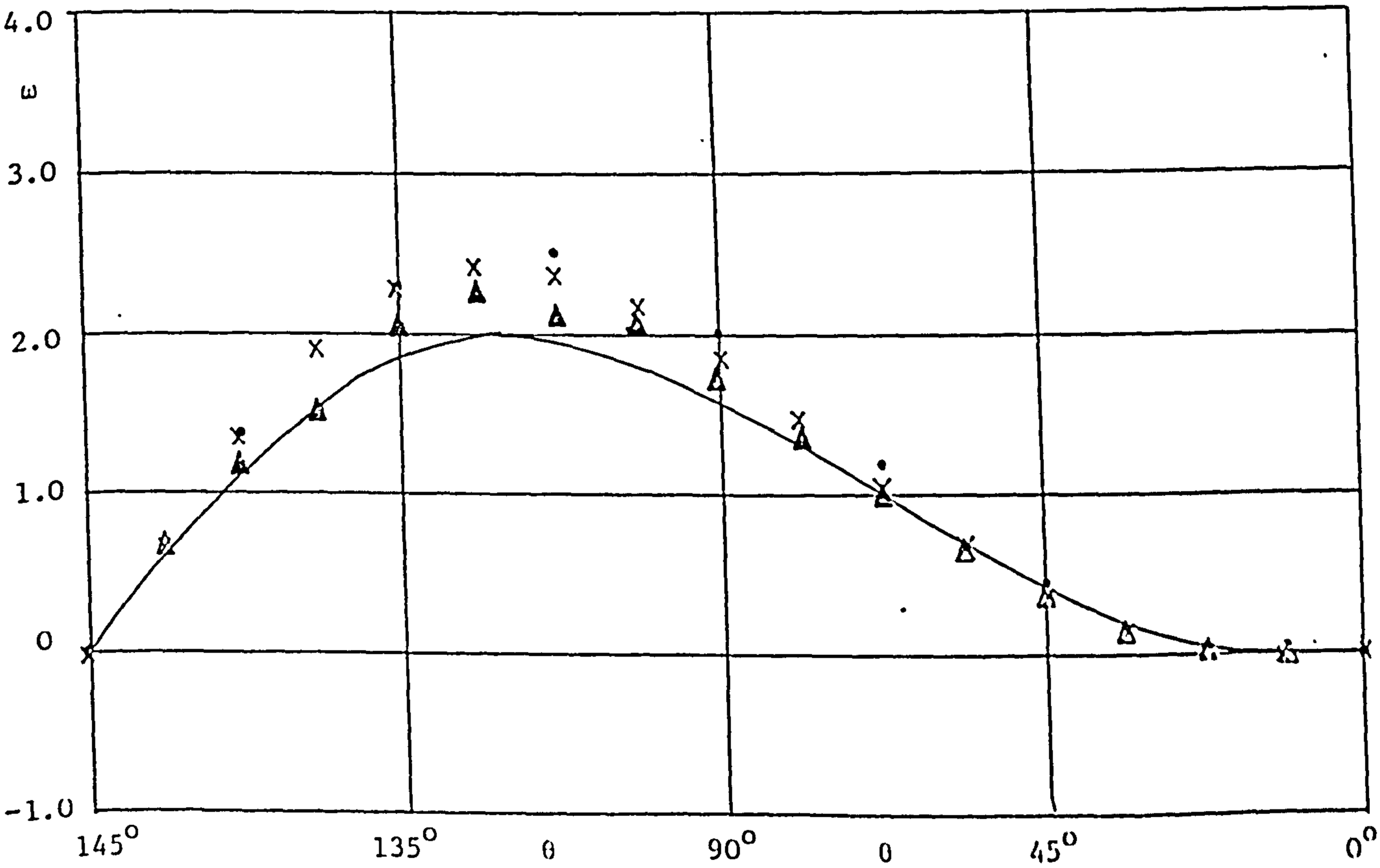

Figure 5.35 The Vorticity About the Wall

(c) $R_e = 7$

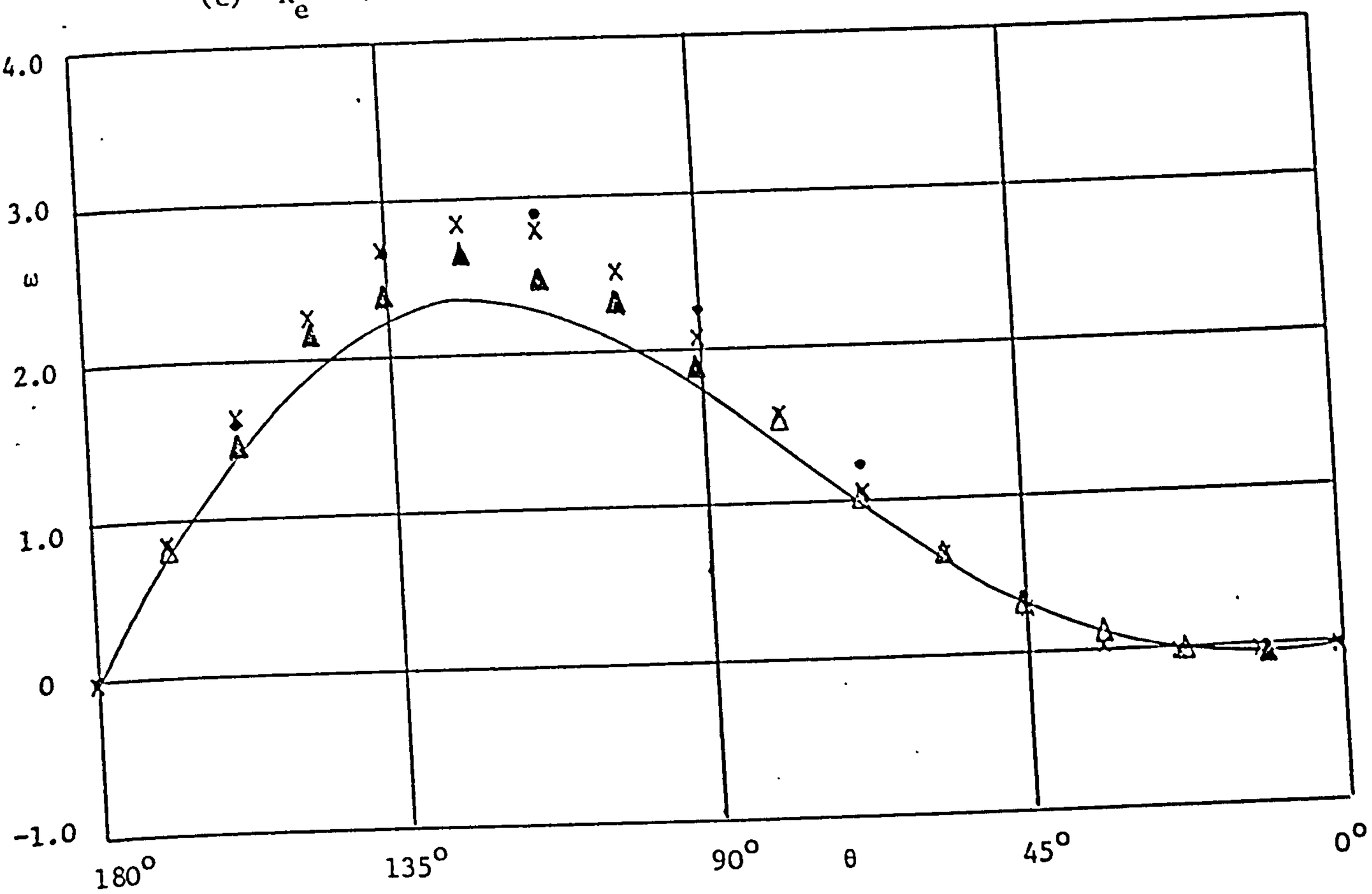

(d) $R_e = 10$

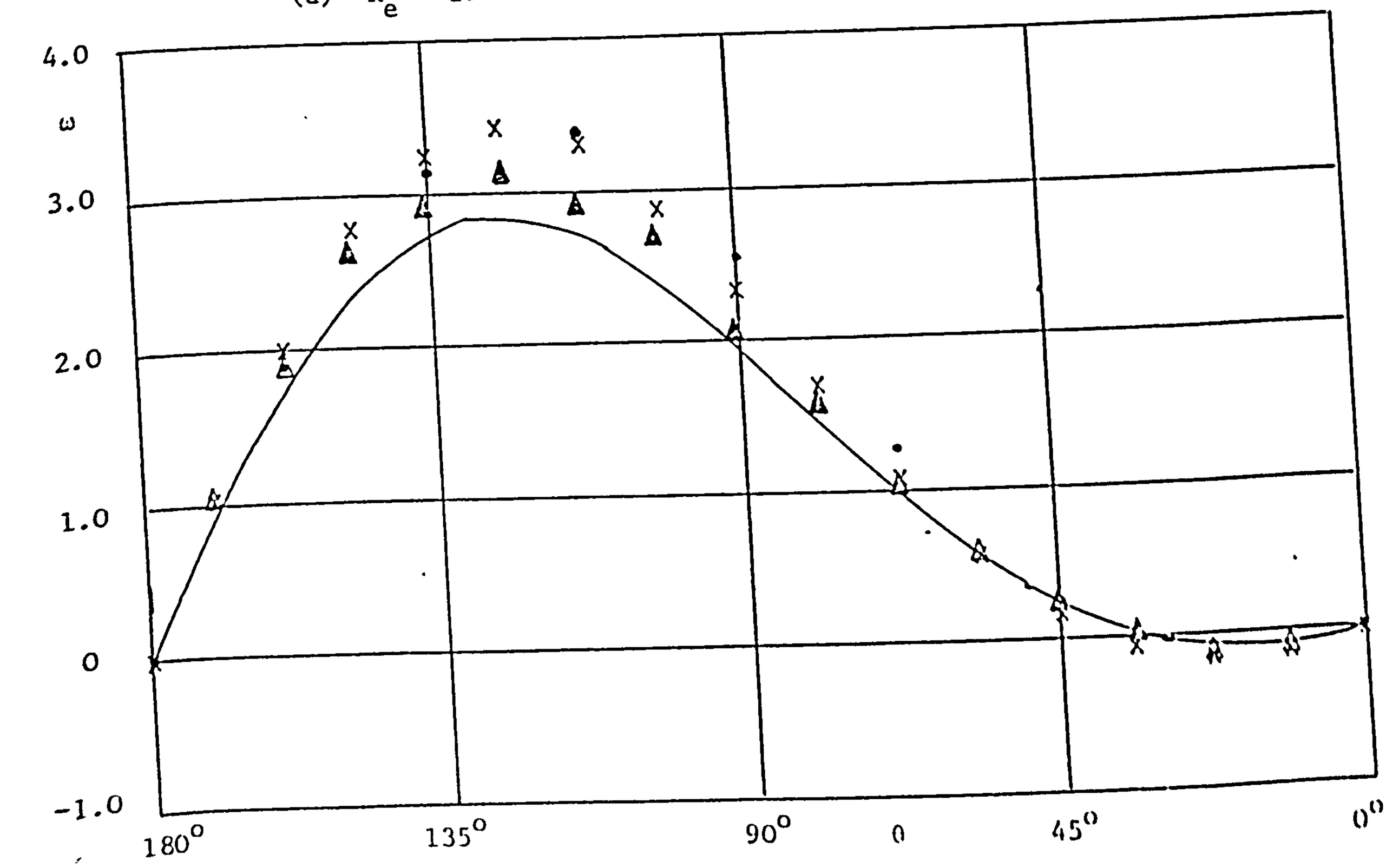

Figure 5.35 Continued

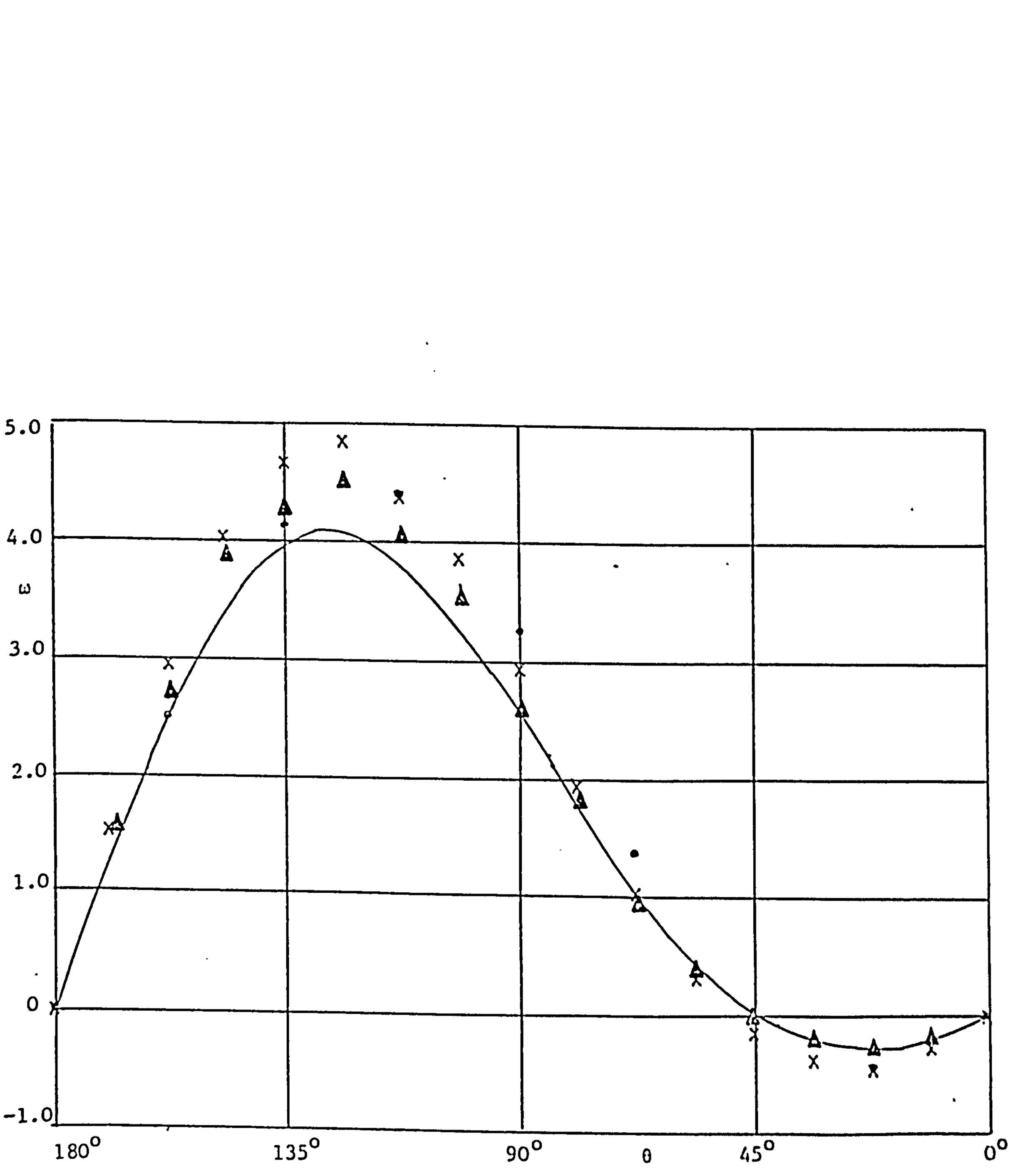

(e) $R_e = 20$

Figure 5.35 Continued

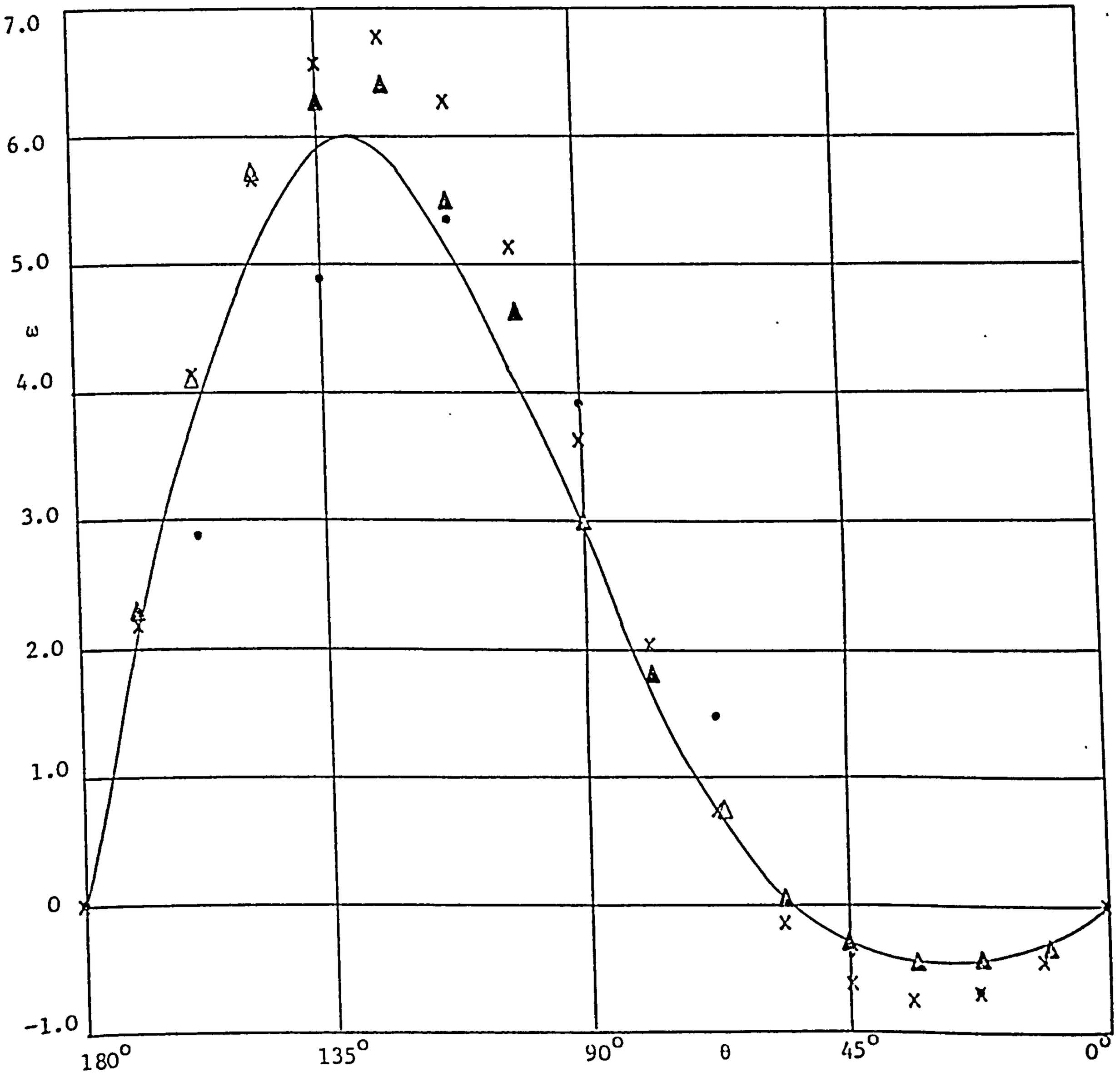

(f) $R_e = 40$

Figure 5.35 Continued

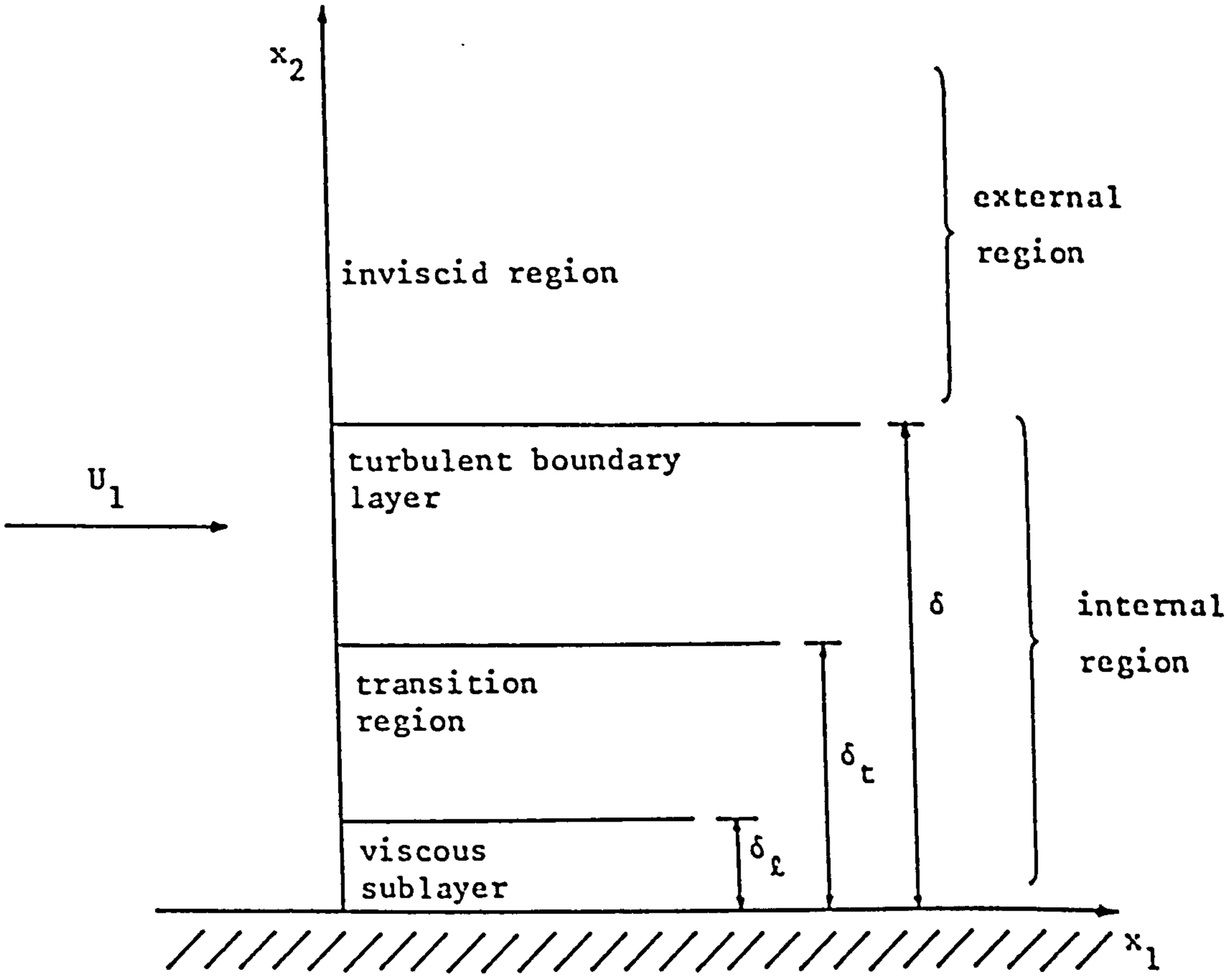

Figure 6.1 The Cross-section of a Turbulent Boundary Layer

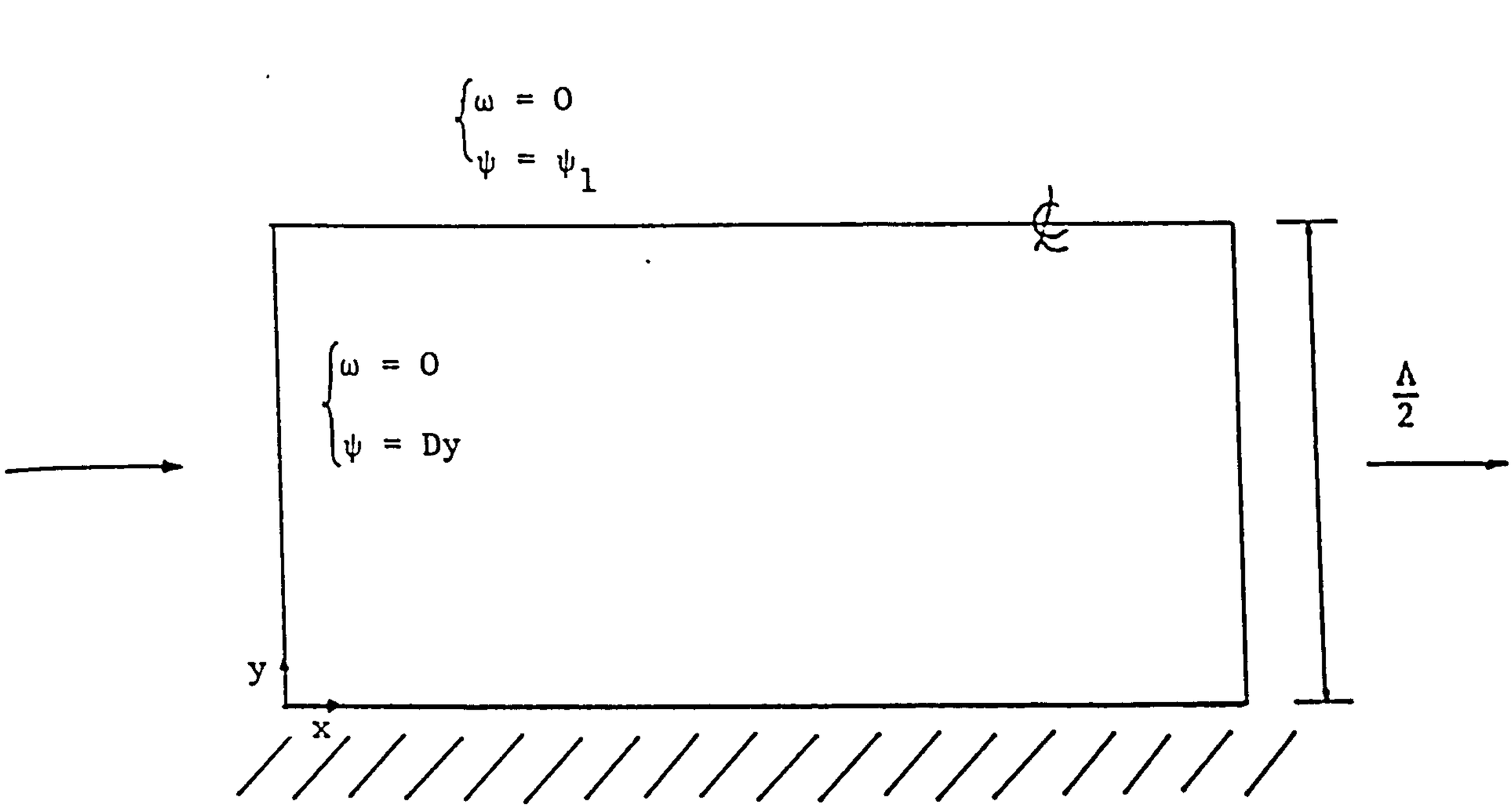

Figure 6.2 The problem of developing flow in a channel, where D is the inlet velocity

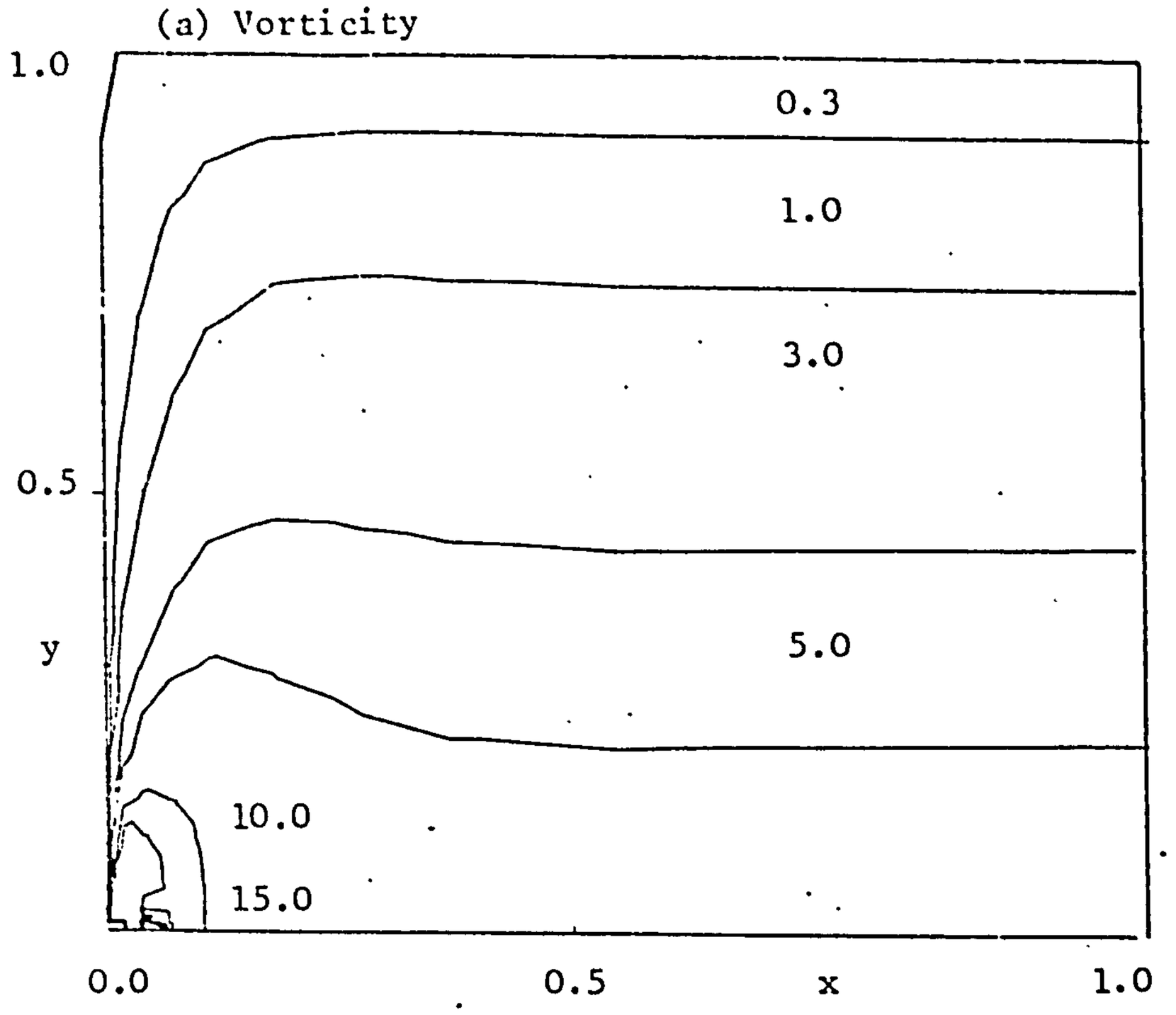

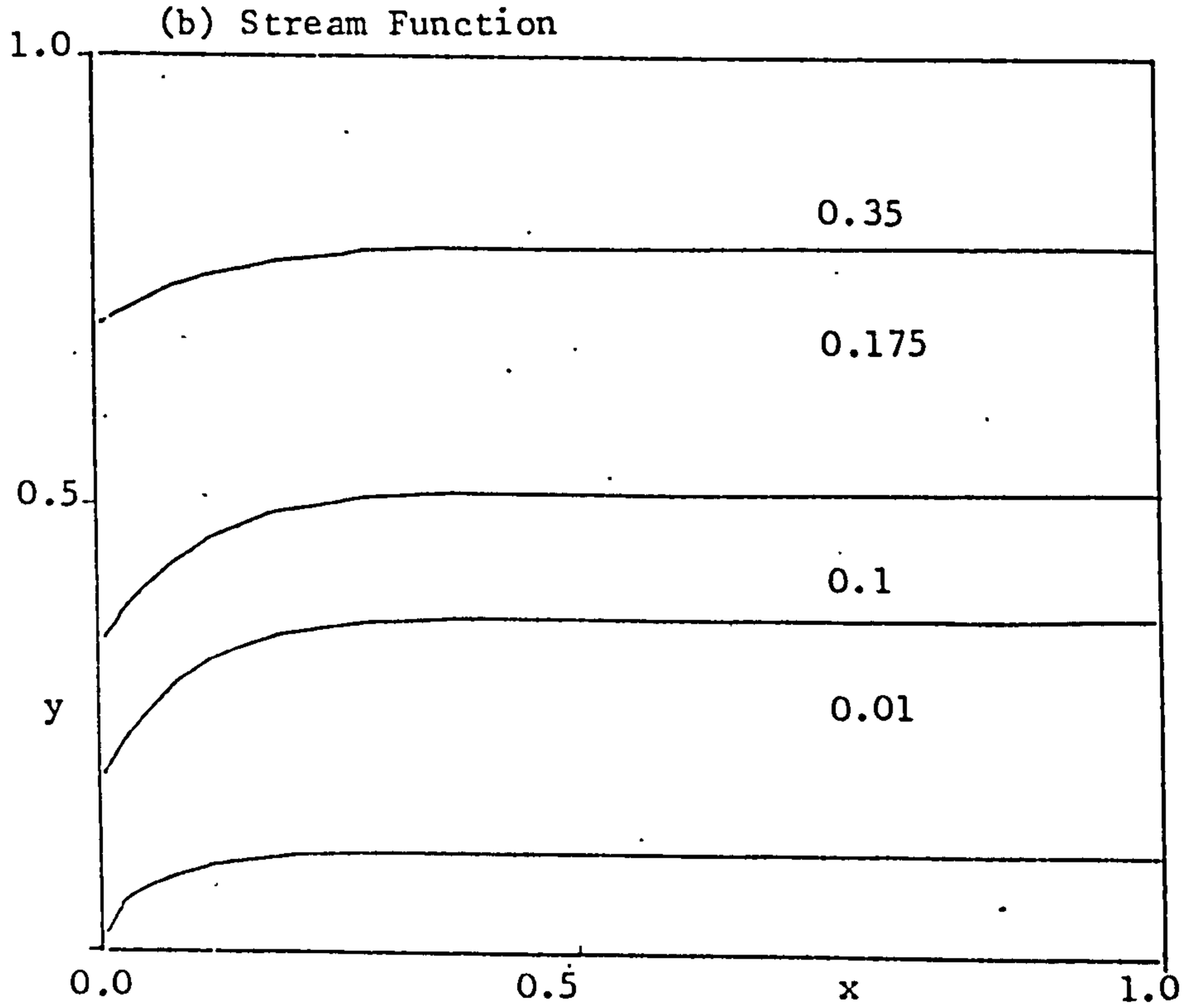

Figure 6.3 Laminar Flow; $R_e = 10.0$

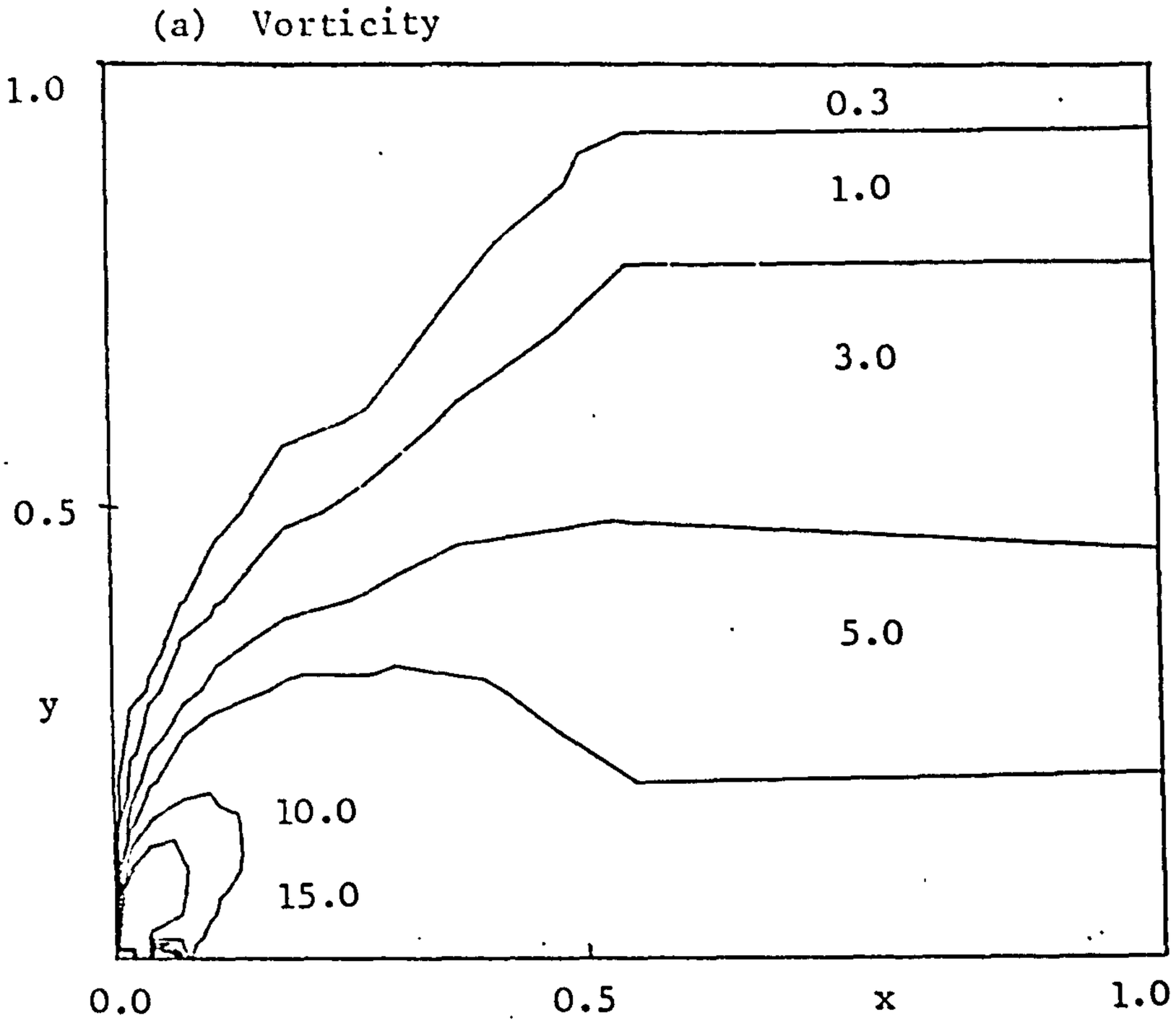

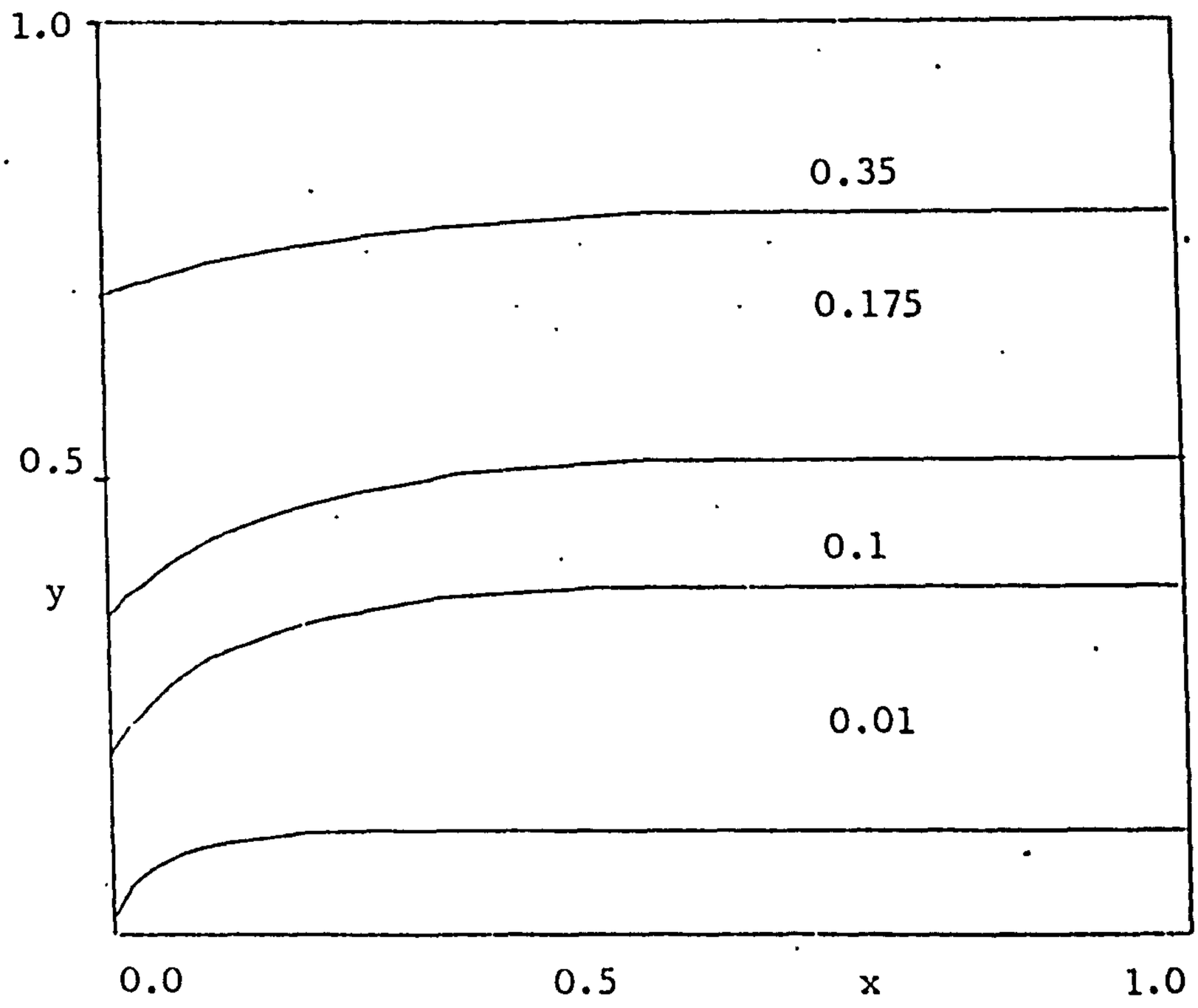

Figure 6.4 Laminar Flow; $R_e = 100.0$

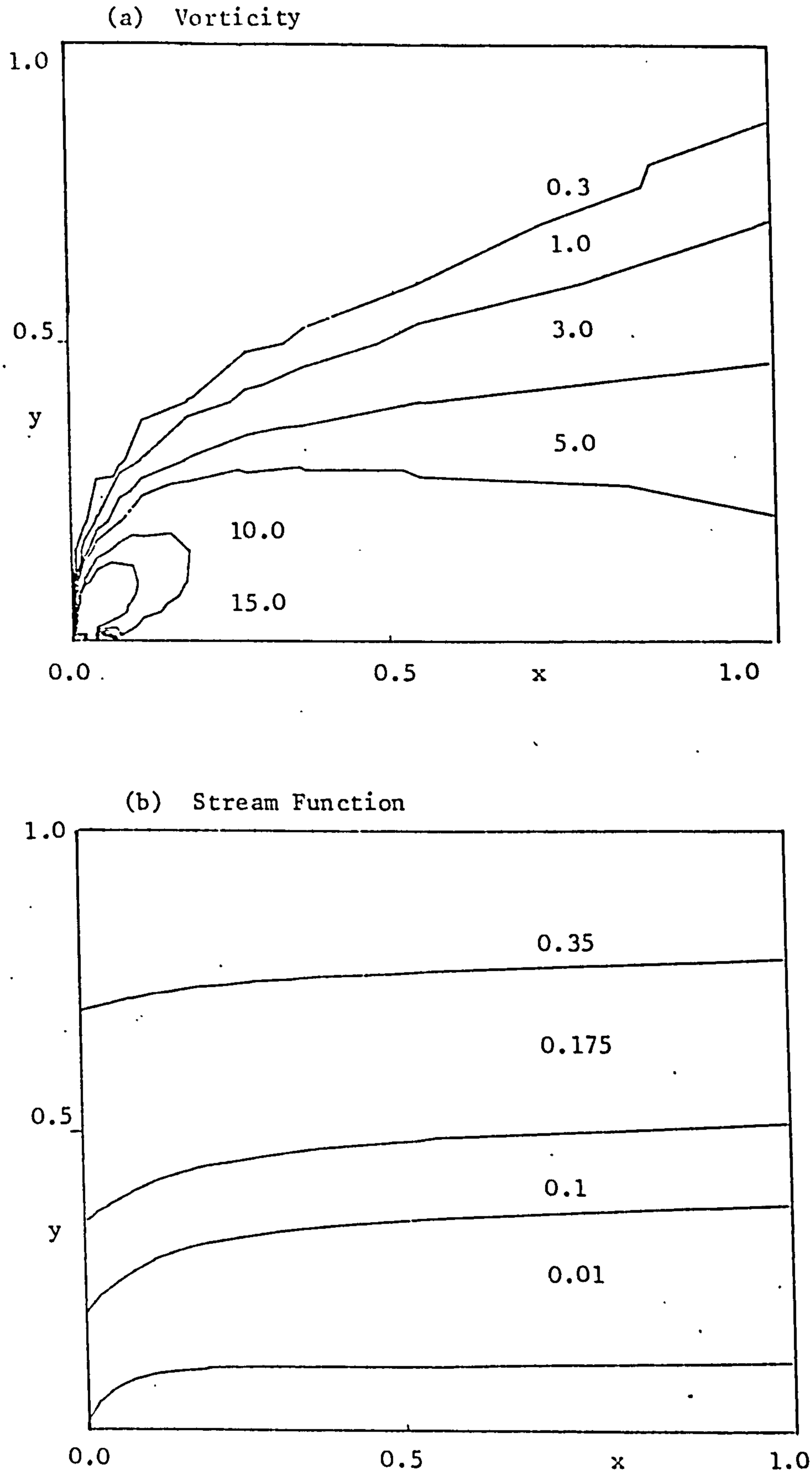

Figure 6.5 Laminar Flow; R_e 200.0

(a) Vorticity

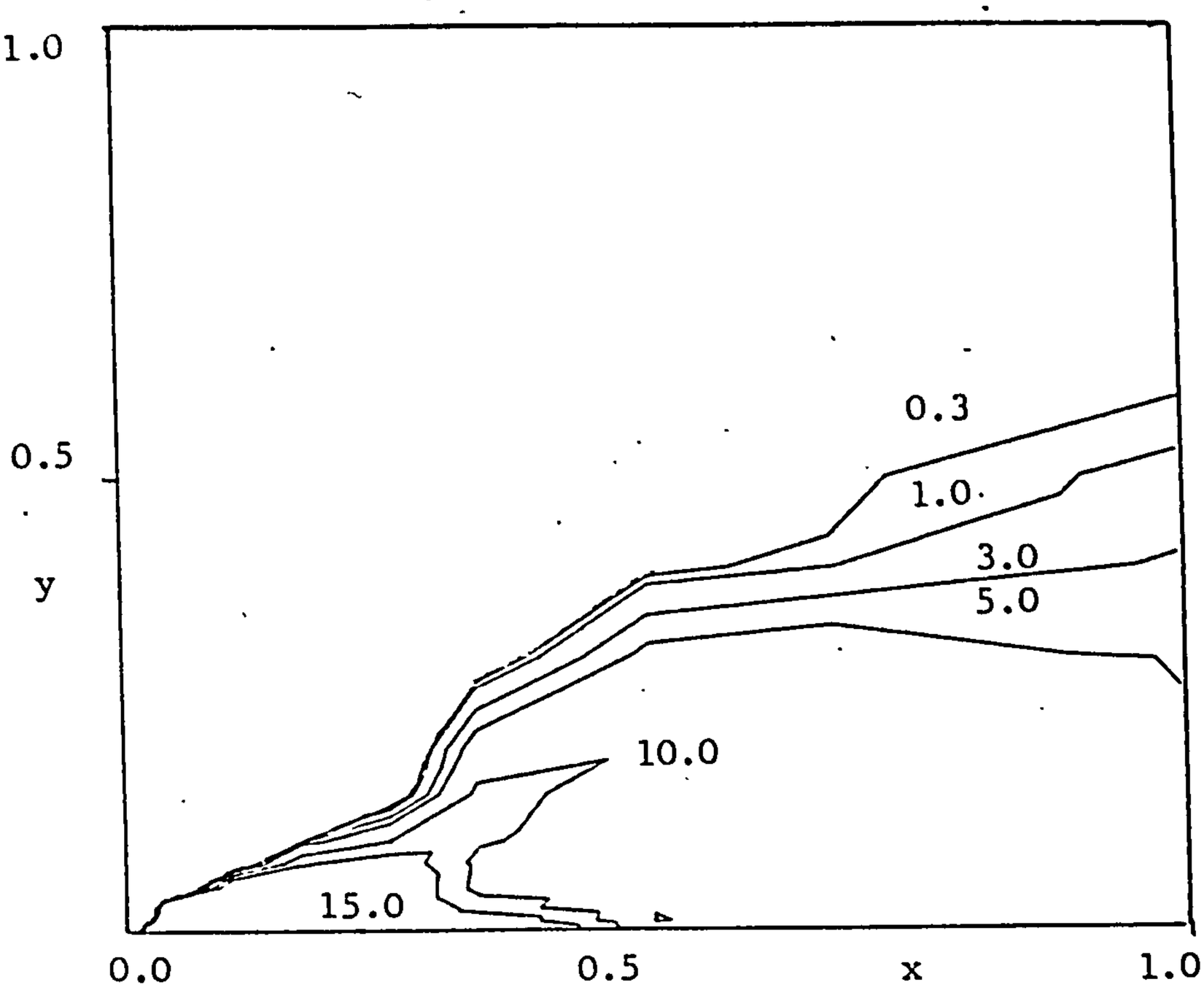

(b) Stream Function

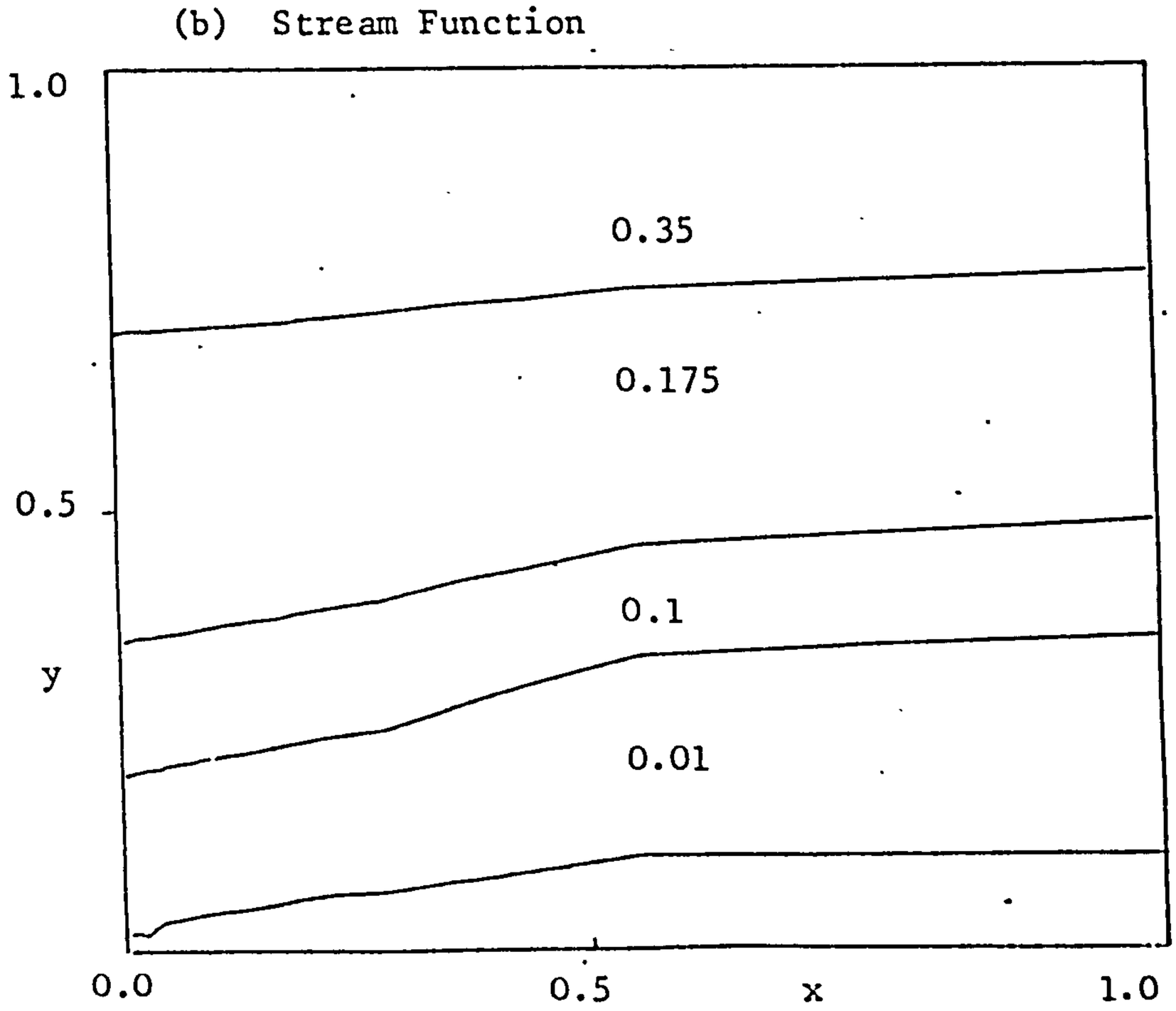

Figure 6.6 Laminar Flow R_e = 2500.0

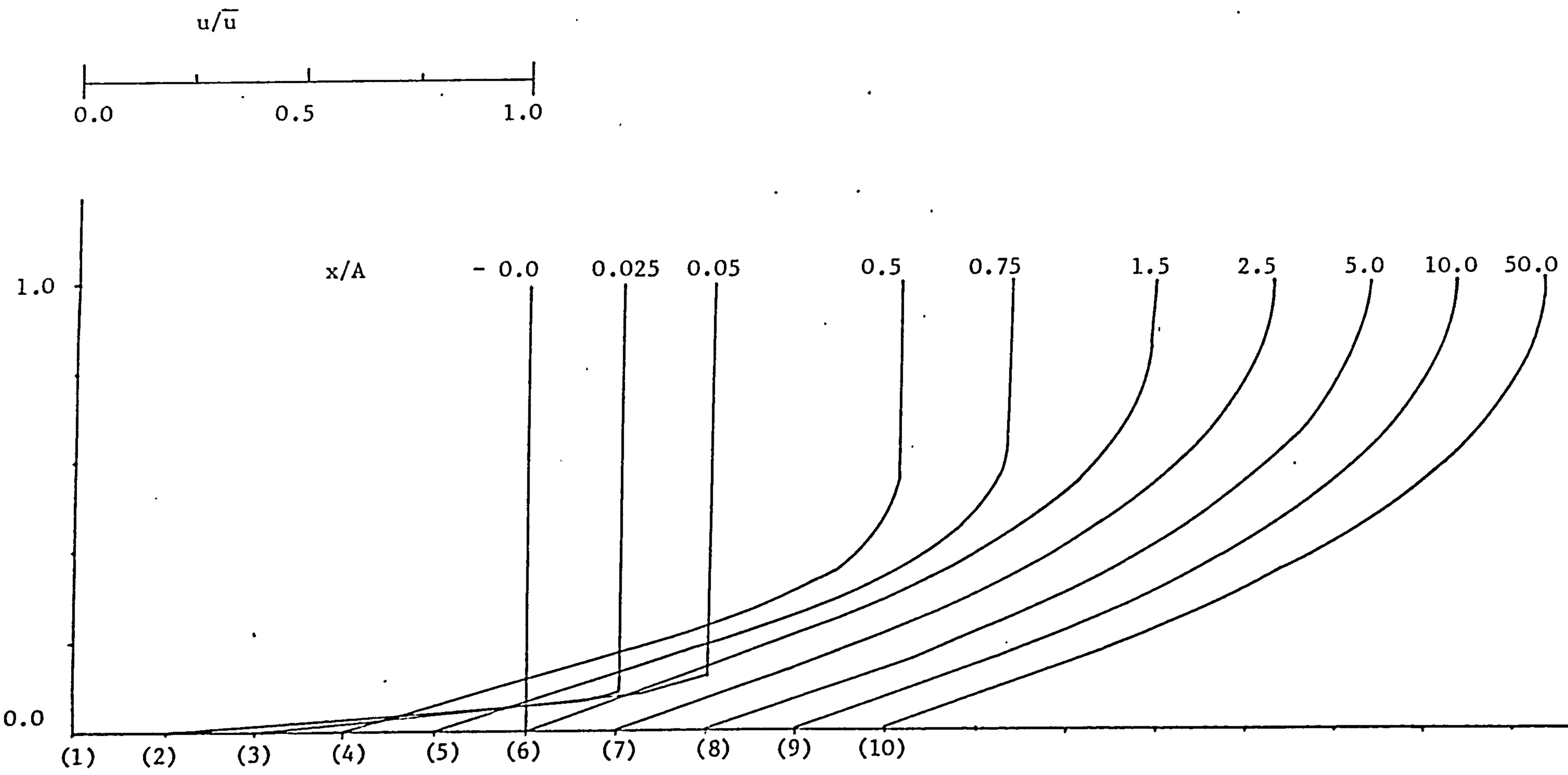

Figure 6.7(a) Laminar Velocity Profiles R_e = 200.0

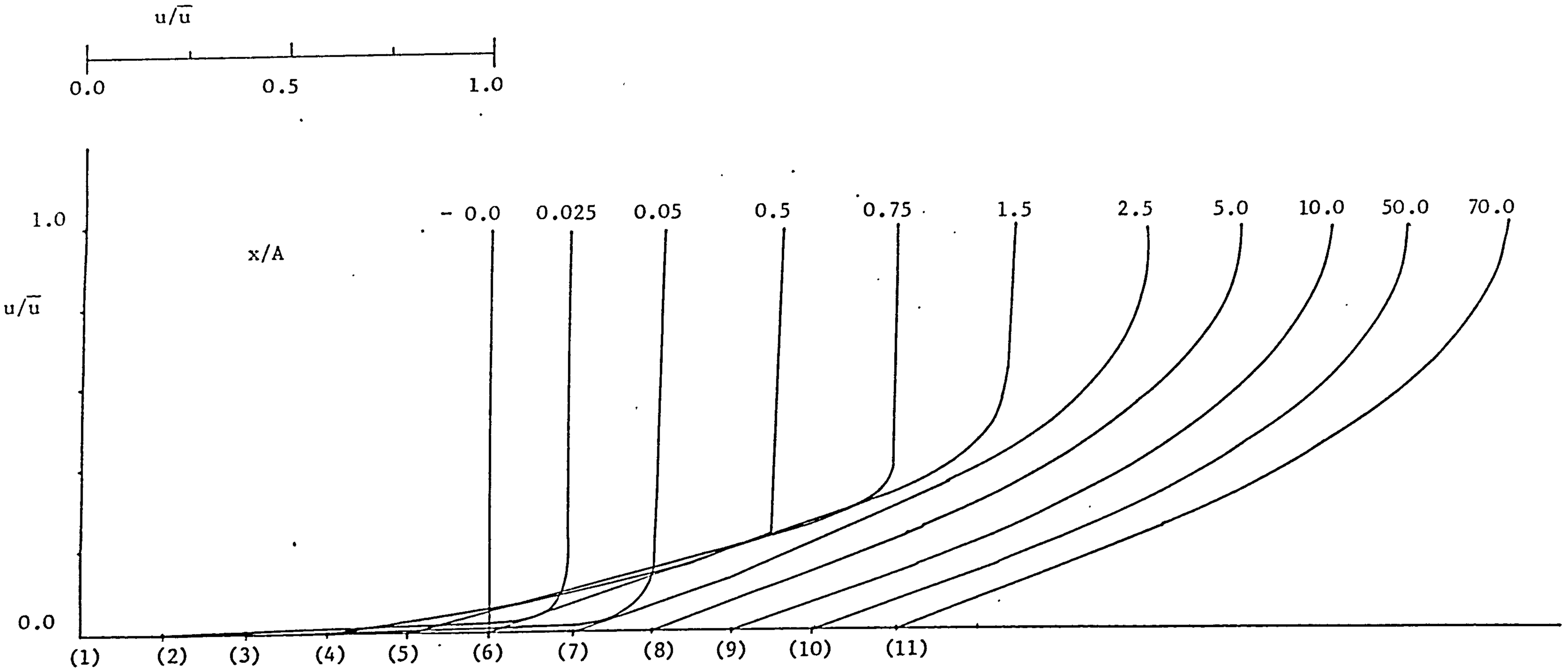

Figure 6.7(b) Laminar Velocity Profiles R_e = 2500

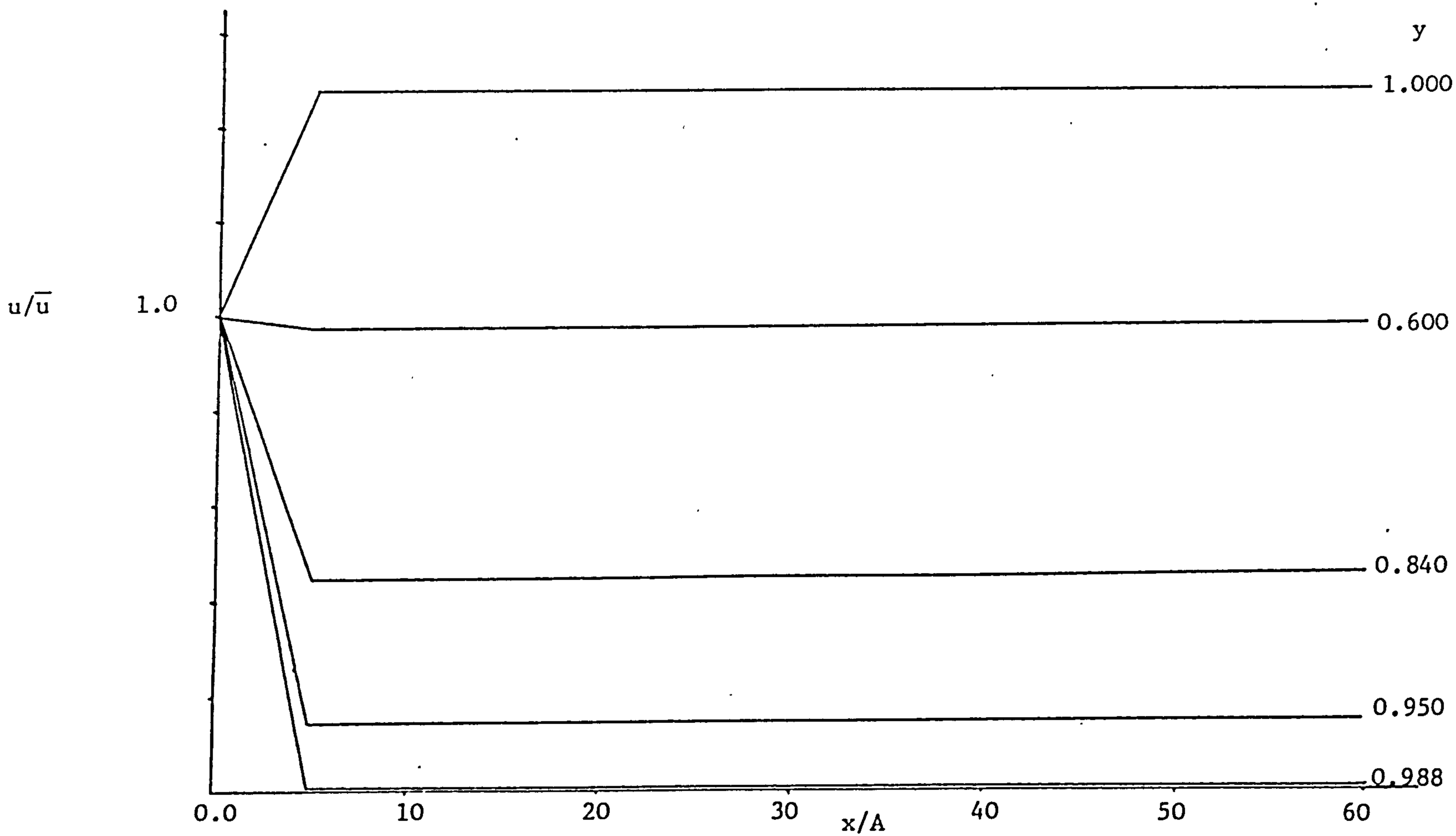

Figure 6.8 Laminar Flow Axial Velocity, R_e = 2500

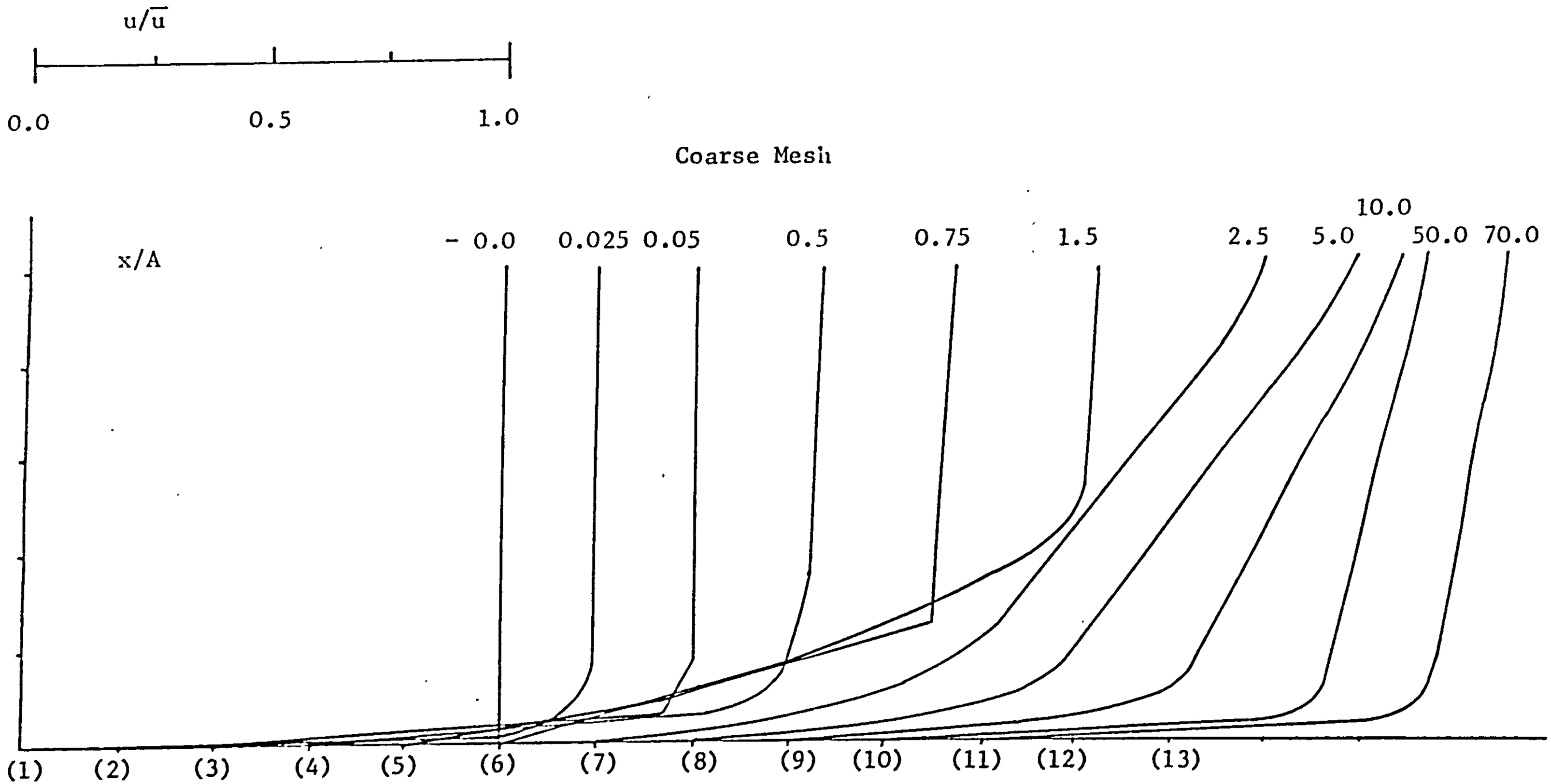

Figure 6.9(a) Turbulent Velocity Profiles R_e = 2500

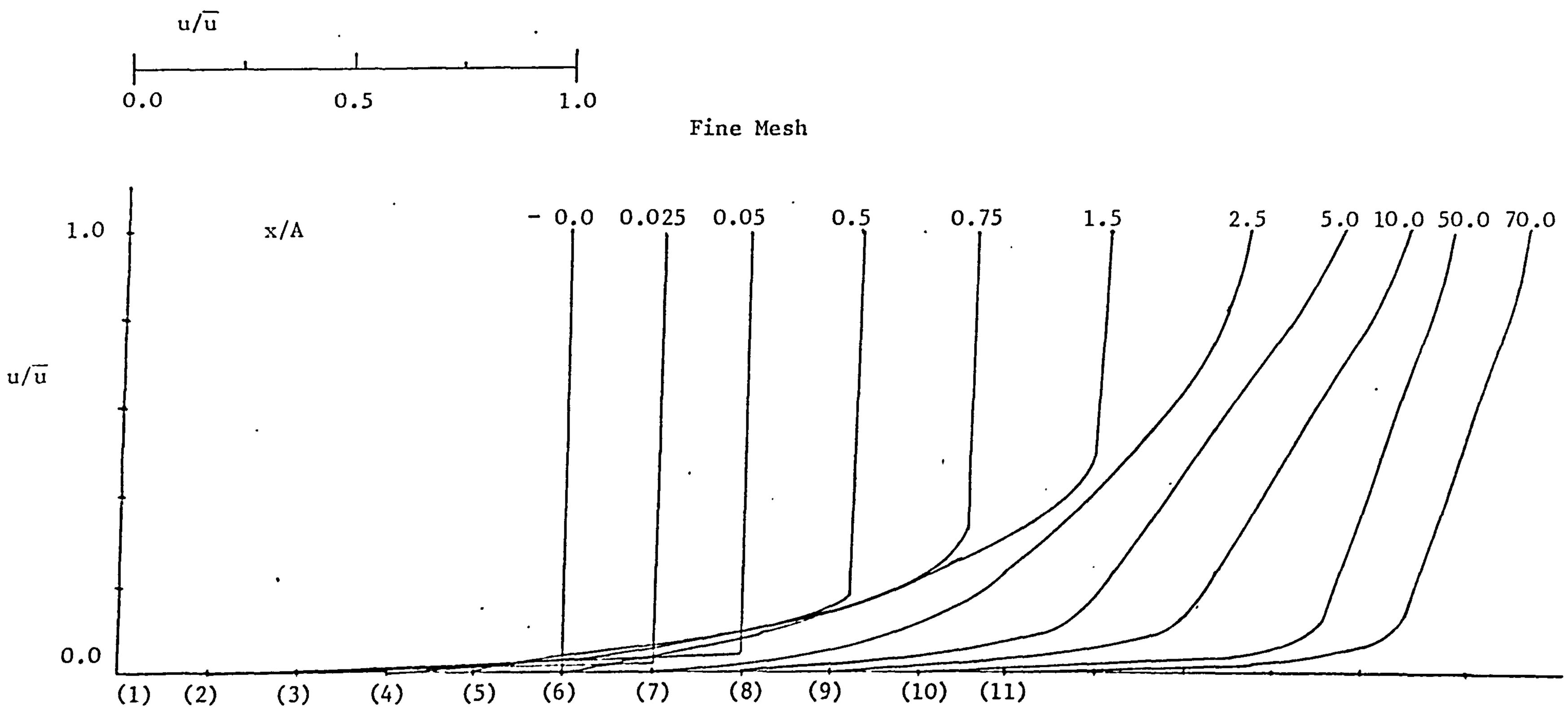

Figure 6.9(b) Turbulent Velocity Profiles R_e = 2500

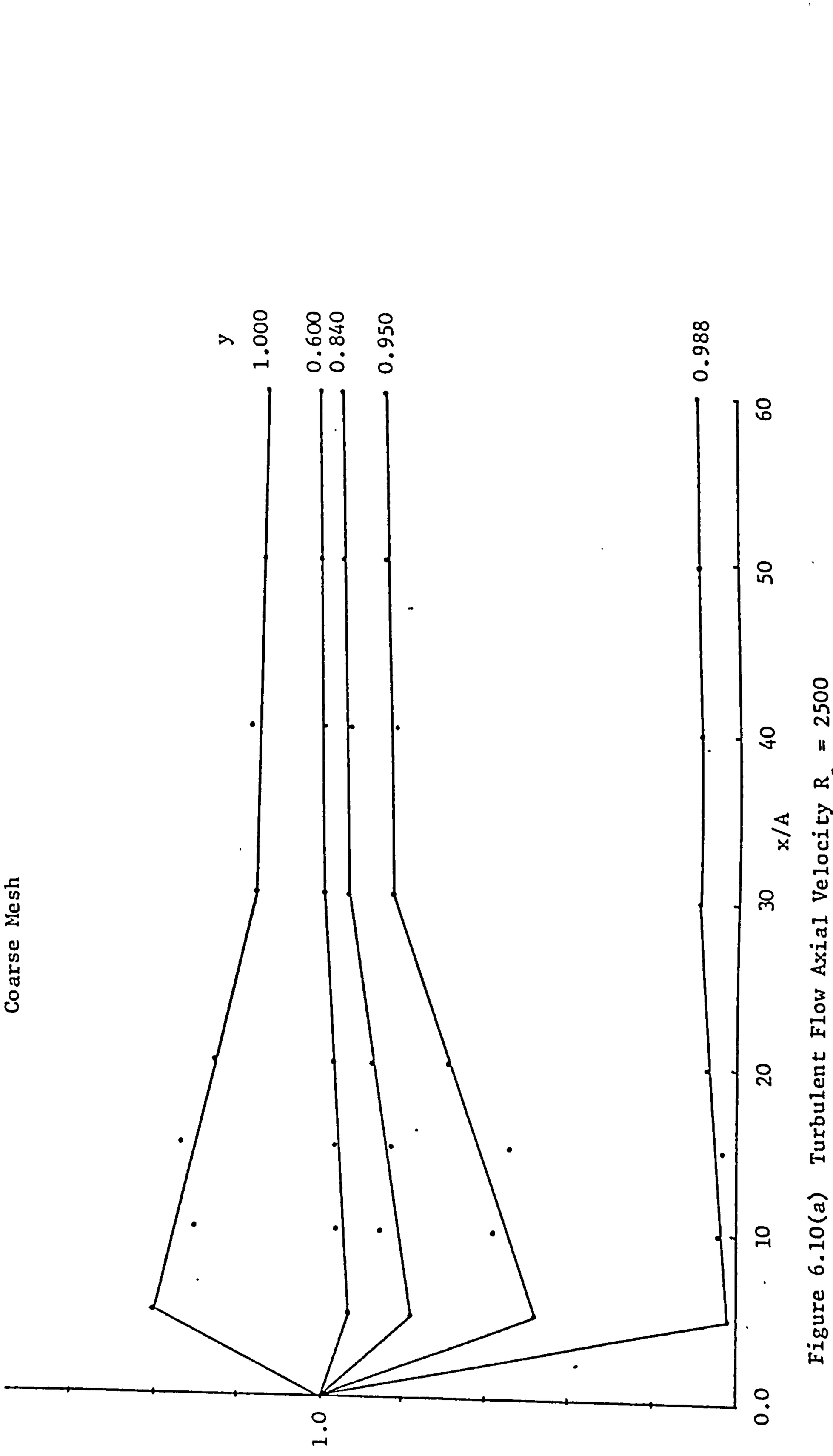

Figure 6.10(a) Turbulent Flow Axial Velocity R_e = 2500

Fine Mesh

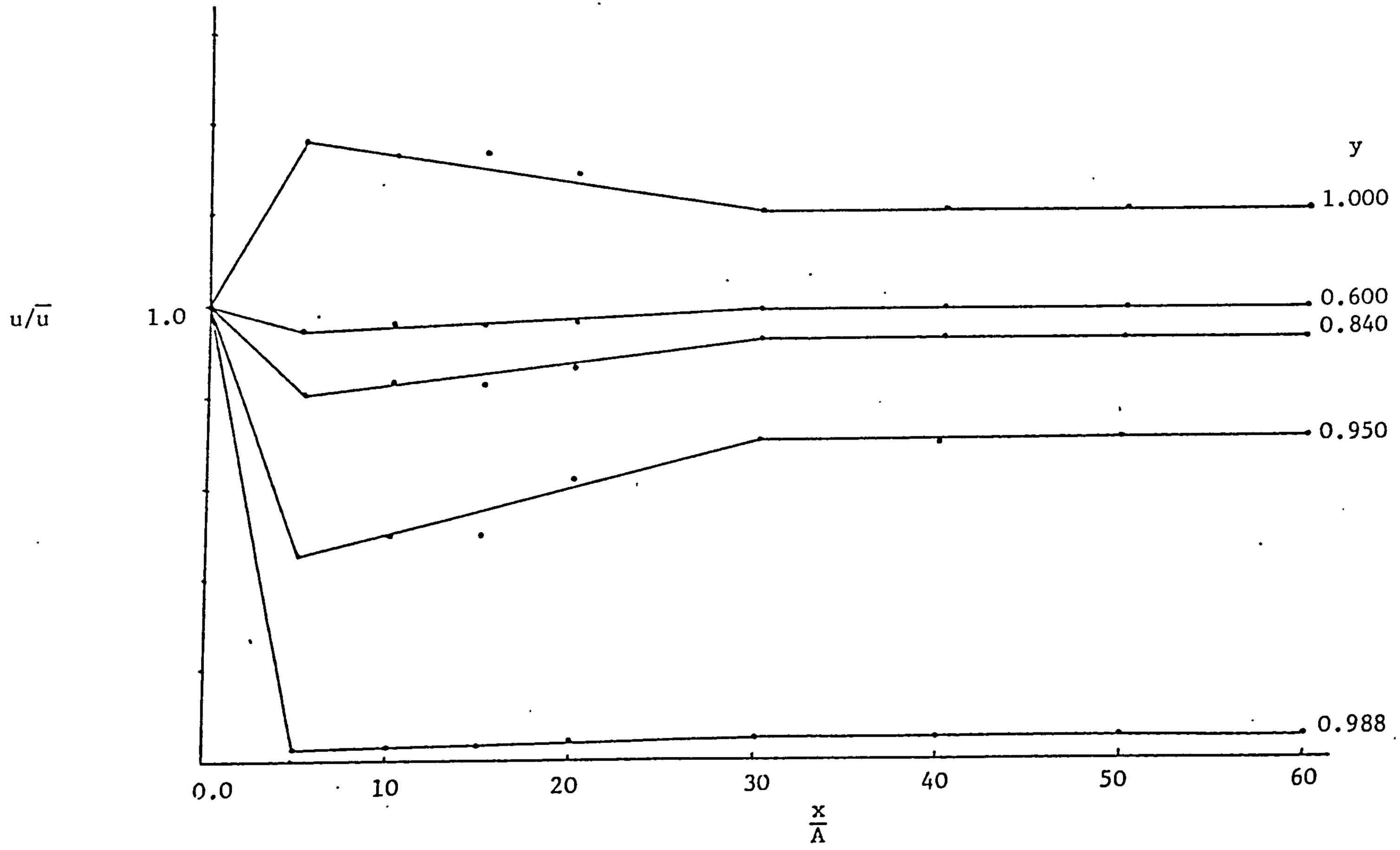

Figure 6.10(b) Turbulent Flow Axial Velocity R_c = 2500

APPENDICES

APPENDIX A.1 - THE STRESS TENSOR

The surface stress tensor T_{ij} has been defined as;

$$T_{ij} = -P\,\delta_{ij} + \lambda\, D_{KK}\,\delta_{ij} + 2\mu\, D_{ij} \qquad (A.1.1)$$

for the case of a fluid continuum.

This may be derived by initially considering an elastic solid continuum. Here again the general equilibrium equation holds:

$$\rho\frac{\partial u_i}{\partial t} = \rho\, b_i + \frac{\partial T_{ij}}{\partial x_j} \qquad (A.1.2)$$

The stress tensor may be split into direct stresses σ_i and shear stresses τ_{ij}. For an elastic solid a linear relationship between stress and strain is assumed by applying Hookes' Law. Considering the direct stresses initially;

$$\sigma_i = \overline{\sigma} - \frac{2}{3}\, G\,\frac{\partial \varepsilon_j}{\partial x_j} + 2\, G\,\frac{\partial \varepsilon_i}{\partial x_i} \qquad (A.1.3)$$

G - shear modulus

ε_i - deformation vector = $\varepsilon_1\underline{x} + \varepsilon_2\underline{y} + \varepsilon_3\underline{z}$

The first term of the above equation is the arithmetric mean of the direct stresses, the second term is caused by the dilatation of the continuum and the third is due to the direct strains.

The second part of the stress tensor the shear stresses are a function of the shear strains alone, producing:

$$\tau_{ij} = G\left(\frac{\partial \varepsilon_i}{\partial x_j} + \frac{\partial \varepsilon_j}{\partial x_i}\right) \qquad (A.1.4)$$

Finally, the total stress tensor becomes:

$$T_{ij} = \overline{\sigma}\,\delta_{ij} - \frac{2}{3}\, G\frac{\partial \varepsilon_K}{\partial x_K}\,\delta_{ij} + G\left(\frac{\partial \varepsilon_i}{\partial x_j} + \frac{\partial \varepsilon_j}{\partial x_i}\right) \qquad (A.1.5)$$

When considering a fluid it is necessary to apply Stokes' Law of friction. The strains are replaced by the rate of strains, the shear

modulus G is replaced by the dynamic viscosity of the fluid μ and the mean direct stress is equated to the fluid pressure - P. Consequently the stress tensor for a fluid may now be expressed as:

$$T_{ij} = -P\,\delta_{ij} - \frac{2}{3}\,\mu\frac{\partial u_K}{\partial x_k}\,\delta_{ij} + 2\,G\left(\frac{\partial u_i}{\partial x_j} + \frac{\partial u_j}{\partial x_i}\right) \qquad (A.1.6)$$

The rate of deformation tensor D_{ij} may now be expressed in terms of velocity

$$D_{ij} = \frac{1}{2}\left(\frac{\partial u_i}{\partial x_j} + \frac{\partial u_j}{\partial x_i}\right) \qquad (A.1.7)$$

Substituting this into equation (A.1.6) produces the expression quoted in Chapter 2.

$$T_{ij} = -P\,\delta_{ij} - \frac{2}{3}\,\mu\,D_{KK}\,\delta_{ij} + 2\,\mu\,D_{ij} \qquad (A.1.8)$$

where

$$\lambda = -\frac{2}{3}\,\mu$$

(c) Continuity

The stream function is defined as:

$$u_1 = \frac{\partial \psi}{\partial x_2} \qquad (A.2.1)$$

$$u_2 = - \frac{\partial \psi}{\partial x_1}$$

The continuity requirement for an incompressible fluid is:

$$\frac{\partial u_i}{\partial x_i} = 0 \qquad (A.2.2)$$

Substituting equation (A.2.1) into this produces:

$$\frac{\partial}{\partial x_1} \left(\frac{\partial \psi}{\partial x_2} \right) + \frac{\partial}{\partial x_2} \left(- \frac{\partial \psi}{\partial x_1} \right) = 0$$

$$\frac{\partial^2 \psi}{\partial x_1 \partial x_2} = \frac{\partial^2 \psi}{\partial x_2 \partial x_1}$$

This is the case if the stream function is taken to be a normal continuous function. Consequently the continuity of the fluid is inherent in the definition of stream function.

(ii) The vorticity - stream function relation

Vorticity describes the local rotation of a fluid and in two-dimension may be considered as a scalar defined by:

$$\omega = \frac{\partial u_2}{\partial x_1} - \frac{\partial u_1}{\partial x_2} \qquad (A.2.3)$$

Substituting equation (A.2.1) into this produces:

$$\omega = \frac{\partial}{\partial x_1} \left(- \frac{\partial \psi}{\partial x_1} \right) - \frac{\partial}{\partial x_2} \left(\frac{\partial \psi}{\partial x_2} \right)$$

$$\therefore \omega = - \frac{\partial^2 \psi}{\partial x_j^2}$$

APPENDIX B - THE ELEMENT MATRICES OF THE GOVERNING FORMULATION

The element matrices are integrated analytically in order to improve the efficiency and accuracy of the solution. In order to standardize the integration of a general element in the domain, a homogeneous coordinate system is adopted.

The background to this coordinate system being presented below .

Writing the interpolation functions in terms of the homogeneous coordinates along each element sides i.e. L_1, L_2, L_3, where;

$$L_1 = \frac{A_1}{A} \quad , \quad L_2 = \frac{A_2}{A} \quad , \quad L_3 = \frac{A_3}{A} \qquad (B.1)$$

refer to figure B.1.

Any point within the triangle may now be expressed in terms of this coordinate system. For example, the values of L_1, L_2, L_3 at the three nodal points of the triangle are presented in Table A.1 below.

NODE	L_1	L_2	L_3
1	1	0	0
2	0	1	0
3	0	0	1

Table A.1

The value of a given unknown at any point within the triangle depends on the relative influence of each nodal value. In this case a linear variation of the unknowns within the triangle has been chosen, and so it can be seen from inspection that the interpolation function takes the simple form:

$$\phi_j^T = [\phi_1, \phi_2, \phi_3] = [L_1, L_2, L_3] \tag{B.2}$$

The relationship between the homogeneous and the cartesian coordinate system is:

$$\begin{bmatrix} 1 \\ x \\ y \end{bmatrix} = \begin{bmatrix} 1 & 1 & 1 \\ x_1 & x_2 & x_3 \\ y_1 & y_3 & y_3 \end{bmatrix} \begin{bmatrix} L_1 \\ L_2 \\ L_3 \end{bmatrix} \tag{B.3}$$

This may be inverted to produce:

$$\begin{bmatrix} L_1 \\ L_2 \\ L_3 \end{bmatrix} = \frac{1}{2A} \begin{bmatrix} \alpha_1 & b_1 & c_1 \\ \alpha_2 & b_2 & c_2 \\ \alpha_3 & b_3 & c_3 \end{bmatrix} \begin{bmatrix} 1 \\ x \\ y \end{bmatrix} \tag{B.4}$$

where

$$\alpha_1 = x_2 y_3 - y_2 x_3; \quad \alpha_2 = x_3 y_1 - x_1 y_3; \quad \alpha_3 = x_1 y_2 - x_2 y_1$$

$$b_1 = y_2 - y_3; \quad b_2 = y_3 - y_1; \quad b_3 = y_1 - y_3$$

$$c_1 = x_3 - x_2; \quad c_2 = x_1 - x_3; \quad c_3 = x_2 - x_1$$

The derivatives of the interpolation functions may be expressed using the chain rule:

$$\frac{\partial \phi_j}{\partial x}(L_1, L_2, L_3) = \frac{\partial \phi_j}{\partial L_1}\frac{\partial L_1}{\partial x} + \frac{\partial \phi_j}{\partial L_2}\frac{\partial L_2}{\partial x} + \frac{\partial \phi_j}{\partial L_3}\frac{\partial L_3}{\partial x}$$

$$= \frac{1}{2A}\left[\frac{\partial \phi_j}{\partial L_1} b_1 + \frac{\partial \phi_j}{\partial L_2} b_2 + \frac{\partial \phi_j}{\partial L_3} b_3\right]$$

Using a linear interpolation this becomes:

$$\frac{\partial \phi_j}{\partial x}(L_1, L_2, L_3) = \frac{1}{2A}\begin{bmatrix} b_1 \\ b_2 \\ b_3 \end{bmatrix} \tag{B.5}$$

Consequently

$$\frac{\partial \phi_j}{\partial y}(L_1, L_2, L_3) = \frac{1}{2A}\begin{bmatrix} c_1 \\ c_2 \\ c_3 \end{bmatrix}$$

The integration of the homogeneous coordinates over an element or boundary side may be generalized:

$$\int_A L_1^i L_2^j L_3^K \, dA = \frac{i!j!K!}{(i+j+K+2)!} 2A$$

$$\int_S L_1^i L_2^j \, dS = \frac{i!j!}{(i+j+1)!} S$$

A - the area of the triangular element

S - the length of the element side, 1-2.

This clearly illustrates how each particular integral may be generalized as a function of the particular triangle's area, or an element side's length.

Below the element matrices for a general triangular element and side are presented.

Here the standard matrices which are well reported in earlier (F.E.) work shall simply be quoted in their final form. The less common non-linear matrices and the no-slip force vector shall be derived later.

The element mass matrix:

$$\underline{m} = \frac{A}{12}\begin{bmatrix} 2 & 1 & 1 \\ 1 & 2 & 1 \\ 1 & 1 & 2 \end{bmatrix} \qquad (B.7)$$

The element stiffness matrix:

$$\underline{K} = \frac{1}{4A^2}\left\{\begin{bmatrix} b_1 \\ b_2 \\ b_3 \end{bmatrix}[b_1, b_2, b_3] + \begin{bmatrix} c_1 \\ c_2 \\ c_3 \end{bmatrix}[c_1, c_2, c_3]\right\} \qquad (B.8)$$

The force vector acting over an element side:

$$\underline{b} = \frac{S}{2}\begin{bmatrix}1\\1\end{bmatrix} \tag{B.9}$$

From equation (3.2.10) the element convective matrix is defined as:

$$\underline{a}\ (\underline{\psi}) = \int_A \left[\phi_j \left(\frac{\partial \phi_j^T}{\partial y}\ \underline{\psi}^n\ \frac{\partial \phi_j^T}{\partial x} - \frac{\partial \phi_j^T}{\partial y}\ \underline{\psi}^n\ \frac{\partial \phi_j^T}{\partial x}\right)\right]\ dA$$

This may be expanded as:

$$\underline{a}\ (\underline{\psi}) = \frac{1}{4A^2}\int_A \begin{bmatrix}L_1\\L_2\\L_3\end{bmatrix}\left\{ [c_1,\ c_2,\ c_3]\begin{bmatrix}\psi_1\\\psi_2\\\psi_3\end{bmatrix}[b_1,\ b_2,\ b_3] - \right. \tag{B.10}$$

$$\left. [b_1,\ b_2,\ b_3]\begin{bmatrix}\psi_1\\\psi_2\\\psi_3\end{bmatrix}[c_1,\ c_2,\ c_3]\right\}\ dA$$

This may now be integrated producing:

$$\underline{a}\ (\underline{\psi}) = \frac{1}{12A}\left[\begin{bmatrix}1\\1\\1\end{bmatrix}\left\{ [c_1,\ c_2,\ c_3]\begin{bmatrix}\psi_1\\\psi_2\\\psi_3\end{bmatrix}[b_1,\ b_2,\ b_3] - \right.\right.$$

$$\left.\left. [b_1,\ b_2,\ b_3]\begin{bmatrix}\psi_1\\\psi_2\\\psi_3\end{bmatrix}[c_1,\ c_2,\ c_3]\right\}\right] =$$

$$= \frac{1}{12A}\begin{bmatrix}1\\1\\1\end{bmatrix}\{[b_1(c_1\ \psi_1 + c_2\ \psi_2 + c_3\ \psi_3) - c_1(b_1\ \psi_1 + b_2\ \psi_2 + b_3\ \psi_3)];$$

$$[b_2(\quad " \quad) - c_2(\quad " \quad)];$$

$$[b_3(\quad " \quad) - c_3(\quad " \quad)]\}$$

$$= \frac{1}{12A}\begin{bmatrix}1\\1\\1\end{bmatrix}\{[\psi_2\ (b_1\ c_2 - b_2\ c_1) + \psi_3\ (b_1\ c_3 - b_3\ c_1)]$$

$$[\psi_1\ (b_2\ c_1 - b_1\ c_2) + \psi_3\ (b_2\ c_3 - b_3\ c_2)]$$

$$[\psi_1\ (b_3\ b_1 + b_1\ c_3) + \psi_2\ (b_3\ c_2 - b_2\ c_3)]\}$$

$$\therefore\ a\ (\underline{\psi}) = \frac{1}{6}\begin{bmatrix}1\\1\\1\end{bmatrix}\ [(\psi_2 - \psi_3);\ (\psi_3 - \psi_1);\ (\psi_1 - \psi_2)] \qquad (B.11)$$

From section 3.4 the boundary force vector is of the form:

$$\underline{b}_\omega = \left[\int_{S_{NSB}} \phi_j \frac{\partial \phi_j^T}{\partial n}\, dS\right] \omega^e$$

From the chain rule:

$$\frac{\partial \phi_j}{\partial n} = \frac{\partial \phi_j}{\partial x}\,\alpha_x + \frac{\partial \phi_j}{\partial y}\,\alpha_y$$

$$\alpha_x = \frac{\partial x}{\partial n} \quad ; \quad \alpha_y = \frac{\partial y}{\partial n}$$

Along an element side the interpolation function becomes:

$$\phi_j^T = [L_1,\ L_2]$$

$$\frac{\partial \phi_j}{\partial n} = \left\{\left[\frac{\partial \phi_j}{\partial L_1}\frac{\partial L_1}{\partial x} + \frac{\partial \phi_j}{\partial L_2}\frac{\partial L_2}{\partial x}\right]\alpha_x + \left[\frac{\partial \phi_j}{\partial L_1}\frac{\partial L_1}{\partial y} + \frac{\partial \phi_j}{\partial L_2}\frac{\partial L_2}{\partial y}\right]\alpha_y\right\} =$$

$$= \frac{1}{2A}\begin{bmatrix}(c_1\,\alpha_x + b_1\,\alpha_y)\\(c_2\,\alpha_x + b_2\,\alpha_y)\end{bmatrix}$$

$$\therefore \int_{S_{NSB}} \phi_j \frac{\partial \phi_j^T}{\partial n}\, dS = \frac{1}{2A}\int_{S_{NSB}} \left\{\begin{bmatrix}L_1\\L_2\end{bmatrix}\ [(c_1\,\alpha_x + b_1\,\alpha_y)\ ;\ (c_2\,\alpha_x + b_2\,\alpha_y)]\right\}\, dA$$

This may now be integrated:

$$= \frac{S}{4A}\begin{bmatrix}1\\1\end{bmatrix}[(c_1\,\alpha_x + b_1\,\alpha_y)\ ;\ (c_2\,\alpha_x + b_2\,\alpha_y)]$$

The local boundary effect may be expressed:

$$b_\omega = \frac{S}{4A}\begin{bmatrix}1\\1\end{bmatrix}\ [(c_1\,\alpha_x + b_1\,\alpha_y)\ ;\ (c_2\,\alpha_x + b_2\,\alpha_y)]\ \underline{\omega}^e$$

Assuming the vorticity is constant along an element boundary.

$$\underline{b}_{\omega} = \frac{S}{4A} \left((c_1 + c_2)\ \alpha_x + (b_1 + b_2)\ \alpha_y \right)\ \omega_{NSB} \begin{bmatrix} 1 \\ 1 \end{bmatrix}$$

$$= \frac{S^2}{4A}\ \omega_{NSB} \begin{bmatrix} 1 \\ 1 \end{bmatrix} \qquad (B.12)$$

refer to figure (B.2).

ω_{NSB} - is obtained from the local equation at element level, where the non-boundary node is taken as the offset point.

Considering the extra matrices due to the variable viscosity in the turbulent range of flow, see equation (6.5.8).

$$\underline{t}_1\ \underline{\Omega} = \int_a \frac{\partial \nu_t}{\partial x_j} \frac{\partial \Omega}{\partial x_j}\ \delta\ \Omega\ da \qquad (B.13)$$

$$\therefore\ \underline{t}_1 = \frac{\partial \nu_t}{\partial x_j} \int_a \phi_j \frac{\partial \phi_j^T}{\partial x_j}\ da$$

$$= \frac{\partial \nu_t}{\partial x_j} \frac{1}{2A} \int_a \left\{ \begin{bmatrix} L_1 \\ L_2 \\ L_3 \end{bmatrix} \left[(b_1 + c_1)\ ;\ (b_2 + c_2)\ ;\ (b_3 + c_3) \right] \right\} da$$

This may now be integrated:

$$= \frac{\partial \nu_t}{\partial x_j} \frac{1}{6} \begin{bmatrix} 1 \\ 1 \\ 1 \end{bmatrix} \left[a_1,\ a_2,\ a_3 \right]$$

where

$$a_1 = b_1 + c_1\ ;\ a_2 = b_2 + c_2\ ;\ a_3 + b_3 = c_3$$

Assuming a linear variation of viscosity within each element:

$$\frac{\partial \nu_t}{\partial x_j} = \frac{1}{2A} \left[a_1, a_2, a_3\right] \begin{bmatrix} \nu_1 \\ \nu_2 \\ \nu_3 \end{bmatrix}$$

And so the element matrix may be expressed as:

$$\underline{t}_1 = \frac{1}{12A} \left[a_1 \nu_1 + a_2 \nu_2 + a_3 \nu_3\right] \begin{bmatrix} 1 \\ 1 \\ 1 \end{bmatrix} \left[a_1, a_2, a_3\right] \qquad \text{(B.14)}$$

The second term is:

$$\underline{t}_2 \, \underline{\Omega} = \int_a \frac{\partial \nu_t}{\partial x_j} \frac{\partial (\delta \Omega)}{\partial x_j} \Omega \, da \qquad \text{(B.15)}$$

$$\therefore \underline{t}_2 = \frac{\partial \nu_t}{\partial x_j} \int_a \frac{\partial \phi_j}{\partial x_j} \phi_j^T \, da$$

$$= \frac{\partial \nu_t}{\partial x_j} \frac{1}{6} \begin{bmatrix} a_1 \\ a_2 \\ a_3 \end{bmatrix} \left[1, 1, 1\right]$$

Again assuming a linear variation of viscosity

$$= \frac{1}{12A} \left[a_1 \nu_1 + a_2 \nu_2 + a_3 \nu_3\right] \begin{bmatrix} a_1 \\ a_2 \\ a_3 \end{bmatrix} \left[1, 1, 1\right] \qquad \text{(B.16)}$$

The additional boundary term is expressed:

$$\underline{S} \, \underline{\Omega} = \int_s \frac{\partial \nu_t}{\partial n} \delta \, \Omega \, \Omega \, ds \qquad \text{(B.17)}$$

ω_2

Again assuming a linear variation of the viscosity the gradient is constant over an element side:

$$\therefore \underline{S} = \frac{\partial \nu_t}{\partial n} \int_{s_{\omega_2}} \phi_j \phi_j^T \, ds$$

Applying the chain rule:

$$\frac{\partial \nu_t}{\partial n} = \frac{\partial \nu_t}{\partial x}\frac{\partial x}{\partial n}\frac{\partial \nu_t}{\partial y}\frac{\partial y}{\partial n}$$

$$\frac{\partial \nu}{\partial n} = \frac{1}{2A}\left[\ell_x(b_1, b_2, b_3) + \ell_y(c_1, c_2, c_3)\right]\begin{bmatrix}\nu_1\\ \nu_2\\ \nu_3\end{bmatrix}$$

$\ell_x = \cos\theta$; $\ell_y = -\sin\theta$

θ is the angle of x with n

$$\underline{S} = \left[\ell_x(b_1, b_2, b_3) + \ell_y(c_1, c_2, c_3)\right]\begin{bmatrix}\nu_1\\ \nu_2\\ \nu_3\end{bmatrix}\frac{L}{12A}\begin{bmatrix}2 & 1\\ 1 & 2\end{bmatrix} \qquad (B.18)$$

$$A = A_1 + A_2 + A_3$$

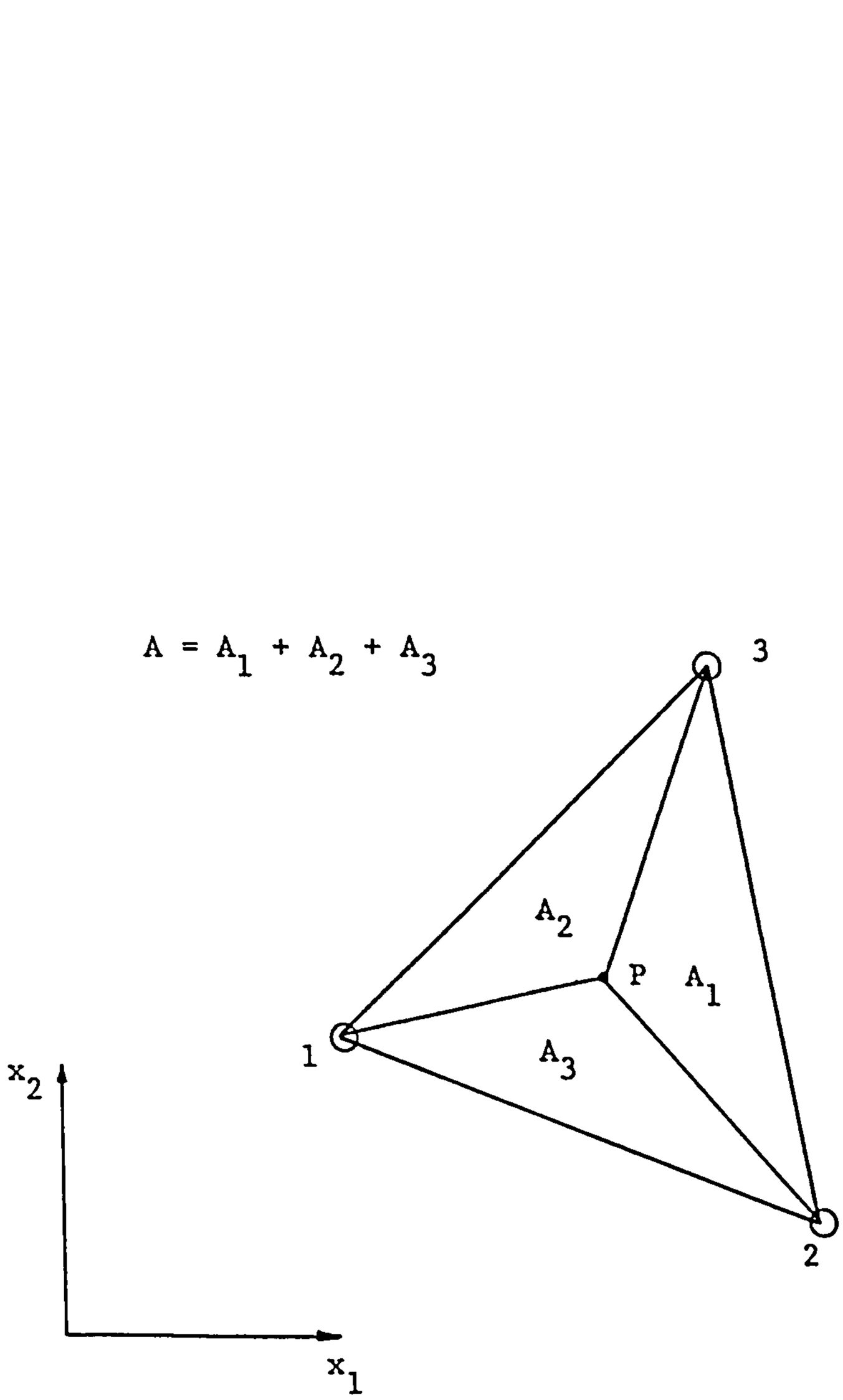

The homogeneous coordinates of point P = (L_1, L_2, L_3)

where

$$L_1 = \frac{A_1}{A} \; ; \quad L_2 = \frac{A_2}{A} \; ; \quad L_3 = \frac{A_3}{A}$$

Figure B.1 The Homogeneous Coordinate System

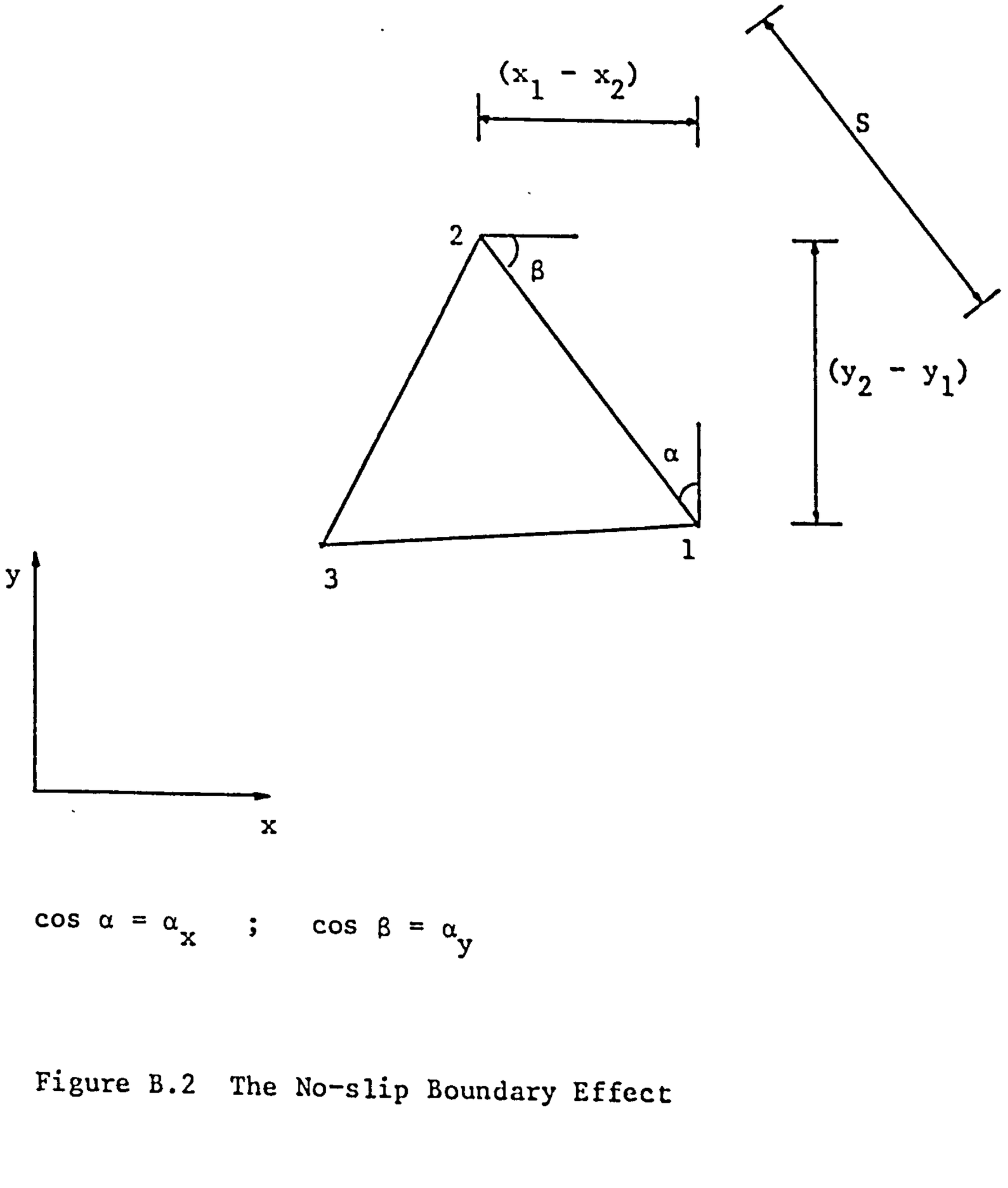

$\cos \alpha = \alpha_x$; $\cos \beta = \alpha_y$

Figure B.2 The No-slip Boundary Effect

APPENDIX C - A LIST OF SOLVER ABORT CODES

Two expressions are available to calculate the size of the two main arrays used in the (N.S) solver; i.e. real and integer array. This ensures the most efficient use of program space.

Where:

N1 - the size of solution matrix.

Two such arrays are required in order to store both the upper and lower diagonal parts of the non-linear matrix.

N2 - the size of the unknown array.

Since the solver deals with stream function and vorticity separately, this is equivalent to the number of nodes.

N3 - the size of the boundary array.

N4 - the maximum number of elements.

The storage scheme is split into two main arrays storing the real variables and integers separately where,

$$A(NR),\ NR = 3 \times N1 + 12 \times N2 + 27 \times N3$$
$$B(NI),\ NI = 3 \times N4 + 2 \times N2 + 16 \times N3 \qquad (C.1)$$

NX - the real array size

NY - the integer array size

List of Abort Codes

When the subroutine FPSTOP(n) is called anywhere in the program, execution stops and the abort number n is printed.

Below a list of such abort numbers related to the solution part of the program is presented:

(1) - error in subroutine USER1, where the main real array size is exceeded.

(2) - error in subroutine USER1, where the main integer array size is exceeded.

(3) - error in subroutine USER2, where the element array size is too small, i.e. NELMS>N4.

(4) - error in subroutine USER2, where the nodal array size is too small, i.e. NN>N2.

(5) - error in subroutine USER2, where the restricted array size is too small, i.e. NRN>N3.

(6) - error in subroutine USER2, when the boundary element array is too large, i.e. NBEL>N3.

(7) - error in subroutine USER2, where the size of the solution matrix is too small, i.e. NNNV>N1.

(8) - error in subroutine USER2, where the size of the no-slip boundary element array is too small, i.e. NSEL>N3.

(9) - error in subroutine USER2 before subroutine INSLIP is called. To check that there is enough auxilary space required in INSLIP, i.e. 4xN3>N1.

(10) - error in subroutine INSLIP unable to find any nodes adjacent to the current one on the no-slip boundary.

(11) - error in subroutine INSLIP unable to find an adjacent node to the first or last node of the no-slip boundary.

(12) - error in subroutine USER1 check the size of parameters NELMS, NN, NNNV before reading in the mesh.

(13) - error in subroutine RENUM, cannot find a suitable starting node for renumbering.

where

NELMS - the number of elements

NN - the number of nodes

NNNV - the size of the solution array required

NRN - the number of restricted nodes

NBEL - the number of boundary elements

NSEL - the number of elements containing one boundary side.